Modeling the gas and aqueous phase chemistry of the marine boundary layer

Dissertation
zur Erlangung des Grades
„Doktor der Naturwissenschaften"

am Fachbereich Physik der
Johannes Gutenberg-Universität
in Mainz

Roland von Glasow

geboren in Essen

Mainz, 2000

Tag der mündlichen Prüfung: 25.01.2001

Contents

Zusammenfassung

Ein eindimensionales numerisches Modell der maritimen Grenzschicht (MBL) wurde erweitert, um chemische Reaktionen in der Gasphase, von Aerosolpartikeln und Wolkentropfen zu beschreiben. Ein Schwerpunkt war dabei die Betrachtung der Reaktionszyklen von Halogenen. Soweit Ergebnisse von Meßkampagnen zur Verfügung standen, wurden diese zur Validierung des Modells benutzt.

Die Ergebnisse von früheren Boxmodellstudien konnten bestätigt werden. Diese zeigten die säurekatalysierte Aktivierung von Brom aus Seesalzaerosolen, die Bedeutung von Halogenradikalen für die Zerstörung von O_3, die potentielle Rolle von BrO bei der Oxidation von DMS und die von HOBr und HOCl in der Oxidation von S(IV).

Es wurde gezeigt, daß die Berücksichtigung der Vertikalprofile von meteorologischen und chemischen Größen von großer Bedeutung ist. Dies spiegelt sich darin wider, daß Maxima des Säuregehaltes von Seesalzaerosolen und von reaktiven Halogenen am Oberrand der MBL gefunden wurden. Darüber hinaus wurde die Bedeutung von Sulfataerosolen bei dem aktiven Recyceln von weniger aktiven zu photolysierbaren Bromspezies gezeigt.

Wolken haben große Auswirkungen auf die Evolution und den Tagesgang der Halogene. Dies ist nicht auf Wolkenschichten beschränkt. Der Tagesgang der meisten Halogene ist aufgrund einer erhöhten Aufnahme der chemischen Substanzen in die Flüssigphase verändert. Diese Ergebnisse betonen die Wichtigkeit der genauen Dokumentation der meteorologischen Bedingungen bei Meßkampagnen (besonders Wolkenbedeckungsgrad und Flüssigwassergehalt), um die Ergebnisse richtig interpretieren und mit Modellresultaten vergleichen zu können.

Dieses eindimensionale Modell wurde zusammen mit einem Boxmodell der MBL verwendet, um die Auswirkungen von Schiffemissionen auf die MBL abzuschätzen, wobei die Verdünnung der Abgasfahne parameterisiert wurde. Die Auswirkungen der Emissionen sind am stärksten, wenn sie in sauberen Gebieten stattfinden, die Höhe der MBL gering ist und das Einmischen von Hintergrundluft schwach ist. Chemische Reaktionen auf Hintergrundaerosolen spielen nur eine geringe Rolle. In Ozeangebieten mit schwachem Schiffsverkehr sind die Auswirkungen auf die Chemie der MBL beschränkt. In stärker befahrenen Gebieten überlappen sich die Abgasfahnen mehrerer Schiffe und sorgen für deutliche Auswirkungen. Diese Abschätzung wurde mit Simulationen verglichen, bei denen die Emissionen als kontinuierliche Quellen behandelt wurden, wie das in globalen Chemiemodellen der Fall ist. Wenn die Entwicklung der Abgasfahne berücksichtigt wird, sind die Auswirkungen deutlich geringer da die Lebenszeit der Abgase in der ersten Phase nach Emission deutlich reduziert ist.

Abstract

A numerical one-dimensional model of the marine boundary layer (MBL) was extended with a module that describes chemical reactions of the gas phase, aerosol particles and cloud droplets. A special focus was the study of the reaction cycles of halogen compounds. Where measurements are available they were used for validation of the model results.

Results of earlier box model studies could be confirmed. They showed the acid catalyzed activation of bromine from sea salt aerosol, the role of halogen radicals in the destruction of O_3, the potential role of BrO in the oxidation of DMS and that of HOBr and HOCl in the oxidation of S(IV).

The importance of the consideration of vertical variations of the meteorological and chemical properties in the MBL was shown. They are manifested in maxima of sea salt acidity and reactive halogen species at the top of the MBL. The importance of sulfate aerosol particles in the active recycling of less reactive bromine species to photolyzable species was shown.

The effects of clouds on the evolution and diurnal cycle of halogen species are widespread; they are not restricted to cloud layers. The diurnal variation of most halogen species near the surface is changed due to a different partitioning of the chemical species between the gas and aqueous phase. These findings point to the importance of an exact description of the meteorological circumstances of field measurements (esp. cloud cover, liquid water content) to be able to interpret them correctly and to compare them with model results.

The same model and a box-model of the MBL were applied to the study of the effects of emissions of ocean-going ships on the MBL. The dilution of the air in the plume was parameterized. It could be shown that the effect of emissions are strongest when they take place in clean regions, when the height of the MBL is smallest and when dilution of the plume by backgrond air is weak. Chemical reactions on background aerosol particles play only a minor role. In ocean regions that are distant from the main traffic regions the effect on the chemistry of the MBL is only small. The effect of the overlap of the plumes of several ships in more heavily traversed regions was investigated showing significant impacts there. The simulation of overlapping ship plumes was compared with simulations where the ship emissions are treated as continuous sources as it is done in global chemistry models. The impacts of ship emissions are significantly smaller when the plume evolution is accounted for due to strongly reduced chemical lifetimes of pollutants in early plume stages.

Chapter 1

Introduction

The subject of this thesis is the chemistry and physics of the marine boundary layer (MBL). Over large regions of the remote oceans the boundary layer is affected only to a small extent by anthropogenic emissions. The emissions of ocean-going ships, however, can pollute these regions of the MBL significantly. Both of these extremes are studied in this thesis. A special emphasis in the examination of the clean MBL is on the chemistry of halogen compounds. The basic properties of the MBL and the origin of halogens in the MBL are explained briefly. Then the role of halogen reactions in other parts of the atmosphere is mentioned where they were first discovered to be of importance.

The MBL is the lowest part of the troposphere that is in direct contact with the sea surface. It is separated from the free troposphere by a temperature and humidity inversion and is generally well mixed. As a consequence, the absolute humidity is constant with height in a cloud-free MBL. In the MBL the temperature decreases with height and therefore the relative humidity increases with height (see e.g. *Stull* (1988)). Below the inversion stratiform clouds occur frequently. Figure 1.1 shows schematically the structure of the MBL with typical vertical profiles of the relative humidity, temperature and potential temperature. When the potential temperature is constant with height, this indicates a well mixed MBL. For the cloudy MBL also a typical profile of liquid water content of the cloud is shown. In the cloud the potential temperature increases with height due to the release of latent energy during condensation.

Approximately 70 % of the earth's surface is covered by oceans, making processes in the MBL potentially significant for the whole troposphere and atmosphere, as trace gases and aerosol can be exchanged between the MBL and the free troposphere. The net radiative forcing of stratiform clouds in the MBL is negative, which is important for the total radiation budget of the atmosphere (e.g. *Albrecht* (1989)). *Lelieveld et al.* (1989) provided values for the latitudinally averaged cloud coverage for different types of clouds, which show that in the latitude bands of the southern hemisphere where the fraction of land is below 4 % the coverage by stratiform clouds is in all seasons greater than 20 % and often greater than 40 %. But even when no clouds are present in the MBL the relative humidity is usually high enough to allow aerosol particles to be deliquescent and

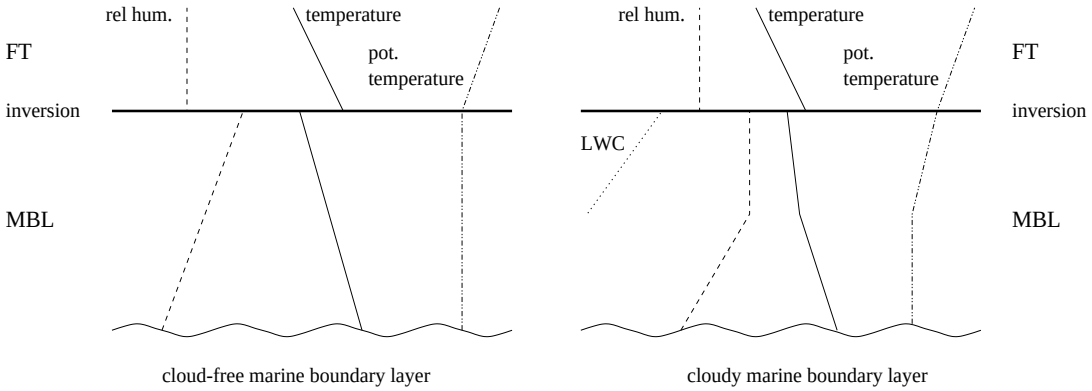

Figure 1.1: Schematic depiction of the vertical profiles of relative humidity, temperature, potential temperature (Θ) and liquid water content (LWC) in the cloud-free and cloudy MBL, FT stands for free troposphere. The LWC is only shown where a cloud is present.

therefore active aqueous chemistry to occur.

Chemical reactions on and inside atmospheric particles (e.g. aerosol particles and cloud droplets) can have a significant influence on the chemistry of the gas phase (see *Jacob* (2000) for a review). The aerosol particles in the unpolluted MBL are usually particles with sulfate as a main component as well as aerosol particles derived from the sea surface, the so-called sea salt aerosols. During episodes of strong influence of continental air, e.g. dust outbreak from deserts or biomass burning, these particles can significantly contribute to the aerosol loading. Usually the number of aerosols in the MBL is dominated by sulfate particles, whereas the mass is dominated by the sea salt fraction.

Sea salt aerosols are produced at the sea surface by the bursting of air bubbles that had been entrained from the atmosphere at wave crests. This process produces small droplets from the film of the air bubbles and large jet droplets (see Figure 1.2). Even larger droplets are produced by strong winds blowing over wind crests and producing spray droplets (*Pruppacher and Klett* (1997)). When these droplets remain airborne they evaporate partly to form sea salt aerosol particles. Sea salt aerosol consists mainly of sea water, sometimes an organic film is present on the sea surface which might be incorporated into the particles. The major component of sea salt aerosol is NaCl, but other components are also included (see Table 1.1), e.g. the halogen bromine which is very reactive once it is liberated from the sea salt aerosol. The composition of the major ions in sea water is very constant due to the long residence times of the ions in the oceans (10^4 to 10^8 years, *Andrews et al.* (1996), p. 121).

Sea salt aerosol is important on a global scale because it contributes about 2/3 of the total natural sources of aerosol particles (by mass), if gas-to-particle conversion is included as particle source it still contributes more than 40 % - 60 % (different estimates) to the total naturally produced aerosol mass (*Pruppacher and Klett* (1997)).

Apart from the halogens chlorine and bromine, the halogen iodine is also

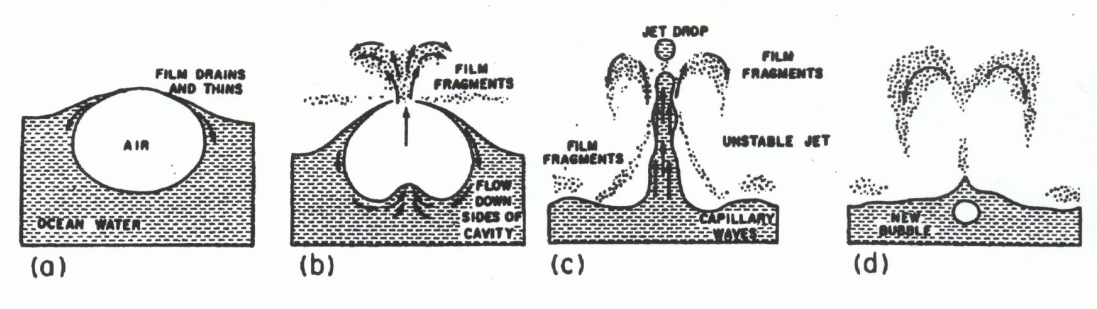

Figure 1.2: Four stages in the production of sea salt aerosol by the bubble-burst mechanism. (a) Film cap protrudes from the ocean surface and begins to thin. (b) Flow down the sides of the cavity thins the film which eventually ruptures into many small fragments. (c) Unstable jet breaks into few drops. (d) Tiny salt particles remain as drops evaporate; new bubble is formed. From *Pruppacher and Klett* (1997).

Table 1.1: Composition of sea water.

ion	Cl^-	Na^+	Mg^{2+}	SO_4^{2-}	K^+	Ca^{2+}	HCO_3^-	Br^-
conc. [mmol/l]	550	470	53	28	10	10	2	0.85 [1]

The data is after *Andrews et al.* (1996), p. 121, except for [1] which is calculated after *Jaenicke* (1988).

present in the MBL. It is mainly emitted in the form of biogenic alkyl iodides that are rapidly photolysed in the MBL.

Reactions of halogens in the atmosphere received most attention in the study of the "ozone hole" that occurs in the Antarctic stratosphere during spring. This very strong O_3 destruction could be explained by fast, catalytic reactions involving halogen (mainly chlorine and bromine) radicals. The importance of interactions between the gas and the particulate phase was shown to be of particular importance (see e.g. *Brasseur et al.* (1999) for an overview).

The reaction mechanisms involved in the destruction of O_3 in the stratosphere are not restricted to the stratosphere as shown by the occurence of sudden O_3 destructions during spring ("polar sunrise") in the Arctic boundary layer. There BrO was found to be very important in O_3 destruction e.g. by the cycle:

$$\begin{aligned} \mathrm{Br} + \mathrm{O_3} &\longrightarrow \mathrm{BrO} \\ \mathrm{BrO} + \mathrm{HO_2} &\longrightarrow \mathrm{HOBr} \\ \mathrm{HOBr} + h\nu &\longrightarrow \mathrm{Br} + \mathrm{OH} \\ \hline net: \mathrm{O_3} + \mathrm{HO_2} &\longrightarrow \mathrm{O_2} + \mathrm{OH} \end{aligned}$$

Other reaction cycles as well as the uptake of HOBr on particles were also found to be of importance. This cycle stands as an example for quick catalytic O_3 destruction and that radicals that are present at very small concentrations (the BrO to O_3 ratio is about 1:1000) can have a large impact. The source for

bromine during these episodic events are probably deposits on the snow pack (see e.g. *Barrie et al.* (1988), *Bottenheim et al.* (1990), *Barrie et al.* (1994), *Barrie and Platt* (1997)).

As halogen compounds as well as particles are present in the MBL, the question arose, if similar reaction cycles with influence on O_3 or other species can be important in the MBL as well. Destruction of O_3 in the troposphere would change the oxidative capacity of the atmosphere which determines e.g. the lifetime of short- and longlived trace gases.

In the first part of this thesis (chapters 2 to 5), the gas phase and aqueous phase chemistry of the cloud-free and cloudy MBL with a focus on halogen reactions is studied in detail with a numerical model. In the text "aqueous phase chemistry" is understood as a generic term for all reactions involving aqueous particles. Aqueous particles in this context are deliquescent aerosols or cloud droplets. The reactions involving aqueous particles are uptake from the gas phase, reactions on the surface of particles, chemical reactions and equilibria within the particles.

In chapter 2 the literature is briefly reviewed, listing the studies that were made in the laboratory, in the field and with models to understand chemical processes involving halogens in the MBL.

To further elucidate the role of halogens in the MBL, I extended the one-dimensional boundary layer model MISTRA to include chemical reactions in the gas phase as well as in and on aerosol (sea salt and sulfate particles) and cloud particles that grew on each type of aerosol. The new model is designed for detailed process studies, it is explained in chapter 3. In chapter 4 the results of sensitivity studies are shown for cloud-free situations, whereas the cloudy MBL is studied in chapter 5.

Where available, data from measurement campaigns were used to discuss the model results. My findings might also help to design future field campaigns or laboratory studies.

The second part of this thesis (chapters 6 to 9) deals with the anthropogenic influence of ocean-going ships on the MBL. Contrary to the intermittent advection of anthropogenic emissions from the continents to the sea, the emissions by the global ship fleet along the most important ship routes is more continuous. An overview of the relevant literature and a more in-depth discussion of the problem is given in chapter 6.

To assess the effects of ship emissions on the MBL, the box model MOCCA was modified. These modifications as well as changes in the one-dimensional model MISTRA to account for ship emissions are explained in chapter 7. In chapter 8 the evolution of the ship exhaust plumes is studied using the modified box model, whereas in chapter 9 results from model runs with the one-dimensional model are discussed.

In chapter 10 a summary of the major results of this thesis is given. The appendix contains a list of all reaction rates and coefficients used in the model, the discussion of specific topics that would distract in the main text, a list of the symbols used, and a depiction of the major reaction cycles.

Chapter 2

Halogen chemistry in the MBL: An overview

Sea salt aerosol particles contain Cl^- and Br^-, but in order to get reactive gas phase halogen compounds these substances have to be liberated from the sea salt aerosol.

2.1 Laboratory and modeling studies

Fan and Jacob (1992) proposed that the following acid catalyzed reaction plays a role in the rapid cycling of bromine in the Arctic in atmospheric sulfate particles:

$$HOBr_{aq} + H^+ + Br^- \longrightarrow Br_{2,aq}. \tag{2.1}$$

They assumed that HOBr and HBr (which they considered to be the source of Br^-) would be produced by gas phase reactions. *Mozurkewich* (1995) proposed a reaction involving Caro's acid (HSO_5^-) that can release bromide from the sea salt aerosol by transforming it into the reactive $HOBr_{aq}$:

$$HSO_5^- + Br^- \longrightarrow SO_4^{2-} + HOBr_{aq} \tag{2.2}$$

The hypobromous acid, HOBr, which is formed in this reaction can react further to species that degas from the aerosol. *Mozurkewich* (1995) also proposed an auto-catalytic cycle, that would be active after starter reactions like reaction (2.2) converted Br^- into reactive species in the aqueous phase (Br_2). *Sander and Crutzen* (1996) showed the importance of these cycles also at midlatitudes and *Vogt et al.* (1996) proposed reaction cycles that couple bromine and chlorine chemistry. Br_2 and BrCl can degas from the particles, be photolyzed in the gas phase and destroy O_3 in a catalytic cycle. HOBr, which is produced during this cycle can be taken up by the aerosol particles, thereby closing the reaction cycles:

$$\mathrm{Br_2} + h\nu \longrightarrow 2\mathrm{Br} \quad (2.3)$$
$$2(\mathrm{Br} + \mathrm{O_3}) \longrightarrow 2(\mathrm{BrO} + \mathrm{O_2}) \quad (2.4)$$
$$2(\mathrm{BrO} + \mathrm{HO_2}) \longrightarrow 2\mathrm{HOBr} \quad (2.5)$$
$$2\mathrm{HOBr} \longrightarrow 2\mathrm{HOBr_{aq}} \quad (2.6)$$
$$2(\mathrm{HOBr_{aq}} + \mathrm{H^+} + \mathrm{Br^-}) \longrightarrow 2\mathrm{Br_{2,aq}} \quad (2.7)$$
$$2\mathrm{Br_{2,aq}} \longrightarrow 2\mathrm{Br_2} \quad (2.8)$$

and

$$\mathrm{BrCl} + h\nu \longrightarrow \mathrm{Br} + \mathrm{Cl} \quad (2.9)$$
$$\mathrm{Br} + \mathrm{O_3} \longrightarrow \mathrm{BrO} + \mathrm{O_2} \quad (2.10)$$
$$\mathrm{BrO} + \mathrm{HO_2} \longrightarrow \mathrm{HOBr} \quad (2.11)$$
$$\mathrm{HOBr_{aq}} + \mathrm{H^+} + \mathrm{Cl^-} \longrightarrow \mathrm{BrCl_{aq}} \quad (2.12)$$
$$\mathrm{BrCl_{aq}} \longrightarrow \mathrm{BrCl} \quad (2.13)$$

The reaction cycles will be discussed in more detail in sections 4.2 and 4.5 and are depicted in Figure G.1.

In different laboratory studies the release of Br_2 and BrCl from sea salt solutions and the importance of HOBr could be shown. *Abbatt and Waschewsky* (1998) studied the kinetics of the uptake of HOBr, HNO_3, O_3, and NO_2 on deliquescent NaCl aerosols using an aerosol kinetics flow tube technique, showing quick uptake of HOBr that is needed in order to maintain the autocatalytic reaction cycle proposed by *Vogt et al.* (1996) (see reactions (2.6), (2.7), (2.8)).

Mochida et al. (1998a) studied the uptake of HOBr on solid NaCl and KBr crystals observing Br_2 and BrCl (only for NaCl) as the main products. Br_2 was even formed for HOBr interacting on solid $NaNO_3$, a non-halogen containing substrate.

Hirokawa et al. (1998) showed in a reaction chamber experiment that reactive bromine species can be released from sea salt particles in the absence of nitrogen oxides again pointing to the importance of HOBr, possibly involving reactions of O_3 as an intermediate step in the formation of HOBr in the aqueous phase. In another study using a Knudsen cell reactor *Mochida et al.* (2000) measured the uptake coefficients of O_3 on synthetic and natural sea salt, which were about 3 orders of magnitude greater than those known from bulk bromide solutions.

Fickert et al. (1999) showed the production of Br_2 and BrCl from the uptake of HOBr onto aqueous salt solutions in a wetted-wall flow tube reactor. The yield of Br_2 and BrCl was found to depend on the Cl^- to Br^- ratio, with more than 90 % yield of Br_2 when $[Cl^-]/[Br^-]$ (in mol/l) was less than 1000. With increasing $[Cl^-]/[Br^-]$ BrCl was the main product. They also found a pH dependency of the outgassing of Br_2 and BrCl with greater release rates for lower pH.

The results of *Disselkamp et al.* (1999), who examined the chemistry in NaBr/ $NaCl/HNO_3/O_3$ solutions support the HOBr mediated Cl^- oxidation process pro-

posed by *Vogt et al.* (1996) because they are consistent with the reaction sequence $O_3 + H^+ + Br^- \longrightarrow O_2 + HOBr$ and $HOBr + Cl^- + H^+ \longrightarrow BrCl + H_2O$.

The experiments of *Behnke et al.* (1999) in a smog chamber verified the above listed chain reaction (2.3) to (2.12). They also studied the reduction of Br_2 by oxalic acid.

Reactions of NO_y compounds with sea salt were studied e.g. by *Behnke et al.* (1993, 1994), who showed the production of $BrNO_2$, Br_2 and $ClNO_2$ from the reaction of N_2O_5 with sea salt aerosol. *Seisel et al.* (1997) studied the reaction of NO_3 with solid halogen salts.

Further studies regarding sea salt aerosols that were undertaken in the framework of European projects have been summarized by *Crowley et al.* (1998) and *Zetzsch et al.* (1998).

All these studies that were made with very different techniques show basically the same behaviour of the reaction system. For an overview of the various experimental techniques see *Finlayson-Pitts and Jr* (1999).

Numerous studies dealt with reactions involving chlorine. A major reaction for the main halogen compound of sea salt, Cl^-, is the release of HCl from sea salt aerosol by acid displacement (e.g. *Brasseur et al.* (1999), p. 314):

$$HNO_{3,g} + NaCl_{aq} \longrightarrow HCl_g + NaNO_{3,aq} \quad (2.14)$$

$$H_2SO_{4,g} + 2NaCl_{aq} \longrightarrow HCl_g + Na_2SO_{4,aq} \quad (2.15)$$

Other acids that displace Cl^- from the sea salt aerosol are methanosulfonic acid (MSA) and oxalic acid (*Kerminen et al.* (1998)).

The search for possible mechanisms for the release of reactive chlorine from sea salt aerosol was the motivation of many laboratory studies (e. g. *Zetzsch et al.* (1988), *Finlayson-Pitts et al.* (1989), *Zetzsch and Behnke* (1992) for reactions of NO_y with NaCl).

Fickert et al. (1998) studied the uptake of $ClNO_2$ on aqueous bromide solutions and found Br_2 and $BrNO_2$ to be the major products and BrCl a minor product. Br_2 is produced by secondary reactions in the aqueous phase.

Mochida et al. (1998b) studied reactions of Cl_2 on synthetic and natural sea salt aerosol in a Knudsen cell reactor finding that uptake of Cl_2 leads to the production of Br_2.

Very recently the phenomen of surface segregation of halide ions in sea salt aerosol has been shown theoretically by *Knipping et al.* (2000) (for Cl^-) and experimentally by *Ghosal et al.* (2000) (for Br^-).

A link between sulfur and halogen chemistry was suggested by *Toumi* (1994), who proposed that the reaction of DMS with BrO could be important for the production of DMSO by the reaction :

$$\begin{array}{rcl} BrO + DMS & \longrightarrow & Br + DMSO \\ Br + O_3 & \longrightarrow & BrO + O_2 \\ \hline \text{net: } DMS + O_3 & \longrightarrow & DMSO + O_2. \end{array}$$

As shown in the net reaction, this is no sink for BrO which is reformed in the reaction with O_3, but rather a sink for O_3. *Ingham et al.* (1999) presented updated kinetic data and a model study of the importance of this reactions.

Another link between sulfur and halogen chemistry was proposed by *Vogt et al.* (1996). They studied the potential importance of HOCl and HOBr in the production of sulfate in sea salt aerosol.

Numerical studies of halogen chemistry in the MBL, that incorporated data from kinetic studies in box models, could show the activation of reactive bromine in the MBL (*Sander and Crutzen* (1996), *Vogt et al.* (1996), *Sander et al.* (1999), *Dickerson et al.* (1999)) and the dependence of bromine activation mechanism on pH (*Keene et al.* (1998)). Using a general circulation model based approach, *Erickson et al.* (1999) showed the release of HCl and $ClNO_2$ from sea salt aerosol under different ambient conditions.

2.2 Field measurements

Field measurements of sea salt aerosol composition in the MBL have been made for a long time. They often show a decrease of the Br^-/Na^+ ratio of aged sea salt aerosol compared to sea water (e.g. *Duce et al.* (1965), *Moyers and Duce* (1972), *Kritz and Rancher* (1980), *Duce et al.* (1983), *Ayers et al.* (1999)). This can only be explained by a release of bromine from the sea salt aerosol.

The total gas phase bromine concentrations in the measurements of *Moyers and Duce* (1972) were 4 to 10 times higher than the particulate concentrations. In contrast to this, most samples of *Kritz and Rancher* (1980) showed comparable gas and aqueous phase concentrations of bromine. *Moyers and Duce* (1972) noted also that the lifetime of gaseous bromine would be approximately 7 times that of particulate bromine. *Ayers et al.* (1999) presented measurements from Cape Grim, Tasmania that showed bromine deficits of 30 % to 50 % on an annual average and maximum monthly mean values of more than 80 % and that Br^- and Cl^- deficits were linked to the availability of strong sulfur acidity in the aerosol, pointing to the importance of acid catalysis in the dehalogenation process as shown by *Fickert et al.* (1999) in the laboratory.

Pszenny et al. (1993) presented evidence for the existence of inorganic chlorine gases other than HCl in the MBL. *Spicer et al.* (1998) found very high mixing ratios of Cl_2 (up to 150 pmol/mol) at a coastal site in Long Island, New York. *Graedel and Keene* (1995) discuss in great detail measurements and possible reaction mechanisms of different reactive chlorine compounds in the gas and aqueous phase. Indirect determination of Cl radicals in the MBL ranged from upper limits of 10^3 atoms/cm^3 (*Jobson et al.* (1998)) to 720 atoms/cm^3 (*Wingenter et al.* (1999)) and up to 10^5 atoms/cm^3 (*Singh et al.* (1996a), *Wingenter et al.* (1996)). *Rudolph et al.* (1996, 1997) estimated tropospheric average Cl concentrations on the order of 10^3 atoms/cm^3 and stated as well as *Singh et al.* (1996b) that on a global scale mean Cl concentrations would be too small to compete with OH in influencing the oxidizing capacity of the troposphere.

Reactive gas phase halogen species are difficult to detect because of their relatively low mixing ratios. Most available measurements of single bromine species are for BrO using the differential optical absorption spectroscopy (DOAS) technique. Rather large BrO mixing ratios of 20 - 30 pmol/mol were found in the Arctic boundary layer during polar sunrise (*Hausmann and Platt* (1994), *Tuckermann et al.* (1997)) which were always associated with a dramatic loss of ozone (see also *Platt and Moortgat* (1999) and references therein). *McElroy et al.* (1999) provided evidence for the presence of BrO in the free troposphere during Arctic polar sunrise. Measurements with the GOME instrument aboard the ERS-2 satellite show large tropospheric column integrated values of BrO in some areas. This is restricted to high northern latitudes, namely to areas around the Hudson Bay, parts of the Canadian Arctic, along the coast lines of the Arctic Sea and over the polar ice. It can be observed from February until the end of May and is probably related to the "polar sunrise" O_3 destruction in the boundary layer that was discussed above (*Richter et al.* (1998), *Wagner and Platt* (1998) and *Chance* (1998)). Bromine related ozone loss, however, is not only dependent on the availability of ice surfaces as was proposed for the Arctic. In a very different environment, namely the Dead Sea, BrO mixing ratios of up to 90 pmol/mol (*Hebestreit et al.* (1999)) were found, which are due to the special location of the measurement site downwind of large salt pans. These extreme events were also correlated with low boundary layer O_3 mixing ratios.

In the MBL several groups tried to measure BrO with the DOAS technique at Mace Head/Ireland, Hawaii, Tenerife and Cape Grim/Tasmania. During these campaigns the detection limit for BrO was between 1 - 10 ppt and when BrO was measured, it was at the detection limit (personal communication with: D. Perner, B. Allan, K. Hebestreit). Therefore these measurements only provide upper limits for BrO that are consistent with model results.

Iodine compounds may also be important for the chemistry of the MBL. Measurements show that iodine is strongly enriched in sea salt aerosol compared to sea water (see overview in *Vogt* (1999)), indicating that the main source for iodine is not the sea salt aerosol, which is rather a sink. Organisms living in the upper ocean emit iodocarbons like CH_3I, CH_2ClI or CH_2I_2 (*Vogt* (1999)) which are probably used by these organisms for pest control. In the gas phase these iodocarbons are photolyzed to produce chemically active species like I and IO. IO has been measured in the pmol/mol range at coastal areas (*Alicke et al.* (1999)) and recently also at background ocean stations (*Allan et al.* (2000)). In some coastal regions also OIO could be detected (*Hebestreit et al.* (2000), *Plane et al.* (2000)).

In the discussions of the model results the different points raised here briefly will be discussed, e.g. the activation of halogens, O_3 destruction, the coupling between halogen and sulfur chemistry, and the importance of iodine chemistry.

Chapter 3

Description of the MBL model

3.1 Meteorology, microphysics and thermodynamics

For this modeling study a one-dimensional model is used. The meteorological and microphysical part is the boundary layer model MISTRA described in detail by *Bott et al.* (1996) and *Bott* (1997). Apart from dynamics and thermodynamics it includes a detailed microphysical module that calculates particle growth explicitly and treats feedbacks between radiation and particles. Figure 3.1 shows schematically the most important processes that are included in the model for a cloudy MBL. Gas phase chemistry is active in all model layers, aerosol chemistry only in layers where the relative humidity (of which a typical vertical profile is shown) is greater than the deliquescence / crystallization humidity (see discussion on page 21). When a cloud forms, cloud droplet chemistry is also active. Fluxes of sea salt aerosol and gases from the ocean are included and the main meteorological processes (turbulence, radiation) are also shown.

The set of prognostic variables comprises the horizontal components of the wind speed u, v, the specific humidity q, and the potential temperature Θ:

$$\frac{\partial u}{\partial t} = -w\frac{\partial u}{\partial z} + \frac{\partial}{\partial z}\left(K_m\frac{\partial u}{\partial z}\right) + f(v - v_g) \tag{3.1}$$

$$\frac{\partial v}{\partial t} = -w\frac{\partial v}{\partial z} + \frac{\partial}{\partial z}\left(K_m\frac{\partial v}{\partial z}\right) - f(u - u_g) \tag{3.2}$$

$$\frac{\partial q}{\partial t} = -w\frac{\partial q}{\partial z} + \frac{\partial}{\partial z}\left(K_h\frac{\partial q}{\partial z}\right) + \frac{C}{\rho} \tag{3.3}$$

$$\frac{\partial \Theta}{\partial t} = -w\frac{\partial \Theta}{\partial z} + \frac{\partial}{\partial z}\left(K_h\frac{\partial \Theta}{\partial z}\right) - \left(\frac{p_0}{p}\right)^{R/c_p}\frac{1}{c_p\rho}\left(\frac{\partial E_n}{\partial z} + LC\right) \tag{3.4}$$

where f is the Coriolis parameter, u_g and v_g are the geostrophic wind components, K_m and K_h are the turbulent exchange coefficients for momentum and heat, L is the latent heat of condensation, C the condensation rate, ρ the air density, p

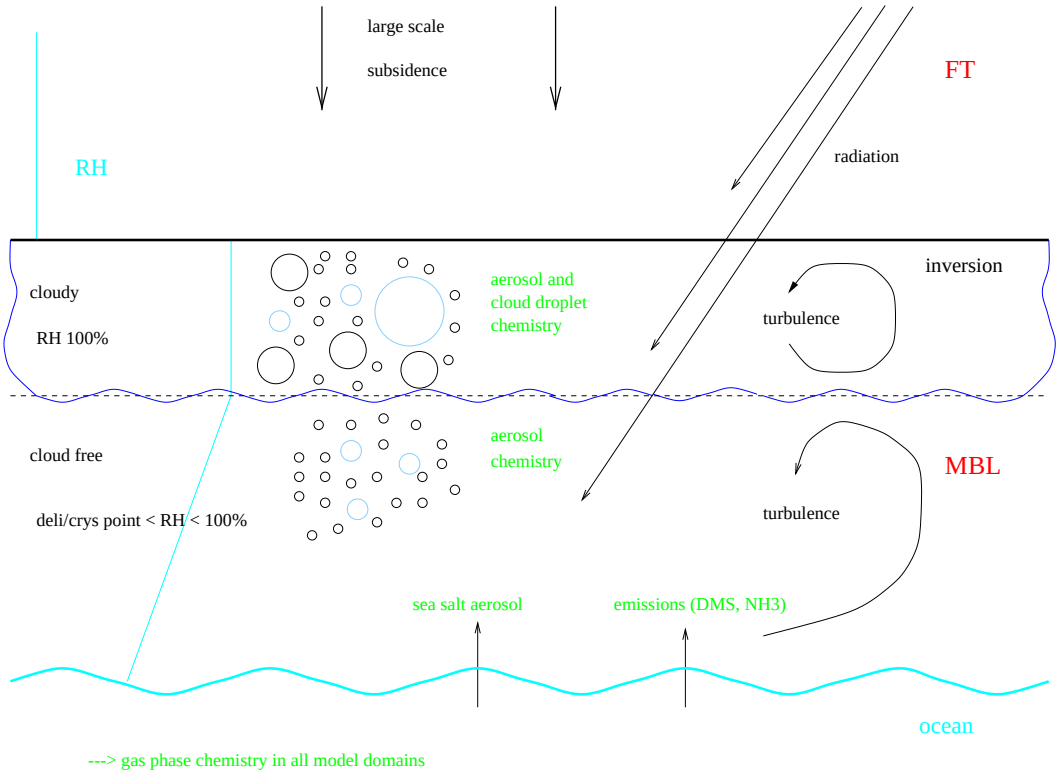

Figure 3.1: Schematic depiction of the most important processes included in the one-dimensional boundary layer model MISTRA. The free troposphere is denoted as FT, relative humidity as RH.

the air pressure, p_0 the air pressure at the surface, R the gas constant for dry air, c_p the specific heat of dry air at constant pressure, and E_n the net radiative flux density, respectively. The first term on the right of each equation is the large scale subsidence. Strictly in a one-dimensional framework the vertical velocity $w = 0$ everywhere. To correctly model the evolution of stratiform clouds this term is essential as pointed out by several authors (e.g. *Driedonks and Duynkerke* (1989)). Mass balance, however, is violated if subsidence is included. In runs where only aerosol chemistry is studied, i.e. in runs without clouds, the vertical velocity is set to zero ($w = 0$) to avoid this problem, for the cloud runs subsidence is included.

Turbulence is treated with the level 2.5 model of *Mellor and Yamada* (1982) with the modifications described in *Bott et al.* (1996). The turbulent exchange coefficients K_m and K_h are calculated via stability functions $S_{m/h}$ and $G_{m/h}$. The prognostic equation for the turbulence kinetic energy e is:

$$\frac{\partial e}{\partial t} = -w\frac{\partial e}{\partial z} + \frac{\partial}{\partial z}\left(K_e\frac{\partial e}{\partial z}\right) + \frac{(2e)^{3/2}}{l}\left(S_m G_m + S_h G_h - \frac{1}{16.6}\right) \tag{3.5}$$

assuming a constant dissipation ratio (last term on the right). For more details and an explanation of the calculation of the mixing length l, the exchange coef-

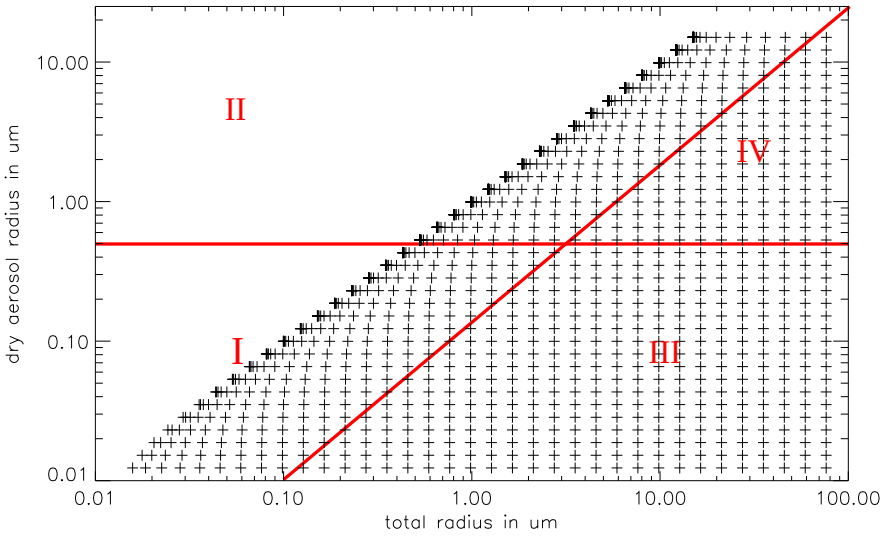

Figure 3.2: The two-dimensional particle spectrum as function of the dry aerosol radius a and the total particle radius r. Added are the chemical bins. I: sulfate aerosol bin, II: sea salt aerosol bin, III: sulfate cloud droplet bin, IV: sea salt droplet bin. For simplicity a 35 x 35 bin grid is plotted, in the model 70 x 70 bins are used.

ficient K_e for the turbulent kinetic energy, and the functions $S_{m/h}$ and $G_{m/h}$ see *Mellor and Yamada* (1982) and *Bott et al.* (1996).

The microphysics is treated using a joint two-dimensional particle size distribution function $f(a,r)$ with the total particle radius r and the dry aerosol radius a the particles would have, when no water were present in the particles. The two-dimensional particle grid (see Figure 3.2) is divided into 70 logarithmically equidistant spaced dry aerosol classes, with the minimum aerosol radius being 0.01 μm and the maximum radius 15 μm. Chosing these values allows to account for all accumulation mode particles and most of the coarse particles.

Each of the 70 dry aerosol classes is associated with 70 total particle radius classes, ranging from the actual dry aerosol radius up to 60 μm (150 μm in cloud runs). The prognostic equation for $f(a,r)$ is:

$$\frac{\partial f(a,r)}{\partial t} = -w\frac{\partial f(a,r)}{\partial z} + \frac{\partial}{\partial z}\left(K_h\rho\frac{\partial f(a,r)/\rho}{\partial z}\right) - \frac{\partial}{\partial z}\left(w_t f(a,r)\right) - \frac{\partial}{\partial r}\left(\dot{r} f(a,r)\right). \quad (3.6)$$

Again, subsidence is the first term on the right, followed by turbulent mixing, particle sedimentation (w_t is the sedimentation velocity) and changes in f due to particle growth ($\dot{r} = dr/dt$). Upon model initialization the particles are initialized with a water coating according to the equilibrium radius of the dry nucleus at the ambient relative humidity. During the integration, particle growth is calculated

explicitly for each bin of the 2D particle spectrum using the growth equation after *Davies* (1985) (see also *Bott et al.* (1996)):

$$r\frac{d\,r}{d\,t} = \frac{1}{C_1}\left[C_2\left(\frac{S_\infty}{S_r} - 1\right) - \frac{F_d(a,r) - m_w(a,r)c_w dT/dt}{4\pi r}\right] \tag{3.7}$$

with the ambient supersaturation S_∞ and the supersaturation at the droplet's surface S_r according to the Köhler equation:

$$S_r \;=\; exp\left[\frac{A}{r} - \frac{Ba^3}{r^3 - a^3}\right]. \tag{3.8}$$

The change in particle radius is not determined by changes in water vapor saturation alone, but also by the net radiative flux at the particle's surface $F_d(a,r)$. The constants C_1 and C_2 in eq. (3.7) are:

$$C_1 = \rho_w L + \frac{\rho_w C_2}{D'_v S_r \rho_s} \qquad\qquad C_2 = k'T\left[\frac{L}{R_v T} - 1\right]^{-1}, \tag{3.9}$$

$m_w(a,r)$ is the liquid water mass of the particle, c_w and ρ_w are the specific heat and density of water, ρ_s is the saturation vapor density and R_v the specific gas constant for water vapor. The thermal conductivity k' of moist air and the diffusivity of water vapor D'_v have been corrected for gas kinetic effects following *Pruppacher and Klett* (1997). The condensation rate C in eq. (3.4) is determined diagnostically from the partical growth equation.

Collision-coalescence processes are not included in the model because this leads to great difficulties for describing the redistribution of the chemical species in the particles. However a version of MISTRA including collision-coalescence without considering chemistry does exist (*Bott* (2000)).

For the calculation of the radiative fluxes a δ-two stream approach is used (*Zdunkowski et al.* (1982), *Loughlin et al.* (1997)). The radiative fluxes are used for calculating heating rates and the effect of radiation on particle growth. The radiation field is calculated with the aerosol/cloud particle data from the microphysical part of the model, so feedbacks between radiation and particle growth are fully implemented.

3.2 Chemistry

The multiphase chemistry module comprises chemical reactions in the gas phase as well as in aerosol and cloud particles. Transfer between gas and aqueous phase and surface reactions on particles are also included. Tables D.1 to D.5 show a complete listing of the reactions. The reaction set is an updated version of *Sander and Crutzen* (1996) (see also http://www.mpch-mainz.mpg.de/˜sander/mocca) plus some organic reactions from *Lurmann et al.* (1986). In the following the term

aqueous phase is used as generic term for sub-cloud aerosol, interstitial aerosol, and cloud particles.

The prognostic equation for the concentration of a gas phase chemical species c_g (in mol/m^3_{air}) including subsidence, turbulent exchange, deposition on the ocean surface, chemical production and destruction, emission and exchange with the aqueous phases is:

$$\begin{aligned}\frac{\partial c_g}{\partial t} &= -w\frac{\partial c_g}{\partial z} + \frac{\partial}{\partial z}\left(K_h\rho\frac{\partial c_g/\rho}{\partial z}\right) - \frac{\partial}{\partial t}(v_g^{dry}c_g) \\ &\quad +P - Dc_g + E - \sum_{i=1}^{n_{kc}}\left[\overline{k_{t,i}}\left(w_{l,i}c_g - \frac{c_{a,i}}{k_H^{cc}}\right)\right].\end{aligned} \tag{3.10}$$

Again subsidence is included only in runs with clouds. P and D are chemical production and destruction terms, respectively, k_H^{cc} is the dimensionless Henry constant obtained by $k_H^{cc} = k_H RT$, where k_H is in mol/(m^3Pa), $w_{l,i}$ is the dimensionless liquid water content (m^3_{aq}/m^3_{air}) of bin i (see explanation on p. 21). The emission flux E as well as dry deposition (third term in eq. (3.10)) are effective only in the lowermost model layer. The calculation of the dry deposition velocity v_g^{dry} is explained at the end of this section. The last term in eq. (3.10) describes the transport from the gas phase into the aqueous phases according to the formulation by *Schwartz* (1986) (see also *Sander* (1999)), n_{kc} is the number of the aqueous classes as explained below. For a single particle, the mass transfer coefficient k_t is defined as

$$k_t = \left(\frac{r^2}{3D_g} + \frac{4r}{3\bar{v}\alpha}\right)^{-1} \tag{3.11}$$

with the particle radius r, the mean molecular speed $\bar{v} = \sqrt{8RT/(M\pi)}$ (M is the molar mass), the accommodation coefficient α (see Table D.5), and the gas phase diffusion coefficient D_g. D_g is approximated as $D_g = \lambda\bar{v}/3$ (*Gombosi* (1994), p. 125) using the mean free path length λ.

Chameides (1984) points out that the time needed to establish equilibrium between the gas and aqueous phase differs greatly for individual species and that soluble species never reach equilibrium in cloud droplets, emphasizing the importance of describing phase transfer in the kinetic form that is used here.

Ambient particle populations are never monodisperse, i.e. one has to account for particle with different radii. The mean transfer coefficient $\overline{k_t}$ for a particle population is given by the integral:

$$\overline{k_t} = \frac{4\pi}{3w_l}\int_{logr_{min}}^{logr_{max}}\left(\frac{r^2}{3D_g} + \frac{4r}{3\bar{v}\alpha}\right)^{-1} r^3\frac{\partial N}{\partial logr}dlogr. \tag{3.12}$$

Aqueous chemistry is calculated in four bins (see Figure 3.2): deliquescent aerosol particles with a dry radius less than 0.5 μm are included in the "sulfate

aerosol" bin, whereas deliquescent particles with a dry aerosol radius greater than 0.5 μm are in the "sea salt aerosol" bin. Although the composition of the particles changes over time the terms "sulfate" and "sea salt" aerosol are used to describe the origin of the particles. The particles get internally mixed by exchange with the gas phase but, as mentioned earlier, not by particle collisions. For the description of the initial composition of the aerosol bins see section 4.1.

When the total particle radius exceeds the dry particle radius by a factor of 10, i.e. when the total particle volume is 1000 times greater than the dry aerosol volume, the particle and its associated chemical species are moved to the corresponding sea salt or sulfate derived cloud particle class. This threshold roughly coincides with the critical radius derived from the Köhler equation. When particles shrink they are redistributed from the droplet to the aerosol bins.

Therefore in a cloud-free layer there are 2 ($n_{kc} = 2$) aqueous chemistry classes (sulfate and sea salt aerosol) and in a cloudy layer 2 cloud droplet (sulfate and sea salt derived) and 2 interstitial aerosol (sulfate and sea salt) classes, giving a total of 4 ($n_{kc} = 4$) aqueous chemistry classes. In each of these classes the following prognostic equation is solved for each chemical species $c_{a,i}$ (in mol/m$^3_{\text{air}}$), where the index i stands for the i-th aqueous class:

$$\begin{aligned}\frac{\partial c_{a,i}}{\partial t} &= -w\frac{\partial c_{a,i}}{\partial z} + \frac{\partial}{\partial z}\left(K_h\rho\frac{\partial c_{a,i}/\rho}{\partial z}\right) - \frac{\partial}{\partial t}(v_{a,i}^{dry}c_{a,i}) \\ &\quad +P - Dc_{a,i} + E + P_{pc} + \overline{k_{t,i}}\left(w_{l,i}c_g - \frac{c_{a,i}}{k_H^{cc}}\right)\end{aligned} \tag{3.13}$$

The individual terms have similar meanings as in eq. (3.10). The calculation of the sedimentation velocity $v_{a,i}^{dry}$ is explained at the end of this section. The additional term P_{pc} accounts for the transport of chemical species from the aerosol to the cloud droplet regimes and vice versa. If only phase transfer is considered, this equation reduces in steady state conditions ($\partial c_{a,i}/\partial t = 0$) to the Henry equilibrium $c_{a,i} = w_{l,i}c_g k_H^{cc}$.

The concentration of H^+ ions is calculated like any other species, i.e. no further assumptions are made. The charge balance (sometimes used to derive the pH) is satisfied implicitly.

Cloud-processing, i.e. the change of aerosol mass due to uptake of gases, is included in the model based on *Bott* (1999).

It is assumed that water is associated with sea salt aerosol particles above their crystallization point rather than their deliquescence point because they are produced as droplets at the sea surface. Therefore the hysteresis effect ensures that, upon drying, the particles remain in a metastable highly concentrated solution state above their crystallization point, which is about 45 % relative humidity for NaCl (*Shaw and Rood* (1990), *Tang* (1997), *Pruppacher and Klett* (1997), and *Lee and Hsu* (2000)). As long as the relative humidity in the MBL is well above the crystallization point, sea salt aerosol is not present in crystalline form.

The crystallization humidity for many mixed aerosol particles containing sulfate or nitrate is below 40 % relative humidity (*Seinfeld and Pandis* (1998) and

references therein), implying that aerosol particles that already had been involved in cloud cycles will also be in an aqueous metastable state. Therefore many soluble aerosol particles will be present in the atmosphere as metastable aqueous particles below their deliquescence humidity. A relative humidity of 60 % is used as threshold for sulfate particles to be in aqueous form. With the above discussion in mind, this might lead to an underestimation of aqueous sulfate particles, but, at least in the model runs presented here, the ambient relative humidity is always above 60 %, so all aerosol particles are assumed to be present in aqueous form. The only exception from this is the "high BL" run as discussed in section 4.4.

Aerosols are usually highly concentrated solutions. Laboratory measurements show that NaCl molalities can be in excess of 10 mol/kg (*Tang* (1997)) implying also very high ionic strengths. Therefore it is necessary to account for deviations from ideal behaviour, i.e. to include activity coefficients. The Pitzer formalism (*Pitzer* (1991)) is used to calculate the activity coefficients for the actual composition of each aqueous size bin.

In the atmosphere each aerosol or cloud particle is a closed "reaction chamber" with its own pH and concentrations of the species. In models the particles have to be lumped in bins where the individual properties of the particles vanish. In the model freshly emitted, alkaline sea salt particles are put into the same chemistry bin as aged acidic particles leading to mean conditions and reaction paths that can be distinctly different from what is happening in the atmosphere. Especially in the case of high wind, when sea salt aerosol production and therefore also sea salt aerosol loadings are high, the pH might be overestimated and reactions involving acidity might be underestimated because the buffer capacity of the few large particles would dominate the smaller, more acidic particles. In future versions of this model a finer resolution for the aqueous chemistry bins will be achieved.

Photolysis is calculated online using the method of *Landgraf and Crutzen* (1998). The photolysis rate (or photo dissociation coefficient) J_{X} for a gas X can be calculated from the spectral actinic flux $F(\lambda)$ via the integral:

$$J_{\mathrm{X}} = \int_I \sigma_{\mathrm{X}}(\lambda)\phi_{\mathrm{X}}(\lambda)F(\lambda)d\lambda \tag{3.14}$$

where λ is the wavelength, σ_{X} the absorption cross section, ϕ_{X} the quantum yield and I the photochemically active spectral interval. If the integral in eq. (3.14) would be approximated with a sum, the number of wavelength bins needed for an accurate approximation of the integral would be in the order of 100 which would lead to excessive computing times. *Landgraf and Crutzen* (1998) suggested a method using only 8 spectral bins (see Table 3.1) approximating (3.14) by:

$$J_{\mathrm{X}} \approx \sum_{i=1}^{8} J^a_{i,\mathrm{X}} \cdot \delta_i \tag{3.15}$$

Table 3.1: Subdivision of the spectral range of the photolysis module.

interval	1	2	3	4	5	6	7	8
λ_a [nm]	178.6	202.0	241.0	289.9	305.5	313.5	337.5	422.5
λ_b [nm]	202.0	241.0	289.9	305.5	313.5	337.5	422.5	752.5
λ_i [nm]	see LC98	205.1	287.9	302.0	309.0	320.0	370.0	580.0

The spectral range 178.6 nm $\leq \lambda \leq$ 752.5 nm is subdivided into eight intervals, λ_a and λ_b are the initial and the final, and λ_i the fixed wavelength in interval I_i (after *Landgraf and Crutzen* (1998)). The intervals 1 and 2 are important only for the stratosphere, as only light with wavelengths greater than about 290 nm reaches the troposphere.

where $J^a_{i,\mathrm{X}}$ is the photolysis rate for a purely absorbing atmosphere. The factor δ_i:

$$\delta_i := \frac{F(\lambda_i)}{F^a(\lambda_i)} \tag{3.16}$$

describes the effect of scattering by air molecules, aerosol and cloud particles, which is significant in the spectral range 202.0 nm $\leq \lambda \leq$ 752.5 nm. $F^a(\lambda_i)$ is the actinic flux of a purely absorbing atmosphere. For the Schumann-Runge band (spectral range 178.9 nm $\leq \lambda \leq$ 202.0 nm), scattering effects can be neglected because of the strong absorption by O_2 ($\delta_1 = 1$). The factor δ_i is calculated online for one wavelength for each interval (see λ_i in Table 3.1).

The $J^a_{i,\mathrm{X}}$ are precalculated with a fine spectral resolution and are approximated during runtime from lookup tables or by using polynomials. The advantage of this procedure is that the fine absorption structures that are present in σ_X and ϕ_X are considered and only Rayleigh and cloud scattering, included in $F(\lambda_i)$, are treated with a coarse spectral resolution which is justified.

For the calculation of the actinic fluxes a four stream radiation code is used in addition to the two stream radiation code used for the determination of the net radiative flux density E_n because different spectral resolutions and accuracies are needed for these different purposes. Based on the findings of *Ruggaber et al.* (1997) a factor 2 is applied to photolysis rates inside aqueous particles to account for the actinic flux enhancement inside the particles due to multiple scattering.

All chemical reactions in gas and aqueous phases, equilibria and phase transfer reactions are calculated as one coupled system using the kinetic preprocessor KPP (*Damian-Iordache* (1996)) which allows rapid change of the chemical mechanism without major changes in the source code.

Constant emission fluxes for the gases DMS and NH_3 from the sea surface are applied with 2×10^9 molec/(cm^{2}s) (*Quinn et al.* (1990)) and 4×10^8 molec/(cm^{2}s) (*Quinn et al.* (1990), scaled to model their measured gas phase mixing ratios of 19 noml/mol in clean air masses), respectively.

Sea salt particles are emitted by bursting bubbles at the sea surface (e.g. *Woodcock et al.* (1953), *Pruppacher and Klett* (1997)). The parameterization of *Monahan et al.* (1986) is used that estimates the flux F of particles with radius

r at a relative humidity of 80 % per unit area of sea surface, per increment of droplet radius and time (in particles m^{-2} s^{-1} μm^{-1}):

$$\frac{dF}{dr} = 1.373 u_{10}^{3.41} r^{-3} (1 + 0.057 r^{1.05}) \times 10^{1.19 exp(-B^2)} \tag{3.17}$$

where $B = (0.380 - \log r)/0.65$ and u_{10} is the windspeed at 10 m height. *Monahan et al.* (1986) also parameterize the emission for particles with radii larger than r=10 μm by additional terms, but only the bubble burst mechanism and not the spume production terms are included because as pointed out by e.g. *Wu* (1993), *Gong et al.* (1997) and *Andreas* (1998) these additional terms lead to an overestimation of the particle flux compared to measurements.

Large sea spray droplets (r=10 – 300 μm) can contribute to the transport of heat and moisture between ocean and atmosphere. According to *Andreas et al.* (1995) this is important for high windspeeds above about 15 m/s. As the model studies are mainly for moderate wind speeds where only very small amounts of particles of that size are produced this process is neglected.

For each dry aerosol radius bin of the 2D microphysical spectrum the equilibrium radius for the actual relative humidity is calculated and the appropriate number of particles according to eq. (3.17) is added in the lowermost model layer. The *Monahan et al.* (1986) estimate of the sea salt aerosol flux based on wind tunnel experiments is believed to yield good results for small particles (*Andreas* (1998)). For higher wind speeds the resulting mass flux of sea salt particles is less realistic, so for the model runs with high wind speed the parameterization of *Smith et al.* (1993) that is based on measurements off the Scottish coast is used.

The dry deposition velocity for gases v_g^{dry} at the sea surface is calculated using the resistance model described by *Wesely* (1989):

$$v_g^{dry} = \frac{1}{r_a + r_b + r_c}. \tag{3.18}$$

The aerodynamic resistance r_a is calculated using:

$$r_a = \frac{1}{\kappa u_*} \left[\ln\left(\frac{z}{z_0}\right) + \Phi_s(z, L) \right], \tag{3.19}$$

with the friction velocity u_*, the von Kármán constant $\kappa = 0.4$, and the stability function Φ_s which depends on the Monin-Obukhov length L, the roughness length z_0 and a reference height z. The quasi-laminar layer resistance r_b is parameterized as:

$$r_b = \frac{1}{u_* (Sc^{-2/3} + 10^{-3/St})}. \tag{3.20}$$

The Stokes number St can be written as $St = w_t u_*^2/(g\nu)$ and the Schmidt number as $Sc = \nu/D$ with the dynamic viscosity of air ν and the aerosol diffusivity D.

The surface resistance r_c is calculated using the formula by *Seinfeld and Pandis* (1998) (their equation (19.30)):

$$r_c = \frac{2.54 * 10^4}{H^* T u_*}, \tag{3.21}$$

with the effective Henry constant H^*.
The dry deposition velocity of particles $v_{a,i}^{dry}$ is calculated after *Seinfeld and Pandis* (1998):

$$v_{a,i}^{dry} = \begin{cases} \frac{1}{r_a + r_b + r_a r_b w_t} + w_t & \text{lowest model layer} \\ w_t & \text{rest of model domain} \end{cases}. \tag{3.22}$$

The particle sedimentation velocity w_t is calculated in the microphysical module assuming Stokes flow and taking into account the Cunningham slip flow correction for particles with $r < 10\mu$m and after Beard for larger particles (see *Pruppacher and Klett* (1997)).

3.3 Model resolution and integration scheme

The atmosphere between the sea surface and 2000 m is divided into 150 layers. The lowest 100 layers have a constant grid height of 10 m, the layers above 1000 m are spaced logarithmically. For the "high boundary layer" run the grid height in the lowest 100 layers was increased to 20 m and the model domain was extended to 3500 m.

The dynamical timestep is 10 s and the chemical timestep is chosen to differ between 1 ms for layers with low LWC associated to the particles or layers including freshly formed particles and 60 s for gas phase only layers.

The very stiff chemical differential equation system is solved with a second order Rosenbrock method (ROS2 by *Verwer et al.* (1997)).

Chapter 4

Chemistry of the cloud-free MBL

4.1 Overview of the runs

With the base run for the study of aerosol chemistry (i.e. without clouds) it was not intended to mimic a situation that has been observed in a field campaign, it is rather intended to demonstrate the evolution of the gas and aerosol chemistry under idealized conditions. The latitude chosen for this run is $\varphi = 30°$ at the end of July. The boundary layer height is roughly 700 m, moisture and heat fluxes from the sea surface are adjusted to yield a stable boundary layer. The relative humidity at the sea surface is roughly 65 %, increasing to around 90 % below the inversion that caps the MBL. As a result of the prescribed heat fluxes from the sea surface, the potential temperature in the well mixed MBL is slowly decreasing from $\Theta = 14.5°$C to 13.5 °C. The relative humidity in the different layers stays constant apart from a minor diurnal variation ($\pm 3\%$). After a spin-up of the dynamical part of the model for 2 days the complete model was integrated for 3 days.

Many different sensitivity studies were performed and some of them and the differences between them are described here. See Table 4.3 for an overview of the runs.

First the halogen chemistry was turned off in the run "halogen off" and in another run both, halogen and aerosol chemistry ("aerosol off") were switched off. In the run "low O_3 low SO_2" low initial values for these gases were chosen in the initialization of the run to see the effects of very clean air. The contrary was simulated at with the "continental influence" run where high initial values of NO_x, SO_2, O_3 and other pollutants were chosen. To see the influence of the season a "winter" and a "spring" run were performed. The implications of different heights of the MBL were the object of the "high BL" run. In the run "strong wind" the wind speed and the parameterization of the sea salt aerosol production were changed to study the effects of the production of more and larger particles at higher wind speeds. Higher mean wind speeds over the ocean could be a consequence of global change with impacts on chemistry and microphysics in the MBL as already mentioned by *Pszenny et al.* (1998). The strength of the DMS flux was varied in the "high DMS" run and iodine chemistry was included in the

Table 4.1: Initial mixing ratios of gas phase species (in nmol/mol).

species	remote (MBL)	remote (FT)	cont. influen. (MBL)	cont. influen. (FT)
CO	70.0		150.0	
NO_2	0.02	0.03	0.5	
HNO_3	0.01	0.05	0.1	
NH_3	0.08		0.2	
SO_2	0.09		1.0	
O_3	20.0	50.0	50.0	70.0
CH_4	1800.0		1800.0	
C_2H_6	0.5		5.0	
HCHO	0.3		0.3	
H_2O_2	0.6		0.8	
PAN	0.01	0.1	0.1	1.0
HCL	0.04		0.04	
DMS	0.06		0.06	
CH_3I	0.002			
C_3H_7I	0.001			

Values are for the 2 scenarios "remote" and "continentally influenced". A value for the free troposphere (FT) is given only when it is different from the MBL value. CH_3I and C_3H_7I are accounted for only in the "iodine" run.

Table 4.2: Initial size distribution of the aerosol.

mode	$N_{tot,i}$ $(1/cm^3)$	$R_{N,i}$ (μm)	σ_i
1	100	0.027	1.778
2	120	0.105	1.294
3	6	0.12	2.818

The data is after *Hoppel and Frick* (1990). The particle size distribution is calculated according to $\frac{dN(r)}{dlgr} = \sum_{i=1}^{3} \frac{N_{tot,i}}{lg\sigma_i\sqrt{2\pi}} \times \exp\left(-\frac{(lgr-lgR_{N,i})^2}{2(lg\sigma_i)^2}\right)$.

"iodine" run.

Tables 4.1 and 4.2 list the initial gas phase mixing ratios and parameters for the initial lognormal aerosol size distribution. Aerosol particles with dry radii less than r=0.5 μm are assumed to be a mixture of 32 % $(NH_4)_2SO_4$, 64 % NH_4HSO_4 and 4 % NH_4NO_3 (*Kim et al.* (1995)).

The resulting pH of the sulfate aerosols is between 0.5 and 1 (and even lower for the "continentally influenced" run) which is in the range estimated by *Fridlind and Jacobson* (2000) for sulfate aerosol sampled during the ACE-1 campaign. A run where the initial composition of the sulfate aerosol was assumed to be pure $(NH_4)_2SO_4$ showed a pH between 2.5 at model start and 1 after 3 days due to the uptake of acids the gas phase. Consequences for the gas phase were very small, NH_3 increased because of reduced uptake by the sulfate aerosol whereas HCl decreased due to uptake by the sulfate aerosol.

Table 4.3: Overview of the sensitivity runs for the cloud-free MBL.

name	gas phase initialization (see Table 4.1)	MBL height	SST	Differences from base run	Main results
base run	remote	700m	15 °C	-	BrO vertical profile/diurnal variation, vertical profile of sea salt pH, recycling of HBr and HOBr by sulfate, "overall" effects of halogen chemistry
halogen off	remote	700m	15 °C	halogen chemistry switched off	overall importance of halogen chemistry shown
aerosol off	remote	700m	15 °C	halogen and aerosol chemistry switched off	overall importance of aerosol chemistry shown
low O_3 low SO_2	remote, but O_3 = 12 nmol/mol, SO_2 = 20 pmol/mol	700m	15 °C	gas phase initialization	low O_3 reduces Br activation, initial mixing ratios of SO_2 unimportant for steady state conditions
low O_3 low SO_2 large sulfate surface	same as "low O_3 low SO_2"	700m	15 °C	sulfate aerosol mode radius increased by factor 1.5	recycling of HBr, HOBr by sulfate aerosol is important
continental influence	continentally influenced	700m	15 °C	gas phase initialization	quicker Br activation
winter	remote	750m	5 °C	solar declination - 20 ° instead of 20 °	higher BrO mixing ratios than in summer
spring	remote	700m	10 °C	solar declination 0 ° instead of 20 °	similar to winter
high BL	remote	1300m	15 °C	inversion at 1300m instead of 750m, vertical resolution 20m	importance of recycling by sulfate aerosol, less strong Br_x activation
strong wind	remote	700m	15 °C	u_{10} ≈9 m/s (instead of 6 m/s), sea salt aerosol flux param. by *Smith et al.* (1993)	strong increase in S(IV) oxidation in sea salt particles
carbonate	remote	700m	15 °C	carbonate buffer in sea salt increased by 50 % (*Sievering et al.* (1999))	changes in importance of S(IV) oxidation paths
iodine	remote	700m	15 °C	iodine chemistry included	quicker Br activation and greater O_3 loss

SST is the sea surface temperature. Further details on the characteristics of the base run are given in section (4.1).

Particles larger than r=0.5 μm are assumed to be sea salt particles. The composition of sea salt aerosol in the model differs somewhat from the sea water composition in Table 1.1, because in the model only Na^+ is considered as cation because the cations are chemically unreactive in the atmospheric aerosol. The anions considered are Cl^-, Br^-, HCO_3^- and for the iodine run also I^- and IO_3^-. Sulfate is not considered as initial component of sea salt aerosol as it is also assumed to be chemically unreactive. Therefore all sulfate that is present in sea salt aerosol in the model runs stems from uptake from the gas phase and can be labelled "non-sea salt sulfate". According to these assumptions, the molar ratio of Br^- to Na^+ (used as the sum of cations in sea water) is about 1 : 640 and HCO_3^- : $Na^+ = 1 : 235$ (see also *Sander and Crutzen* (1996)). Upon model initialization "fresh" sea salt with a pH of about 8 is present everywhere in the MBL. Uptake of acidic gases like HNO_3 from the gas phase rapidly acidifies the sea salt aerosol particles. When fresh sea salt aerosols are emitted from the sea surface they also have a pH around 8.

4.2 Halogen activation

The model runs start at midnight. Figure 4.1 shows the evolution with time of major gas phase species for the base run, the "continental influence" run and the "low O_3 low SO_2" run. Shortly after model start the sea salt aerosol is acidified due to rapid uptake of acids from the gas phase (see Figure 4.2) with pH values ranging between 6 at the surface and less than 3.5 at the top of the MBL (see Figure 4.9 for a depiction and section 4.10 for a discussion of the vertical profile of the sea salt aerosol pH). At the surface fresh alkaline sea salt aerosol is continuously emitted which is added to the pre-existing sea salt particles in the lowest model layer resulting in a mixture of old acidified and fresh alkaline particles. The acidification of the sea salt particles is an important step in the reaction cycles, because many of them are acid catalyzed.

The halogen chemistry is started by reactions that transform Br^- into species that can degas from the aerosol and initiate quick reaction cycles in the gas phase. These starter reactions are reactions of Br^- with OH, HSO_5^- and NO_3 (reactions A49, A107, A50).

The reaction cycles responsible in the model for the degassing of the reactive bromine species (Br_2 and BrCl) involve the following steps as discussed in *Sander and Crutzen* (1996) and *Vogt et al.* (1996) (see also Figure G.1 for an overview of the most important bromine reactions):

$$HOBr \longleftrightarrow HOBr_{aq} \quad \text{(I.1)}$$

$$HOBr_{aq} + Cl^- + H^+ \longleftrightarrow BrCl_{aq} + H_2O \quad \text{(I.2)}$$

Depending on the concentrations of the species involved in aqueous phase equilibria $BrCl_{aq}$ either degasses (when significant Br^- depletion has occured) and is then photolysed:

$$BrCl + h\nu \longrightarrow Br + Cl \qquad \lambda < 560\text{nm} \tag{I.3}$$

or takes part in the following autocatalytic cycles (when sufficient Br^- is available) leading to the production of Br_2:

$$BrCl_{aq} + Br^- \longleftrightarrow Br_2Cl^- \tag{I.4}$$
$$Br_2Cl^- \longleftrightarrow Br_{2aq} + Cl^- \tag{I.5}$$
$$Br_{2aq} \longleftrightarrow Br_2 \tag{I.6}$$
$$Br_2 + h\nu \longrightarrow 2Br \qquad \lambda < 600\text{nm} \tag{I.7}$$
$$2(Br + O_3) \longrightarrow 2(BrO + O_2) \tag{I.8}$$
$$2(BrO + HO_2) \longrightarrow 2(HOBr + O_2) \tag{I.9}$$

Or instead of equilibria (I.2), (I.4) and (I.5):

$$HOBr_{aq} + Br^- + H^+ \longleftrightarrow Br_{2aq} + H_2O \tag{I.10}$$

leading in both cases to the following net reaction:

$$2HO_2 + H^+ + 2O_3 + Br^- + h\nu \xrightarrow{HOBr,Cl^-} HOBr + 4O_2 + H_2O \tag{I.11}$$

This autocatalytic bromine activation cycle consumes H^+ ions which implies the need for acidification of the sea salt aerosol as shown by *Fickert et al.* (1999) in laboratory experiments.

Keene et al. (1998) studied the influence of the pH on halogen activation. They showed that significant sea salt dehalogenation is limited to acidified aerosol but that differences between a pH of 5.5 and 3 are not significant.

Sander et al. (1999) showed that when sufficient NO_x is available, reactions on the surface of aerosols can also lead to the production of Br_2 and BrCl without the need for acid catalysis:

$$BrO + NO_2 \xrightarrow{M} BrNO_3 \tag{II.1}$$
$$BrNO_3 \xrightarrow{H_2O} HNO_{3aq} + HOBr_{aq} \tag{II.2}$$
$$BrNO_3 \xrightarrow{Cl^-} NO_3^- + BrCl_{aq} \tag{II.3}$$
$$BrNO_3 \xrightarrow{Br^-} NO_3^- + Br_{2aq} \tag{II.4}$$

The uptake of $BrNO_3$ is followed by conversion of HOBr as shown in cycle (I) and the degassing of Br_2 and BrCl.

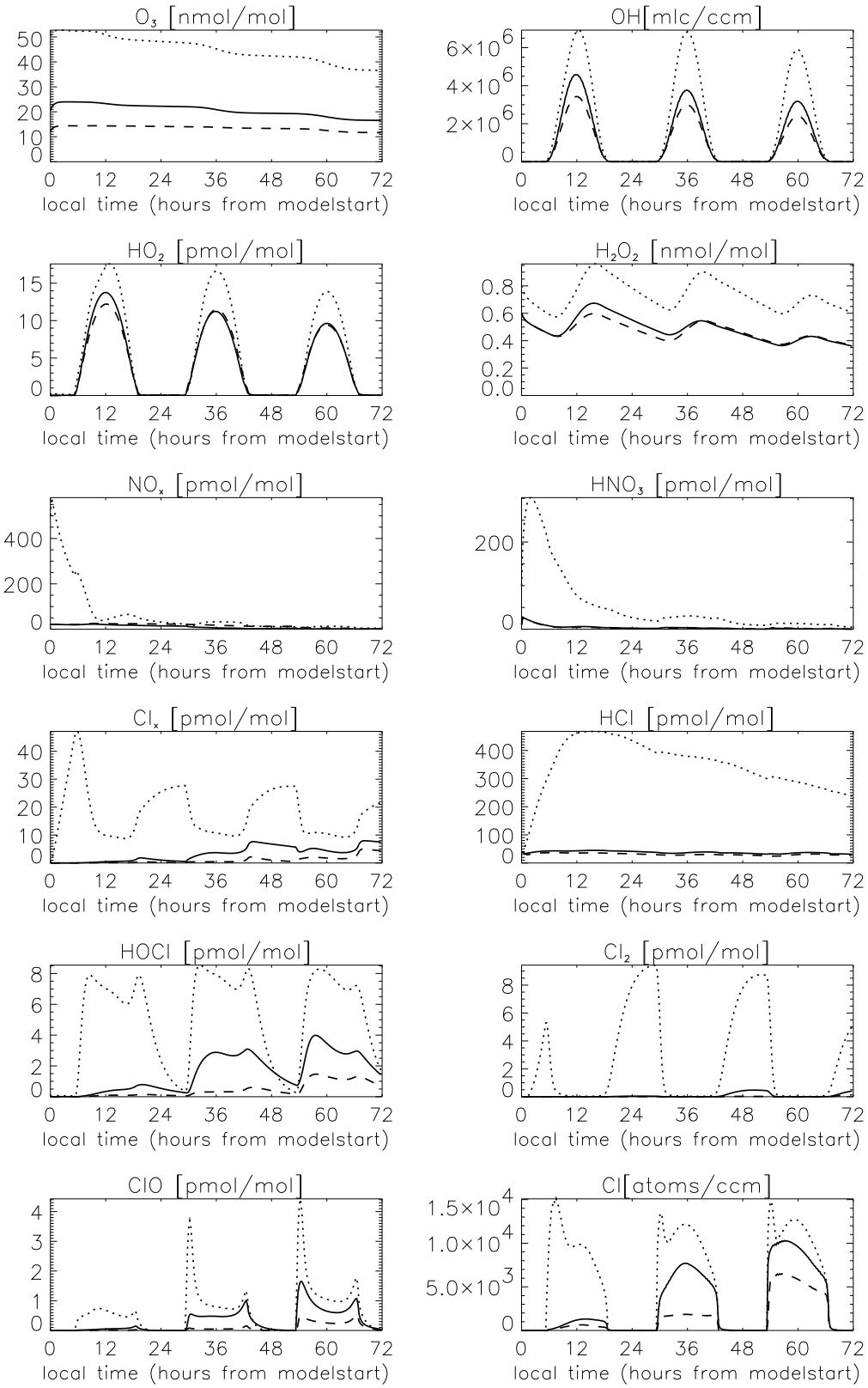

Figure 4.1: Evolution with time of the main gas phase species for the base run (solid line), the "continental influence" run (dotted line) and the "low O_3 low SO_2" run (dashed line) (in 50 m). Cl_x (Br_x) is the sum of all gas phase chlorine (bromine) species except HCl (HBr).

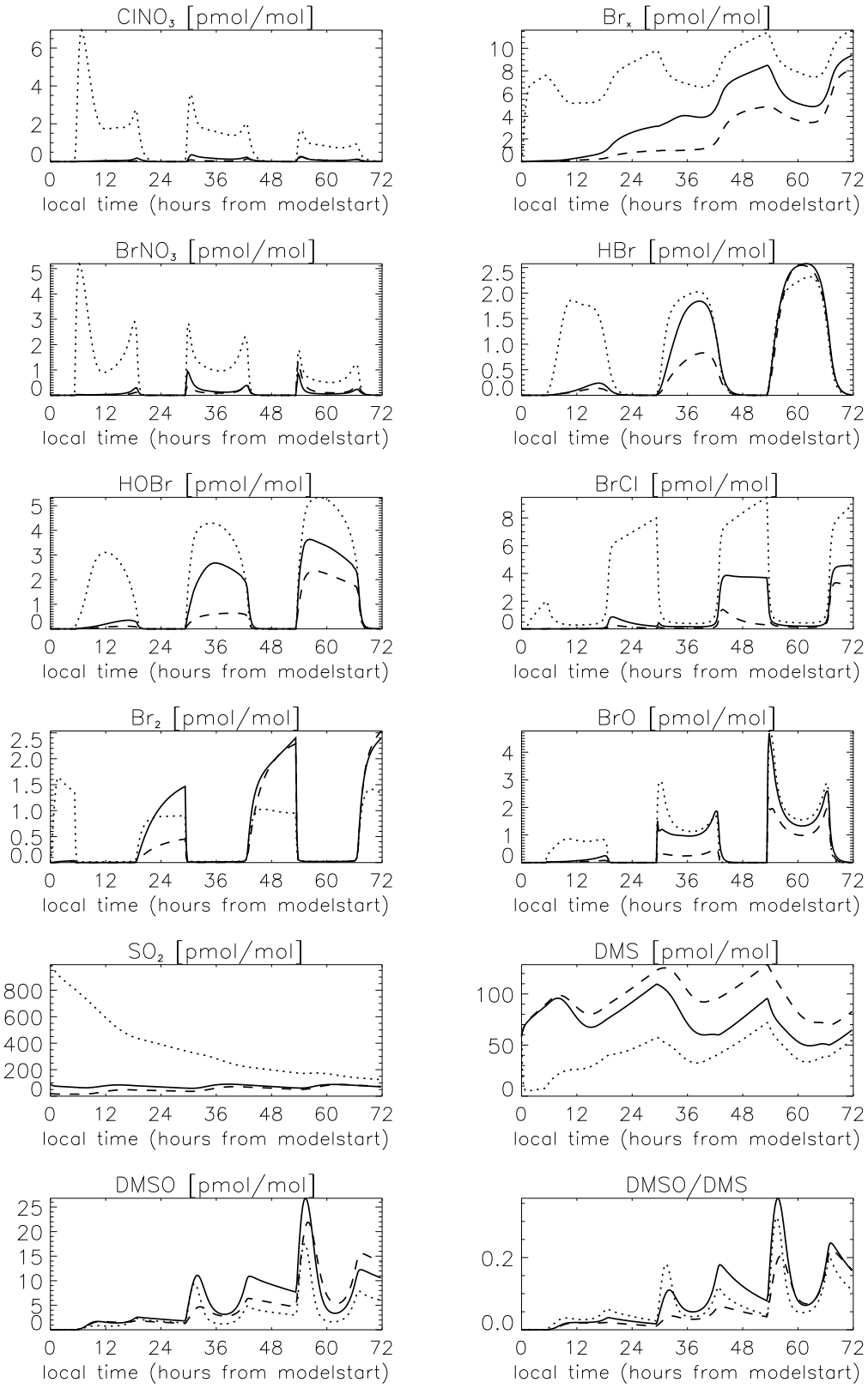

Figure 4.1: Continued.

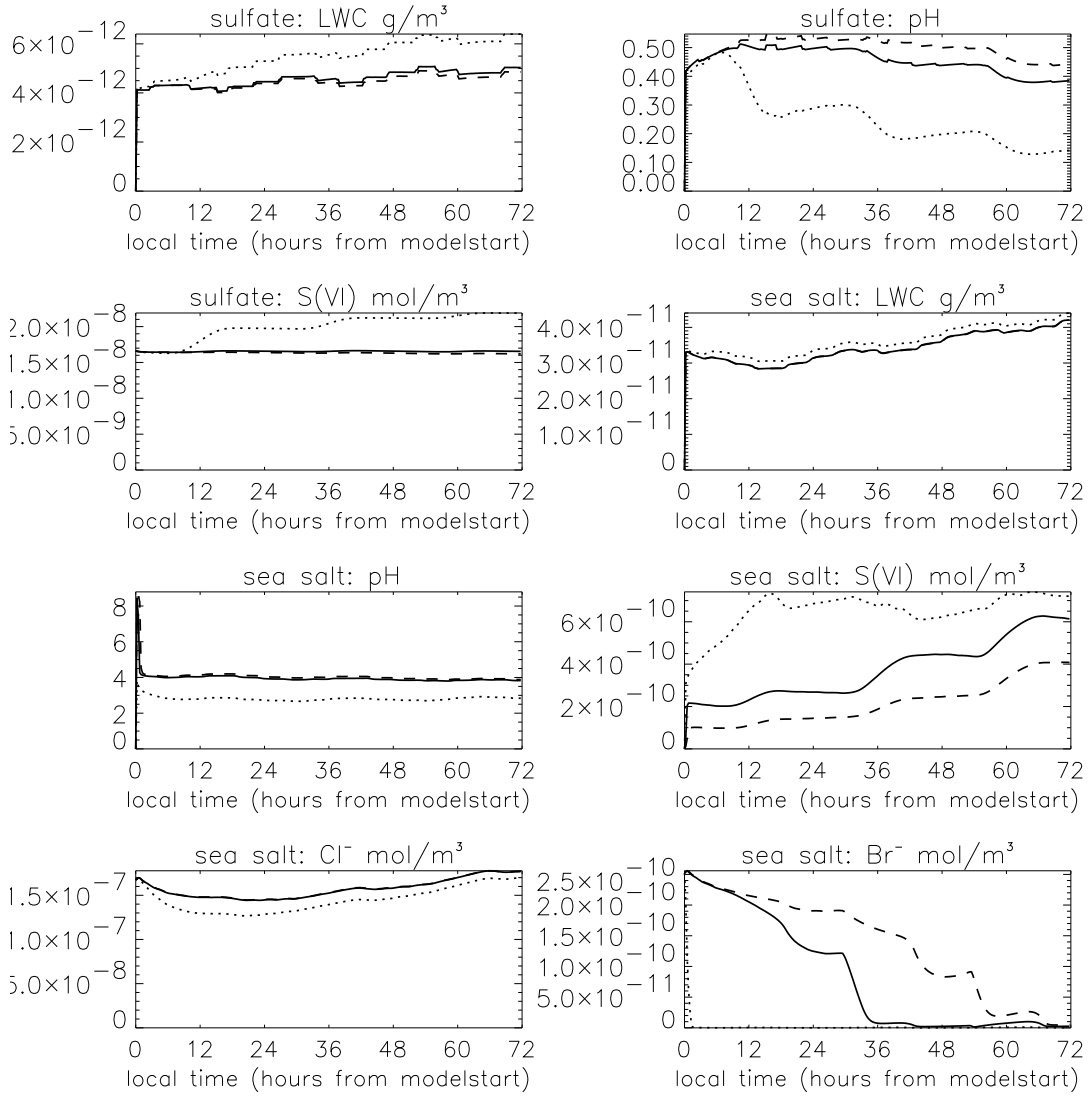

Figure 4.2: Evolution with time of some aqueous phase species as well as liquid water content (LWC) and pH for the base run (solid line), the "continental influence" run (dotted line) and the "low O_3 low SO_2" run (dashed line) in 415 m height in the sulfate and sea salt aerosol. LWC is the liquid water content, units are mol/m^3_{air}.

These reaction cycles lead to gradual build-up of total reactive bromine Br_x (the sum of all gas phase bromine species except HBr) in the gas phase with maximum values between 8 and 10 pmol/mol in the model runs. During daylight the main Br species are HOBr, HBr and BrO, during night this is shifted towards Br_2 and BrCl that are photolyzed readily during daylight (see Figure 4.1). Model calculated bromide deficits are between 70 and 85 % in 50m height, rising to 90 - 99 % in higher model layers due to the lower sea salt aerosol pH in that layers (see section 4.10).

The gas phase mixing ratio of O_3 is important for these cycles because the production of BrO and therefore also the O_3 destruction is catalyzed by O_3 (reaction (I.8). If O_3 mixing ratios are small, halogen activation is slowed down (see run "low O_3 low SO_2").

The order of magnitude of total inorganic gas phase bromine ($Br_t = Br_x$ + HBr) in the model is in the range of the measurements of total inorganic gas phase bromine by *Rancher and Kritz* (1980) that were made during a cruise off the equatorial African coast. The measured daytime gas phase concentrations are about twice the night time values whereas daytime concentrations of particulate bromine were about half the nighttime values. They suggested that there might be a reversible day-night exchange between particulate and gas phase. In the model this diurnal variation cannot be found, total inorganic gas phase bromine peaks at sunrise and has a minimum before sunset. The difference between day and night mixing ratios is only on the order of 20 % close to the surface and a few percent in higher layers of the MBL. It is caused by photolysis shifting the gas phase species from Br_2 and BrCl towards HOBr, $BrNO_3$ and HBr which are taken up by the aqueous phases.

As mentioned by *Rancher and Kritz* (1980) the cloud cover during their cruise was between 0 and 0.5. In model runs that include clouds the model predicts diurnal variation of Br_t that are distinctively different from the ones in runs without clouds. See section 5 for a discussion of this point and note that other measurements did not show a diurnal variation of Br_x (*Moyers and Duce* (1972)).

4.3 Diurnal variation of BrO

The model predicts a distinct diurnal variation of BrO, $BrNO_3$, ClO, and $ClNO_3$ showing a minimum around noon and maxima in the morning and evening (see Figure 4.1). This feature can be explained by differences in the photolysis spectra of O_3 and Br_2 and BrCl. The wavelength dependence of O_3 photolysis is different from that of Br_2 and BrCl that are more rapidly photolysed than O_3 due to absorption at longer wavelengths.

At sunrise (high solar zenith angle) the solar spectrum in the lower troposphere is shifted to longer wavelengths resulting in a delay of O_3 photolysis relative to Br_2 and BrCl (see Figure 4.3). This causes a delay in the photolytically initiated production of OH and HO_2 relative to the production of Br. With low HO_2 the main sink for BrO (reaction (I.9)) apart from photolysis is slow, leading to an increase in BrO mixing ratios (producing the morning peak). Later during the day HO_2 mixing ratios are sufficiently high to reduce BrO mixing ratios leading to the noon minimum. During the afternoon a similar mechanism as in the morning leads to the evening peak of BrO.

If the same wavelength dependence for the photolysis of O_3 and Br_2 are assumed, there is no noon minimum produced by the model but rather a diurnal cycle of BrO that is similar to e.g. OH, showing that the wavelength dependence of the photolysis of the different species is the cause for the noon minimum in BrO

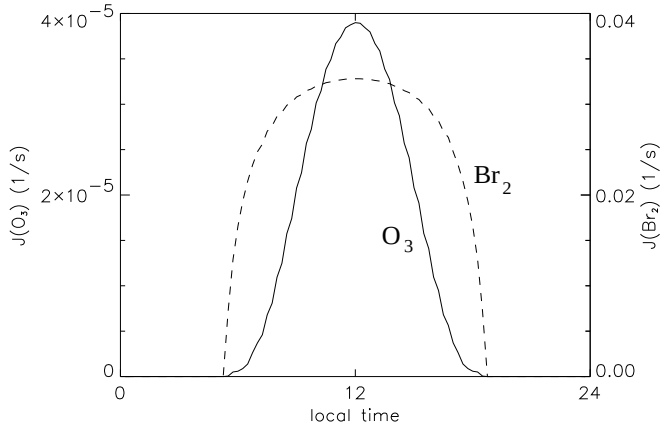

Figure 4.3: Diurnal variation of the photolysis frequencies for O_3 and Br_2 (note the different units). The difference in the shape of the diurnal variation is the cause for the noon minimum in BrO mixing ratios (see text).

and the other affected species. The diurnal variation of BrO is accompanied by an early morning peak in O_3 destruction by XO + YO and XO + NO_2 reactions (X, Y = Br, Cl).

Nagao et al. (1999) found a "sunrise ozone destruction" (SOD) in the diurnal variation of O_3 based on measurements over a 3-year period on an island in the sub-tropical Northwestern Pacific. This SOD could not be explained by photochemistry that neglects halogens. They speculated that bromine spieces might play a role in SOD. A similar feature was found by *Galbally et al.* (2000) in a time series of 13 years of O_3 observations at Cape Grim, Tasmania. They also found a decrease in O_3 concentrations in the first hours after sunrise and speculated about the importance of halogens in this additional O_3 destruction process.

4.4 Active recycling of Br_x by the sulfate aerosol

The presence of sulfate aerosol particles is important for the halogen activation cycle. The large surface area of the sulfate aerosol of 40 to 60 $\mu m^2/cm^3$, compared to the sea salt surface area of 25 to 45 $\mu m^2/cm^3$, is the reason that HBr, HOBr and $BrNO_3$ are also scavenged to a significant amount by the sulfate aerosol and are involved in reactions on and in sulfate particles. Due to the low pH of the sulfate aerosol the acid catalyzed cycle (I) quickly transforms Br^- and Cl^- (from the dissociation of HBr and HCl) and HOBr to BrCl and Br_2 which rapidly degas. As can be seen from Figure 4.4 the magnitude of recycling of bromine species is higher than in the sea salt aerosol by roughly a factor of 5 to 10. Due to this recycling process the sulfate aerosol is not a significant sink for gas phase bromine; some bromine, however, will always be found in the sulfate aerosol.

Particle composition measurements (e.g. *Moyers and Duce* (1972), *Duce et al.* (1983)) sometimes (but not always) showed an increase of the bromine to sodium

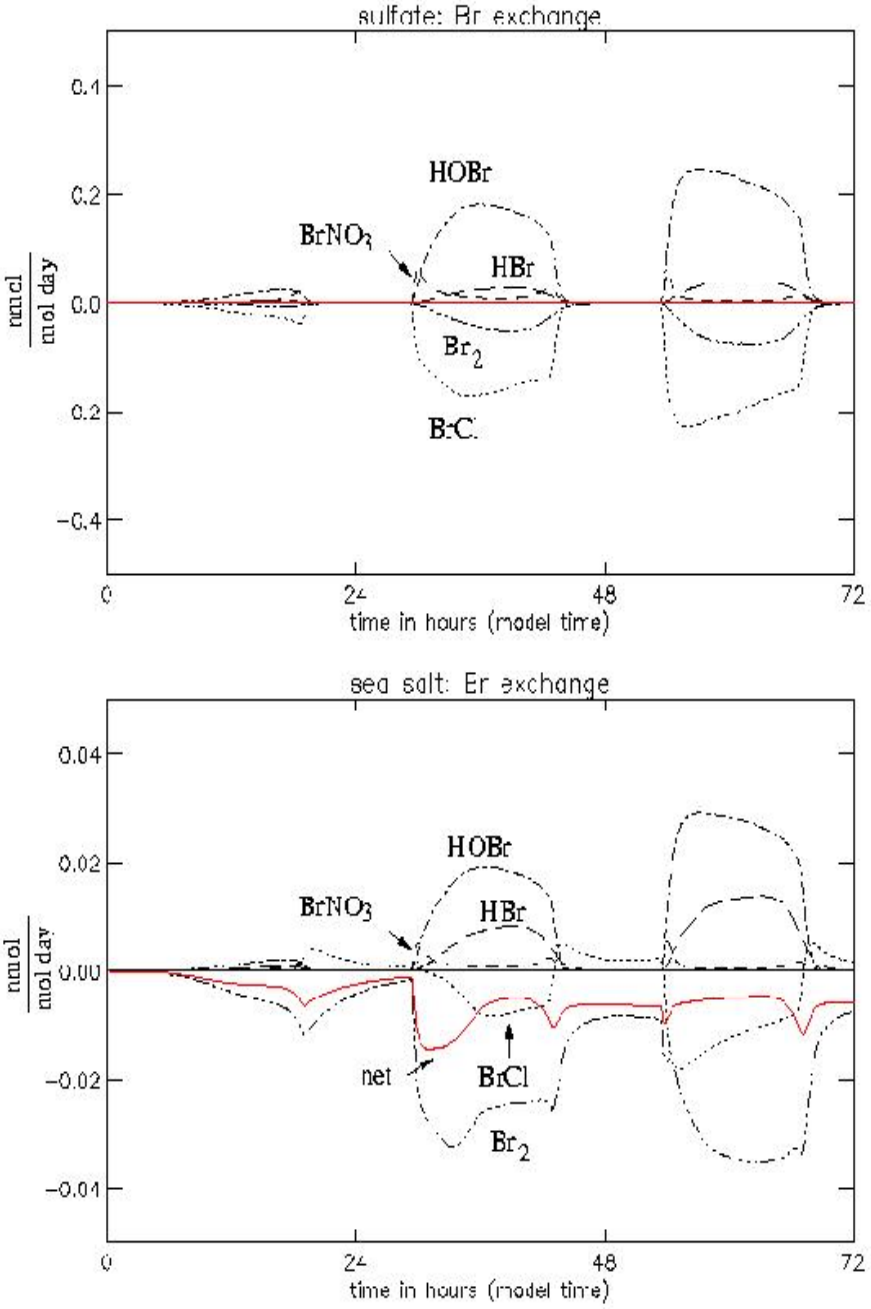

Figure 4.4: Net exchange of Br_x and HBr between sea salt and sulfate aerosol and gas phase (in 215 m). A negative sign implies loss for the aerosol. The solid line is the net flux of Br atoms.

ratio in small particles compared to sea water. Depending on the measurement technique some measurements show the ratio of the ions Br^-/Na^+ whereas oth-

ers show the elemental ratio. The interpretation of this data is difficult because for some samples the chemical state of bromine in the particles is unclear. Further, sodium in the aerosol samples could be a consequence of the sampling of an external mixture of sulfate and sea salt particles or of internally mixed particles that originate from collision-coalescence or cloud processes (or both). The enriched bromine could be in the form of stable bromine containing ions or organic molecules. Known reactions (*Haag and Hoigné* (1983)) for the production of stable ions like BrO_3^- in the aqueous phase are too slow to lead to significant production in the aerosol. See also section 5 for a discussion of this topic for the cloud runs.

To further highlight the importance of the sulfate aerosol as active recyclers the "low O_3 low SO_2" run was repeated (called "low O_3 low SO_2 sulf"), with an increase the particles mode radius of the initial sulfate aerosol by 50 % thereby increasing the total (dry) sulfate aerosol surface by a factor of 2.25. This led to a strong increase in the recycling of bromine through sulfate aerosol compared to the base run. After 43 hours Br_x was the same as in the base run whereas in the "low O_3 low SO_2" (with smaller sulfate aerosol particles) this is never achieved. The bromine fluxes of HOBr and HBr to and of Br_2 and BrCl from the sulfate aerosol were 3.4 times greater on the second model day compared to the "low O_3 low SO_2" run and 2 times greater on the third model day.

In the "high BL" run the MBL has a depth of 1250 m, relative humidity at the sea surface is 50 % increasing to 90 % below the inversion. This implies that sulfate aerosol chemistry is not active in the lowest 400 m where relative humidity is too small (see page 22). During the day the gas phase mixing ratios of Br_2 and BrCl are mainly determined by the flux from the aerosols and loss by photolysis, mixing is much slower than these processes. Br_2 and BrCl increase roughly by a factor of ten from the layers without sulfate aerosol chemistry to higher layers where it is active. $BrNO_3$ and HOBr decrease by the same absolute amount but the relative change is smaller due to higher mixing ratios. This points again to the importance of the sulfate aerosol in recycling these species. Furthermore due to the low relativ humidity and a stronger vertical dilution the sea salt aerosol pH is quite high, decreasing from 8 near the surface to 6 in 500 m and 4 in 1000 m. This allows rapid bromine release only in the highest layers of the MBL.

4.5 Nighttime fluxes of bromine

During daylight, photolysis is the driving force for the net transport of bromine from the aqueous to the gas phase as formation of HOBr is dependent on photolysis. During night Br_2 also degasses as evident from Figure 4.4. This is caused by a sudden rise in BrCl mixing ratios after sunset due to absent photolytical loss. Thus the gas-aqueous partitioning of these species is perturbed leading to the reaction sequence:

$$
\begin{aligned}
BrCl &\longrightarrow BrCl_{aq} && \text{(III.1)}\\
BrCl_{aq} + Br^- &\longrightarrow Br_2Cl^- && \text{(III.2)}\\
Br_2Cl^- &\longrightarrow Cl^- + Br_{2aq} && \text{(III.3)}\\
Br_{2aq} &\longrightarrow Br_2 && \text{(III.4)}
\end{aligned}
$$

where in equilibria the net direction is indicated. This cycle results in net transfer of Br from the aqueous to the gas phase:

$$BrCl + Br^- \longrightarrow Cl^- + Br_2.$$

If the bromide depletion in the sea salt aerosol is close to complete, another sequence gains in importance (in agreement with laboratory experiments of *Fickert et al.* (1999)):

$$
\begin{aligned}
Br_2 &\longrightarrow Br_{2aq} && \text{(IV.1)}\\
Br_{2aq} + Cl^- &\longrightarrow Br_2Cl^- && \text{(IV.2)}\\
Br_2Cl^- &\longrightarrow Br^- + BrCl_{aq} && \text{(IV.3)}\\
BrCl_{aq} &\longrightarrow BrCl && \text{(IV.4)}
\end{aligned}
$$

The Br^- produced in step (IV.3) can then take part in the following reaction sequence:

$$
\begin{aligned}
Cl_2 &\longrightarrow Cl_{2aq} && \text{(V.1)}\\
Cl_{2aq} + Br^- &\longrightarrow BrCl_2^- && \text{(V.2)}\\
BrCl_2^- &\longrightarrow BrCl_{aq} + Cl^- && \text{(V.3)}\\
BrCl_{aq} &\longrightarrow BrCl && \text{(V.4)}\\
& && \text{(V.4)}
\end{aligned}
$$

or in :

$$
\begin{aligned}
HOCl &\longrightarrow HOCl_{aq} && \text{(VI.1)}\\
HOCl + Br^- + H+ &\longrightarrow BrCl_{aq} + H_2O && \text{(VI.2)}\\
BrCl_{aq} &\longrightarrow BrCl. && \text{(VI.3)}
\end{aligned}
$$

Cycles (IV) and (V) combined give:

$$Br_2 + Cl_2 \longrightarrow 2BrCl$$

cycles (IV) and $2 \cdot$ (VI) combined give:

$$Br_2 + 2HOCl \longrightarrow 2BrCl$$

i.e. these cycles are no net sink for total gas phase bromine, they just shift gas phase bromine from Br_2 to BrCl which is what is observed both in the model for the strongly depleted (e.g. "continental influence run") cases and in the laboratory (*Fickert et al.* (1999)).

4.6 Effect on O_3

In the remote MBL O_3 mixing ratios are believed to be mainly determined by the mixing ratios of HO_x and NO_x and by dynamics, i.e. downmixing of O_3-rich air from the free troposphere (e. g. *Monks et al.* (2000)). Photochemistry in the remote MBL usually leads to a net photochemical destruction of O_3. Here it is shown that halogen radicals can significantly contribute to O_3 loss in the MBL.

To properly asses the effect of chemical reactions on O_3, the odd oxygen family O_x has been defined (based on *Crutzen and Schmailzl* (1983)): $O_x = O_3 + O + O(^1D) + NO_2 + 2 \cdot NO_3 + 3 \cdot N_2O_5 + HNO_4 + ClO + 2 \cdot Cl_2O_2 + 2 \cdot OClO + BrO + IO + 2 \cdot I_2O_2$ (OIO is not included because it is assumed to be photolytically stable in contrary to OClO). Species in this family are readily transfered to O_3 (e.g. NO_2 which photolyses forming O which recombines with O_2 to O_3). Only if there a reaction leads to a change in the mixing ratio of the odd oxygen family ($\Delta O_x \neq 0$) an effective O_3 destruction or production took place.

Chemical O_x production in the MBL is primarily by reaction of NO with HO_2 and CH_3OO, both of which form NO_2. In the base run it sums up to 1.9 nmol/(mol day).

Figure 4.5 shows accumulated rates for the major O_x loss reactions for the base run, the "continental influence" run, and the "low O_3 low SO_2" run. The most important O_x loss reaction is $O(^1D) + H_2O$ which accounts for 52 % of net O_3 destruction followed by $O_3 + HO_2$ with 13 %. The main step in bromine related photochemical O_3 destruction is the production of BrO in reaction (I.8) followed by reactions of BrO with HO_2, CH_3OO, XO (X = Br, Cl) radicals, and NO_2. In the base run the halogen related O_3 destruction reactions account for roughly 30 % of net O_3 destruction.

The most important bromine reaction ($BrO + HO_2$) causes 12 % loss. Chlorine related O_3 destruction is less important than the bromine reactions, they account together for roughly 4 %.

Most of the reactions depicted in Figure 4.5 show the highest rate for the "continental influence" run and smallest rates for the "low O_3 low SO_2" run. The relative importance of reactions involving reactions of XO with YO (X, Y = Cl, Br), however, is highest in the base run because there the loss of XO by reaction with NO_2 is lower than in the "continental influence" run. This also increases the importance of the BrO + DMS reaction.

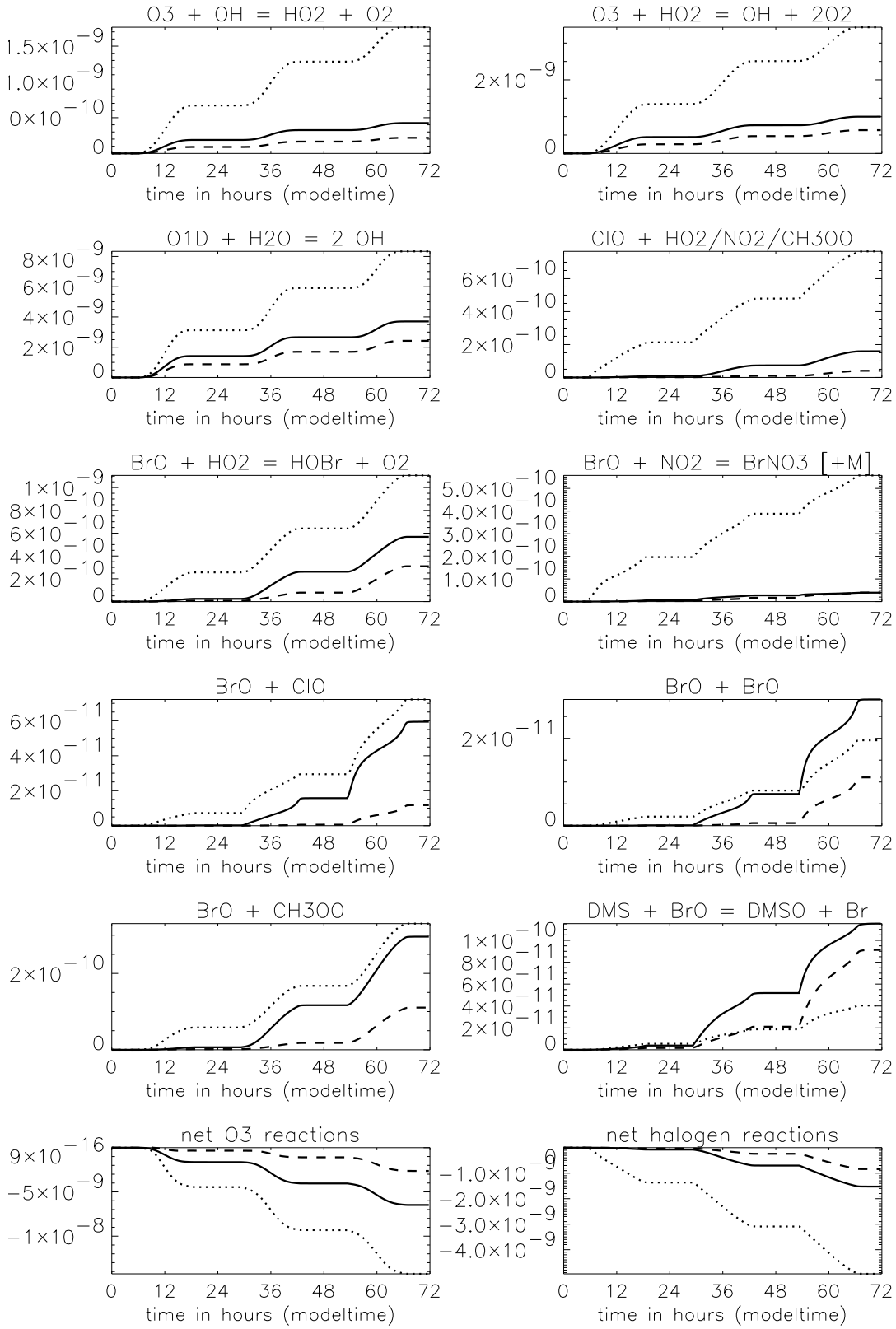

Figure 4.5: Accumulated O_x (see definition in section (4.6)) related reaction rates in mol/mol for the base run (solid line), the "continental influence" run (dotted line) and the "low O_3 low SO_2" run (dashed line) (in 415 m). Note: for the net plots change in O_x is plotted, whereas for the individual reactions the accumulated reaction rates are plotted, i.e. to get ΔO_x from the BrO + BrO reactions multiply with 2.

Table 4.4: O_3 destruction rates.

run	$O(^1D) + H_2O$	$O_3 + HO_2$	$O_3 + OH$	$ClO + HO_2$ / NO_2 / CH_3OO	$BrO + HO_2$	$BrO + ClO$	$BrO + BrO$	$BrO + CH_3OO$	$DMS + BrO$	net O_x destruction	net O_x destruction by halogens
	%	%	%	%	%	%	%	%	%		
base run	52.0	12.6	5.3	3.7	12.4	2.7	1.3	6.6	2.5	1.9	0.6
halogen off	70.1	20.8	7.9							0.7	
aerosol off	70.0	21.0	7.9							0.7	
low O_3 low SO_2	56.4	14.0	4.7	1.7	11.0	0.9	0.8	4.0	3.2	0.6	0.3
low O_3 low SO_2 sulf	49.1	11.1	3.8	3.3	15.0	3.1	2.0	7.0	4.0	1.0	0.5
cont. influence	47.4	15.9	8.7	5.4	8.3	2.6	0.7	4.1	0.7	3.7	1.2
winter	18.0	10.5	2.9	7.3	20.0	18.0	7.1	10.0	10.2	0.8	0.6
spring	39.2	14.5	5.0	4.8	16.0	5.0	2.3	7.1	4.9	1.1	0.5
high BL (in 130 m)	67.0	13.4	7.2	1.7	5.4	0.4	0.3	3.4	0.5	2.9	0.4
strong wind	49.3	12.4	5.5	1.9	14.7	1.8	2.6	7.8	2.6	2.0	0.8
carbonate	52.1	12.7	5.4	3.7	12.3	2.6	1.3	6.5	2.5	1.9	0.6
high DMS	50.6	12.7	4.4	2.1	9.5	1.2	0.8	5.2	11.4	1.8	0.7
iodine	40.2	9.0	4.2	4.7	11.0	4.1	1.4	7.3	2.1	2.4	1.1

Net O_x destruction and net O_x destruction involving halogens are given in nmol/(mol day), the contribution of the different reactions to the total O_3 destruction is expressed in %. For each reaction the appropriate ΔO_x has been used as a factor to evaluate the contribution. The most important O_x destruction paths involving iodine species are $IO + HO_2$: 9.6 % and $IO + BrO$: 5.5 % in the "iodine" run. The data are given as averages of the 2^{nd} and 3^{rd} in 65 m height. Only in the "high BL" run for technical reasons a height of 130 m was chosen.

Figure 4.5 shows furthermore the quicker activation of halogens in the "continental influence" run, which was also apparent from Figure 4.1.

Compared with the "halogen off" run, halogen chemistry causes 1.2 nmol/(mol day) additional O_3 destruction in the base run.

For some runs O_x production and destruction rates have been summarized in Table 4.4. Very interesting is the high relative contribution of halogen chemistry to O_3 destruction in the winter run. The reason for this will be discussed in the next section.

4.7 Winter run

For the winter run temperature and solar zenith angle are chosen to model the conditions at the end of January instead of end of July as in the base run (see Figures 4.6 and 4.7, when looking at the vertical profiles please note that the height of the MBL in slightly different in the base and winter runs). This implies that the solar spectrum is shifted to greater wavelengths reducing the photolysis rates for $O_3 \longrightarrow O(^1D)$ by 66 % leading to a decreased formation of OH and HO_2 compared to summer conditions. The reduction in the photolysis rates of Br_2 and BrCl are only 7.5 and 15 %, respectively, because they absorb at greater wavelengths (see also Figure 4.3 and discussion in section 4.3).

With a strong reduction of the main sink ($XO + HO_2$, $X = Cl, Br$) due to the reduction in O_3 photolysis and therefore of HO_2 production and only a weak reduction in the production of Br and Cl radicals the mixing ratios of BrO and ClO are higher in the winter than in the summer run.

In the "winter" run net O_3 destruction is only 32 % of the destruction in the base run because of the smaller solar radiation intensity reducing OH to a third and HO_2 to 50 % of the summer values. The absolute number of halogen related O_3 loss is approximately as high as in the base run enhancing the halogen contribution to 67 %. This is mainly due to an increase in the BrO and ClO mixing ratios, leading to an increased importance of the XO-YO (X,Y=Br, Cl) reactions, which have a $\Delta O_x = -2$ (see Figure 4.8).

The morning peak in the BrO mixing ratios calculated by the model has increased by approximately 20 %, whereas the noon values increased by more than 90 %. Activation of bromine from the aqueous phase is faster and total reactive bromine (Br_x) increased by 12 to 25 % compared to the base (summer) run at the expense pf HBr which decreased by 1 pmol/mol (roughly 50 %). Also Cl_x (the sum of all gas phase chlorine species except HCl) increased by up to 30 % (see Figure 4.6).

Oxidation of DMS by OH is reduced by approximately two thirds, whereas oxidation by BrO is roughly doubled increasing the relative importance of BrO in DMS oxidation from roughly 44 % in the base run to approximately 75 % in the "winter" run. A corresponding increase in the production of DMSO is observed in the model results (see section 4.12 for a more detailed discussion of the DMS chemistry).

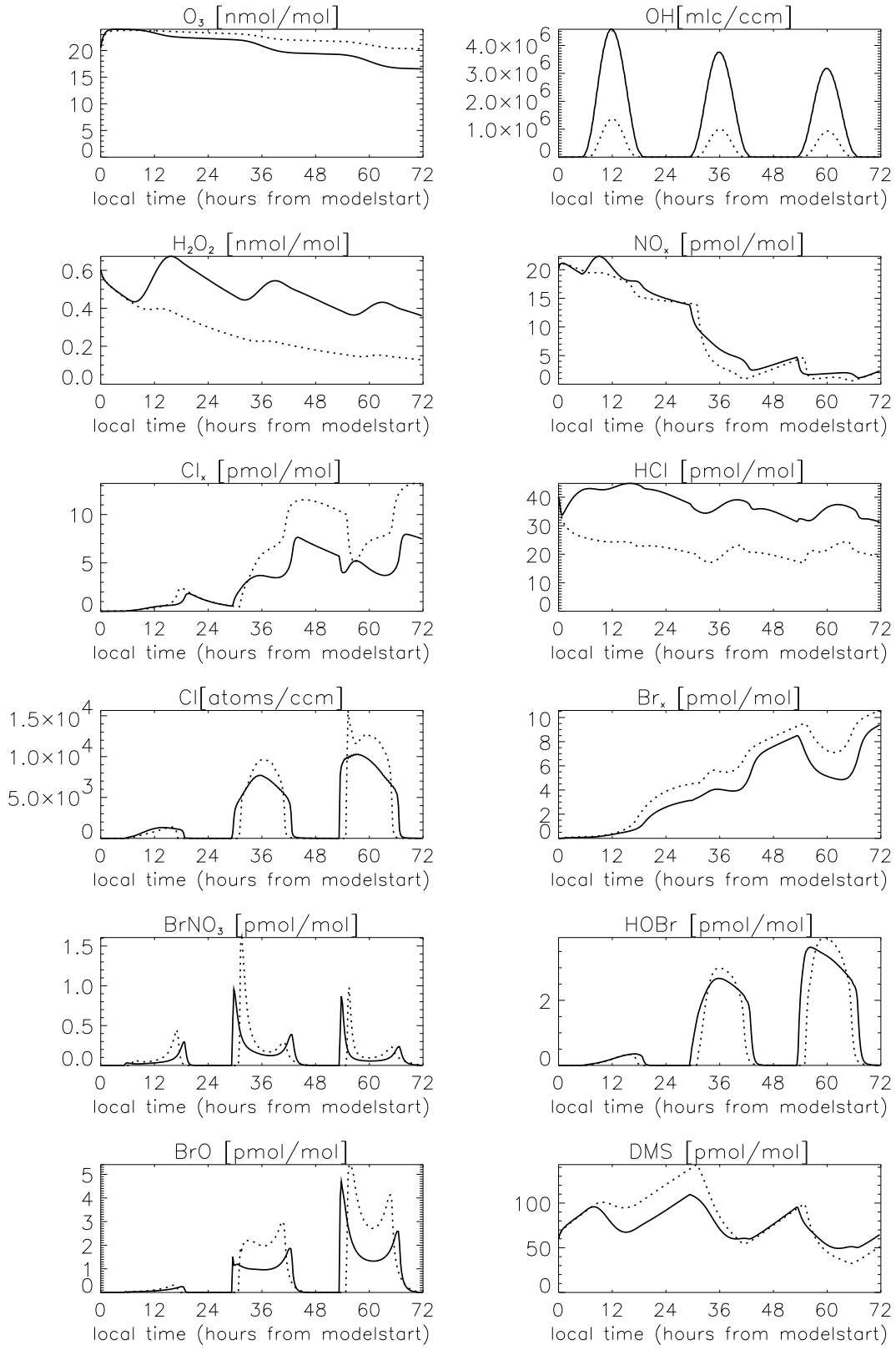

Figure 4.6: Evolution with time of the main gas phase species for the base run (solid line) and for the winter run (dotted line) (in 50 m).

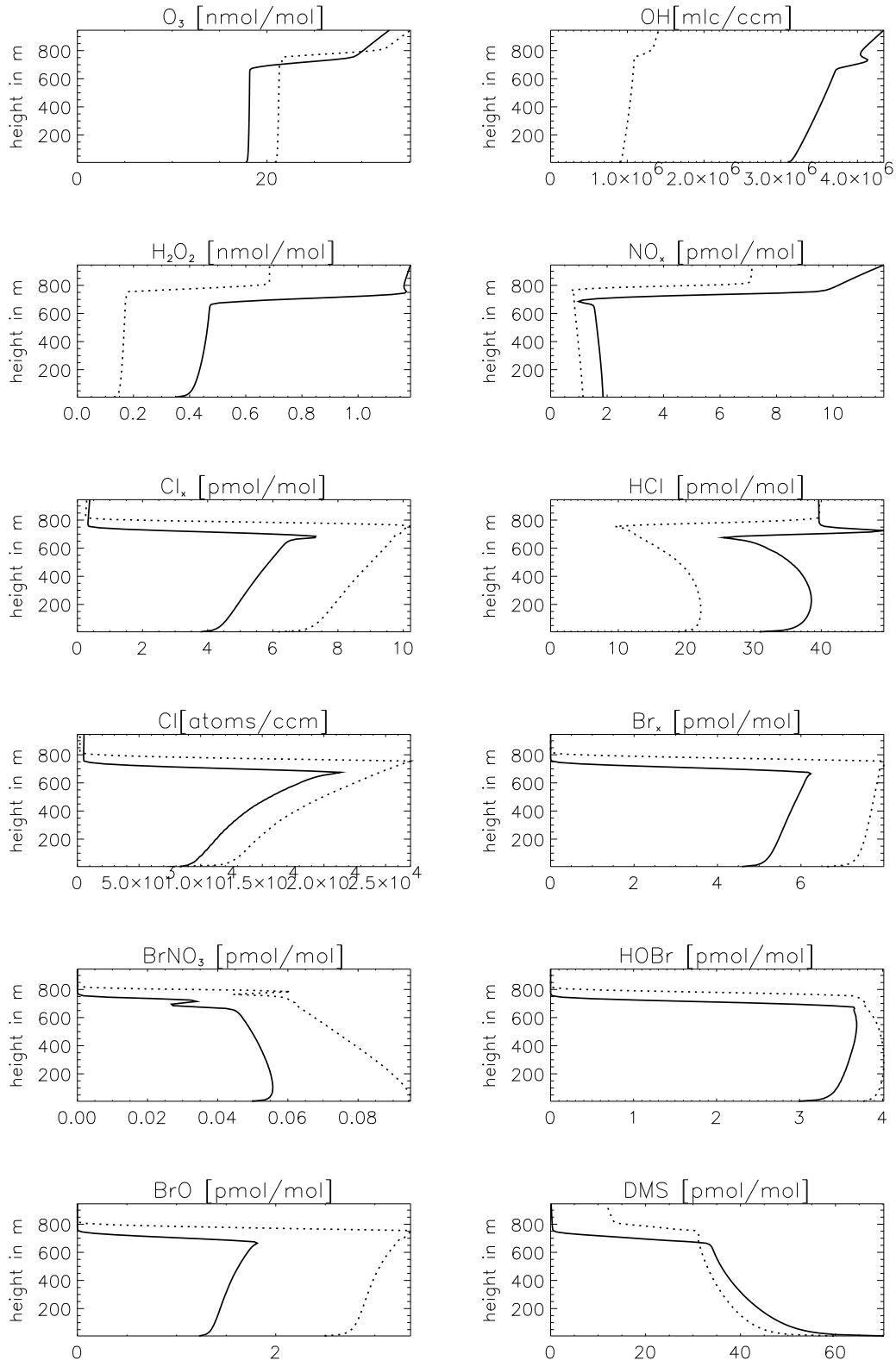

Figure 4.7: Vertical profile of the main gas phase species for the base run (solid line) and for the winter run (dotted line) (at noon of third day). Note that the height of the MBL is slightly different in the two runs.

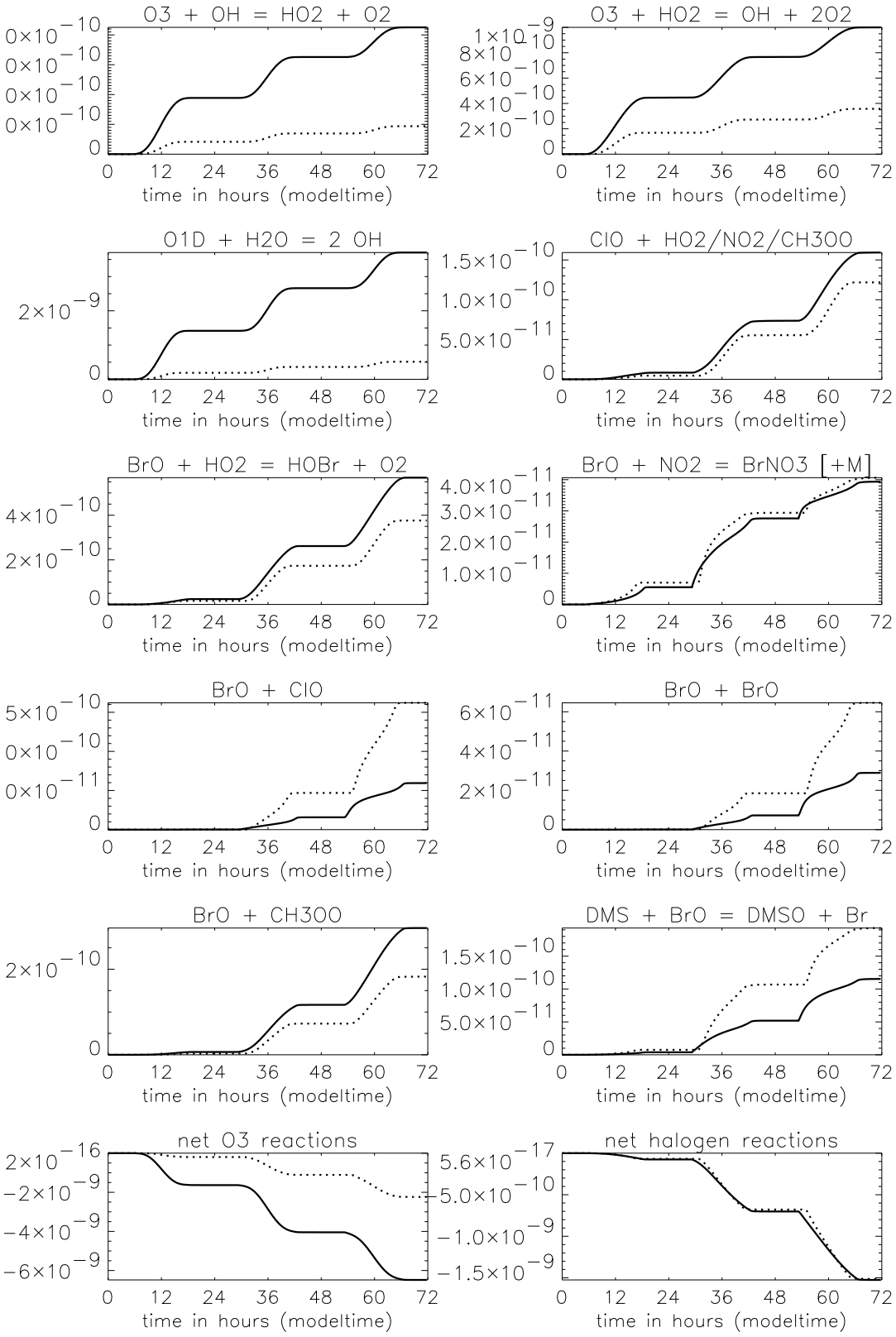

Figure 4.8: Accumulated O_x related reaction rates in mol/mol for the base run (solid line) and the winter run (dotted line) (in 415 m). Note: for the net plots change in O_x is plotted, whereas for the individual reactions the accumulated reaction rates are plotted, .i.e to get ΔO_x from the BrO + BrO reactions multiply with 2.

Cl_x (especially Cl_2) mixing ratios increased significantly compared to the summer run due to greater fluxes from the sea salt aerosol.

Due to lower temperatures compared to the summer case, the solubility of the gases increases. A reduction in the temperature from 15 °C to 0 °C increases the solubility of SO_2 by a factor of 1.8, HNO_3 by a factor of 3.8, and HCl by a factor of 4. Enhanced uptake of acidic gases leads to a lower sea salt aerosol pH. Caused by the lower pH bromine activation is more rapid and bromine depletion even stronger than in the base run. Comparison with the measurements of *Ayers et al.* (1999) shows a difference in the seasonality as they found a minimum in the Br^- deficit in winter. During winter the availability of acids (mainly due to reduced microbial activity which causes a smaller DMS flux) is reduced at their measurement site whereas sea salt loadings are increased due to higher wind speeds in winter (*Ayers et al.* (1999)). In the model run the wind speed (flux of sea salt aerosol), gas phase acid mixing ratios or the DMS flux were not changed to concentrate on differences in radiation and temperature only, therefore these differences between measurements and model results were to be expected.

To test the model under the conditions described by *Ayers et al.* (1999) another run for winter conditions was peformed, where the geostrophic wind speed was increased from 7 to 12 m/s yielding a higher sea salt flux. Further the fluxes of DMS and NH_3 were decreased by a factor of 4 to get typical mixing ratios of 20 pmol/mol for DMS and less than 5 pmol/mol for SO_2 (*Ayers et al.* (1997a)). Other chemical initial values and the meteorology were adjusted to the conditions at Cape Grim (*Ayers et al.* (1997b)). Very little bromine activation was found, the depletion was about 10 % which is even less than in the measurements of *Ayers et al.* (1999) probably pointing to a source of acidity that was not considered in the model. Due to the reduction of the DMS flux and the resulting decrease of SO_2 mixing ratios, the major source for aqueous phase acidity was strongly reduced, whereas the aqueous phase buffer capacity was increased by the increase in sea salt particle mass (roughly a factor of 3). This lead to sea salt aerosol pH values greater than 8 (the value for sea water). When initial gas phase concentrations and fluxes were chosen for summer conditions at Cape Grim (*Ayers et al.* (1997a,b, 1999)), strong bromine occured as in the other runs that were presented here.

The features for the "spring" run (not shown) are the same as for the "winter run" but the reduction in total net O_3 destruction to 58 % of the value in the base run is not as strong as in the "winter" run.

4.8 Influence of NO_x

Nitrogen oxides play a very important role in atmospheric chemistry by acting as catalyst in the photochemical production of O_3. When NO_2 reacts with OH, nitric acid (HNO_3) is formed which is rapidly taken up by aerosol (mainly sea salt aerosol), providing acidity to the aerosol. If halogens are present NO_x mixing ratios are further reduced by reactions of NO_2 with ClO and BrO yielding XNO_3

(X=Cl, Br). XNO_3 can either be photolysed, decomposed or taken up by the aerosol leading to a loss of NO_x from the gas phase and to an increase of NO_3^- in the particles and further activation of bromine (*Sander et al.* (1999)). The scavening of XNO_3 by particles is a significant NO_x loss process, so a NO_x source was introduced in the model to avoid unrealistically small NO_x mixing ratios of less than 0.1 pmol/mol (the source strength is 10 pmol/(mol day) in the MBL which is equivalent to 2.025 $\cdot 10^8$ molec/(cm^2 s) as surface flux). *Monks et al.* (1998) report typical mixing ratios of 2 to 6 pmol/mol for NO_x for clean maritime background conditions (Cape Grim) which are achieved in the model with the NO_x source.

This additional NO_x could be a photolysis product from alkylnitrates that are emitted from the ocean (see e.g. *Blake et al.* (1999) for latitudinal and vertical profiles during the ACE 1 campaign and references therein). Another possibility could be the direct emission of NO from the oceans (formed by photolysis of NO_2^-) as suggested by *Zafiriou et al.* (1980) on the basis of NO measurements in surface waters of the central equatorial Pacific.

Schultz et al. (1999) pointed to the importance of downward transport of PAN from the free troposphere and the subsequent thermolysis in the MBL. This process is included in the model but exchange between the MBL and the free troposphere is weak as long as no clouds are present that strongly increase this exchange.

On the other hand the need to include a NO_x source for runs including aerosol/halogen chemistry might point to the fact, that processes exist that convert aqueous HNO_3/NO_3^- back to NO_x, that are not included in the model. The importance of the photolysis of NO_3^- in aerosol particles was also studied (*Warneck and Wurzinger* (1988), *Zellner et al.* (1990), *Burley and Johnston* (1992)):

$$NO_3^- + h\nu \xrightarrow{H_2O} NO_2 + OH + OH^-, \tag{4.1}$$

Although this reaction was found to be negligible as a source of NO_2, OH concentrations increased significantly speeding up the activation of bromine from the sea salt aerosol because OH is involved in one of the starter reactions (see also p. 29). The resulting differences in the gas phase where only apparent on the first model day.

As already discussed in *Sander et al.* (1999), the $BrNO_3$ uptake rate has been measured only for sulfate particles. They made the assumption that the uptake on sea salt aerosol would be the same. To see the effect of a reduced uptake coefficient, a run was performed (not shown) where its value was changed from $\gamma = 0.8$ to $\gamma = 0.01$. As expected this results in slower activation of Br_x and less pronounced morning peaks of BrO (due to higher NO_x) and less Cl_x. The overall features are unaffected by this variation.

The influence of NO_x on halogen chemistry can be shown when comparing the base with the "continentally influenced" run. If NO_x mixing ratios are small (base run) the morning peak of BrO is quite large (up to 4.5 pmol/mol in 50 m height) because destruction of BrO by reaction with HO_2 or NO_2 is not efficient.

In polluted air there is enough NO_x to make the reaction of BrO with NO_2 important, thereby reducing the morning and afternoon peak of BrO. From the discussion in section 4.3 an evening peak in BrO can be anticipated which is present in all runs except for the first evening of the "continentally influenced" run (see Figure 4.1). In this run it is missing on the first day due to high NO_x mixing ratios that are considerably greater than on the following days. In the continentally influenced run the initially high mixing ratios of NO_2 speed up the bromine activation via reaction cycle (II) and lower sea salt aerosol pH through the uptake of HNO_3. This causes a very quick depletion of bromide from the sea salt aerosol favoring the production of BrCl in the sea salt aerosol instead of Br_2 which leads to a change in the speciation of gas phase Br_x (Br_2 mixing ratios are reduced and BrCl enhanced, see discussion above in section 4.5).

4.9 Cl chemistry

Many field studies found a significant reduction in the ratio of Cl^-/Na^+ in sea salt aerosols compared to the sea water ratio for semi-polluted or polluted cases (*Kritz and Rancher* (1980), *Keene et al.* (1990), *Volpe et al.* (1998), and *Ayers et al.* (1999)). In the model runs a significant chlorine depletion can also be found when enough gas phase acidity is available. Several researchers proposed mechanisms in addition to the acid displacement for the release of chlorine from the sea salt aerosol like reaction of N_2O_5 with sea salt aerosol (*Finlayson-Pitts et al.* (1989), *Zetzsch and Behnke* (1992)), O_3 (*Keene et al.* (1990)) but until now none could be identified as the most important for the MBL. A recent study by *Knipping et al.* (2000) emphasized the role of surface reactions on sea salt aerosols, because their results showed that Cl^- ions are not equally distributed in sea salt particles but more likely to be found at the particle surface. Maybe a mechanism involving other surfaces like sulfate aerosol is also important as could be shown here for the release of bromine.

Like bromine radicals chlorine radicals too can contribute to the oxidative capacity of the MBL, especially for nonmethane hydrocarbons and to a small extent for DMS. Chlorine radical concentrations have indirectly been determined in the MBL by several groups. These estimates ranged from upper limits of 10^3 atoms/cm^3 (*Jobson et al.* (1998)) to 720 atoms/cm^3 (*Wingenter et al.* (1999)) and up to 10^5 atoms/cm^3 (*Singh et al.* (1996a), *Wingenter et al.* (1996)).

Measurements of inorganic chlorine species during night by *Pszenny et al.* (1993) showed mixing ratios between <26 to 254 pmol/mol $Cl_2^\star$ (Cl_2 and a fraction of HOCl). *Spicer et al.* (1998) found <10 to 150 pmol/mol Cl_2. These high mixing ratios of chlorine reservoir species would result in high concentrations of chlorine radicals after sunrise that could have a significant effect on the chemistry in the MBL.

The nighttime mixing ratios of Cl_2 in the model are mostly below 1 pmol/mol; only in the "continental influence" run they are around 9 pmol/mol (Figure 4.1). Total reactive chlorine (the sum of all gas phase chlorine species except HCl) are

shown as Cl_x in the plots and reach values around 10 pmol/mol for the base run and around 30 pmol/mol for the "continental influence" run. Cl_x is elevated in the "continental influence" run because the sea salt aerosol is more acidic than in the base run and therefore acid displacement releases a significant amount of HCl to the gas phase which is partly recycled by the sulfate aerosol to Cl_2. Furthermore the elevated NO_x levels lead to higher $ClNO_3$ mixing ratios via the reaction $ClO + NO_2$. $ClNO_3$ is assumed to react heterogeneously with the aerosol via reactions equivalent to the ones discussed above for $BrNO_3$ yielding Cl_2.

Maximum concentrations of Cl are around $1 \cdot 10^4$ atoms/cm^3 in the base run and $1.5 \cdot 10^4$ atoms/cm^3 in the continentally influenced run. These values are in the range reported by the indirect measurements. Maximum values of 10^5 atoms/cm^3 or the very high mixing ratios of reactive chlorine during night probably imply release processes of chlorine from the sea salt aerosol that are different from the ones that are included in the model.

A recent paper by *Oum et al.* (1998) on the photolytically induced formation of Cl_2 from sea salt particles received considerable attention. However, the assumptions that were made to extrapolate the measurements to the atmosphere are questionable as pointed out by *Jacob* (2000). The proposed mechanism is roughly by a factor of 1000 too slow to be of atmospheric importance (see discussion http://dionysos.mpch-mainz.mpg.de/s̃ander/res/oumetal.html).

4.10 Variation of sea salt aerosol pH and BrO with height

The calculated pH in the sea salt aerosol bin is highest at the sea surface where alkaline particles are emitted and it decreases towards the top of the MBL (see Figure 4.9). The vertical decrease in aerosol pH is associated with increasing relative humidity and aerosol water content. This finding might seem counterintuitive in the first moment because the particles get more diluted when the aerosol water content increases and one would therefore expect the pH to get closer to 7. This increase cannot be explained by vertical gradients in acids, as the concentrations of acids like HCl and HNO_3 do not show a vertical gradient neither in the gas nor in the aqueous phase.

The experimental determination of aerosol pH is difficult because aerosol water contents are usually too small for direct pH measurements. To my knowledge no direct measurements of aerosol pH have been reported in the literature.

Indirect determinations of aerosol pH do exist and some studies either implicitly or explicitly show the phenomenon that has been observed in the model. *Fridlind and Jacobson* (2000) give an overview of estimates of marine aerosol pH. Most studies show acidified aerosol particles (note: in their Table 1 they incorrectly cited the work by *Winkler* (1986) as "observations". The numbers given by *Winkler* (1986) refer to the pH of diluted samples and not to the pH of aerosol particles. He only provided "acid fractions" as information about aerosol pH).

Chameides and Stelson (1992) calculated a decrease in sea salt aerosol pH

with increasing relative humidity in their box model. Their explanation for this behaviour, however, is based on effects of activity coefficients which was found to be insufficient (see below).

Calculations of the pH of sea salt aerosol from simultaneous measurements of gas phase HCl and HNO_3 and aerosol Cl^- and NO_3^- have been performed by *Keene and Savoie* (1998) and *Keene and Savoie* (1999). According to their data the pH in sea salt aerosol can decrease with rising relative humidity. In their table the samples on 23 April and 3 May were associated with roughly similar gas phase HCl (180 and 133 pptv, respectively) and particulate Cl^- (98 and 99 nmol/m^3, respectively). The relative humidity on 23 April was 79% and the calculated pH was 4.43 whereas relative humidity on 3 May was 93% with a calculated pH of 4.11.

Fridlind and Jacobson (2000) used the equilibrium model EQUISOLV II for analysis of the pH of sea salt aerosol from data obtained from the Aerosol Characterization Experiment (ACE 1) campaign. Their results also show a decrease of sea salt aerosol pH with increasing relative humidity. They found that 'relative humidity controlled the influence of HCl on the modeled sea salt pH more than either enrichment by secondary acids or the ambient concentration of HCl'. However, they did not provide an explanation for it.

To find the cause for this effect simulations with a box model of the MBL (based on MOCCA, *Sander and Crutzen* (1996)) were made that showed the same feature as the one-dimensional model, i.e. a decrease of pH with increasing aerosol water content. Setting activity coefficients to unity did not suppress the phenomenon which makes the explanation of *Chameides and Stelson* (1992) insufficient. Repeated reduction of the reaction mechanism in the model showed that even in the very simple system that included only HCl_g, HCl_{aq} and Cl^- and the corresponding Henry and dissociation equilibria the above described feature was still present. This indicated the importance of the high concentration of Cl^- in sea salt particles and the gas phase as reservoir for acidity in the form of HCl. Upon initialization of this idealized system only Cl^- was present, all gas phase HCl was a consequence of degassing from the aqueous phase in order to reach equilibrium between the aqueous and gas phase. It should be pointed out that the actual source of gas phase HCl plays no role. In the MBL, gas phase HCl results from reactions in the gas phase or from acid displacement reactions. Thus freshly produced sea salt particles are immediately exposed to gas phase HCl that e.g. degassed from older, already acidified sea salt particles.

The combination of high concentrations of Cl^- in the sea salt aerosol with the gas phase that acts as a reservoir for acidity mainly in the form of HCl causes this effect. A brief explanation follows.

At low liquid water contents, most HCl is in the gas phase. When the liquid water content changes, it does not affect the gas phase significantly. Relative changes in gas phase HCl (partial pressure $p(\mathrm{HCl})$) are negligible. Henry's law and the dissociation equilibrium for HCl can be combined to:

$$[\mathrm{H^+}] \times [\mathrm{Cl^-}] = k'_{\mathrm{H}} \times p(\mathrm{HCl}), \tag{4.2}$$

where square brackets denote aqueous concentrations in mol/l and $k'_H = k_A k_H$ is the product of the acidity constant (k_A) and Henry constant (k_H). The product $[\mathrm{H^+}] \times [\mathrm{Cl^-}]$ remains almost constant because p(HCl) does not change much and k'_{H} is a constant anyway. In contrast to the gas phase, a change in liquid water content *does* affect the liquid phase. When the liquid water content increases, $[\mathrm{Cl^-}]$ decreases because of the dilution effect. When $[\mathrm{Cl^-}]$ decreases, $[\mathrm{H^+}]$ must increase to keep the product constant. Therefore the pH decreases.

The extra acidity that is needed to decrease the pH comes from the gas phase via HCl. This implies thatthe total amount of both $\mathrm{Cl^-}$ and $\mathrm{H^+}$ in the aqueous phase increase (in units of mol/m^3_{air}) but the relative increase of $\mathrm{Cl^-}$ is negligible, whereas the same increase in $\mathrm{H^+}$ has a large effect. This is simply a consequence of the fact that $\mathrm{Cl^-} \gg \mathrm{H^+}$ in sea salt aerosol.

Charge balance during uptake of HCl is guaranteed as the same amount of anions ($\mathrm{Cl^-}$) as cations ($\mathrm{H^+}$) are produced.

As shown the effect does not depend on particle size but only on the high fraction of salt in the particles.

In the MBL this effect is slightly enhanced by the vertical temperature gradient. Temperature decreases with height and solubility increases with decreasing temperature. This leads to a further uptake of HCl and thereby a further decrease of the aerosol pH.

Appendix C shows an analytical solution for the very simple system HCl - $\mathrm{Cl^-}$ - $\mathrm{H^+}$.

An implication of the vertical gradient of the sea salt particle pH is that acid catalyzed bromine activation is more efficient in higher layers of the MBL. The vertical profiles of both $\mathrm{Br_x}$ and BrO show a maximum directly below the temperature inversion that caps the MBL (see Figure 4.7). In layers close to the sea surface with lower sea salt aerosol water content and high sea salt pH this leads to smaller BrO mixing ratios. The higher mixing ratios of e.g. BrO at the top of the MBL might explain difficulties to detect BrO in surface measurements in the MBL. Based on this finding it would be desirable to modify measurement instruments for the detection of halogen radicals such that information on the vertical distribution in the MBL can be obtained. As a consequence of the maximum in BrO mixing ratios at the top of the MBL, $\mathrm{O_3}$ destruction rates by bromine radicals increase with height in the MBL. If significant detrainment of MBL air into the free troposphere occurs this could lead to enhanced BrO and Br mixing ratios in this region.

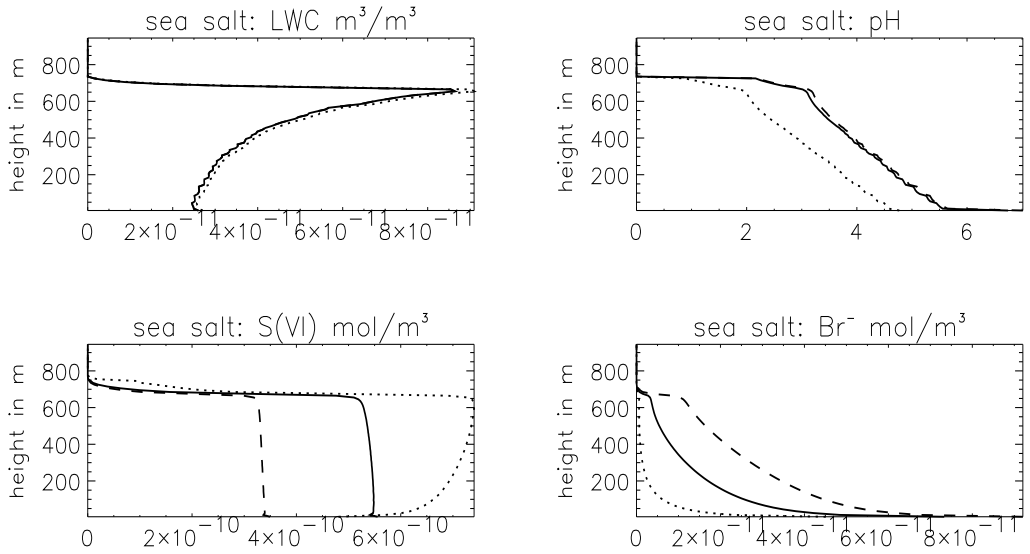

Figure 4.9: Vertical profile of some aqueous phase species as well as liquid water content (LWC) and pH for base run (solid line), the "continental influence" run (dotted line) and the "low O_3 low SO_2" run (dashed line) on the third model day at noon. LWC is the liquid water content, units are mol/m^3_{air}. The stronger decline of pH above 650 m is caused by the entrainment of acids from the free troposphere. This localized effect acts in addition to the one discussed in the text.

4.11 S(IV) oxidation

The production of S(VI) (H_2SO_4 + HSO_4^- + SO_4^{2-}) has been of interest in many studies in the past, experimental as well as model studies. When sulfate is produced in or taken up by particles it changes the microphysical and optical properties of the particles. Oxidation of S(IV) (SO_2 + HSO_3^- + SO_3^{2-}) to S(VI) is strongest in clouds, in the model runs including cloud chemistry 80 - 90 % of the total S(VI) production occurs in cloud droplets (see section 5). In the absence of clouds the mean S(VI) production is reduced to approximately 10 % with the gas phase production of H_2SO_4 by the reaction $SO_2 + OH$ being a significant contributor to total sulfate production (55 % of the mean rate in the base run). Important oxidants in the aqueous phase are H_2O_2 for low pH and O_3 for higher pH. *Vogt et al.* (1996) proposed the importance of halogens (HOCl and HOBr) in the oxidation of sulfur in sea salt aerosol as will be further studied here. Transition metal catalyzed sulfur oxidation was assumed to play a minor role in the marine cases studied here and was therefore neglected.

Oxidation by HOCl in the sea salt aerosol contributes 30 % to the total mean S(IV) oxidation rate (inluding gas phase oxidation of SO_2 by OH) in the base run and between 4 and 45 % in the other runs. 60 % of the non-sea-salt sulfate (nss-sulfate, 18 - 71 % in the other runs) is produced by HOCl. The contribution of HOBr is less as discussed in section 5.2.

Chameides and Stelson (1992) proposed that due to the high alkalinity of fresh sea salt particles O_3 would be the main oxidant for S(IV) in sea salt aerosol. *Keene and Savoie* (1998) and *Keene and Savoie* (1999) obtained sea salt aerosol pH values of 3.5 to 4.5 from measurements in moderately polluted conditions at the Bermudas. *Fridlind and Jacobson* (2000) calculated pH values between 2 and 5 from data collected in the remote MBL during the ACE 1 campaign in the Southern Ocean (40° - 55° S, 135° - 160° E). These measurement based calculations support model estimates of pH and suggest a minor role for the strongly pH dependent sulfur oxidation by O_3. In the base run O_3 contributes roughly 6 % and in the other runs between 0 % and 63 % to the mean S(VI) production in the MBL (Table 4.5). O_3 contributes between 25.1 % and 73.2 % to the nss-sulfate in the sea salt aerosol (Table 4.6, again integrated over the MBL).

Sievering et al. (1999) suggested that the carbonate buffer of the sea salt aerosol collected during the ACE-1 experiment could have been 50 % higher than in seawater due to biogenic carbonate in the ocean's surface microlayer that could have been included in sea salt particles. Sulfate production by reaction with O_3 is proportional to the available alkalinity because it can proceed only as long as the aerosol pH is above 6 and such high pH values can only be sustained while the buffer by HCO_3^- is not exhausted. In the "carbonate" run this higher alkalinity was included and a significant increase in the importance of O_3 oxidation was found. HOCl, however, was still dominating the production of S(VI) (Tables 4.5 and 4.6).

The sea salt aerosol pH in the "strong wind" run is 1 (upper MBL) to 3 (lower MBL) pH units greater than in the base run ensuring that O_3 plays an important role for S(VI) production also after the initial acidification of the aerosol. The importance of O_3 oxidation increased significantly but still approximately 30 % of the nss-sulfate was produced by HOCl and HOBr. This, however, might point to a weakness of the model: all sea salt aerosol particles are lumped together in one chemical "bucket", including small (more acidic) and large (more alkaline) as well as fresh (more alkaline) and aged (more acidic) particles together. In the "strong wind" run sea salt aerosol mass is dominated by very large and fresh particles which results probably in too high pH values and therefore in an overprediction of the importance of the O_3 path in S(VI) production.

Inclusion of halogen chemistry resulted in a 25 % increase of the mean S(IV) oxidation rate (compare the tabulated values of the "halogen off" and base runs).

In Table 4.5 conversion times are given for the gas and aqueous phase. According to these numbers the lifetime of SO_2 against oxidation by OH is of the order of 10^7 s (= 115 days) in the gas phase. The lifetime of S(IV) in the aqueous phase is significantly shorter (0.02 s - 15 min). It is important to mention that uptake by the aerosols is rate limiting with conversion times of the order of 10 - 1000 days.

The availability of SO_2 is a prerequisite for the production of S(VI). In the model a constant flux of DMS was used as the only source for SO_2 (via reactions discussed in the next section). The flux of DMS determines the mixing ratio of

Table 4.5: S(IV) oxidation rates for the cloud-free runs.

run	S(IV) oxidation rate	conversion time (s)			relative contribution to total oxidation rate (%)						
						sulfate		sea salt			
	(mol/(m^3 d))	gas phase	sulfate	sea salt	SO_2+OH	O_3	H_2O_2	O_3	H_2O_2	HOCl	HOBr
base run	$5.39 \cdot 10^{-10}$	$1.4 \cdot 10^{7}$	$2.0 \cdot 10^{-2}$	$0.9 \cdot 10^{3}$	55.4	0.0	0.8	5.7	7.0	29.6	1.5
halogen off	$4.29 \cdot 10^{-10}$	$1.4 \cdot 10^{7}$	$1.6 \cdot 10^{-2}$	$2.7 \cdot 10^{3}$	71.2	0.0	1.3	16.6	10.5	-	-
aerosol off	$2.99 \cdot 10^{-10}$	$1.5 \cdot 10^{7}$	-	-	100	-	-	-	-	-	-
low O_3 low SO_2	$3.38 \cdot 10^{-10}$	$1.3 \cdot 10^{7}$	$1.8 \cdot 10^{-2}$	$1.9 \cdot 10^{3}$	56.6	0.0	1.2	15.9	9.2	15.7	1.4
cont. influence	$18.60 \cdot 10^{-10}$	$1.6 \cdot 10^{7}$	$2.7 \cdot 10^{-2}$	9.4	85.5	0.0	0.6	0.0	9.8	4.0	0.0
winter	$2.73 \cdot 10^{-10}$	$6.7 \cdot 10^{7}$	$3.4 \cdot 10^{-2}$	$1.5 \cdot 10^{3}$	19.5	0.0	0.9	21.0	9.3	45.6	3.5
spring	$3.76 \cdot 10^{-10}$	$2.3 \cdot 10^{7}$	$3.6 \cdot 10^{-2}$	$1.4 \cdot 10^{3}$	44.7	0.0	0.5	11.0	4.2	37.4	2.1
high BL	$5.62 \cdot 10^{-10}$	$1.3 \cdot 10^{7}$	$2.6 \cdot 10^{-2}$	$1.1 \cdot 10^{3}$	71.6	0.0	0.3	1.7	3.5	18.2	4.7
strong wind	$19.45 \cdot 10^{-10}$	$2.1 \cdot 10^{7}$	$4.7 \cdot 10^{-3}$	$0.7 \cdot 10^{3}$	7.6	0.3	0.0	62.5	1.1	16.9	11.5
carbonate	$6.18 \cdot 10^{-10}$	$1.4 \cdot 10^{7}$	$1.9 \cdot 10^{-2}$	$1.2 \cdot 10^{3}$	47.3	0.0	0.7	17.4	6.0	27.2	1.4
iodine	$5.91 \cdot 10^{-10}$	$1.4 \cdot 10^{7}$	$9.1 \cdot 10^{-3}$	$6.9 \cdot 10^{3}$	50.3	1.0	0.6	3.9	5.2	37.5	1.5
high DMS	$10.96 \cdot 10^{-10}$	$1.2 \cdot 10^{7}$	$2.0 \cdot 10^{-2}$	$6.2 \cdot 10^{3}$	74.8	0.5	0.9	0.6	12.6	10.4	0.0

The numbers are means over the MBL over the 2nd and 3rd model day. The contribution of the individual path is given as relative contribution to the total oxidation rate. For the gas and aqueous phases a mean conversion time is given. Note that the conversion time for the aqueous phases includes only reaction within the particles. The conversion time for uptake is on the order of 1000 days for sulfate particles and 10 days for sea salt particles, respectively, imlpying that uptake is the rate limiting step.

Table 4.6: Comparison of oxidation pathways for the cloud-free runs.

run		O_3	H_2O_2	HOCl	HOBr	uptake from gas phase
base run	sulfate	-	1.6 %	-	-	98.4 %
	sea salt	11.7 %	14.4 %	61.0 %	3.0 %	3.8 %
halogen off	sulfate	-	1.9%	-	-	98.1 %
	sea salt	49.4 %	31.3%	-	-	18.2%
low O_3 low SO_2	sulfate	-	2.2 %	-	-	97.8%
	sea salt	33.5 %	19.6%	33.1 %	2.9 %	10.7 %
cont. influence	sulfate	-	0.7 %	-	-	99.3 %
	sea salt	-	47.7 %	19.6 %	-	32.6%
winter	sulfate	-	5.3 %	0.2 %	-	94.5 %
	sea salt	25.6 %	11.4 %	55.6 %	4.3 %	2.9 %
spring	sulfate	-	1.3 %	-	-	98.7 %
	sea salt	18.7 %	7.2 %	63.6 %	3.6 %	6.9 %
high BL	sulfate	-	0.6 %	-	-	99.4 %
	sea salt	4.4 %	9.3 %	48.9 %	12.5 %	24.8 %
strong wind	sulfate	4.2 %	0.9 %	-	-	94.9 %
	sea salt	67.4 %	1.2 %	18.2 %	12.4 %	0.9%
carbonate	sulfate	-	1.6 %	-	-	98.4 %
	sea salt	31.1 %	10.7 %	48.5 %	2.5 %	7.2%
iodine	sulfate	2.0%	1.2 %	-	-	97.0 %
	sea salt	7.4 %	10.0 %	71.3 %	3.0 %	8.3%
high DMS	sulfate	0.8 %	1.3 %	-	-	97.9%
	sea salt	1.8 %	41.5 %	34.4 %	0.3 %	21.9 %

Relative importance of uptake from the gas phase and the different reaction pathways for the production of nss-sulfate in the aerosol (mean over the MBL over the 2nd and 3rd model day).

SO_2 as can be seen from Figure 4.1 where the initially low SO_2 mixing ratio in the run "low O_3 low SO_2" was rapidly increased by the prescribed DMS flux to the same levels as in the base run. In the "high DMS" run the flux of DMS was increased from $2 \cdot 10^9$ to $10 \cdot 10^9$ molec/(cm^2 s) resulting in a significant increase of S(IV) oxidation. The steady state mixing ratio of SO_2 adjusted to the higher flux would roughly be 500 pmol/mol which is not reached during the 3 model days taken as basis for the rates tabulated, the actual implication of the increased DMS flux would therefore be higher.

4.12 DMS chemistry

Charlson et al. (1987) proposed that DMS and its oxidation products play a major role for the production of cloud condensation nuclei in the MBL and thereby in the regulation of climate. DMS is produced by phytoplancton in the oceans and then degasses to the atmosphere.

Using a photochemical box model and laboratory measurements of the reaction of BrO with DMS *Toumi* (1994) postulated that BrO could be an important sink for DMS in the marine atmosphere. *Ingham et al.* (1999) presented new kinetic data for this reaction and stated that the presence of BrO in the atmosphere could be detected by measurements of the ratio of DMSO/DMS which they calculated to be ≤ 0.01 in the absence of BrO and ≥ 0.1 in the presence of 1 pmol/mol BrO. Under the conditions present in the base run, oxidation of DMS by BrO contributes roughly 44 % to the oxidation of DMS. OH is responsible for another 52 % whereas the reaction DMS + NO_3, which is the only chemical loss for DMS during night, contributes only about 4 %, due to the small NO_3 concentrations in the model runs. This implies that oxidation rates of DMS could have been significantly underestimated by models that neglect the chemistry of bromine. In the "low O3, low SO2" run, oxidation of DMS increased SO_2 from initially 20 pmol/mol to the steady state levels of SO_2 of the base run (around 80 pmol/mol, see Figure 4.1).

The product of DMS + BrO is DMSO, which is also partially produced in the reaction of OH with DMS (reaction G118 in Table D.1). Apart from uptake on particles reaction with OH is the only sink for DMSO. Therefore a steady state concentration of DMSO is reached, which shows a diurnal variation (see Figure 4.10). In the absence of BrO the DMSO concentration is rather small. It is significantly enhanced by the inclusion of the production of DMSO by BrO. In a model run without the inclusion of halogen chemistry the ratio DMSO / DMS is roughly between 0.008 at sunrise and 0.02 at local noon. Including halogen chemistry this ratio rises to about 0.1 just before sunrise (0.02 before the halogen chemistry is completely developed) and roughly 0.3 shortly later when BrO reaches its maximum. At local noon the ratio has decreased again to about 0.1.

A recent study by *Falbe-Hansen et al.* (2000) shows that reaction of DMSO with Cl and NO_3 might be important as well, but typical mixing ratios and the rate constants by *Falbe-Hansen et al.* (2000) indicate that reaction with OH should be at least 2 orders of magnitude faster than with NO_3 or Cl.

The diurnal variation of DMSO (Figure 4.10) shows a similar behaviour as BrO (Figure 4.1) with a peak in the morning and the afternoon and a minimum around noon. For an explanation of the diurnal variation of BrO see section 4.3.

Chen et al. (2000) presented a comparison of field data (*Bandy et al.* (1996)) with model results indicating that the reactions included in their model lead to an underestimation of DMSO mixing ratios (10 to 50 pmol/mol, mean 25 pmol/mol) by roughly a factor of 50. They, however, did not consider the production of DMSO by BrO. In my model runs the influence of bromine chemistry leads to a factor of 2 to 25 difference in DMSO between the base run and the run without halogen chemistry (Figure 4.10).

Chen et al. (2000) discussed the potential role of Cl in the oxidation of DMS. They include a constant Cl_2 source into their model that produced a strong Cl peak due to photolysis in the morning which enhances the agreement between model and observation in the morning where observations show an earlier de-

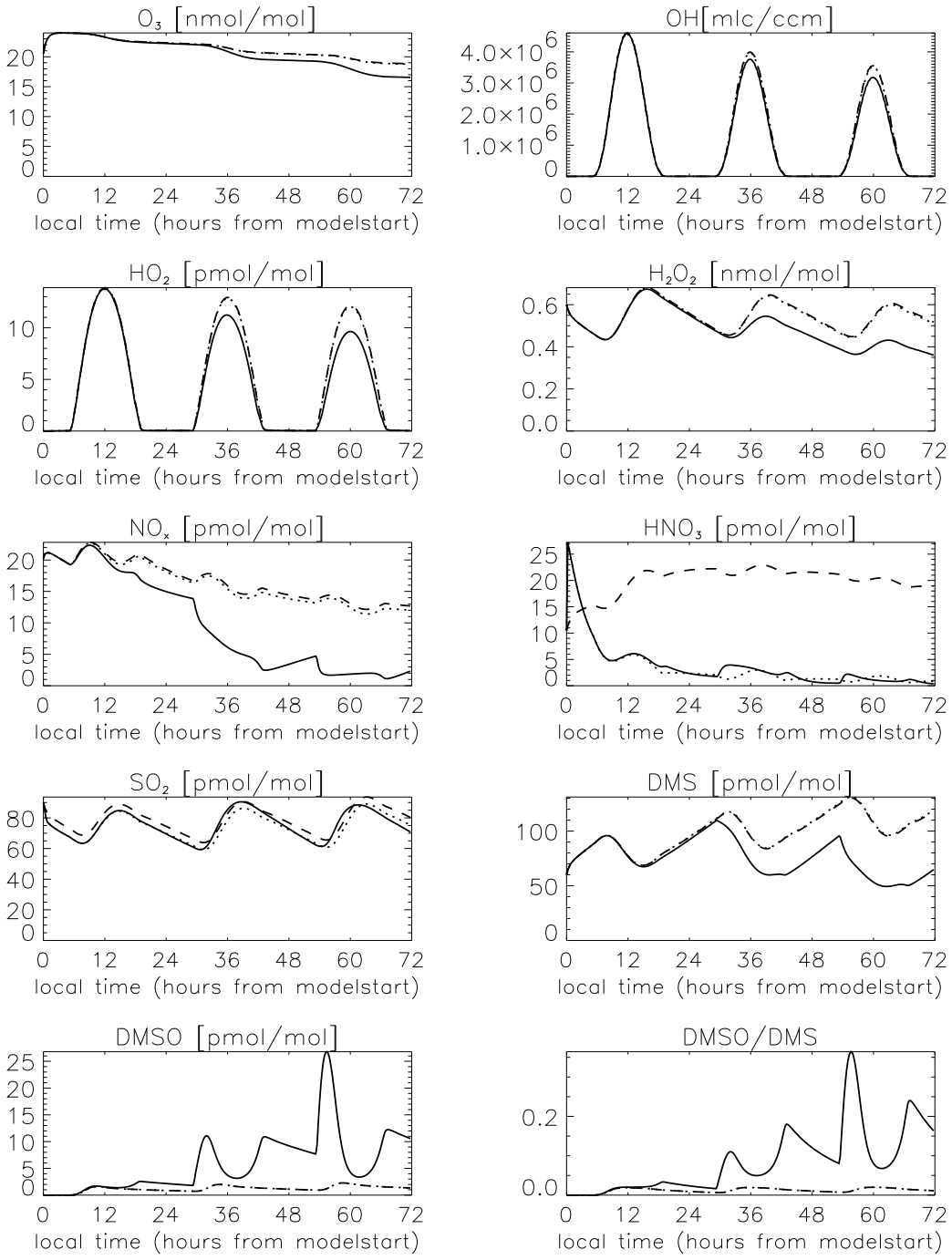

Figure 4.10: Evolution with time of the main gas phase species for the base run (solid line), the run without halogen chemistry (dotted line) and the run without aerosol chemistry (dashed line) (in 50 m). In some plots the dotted and dashed lines lie on top of each other.

crease of DMS than their model without Cl. They show, however, another plot (their Figure 4) where both in the early morning and late afternoon agreement

Table 4.7: Ratio of MSA to nss-sulfate (from uptake from the gas phase and production in the particles) in the aerosol.

	sulfate	sea salt
base run	0 - 0.13	0 - 0.5
hal off	0 - 0.075	0 - 0.42
low O_3 low SO_2	0 - 0.105	0 - 0.7
cont. influence	0 - 0.11	0 - 0.45
winter	0 - 0.16	0 - 0.65
high BL	0 - 0.05	0 - 0.28
strong wind	0 - 0.1	0 - 0.3
carbonate	0 - 0.16	0 - 0.65
iodine	0 - 0.13	0 - 0.47

between their model and observations is less good. In my model runs with halogen chemistry the decrease of DMS mixing ratios starts earlier in the morning than without inclusion of halogen or aerosol chemistry (Figure 4.10). This is due to reaction of DMS with BrO. This reaction could also explain an increased destruction of DMS in the evening when the second peak of BrO leads to higher rates of this reaction than during the day. Reaction rates of Cl + DMS in the model are only 10 % of BrO + DMS, indicating that the importance of chlorine was overestimated by *Chen et al.* (2000) who did not consider the reaction BrO + DMS $\longrightarrow$ Br + DMSO.

Ayers and Gillett (2000) compared the diurnal variation of DMS from measurements with model results that do not include halogen chemistry. In the measurements they showed the DMS loss starts earlier than in their model (their Figure 6) which might again point to the involvement of early morning DMS destruction by BrO.

Methanosulfonic acid (CH_3SO_3H, MSA) is an end product of the DMS oxidation which can be found in the particulate phase due to its high solubility. In the simplified DMS oxidation scheme that is used here, MSA is formed in the reaction of DMSO with OH (*Pham et al.* (1995)) and in CH_3SO_3 with HO_2. The ratio of MSA to nss-sulfate in the aerosol particles is shown in Table 4.7. Measurements (e.g. *Sciare et al.* (2000)) show a strong temperature dependence of this ratio with low values at high temperatures and higher values at lower temperatures. Values determined by field measurements are between 0.02 and 0.5 (e.g. *Capaldo and Pandis* (1997), *Ayers et al.* (1999), *Sciare et al.* (2000)). The model derived values are in this range, indicating that the major features of the chemistry are included in the simple reaction scheme employed for MSA.

4.13 Iodine chemistry

The chemistry of iodine in the MBL has been the subject of some studies in the last decades (see *Vogt et al.* (1999) for an overview) but in recent years it received considerably more attention due to the detection of IO in the MBL (*Alicke et al.* (1999) and *Allan et al.* (2000)). Maximum mixing ratios measured by *Alicke et al.* (1999) were 6 pmol/mol at Mace Head, Ireland. *Allan et al.* (2000) measured IO at Tenerife and Cape Grim, Tasmania with a mean mixing ratio of about 1 pmol/mol. These data suggest a rather widespread presence of IO although it could not be measured on all days of the measurement campaigns. *McFiggans et al.* (2000) used a box model that was constrained with data from measurements and could show the importance of the cycling of iodine species on aerosol particles for the Mace Head and Tenerife measurements. They used a simplified version of the mechanism suggested by *Vogt et al.* (1999).

In recent field campaigns also OIO was detected in the MBL at Mace Head (*Hebestreit et al.* (2000)) and Tasmania (*Plane et al.* (2000)). OIO is known to be formed in the self reaction of IO and in the reaction of IO with BrO (*Bedjanian et al.* (1998), *Misra and Marshall* (1998)). Further reactions of OIO are highly uncertain. *Ingham et al.* (2000) studied the photolysis of OIO and found that OIO is photochemically very stable as already calculated by *Misra and Marshall* (1998). *Cox et al.* (1999) proposed that OIO could be an intermediate in the formation of particulate iodate.

Particulate iodine is found in marine aerosol samples 100 - 1000 times enriched above the sea water ratio (see e.g. *Vogt* (1999) for a review) but it is not clear in which chemical state the iodine is present. Some studies reported it to be IO_3^- but in others no IO_3^- was found (see references and discussion in *McFiggans et al.* (2000)). Based on measurements of aerosol composition, *Baker et al.* (2000) state that "iodine is present in aerosol in varying proportions as soluble inorganic iodine, soluble organic iodine and insoluble, or unextractable, iodine."

In contrast to gas phase chlorine and bromine that is mainly released by sea salt particles, iodine compounds originate from biogenic alkyl iodides released by various types of macroalgae and phytoplankton in the sea. Photodissociation then produces I radicals that mainly react with O_3 to IO. The same oceanic emission rates of alkyl iodides as in *Vogt et al.* (1999) were assumed here: CH_2I_2, CH_2ClI, CH_3I, and iC_3H_7I of $3.0 \cdot 10^7 cm^{-2}s^{-1}$, $2.0 \cdot 10^7 cm^{-2}s^{-1}$, $0.6 \cdot 10^7 cm^{-2}s^{-1}$, and $1.0 \cdot 10^7 cm^{-2}s^{-1}$, respectively.

The chemical mechanism that is used here is based on *Vogt et al.* (1999), see Tables D.1 - D.3 for a listing of the reactions used in the model. The chemistry of OIO has been added. HOI and INO_3, which are formed in the reaction of IO with HO_2 and NO_2, respectively, can be taken up by the aqueous phase where conversion to the much less soluble species ICl, IBr, I_2 takes place. These species degas from the aqueous phase and are photolyzed producing halogen radicals pointing again to the importance of cycling of chemical species between gas and aqueous phase.

The reactions of OIO in the model include production in the self reaction of

IO and in the reaction IO + BrO and sinks by reaction with OH and NO and heterogeneous reaction on aerosol surfaces. The rate constant for OIO + OH was estimated to be the same as for OClO (*DeMore et al.* (1997)) as no other information on OXO + OH is available. For the reaction of OIO with NO the rate constant was assumed to be 5 times faster than the reaction of OBrO with NO (*Li and Tao* (1999)), because the OBrO reaction is also 5 times faster than the OClO reaction (*DeMore et al.* (1997)).

No further reactions of OIO were assumed because too little information is available. Possible reactions of OIO during the night could include reaction with O_3 and NO_3, but for OClO reaction with O_3 is known to be slow (*DeMore et al.* (1997)) and no evidence for a homogeneous reaction between OClO and NO_3 could be found (*Boyd et al.* (1996)). There is clearly a need for more kinetic data on iodine chemistry especially iodine radical and aqueous chemistry.

The uptake coefficient for OIO on aerosol surfaces was assumed to be $\gamma = 0.01$ with the products IO_2^- (10 %) and HOI (90 %). These speculative assumptions were made to reproduce typical mixing ratios of the order of 1 pmol/mol for IO and a decline of OIO during the night with an associated accumulation of particulate iodine in the aerosol. Reaction paths for iodine in the aqueous phase are highly uncertain, so the production of IO_2^- which is assumed to further react to IO_3^- should be understood as one possible way for producing stable iodine compounds in the aqueous phase via OIO as suggested by *Cox et al.* (1999). In the model IO_3^- is the only final stable aqueous phase species but further yet unidentified stable iodine species could exist in the atmosphere. If iodic acid (HIO_3) is a product of OH + OIO, uptake of HIO_3 into the aqueous phase and dissociation could be another possible path of IO_3^- formation.

The amount of particulate iodine formed in the model (4.8 pmol/mol in sulfate and 1.6 pmol/mol in sea salt particles after 3 days) is in the range of measurements reported by *Vogt* (1999).

As already discussed by *Vogt et al.* (1999) the activation of chlorine and bromine chemistry is accelerated by iodine chemistry due to the reaction of HOI in the aqueous phase with Cl^- and Br^- producing ICl and IBr which escape to the gas phase, photolyze and produce halogen radicals that continue the reaction cycles discussed above. Figure 4.11 shows the increases in the mixing ratios of gas phase chlorine and bromine species. Total inorganic iodine consists mainly of OIO during day and of ICl during night. Maxima of ICl and IBr mixing ratios are below the inversion at the top of the MBL. The inclusion of iodine chemistry has a greater effect on gas phase chlorine (Cl_x) than on bromine (Br_x). This is caused by stronger fluxes of ICl from the sea salt aerosol to the gas phase than that of IBr, due to differences in the rate constants of the IX production reactions Ai2 - 5 (keep in mind, that $[Cl^-] \gg [Br^-]$).

The maximum mixing ratios of IO in the model are between 0.7 and 1.0 pmol/mol. Inclusion of iodine chemistry increases chemical net O_3 destruction by up to 20 % compared to the base run; the total contribution of halogens was 39 %. Destruction of O_3 in the IO + HO_2 cycle is more important than by O_3 + HO_2; only photolysis of O_3 followed by the production of OH is more im-

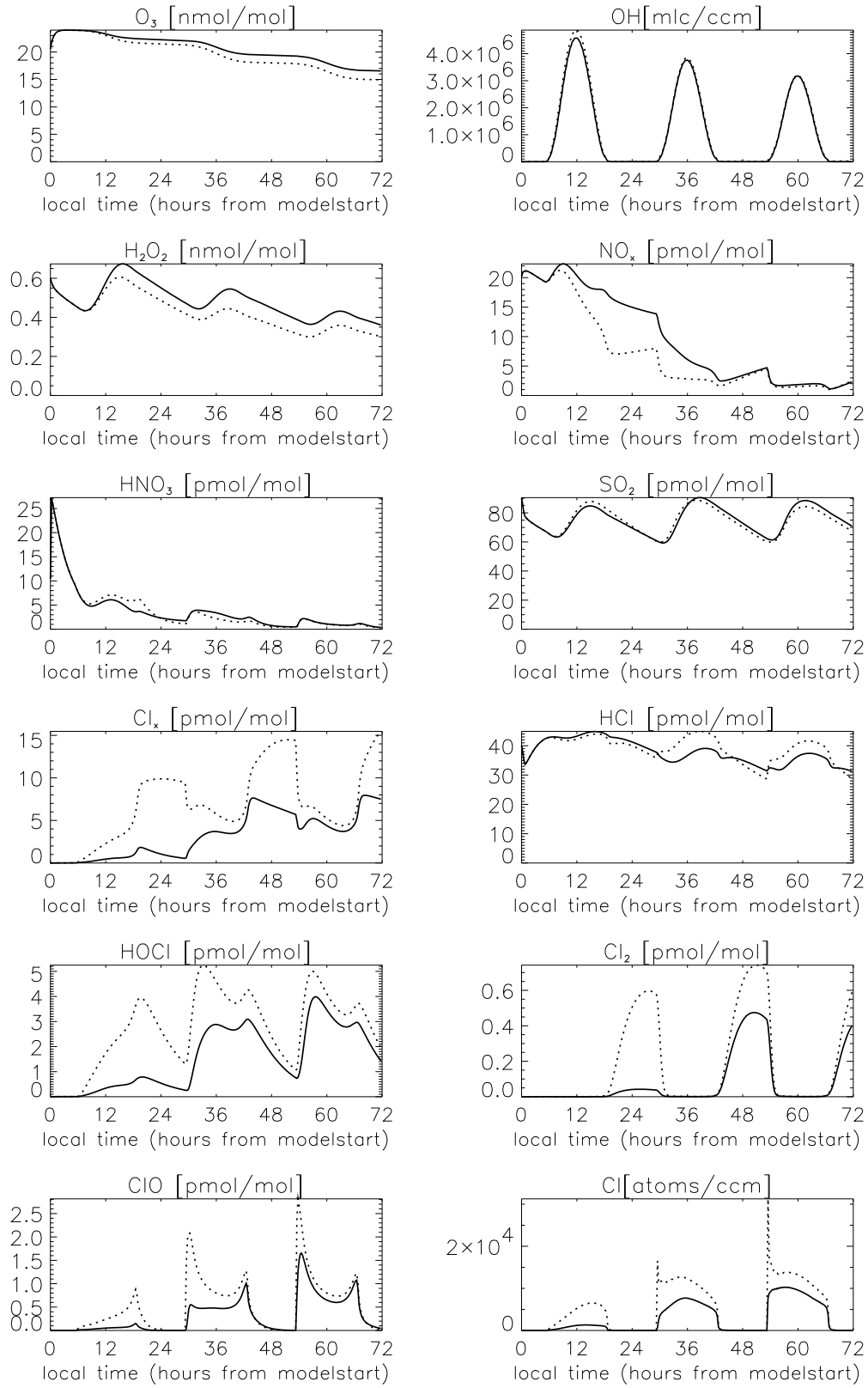

Figure 4.11: Evolution with time of the main gas phase species for the base run (solid line) and for the iodine run (dotted line) (in 50 m).

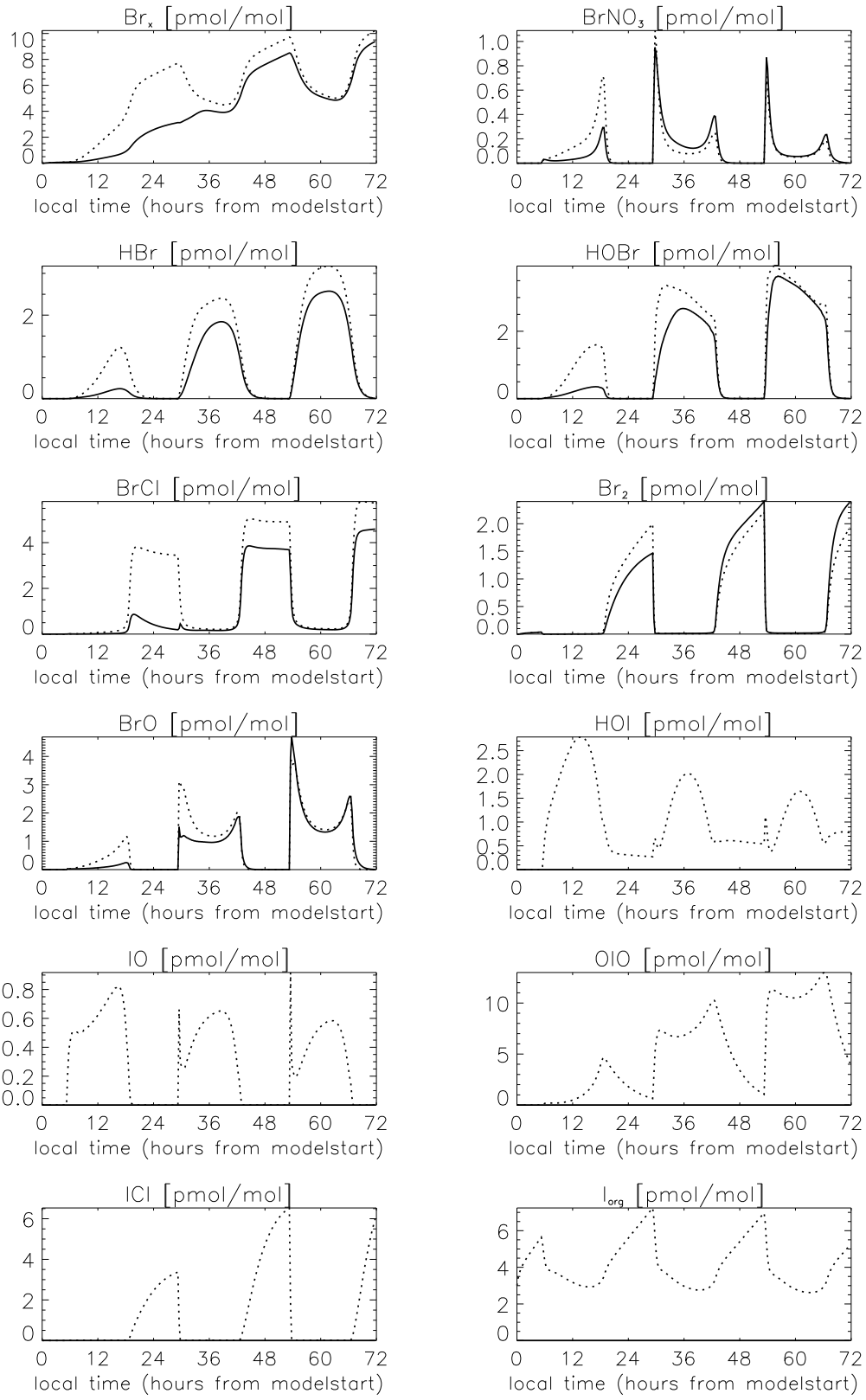

Figure 4.11: Continued.

portant than $IO + HO_2$. IO decreases with height (because the organic precursor gases are emitted at the surface) but the reaction $IO + HO_2$ stays more important than $O_3 + HO_2$. O_3 destruction by bromine and chlorine also increased as a consequence of the increased mixing ratios of these species. These results are in agreement with the findings of *Vogt et al.* (1999).

In the model, the reaction of IO with BrO is the major source for OIO. OIO is already produced at sunrise but maximum mixing ratios are calculated for the late afternoon, when loss of OIO by reaction with NO and OH is already slow but sufficient BrO is still available to produce OIO. This delay of the appearance of the maximum OIO mixing ratios with regard to IO was observed in the field (*Hebestreit et al.* (2000), *Plane et al.* (2000)). The reaction cycle as included in the model would imply the presence of BrO at these sites, although it could not be measured above the detection limit of roughly 3 pmol/mol (B. Allan, pers. comm.). Again it should be said that the results of the OIO chemistry rely on the assumptions that were made.

The diurnal variation of IO does not show the same behaviour as that of ClO and BrO, whereas in the model runs conducted by *Vogt et al.* (1999) a double peak in the diurnal variation of IO appeared. The difference is due to the change of the product of the reaction IO + BrO. In *Vogt et al.* (1999) Br and I were assumed to be the products of this reaction. Here OIO is formed which is supported by recent laboratory experiments (*Bedjanian et al.* (1998)). Br and I react rapidly with O_3 to produce BrO or IO but the assumed reactions of OIO are slower, preventing rapid recycling of IO. This makes the reaction IO + BrO an important sink for IO especially at high solar zenith angles. The peak of IO at sunrise is caused by rapid photolysis of mainly ICl to I and Cl followed by reaction of I with O_3.

Chapter 5

Chemistry of the cloudy MBL

To study the influence of clouds on the cycles of halogen species that were discussed above and to see the effects of halogens on the oxidation of sulfur in clouds, several model runs were performed where the initial and boundary conditions were chosen such that a stratiform cloud develops in the model. Results from 2 runs with different wind velocities are discussed.

In the standard cloud run the cloud top is stable at 750 m and the cloud depth varies between 200 m during the day and 450 m during the night. Maximum liquid water content (LWC) is roughly 0.75 g/m^3 before sunrise and 0.45 g/m^3 in the afternoon.

In the "strong wind" run the geostrophic windspeed was increased resulting in surface windspeeds of roughly 11 m/s compared to 6 m/s in the base cloud run. The resulting increase in emissions of sea salt aerosol particles and exchange of heat and moisture between ocean and atmosphere lead to a higher maximum cloud LWC (0.95 g/m^3), higher maximum cloud depths (up to 600 m now), increased temperatures (0.5 to 1 K), increased absolute and relative humidity, and a very slow growth of the MBL height (ca. 25 m in 3 days). Turbulent kinetic energy increased two- to threefold in the sub-cloud layer.

The difference of cloud depth during day and night is a consequence of the dynamical decoupling of cloud and sub-cloud layer during day which results in a smaller supply of humidity from the sea surface to the cloud layer during day. Furthermore the entrainment of dry and warm air from the free troposphere is confined to the cloud layer only, resulting in smaller LWC. The main cause for this decoupling are vertical differences in the short- and longwave radiative heating rates. Solar heating of the cloud during daylight hours is effective over the whole cloud depth, whereas the longwave radiative cooling of the cloud is effective only in the uppermost layers of the cloud. Furthermore, droplet evaporation (and therefore cooling of the air) is reduced at the cloud base when solar heating is active during the day. This leads to a temperature increase at the cloud base and a stabilization of the sub-cloud air and therefore to the decoupling (see e.g. *Duynkerke* (1989), *Driedonks and Duynkerke* (1989) and *Bott et al.* (1996)) which is for instant apparent as a minimum in the turbulent kinetic energy at cloud base (see Figures in *Bott et al.* (1996)).

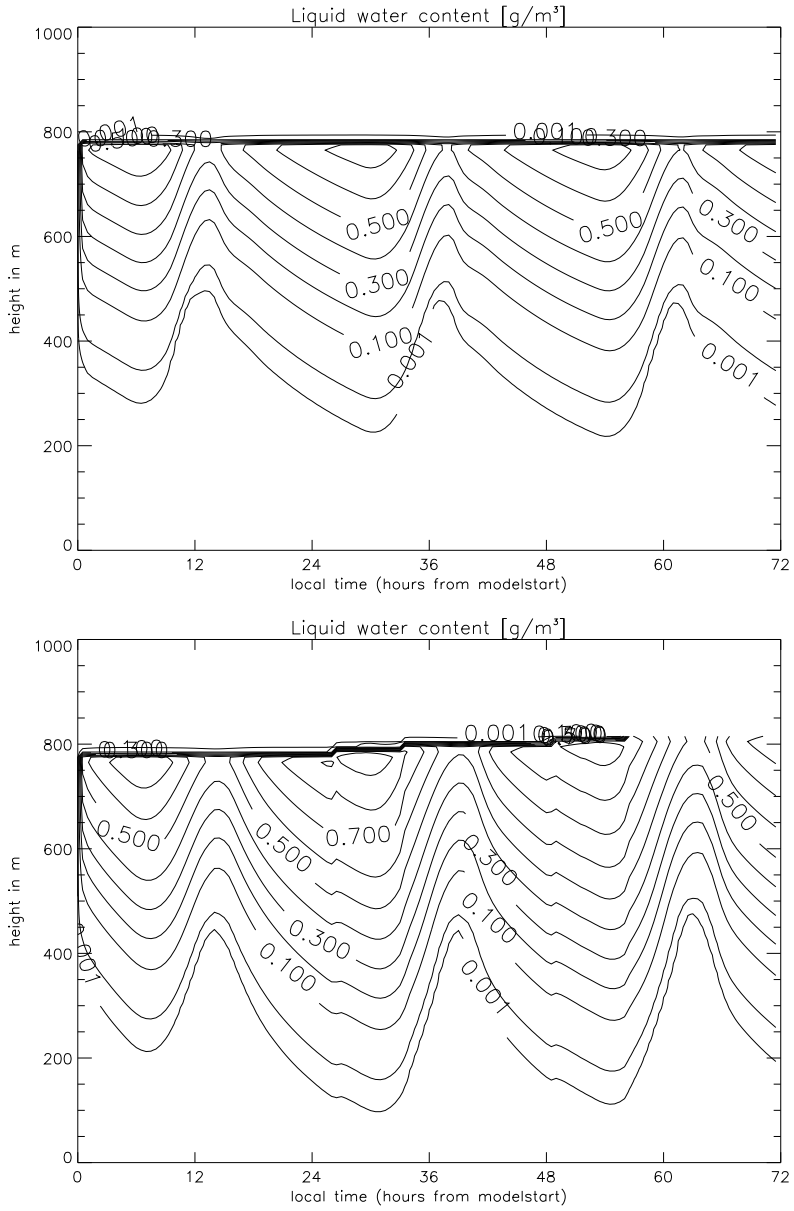

Figure 5.1: Contour plot of the LWC (in g/m^3) as a function of time and height of the standard cloudy run (top panel) and the "strong wind" cloud run (lower panel). Contour levels are 0.001, 0.01, 0.1, 0.2, 0.3, 0.4, 0.5, 0.6, 0.7, 0.8, 0.9 g/m^3.

Figure 5.1 shows a contour plot of the LWC where the diurnal variation in cloud base height can clearly be seen.

In the cloud runs soluble species like NH_3 or SO_2 are rapidly taken up by the cloud and are also depleted below cloud base during the first night. This is a consequence of the well mixed MBL during night that ensures a rapid exchange of cloud and sub-cloud air. The dynamical decoupling of cloud and sub-cloud layers during day is reflected in the vertical gradient of the insoluble DMS. DMS

is emitted from the sea surface at the same rate during day and night but is accumulated below the cloud only during day, even though the chemical sinks for DMS are stronger than during the night. At noon DMS is roughly 55 pmol/mol below cloud and less than 40 pmol/mol within the cloud, whereas at midnight the mixing ratio is around 45 pmol/mol throughout the MBL, showing no vertical gradient below and within the cloud. DMS starts to rise shortly after noon in the "strong wind" cloud run (see Figure 5.2) but drops significantly shortly after. In this run the sub-cloud layer is less deep than in the base cloud run, so DMS emissions are confined to a smaller column of air leading to a greater increase. The drop is caused by the re-coupling of cloud and sub-cloud air followed by vertical equilibration of DMS mixing ratios in the MBL.

5.1 Gas phase chemistry

The most striking difference in the gas phase halogen species between aerosol only and cloud model runs are the diurnal cycles of Cl_x and Br_x (see Figure 5.2 vs. Figure 4.1) which show maxima during daylight and very small mixing ratios during night in the cloudy runs. These differences occur also close to the surface and not only in cloudy layers. Furthermore, in the cloud runs, total gas phase bromine and chlorine is less than in the cloud-free runs, but the activation is quicker due to a lower pH and a higher LWC of the sea salt aerosol. Sub-cloud halogen mixing ratios of halogens are a lot higher than in the cloud due to the high LWC of the cloud and the associated high aqueous fractions.

During day the gas phase halogen mixing ratios are a lot higher in the sub-cloud layers than inside the cloud as can be seen from comparison of Figures 5.2 and 5.3. The soluble species like HOBr are mainly partitioned to the cloud droplets but BrO mixing ratios are comparable to sub-cloud layers.

In the cloud-free runs Br_2, BrCl and Cl_2 accumulate during the night resulting in highest Cl_x and Br_x mixing ratios (see above). Degassing of Br_x from sub-cloud aerosol particles is weak during night and most of it is immediately taken up by cloud droplets at higher levels. Br^- remains in the sea salt and the acidic sulfate aerosol particles during night because HOBr, which is needed for the acid-catalyzed activation mechanism (equilibria I.2 and I.10) is almost exclusively partitioned to the cloud droplets during night. In the cloud droplets the net direction of the equilibria I.2 and I.10 is towards Br^- and Cl^- because the forward rates are third order and therefore a lot slower in the diluted cloud droplets, whereas the backward reactions are first order and therefore not as strongly influenced by dilution. Uptake of gas phase Br_x during afternoon and night by the cloud droplets is further enhanced by the growth of the cloud depth and the stronger mixing and re-coupling of cloud and sub-cloud layers. The scavenging of bromine and chlorine is so efficient that hardly any halogens can be found in the gas phase during the night over the whole depth of the MBL.

The accumulation of photolyzable bromine in the cloud-free runs during the night in the gas phase leads to the above described rapid increases in BrO during

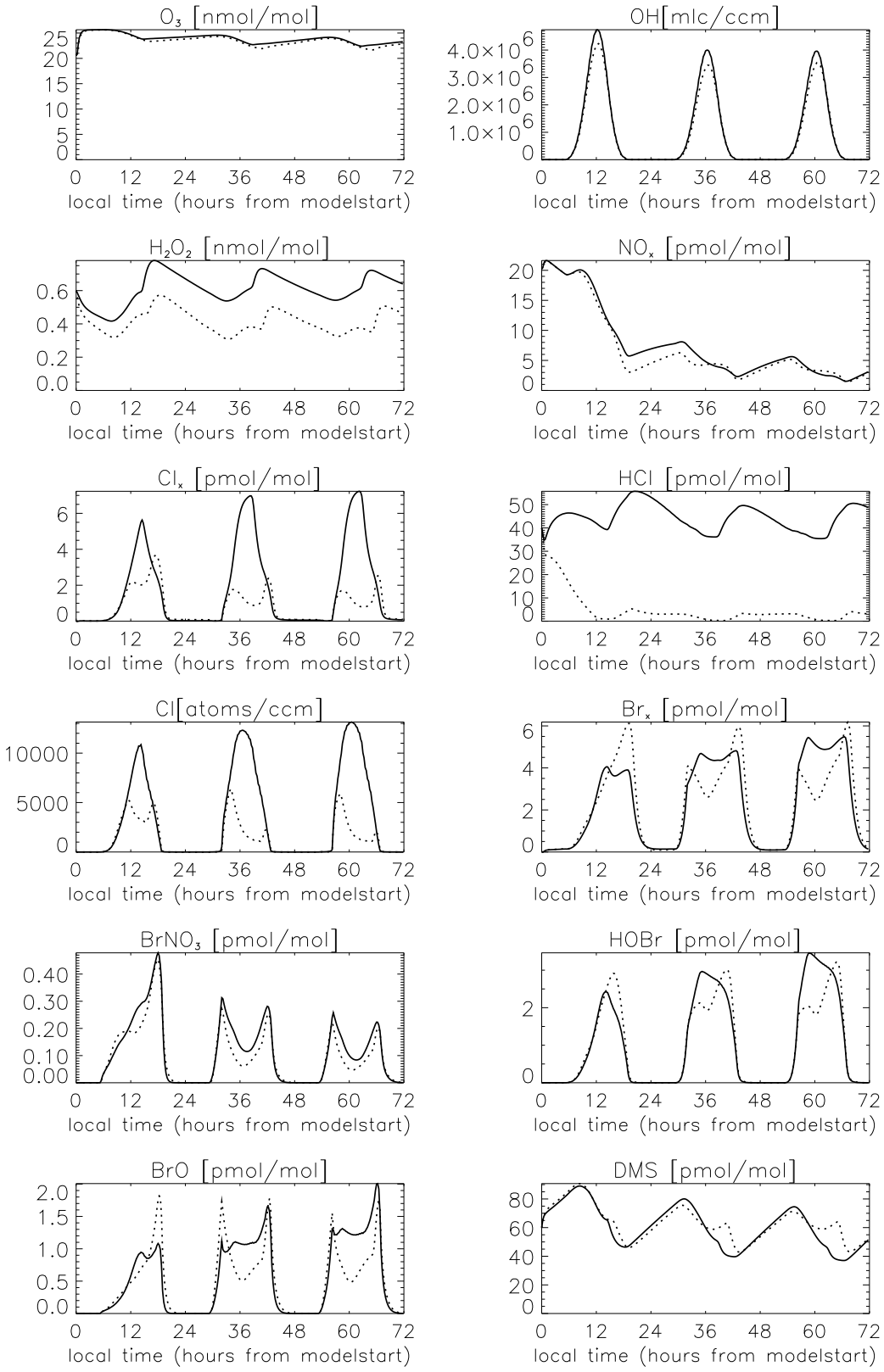

Figure 5.2: Evolution with time of the main gas phase species for the cloud base run (solid line) and the cloud "strong wind" run (dotted line) (in 50m).

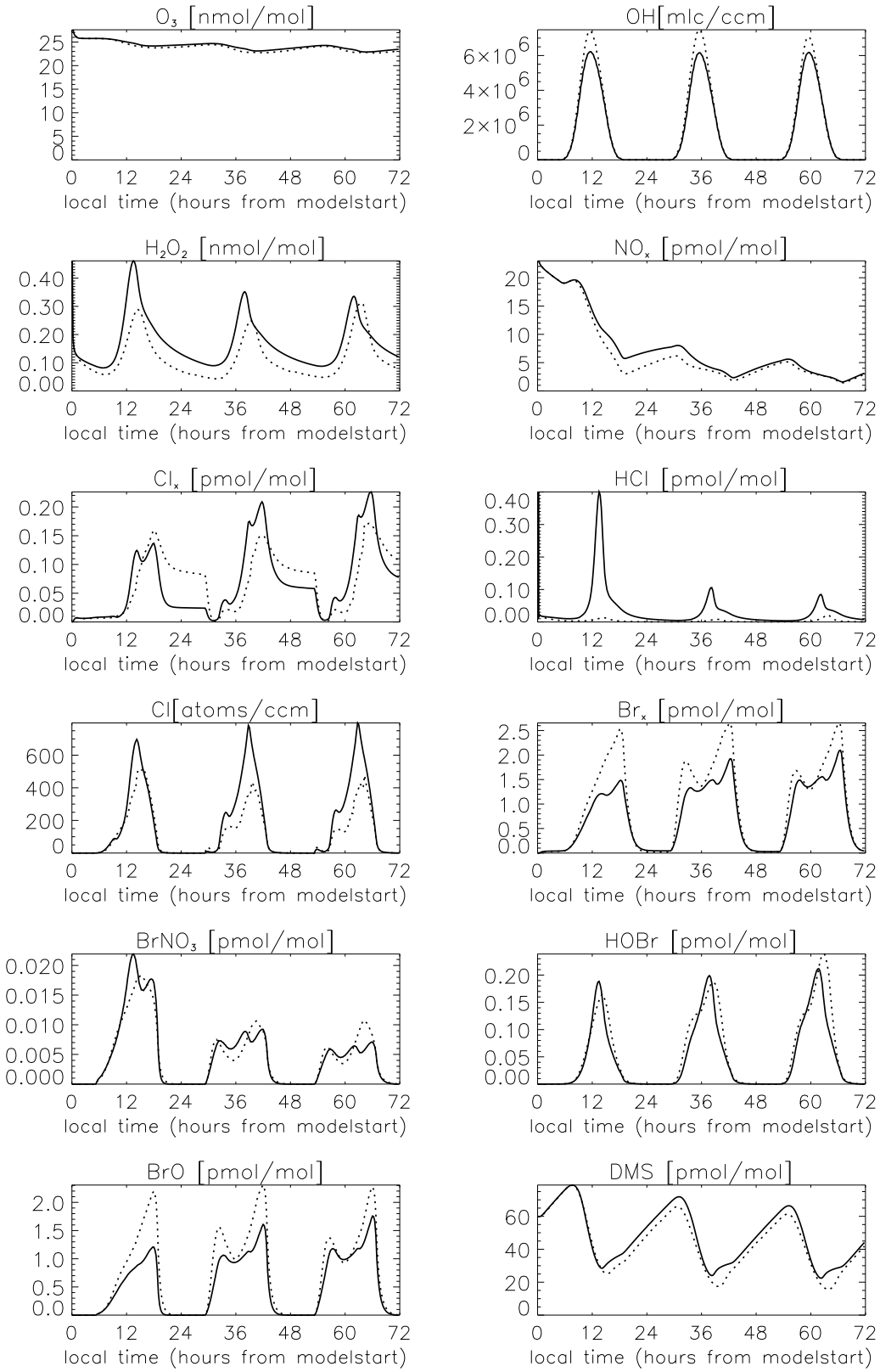

Figure 5.3: Evolution with time of the main gas phase species for the cloud base run (solid line) and the cloud "strong wind" run (dotted line) (in 650m, i.e. within the cloud).

sunrise. In the cloud runs production of BrO is delayed because no photolyzable bromine is present in the gas phase at sunrise. In the cloud runs every morning the halogen chemistry has to be restarted by the reaction cycles explained in detail in previous sections. This, however, takes place quite rapidly because it is supported by the evaporation of cloud droplets with a rather high halogen loading to highly concentrated aerosol particles. Cloud particles (grown on either sea salt or sulfate aerosol particles) with high bromine loadings sediment from near the cloud top, where the LWC is highest, to layers where shrinking and therefore degassing takes place. Thus also sulfate particles provide a source for gas phase bromine. This is shown in Figure 5.4 that depicts the exchange of Br species between gas and aerosol phase in 315 m height. The sulfate aerosol is only around noon when the liquid water content is less than 0.001 g/m^3 (see Figure 5.1) no net source for Br. During the daylight hours when the cloud extends into this layer cloud droplets grown on sulfate particles that took up bromine shrink to aerosol particles that liberate Br_2 and BrCl. Br_2 degasses in the early morning and afternoon when shrinking of cloud droplets takes place, while during the day, when Br^- decreased in the sulfate particles, BrCl escapes from the sulfate aerosol in agreement with the activation cycles discussed in section 4.5. The diurnal variation of Br^- is similar for all aqueous phases with a maximum during night and minimum during day, which is the opposite from cloud-free model runs. The dynamical decoupling of the cloud and sub-cloud layer reduces the loss of gas phase halogens from sub-cloud layers to the cloud droplets during day leading to a strong vertical gradient of the bromine species.

These model results might help explain findings from field measurements where an enrichment of bromine in small particles was found. These particles could have been cloud-processed by the above described mechanism and therefore been enriched in bromine. Also the observations of *Rancher and Kritz* (1980) that show a strong diurnal cycle in gas and aqueous phase bromine (see also discussion in section 4.2) could be explained with these model results. In the model a strong diurnal cycle is simulated in the presence of clouds which is not confined to the cloud layers. In the cloud runs the partitioning between gas and aqueous phase is almost exclusively to the aqueous phase (near the surface to both the sulfate and the sea salt aerosol) during night and, at least for the sub-cloud layers, to the gas phase during day. In the data of *Rancher and Kritz* (1980) such an exclusive partitioning was not seen, but one should not overemphasize these differences because the model runs were not adjusted to the conditions during the measurement period of *Rancher and Kritz* (1980). Furthermore a fractional cloud cover cannot be simulated in the present model version so an exact comparison between their data at reported cloud fractions of 0 to 0.5 cannot be made.

In the run with increased wind velocity larger sea salt particles are emitted leading to a higher pH of the sea salt aerosol. The total gas phase bromine is, unlike in the cloud-free runs with different wind speeds, roughly the same in both runs. This is caused by greater sinks for Cl_x and Br_x (uptake by cloud droplets) in the "strong wind" run due to a decreased height of the sub-cloud layer and the increased deposition velocity due to the higher wind speed.

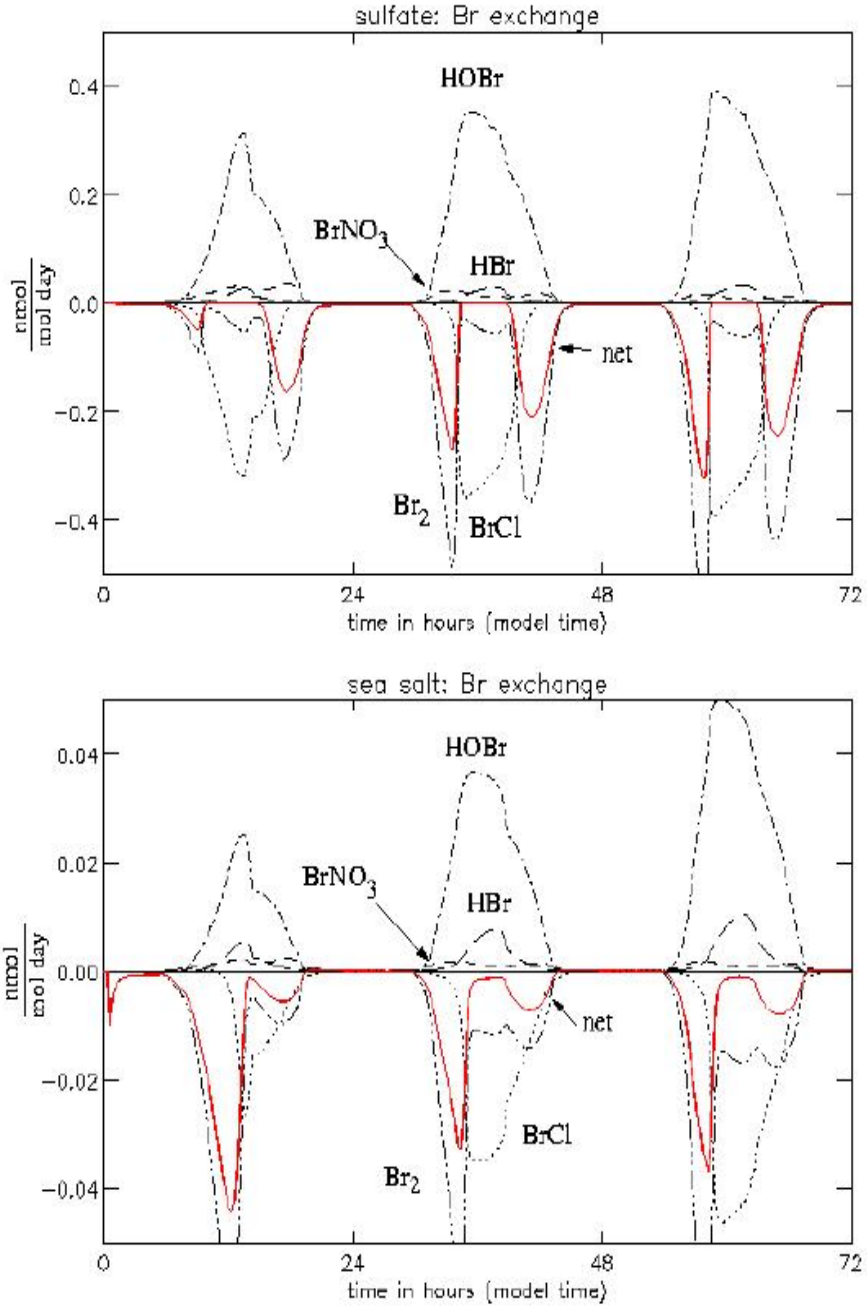

Figure 5.4: Net exchange of Br_x between sea salt and sulfate aerosol and gas phase in the base cloud run. A negative sign implies loss for the aerosol (in 315 m). The solid line is the net flux of Br atoms.

The diurnal variation of active halogen species show some differences with more pronounced morning and evening peaks in the "strong wind" run than in

the base cloud run (see Figure 5.2). The cause for this lies again in the diurnal cycle of the photolysis of O_3. The LWC of the cloud and therefore also the attenuation of solar radiation is greater in the "strong wind" run than in the standard cloud run. This results in smaller early morning photolysis rates of O_3 and smaller HO_2 mixing ratios in the "strong wind" run. Thus the sink for BrO is weaker and early morning and late afternoon peaks in BrO as in the aerosol only runs can be observed.

Maxima in OH and HO_2 appear later in the "strong wind" run than in the base run, because the minimum in the cloud water column and therefore the maximum in O_3 photolysis are delayed.

Photolysis of O_3 produces $O(^1D)$ which reacts with H_2O to OH. The vertical profile of $O(^1D)$ shows an enhancement above the cloud and in higher cloud layers (Figure 5.5) compared to the base cloud-free run. Only below 550 m $O(^1D)$ is smaller in the cloudy run than in the cloud-free run. The cause for this is the increase of the actinic flux in the higher layers of the cloud and above the cloud due to multiple scattering of photons by the cloud droplets (for a detailed explanation see *Landgraf* (1998) and *Trautmann et al.* (1999)). The effect is an enhancement of OH concentrations in a cloudy atmosphere. In the model OH is greater in all levels in the cloudy run than in the cloud-free run and not only where $O(^1D)$ is greater, because water vapour is more abundant than in the cloud-free run.

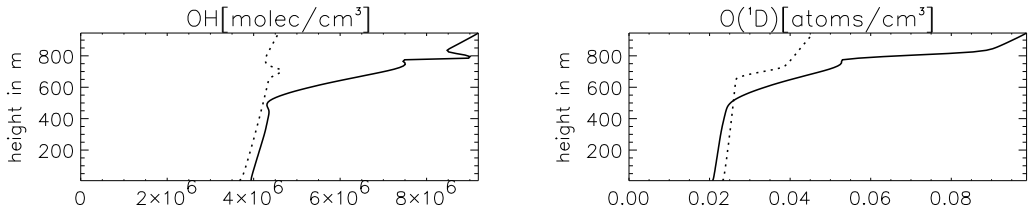

Figure 5.5: Vertical profile of OH and $O(^1D)$ at noon on the second model day for the base cloudy run (solid line) and the base cloud-free run (dotted line).

5.2 Aqueous phase chemistry

The in-cloud interstitial aerosol grew substantially compared to the aerosol in the cloud-free runs in similar heights due to the higher relative humidity. This results in higher pH values for the interstitial aerosol particles. Sea salt particles grew enough to make dilution more important than the pH decreasing process discussed in section 4.10 and in *von Glasow and Sander* (2001). Below the cloud, however, the pH was significantly smaller for sea salt aerosol particles (1 - 2 pH units) and unchanged for the sulfate particles compared to the same height in cloud-free runs. This can be seen in Figure 5.6 where the evolution of the aerosol phases is depicted in 315 m height. Especially the "strong wind" run shows large variations in liquid water content and pH. High liquid water content and pH

correspond to the time when the cloud extends down to this layer (i.e. strong growth of aerosol particles) and low values correspind to the cloud-free times.

Clouds play a very important role in the oxidation of S(IV) (see e.g. *Seinfeld and Pandis* (1998) for an overview). The rates are several times higher than in the gas phase or in aerosol particles. Table 5.1 gives an overview of the mean nss-sulfate production rates and of the paths for sulfur oxidation in the cloud runs compared to the standard cloud-free run. Mean sulfur oxidation rates increased by 250 % in the base cloud run and by 275 % in the "strong wind" cloud run. Mean oxidation rates are now roughly $2 \cdot 10^{-9}$ mol/(m^3 day) (averaged over the depth of the MBL). Most oxidation occurs in the cloud droplets with 80 - 90 % of the total. Oxidation in the gas phase accounts now only for roughly 2 % and in the sea salt aerosol for 1 - 17 % of the total column sulfate production. The absolute values of the gas phase sulfur oxidation also changed significantly compared to the standard cloud-free run showing reductions of 83 % and 94 % in the standard and the "strong wind" cloud runs, respectively.

When comparing the rates for cloud-free and cloudy model runs one should always be aware of the large variability in sulfur oxidation for different conditions as was shown for the different aerosol only runs.

The relative importance of the different pathways of sulfur oxidation in the aqueous phases is listed in Table 5.2.

In the cloud droplets grown on sulfate aerosol particles oxidation by H_2O_2 is dominating followed by oxidation by HOBr. In both droplet classes oxidation of S(IV) by HOBr is more important than by HOCl. This changed behaviour compared to the aerosol particles is caused by the dilution in cloud droplets. The main sink for HOBr in the concentrated sea salt aerosols is the acid catalyzed reaction with Cl^-, producing BrCl, making HOBr less available for S(IV) oxidation. In the diluted cloud droplets (note that the concentration of Cl^- in mol/l, which is strongly dependent on the LWC, is determining the rate) this reaction path is weaker making the S(IV) oxidation by HOBr more important than by HOCl because the higher rate coefficient for HOBr + S(IV) more than compensates the smaller concentrations of HOBr compared with HOCl (see Figure 5.6 and 5.7).

Chameides and Davis (1982) and *Jacob* (1986) proposed the importance of the reaction S(IV) + OH. In the cloud runs between 3 and 10 % of S(IV) in the droplet bins were produced by this reaction. In droplets grown on sulfate aerosol particles oxidation by O_3 is not important, whereas the higher pH in the cloud droplets grown on sea salt aerosol particles makes oxidation by O_3 more important here, especially in the "strong wind" run.

Uptake of H_2SO_4 from the gas phase to the aqueous phases (bins I - IV) in the cloud runs mainly happens at cloud top where entrainment from the free troposphere takes place. This might be overestimated because no loss processes for H_2SO_4 like new particle formation or condensation on solid aerosol particles are considered in the free troposphere.

Many published field measurements in the MBL were made only near the sea surface and did not provide vertical profiles of meterorological and chemical parameters. As shown here and in previous sections, it is very important to

Table 5.1: S(IV) oxidation rates for the cloudy runs.

run	total column S(VI)	gas phase		sulfate aerosol		sea salt aerosol		sulfate droplets		sea salt droplets	
	mol/(m^3 d)	%	s	%	s	%	s	%	s	%	s
base cloud-free run	$5.39 \cdot 10^{-10}$	55.4 %	$1.4 \cdot 10^7$	0.8%	0.02	43.8 %	$0.9 \cdot 10^3$	-	-	-	
base cloud run	$1.91 \cdot 10^{-9}$	2.6 %	$0.9 \cdot 10^7$	0.6%	0.31	1.0 %	$1.0 \cdot 10^3$	93.0 %	22.7	2.8 %	28.3
"strong wind" cloud run	$2.02 \cdot 10^{-9}$	0.9 %	$3.1 \cdot 10^7$	0.5%	0.95	17.1 %	$1.2 \cdot 10^3$	74.0 %	35.0	7.5 %	32.6

The numbers are means over the MBL over the 2$^{\text{nd}}$ and 3$^{\text{rd}}$ model day. The contribution of the individual path is given as relative contribution to the total oxidation rate. For the gas and aqueous phases a mean conversion time is given. Note that the conversion time for the aqueous phases includes only reaction within the particles. The conversion time for uptake is on the order of days for the aerosols and on the order of 10 min to several hours for the droplets, respectively, imlpying that uptake is the rate limiting step but at significantly reduced times scale for droplets.

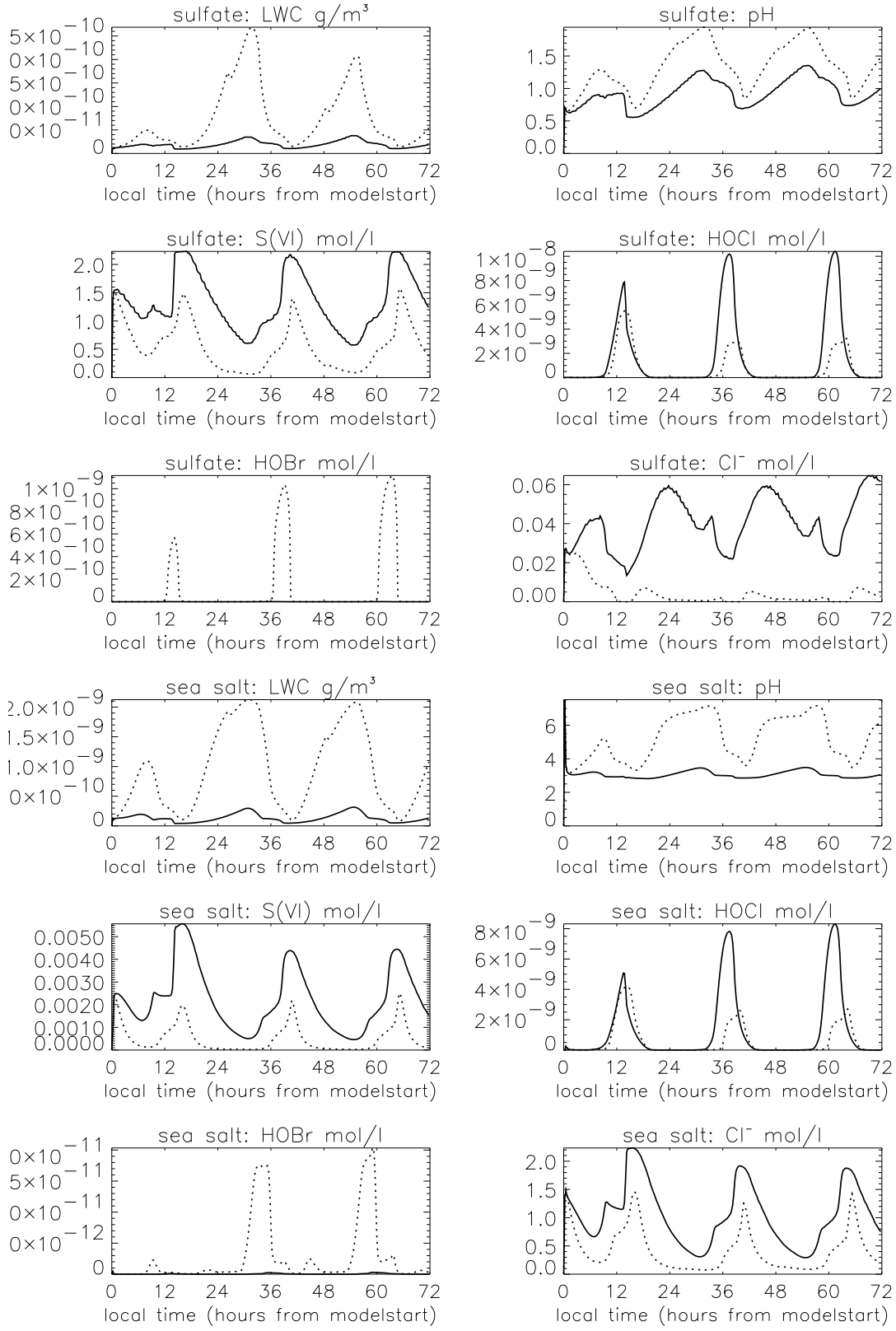

Figure 5.6: Evolution with time of the main aerosol phase species for the cloud base run (solid line) and the cloud "strong wind" run (dotted line) in 315 m. Concentrations are in mol/l. This level is cloud-free during day and in cloud during the night. In the "strong wind" run it is longer part of the cloud.

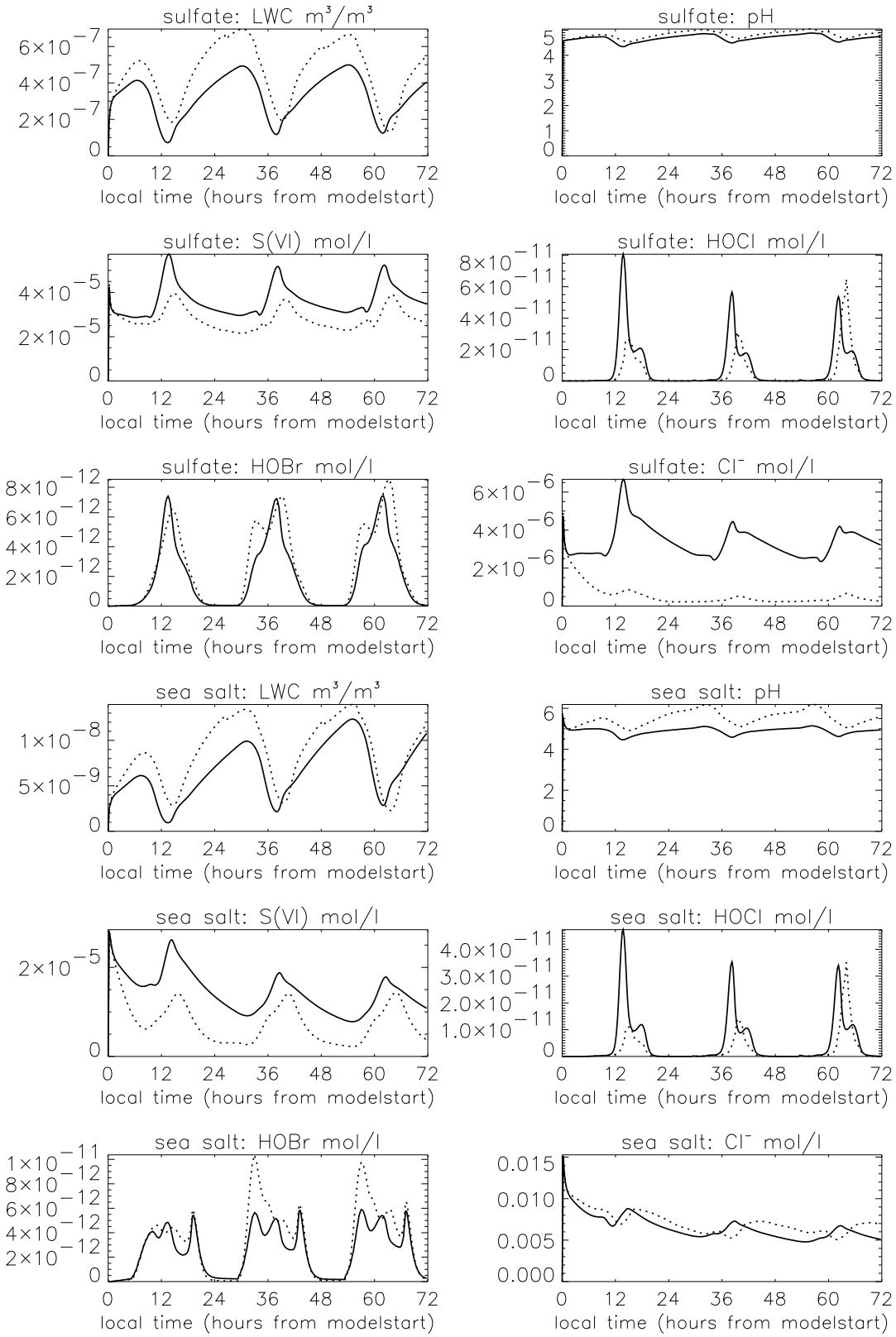

Figure 5.7: Evolution with time of the main droplet phase species for the cloud base run (solid line) and the cloud "strong wind" run (dotted line) in 615 m. Concentrations are in mol/l.

Table 5.2: Comparison of oxidation pathways for the cloudy runs.

S(IV) oxidation path		cloud-free base run	cloud base run	"strong wind" cloud run
sulf. aer.	O_3	-	2.2 %	3.9 %
	H_2O_2	1.6 %	1.0 %	0.9 %
	HOCl	-	-	-
	HOBr	-	-	-
	uptake	98.4 %	96.8 %	95.2 %
	mean rate	$4.47 \cdot 10^{-12}$ mol/(m^3 d)	$1.15 \cdot 10^{-11}$ mol/(m^3 d)	$1.04 \cdot 10^{-11}$ mol/(m^3 d)
sea salt aer.	O_3	11.7 %	1.7 %	44.1 %
	H_2O_2	14.4 %	36.8 %	1.6 %
	HOCl	61.0 %	23.1 %	28.3 %
	HOBr	3.0 %	1.4 %	24.7 %
	uptake	9.8 %	36.9 %	1.1 %
	mean rate	$2.36 \cdot 10^{-10}$ mol/(m^3 d)	$2.00 \cdot 10^{-11}$ mol/(m^3 d)	$3.46 \cdot 10^{-10}$ mol/(m^3 d)
sulf. drop	O_3	-	2.5 %	5.5 %
	H_2O_2	-	54.9 %	33.2 %
	OH	-	8.2 %	14.7 %
	HOCl	-	9.0 %	6.0 %
	HOBr	-	24.2 %	38.9 %
	uptake	-	1.0 %	1.6 %
	mean rate	-	$1.78 \cdot 10^{-9}$ mol/(m^3 d)	$1.50 \cdot 10^{-9}$ mol/(m^3 d)
sea salt drop	O_3	-	6.5 %	48.9 %
	H_2O_2	-	43.2 %	5.2 %
	OH	-	6.0 %	2.7 %
	HOCl	-	6.3 %	1.8 %
	HOBr	-	37.6 %	41.1 %
	uptake	-	0.2 %	-
	mean rate	-	$5.33 \cdot 10^{-11}$ mol/(m^3 d)	$1.50 \cdot 10^{-10}$ mol/(m^3 d)

Relative importance of the uptake from the gas phase and different reaction pathways for the production of nss-sulfate in the particles (mean over the MBL over the 2nd and 3rd model day).

differentiate measurements that were made under clear-sky conditions from those that were done in a cloud-topped MBL as the effects of clouds are also strongly influencing the conditions near the surface of the ocean. It this therefore very important that information about the cloud cover and the vertical structure of the MBL like height of the MBL, cloud depth, or liquid water content are provided when surface measurements are reported.

Chapter 6

The effect of ocean-going ships on the MBL: An introduction

The marine boundary layer is influenced by anthropogenic emissions that are advected from land but also from the exhaust of ocean-going ships. *Conover* (1966) was the first to describe "anomalous cloud lines" that were detected from satellite pictures and assumed to be caused by ships. Later these anomalous cloud lines have been called ship tracks. Ship tracks are regions of increased cloud albedo and modified microphysics that can easily be distinguished from the surrounding clouds (see Figure 6.1) and that are caused by more and smaller cloud droplets. The particles on which the additional cloud droplets grow are either directly emitted by ships or formed from gas-to-particle formation in the plume of the ship. Sometimes ship tracks evolve where no clouds have been before but usually they form in pre-existing low stratiform MBL clouds.

An increasing number of observational and modeling studies were made in the last decades on the formation, evolution and consequences of ship tracks because they can be viewed as an experiment of the influence of anthropogenic particle emissions on clouds and can therefore be used to study the indirect aerosol effect. In June 1994 the Monterey Area Ship Track Experiment (MAST) was conducted to investigate the processes behind anthropogenic modifications of cloud albedo (*Durkee et al.* (2000b) and references therein). A lot of information about the conditions at which ship tracks form was gained.

Based on data from MAST, *Liu et al.* (2000) studied conditions under which ship tracks develop in stratocumulus clouds using a LES model. They found that in a well mixed MBL, where the sub-cloud and the cloud layers are dynamically coupled usually a ship track developed, whereas in decoupled cases the appearance of a ship track depended on the stratification in the MBL and the availability of surface heat fluxes to produce buoyancy to lift the aerosol particles from the ship plume into the cloud layers (see also section 5 for a discussion of coupling and decoupling effects in the cloud-topped MBL). The source for these heat fluxes could either be a change in sea surface temperature or heat from the ship's exhaust.

Coakley et al. (2000) observed an "on-off behaviour" of ship tracks during

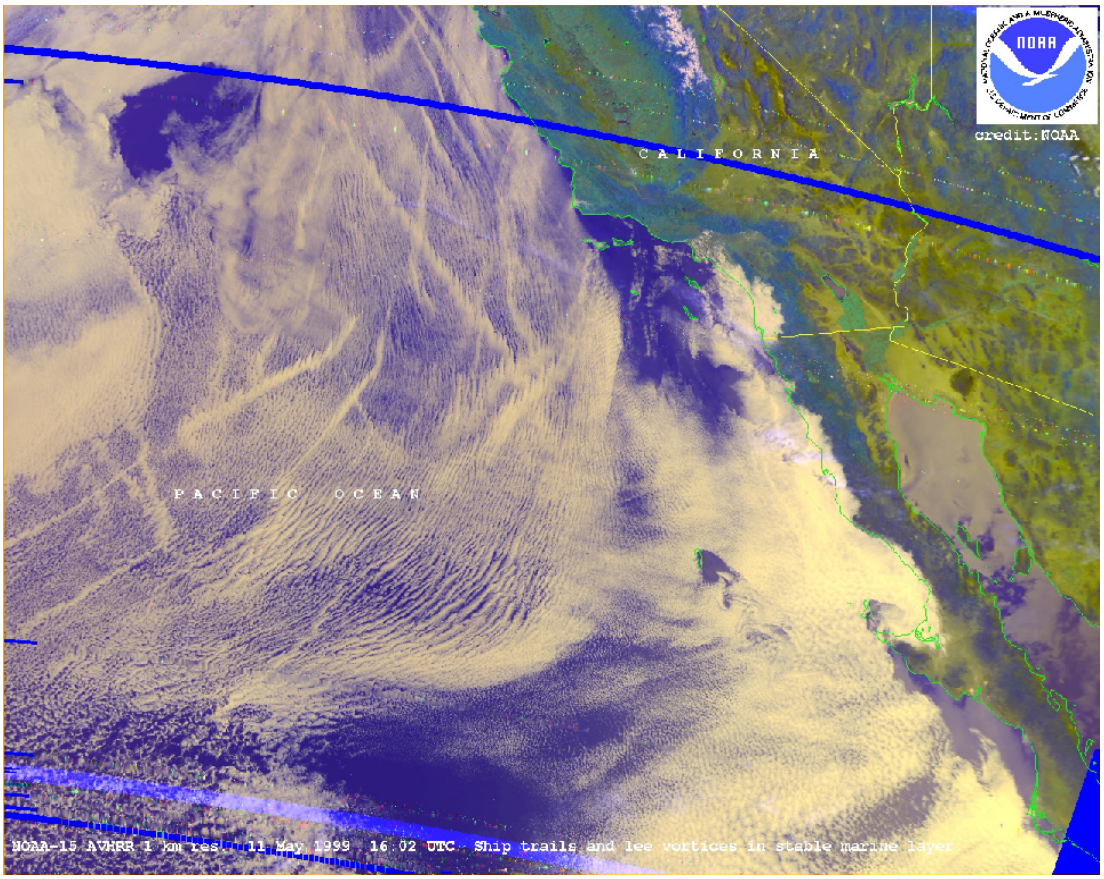

Figure 6.1: Ship tracks off California and Baja California (NOAA-15 AVHRR 1 km resolution 11. May 1999 16:02 UTC, courtesy of U.S. National Oceanic and Atmospheric Administration).

MAST, i.e. either many ship tracks in a certain area or the absence of ship tracks in a large region. This would suggest that the appearance of ship tracks is not only determined by small-scale cloud physics but subject to large-scale forcings. They found a correlation between cloud height and the appearance or absence of ship tracks based on satellite observations. They state that clouds have to be close to the sea surface for ship tracks to form. If coupling of cloud and sub-cloud layer determines whether or not a ship track is formed, than cloud height could be indicative of the coupling.

According to *Hobbs et al.* (2000) heat fluxes from ships are negligible. They argue that under the same meteorological conditions ships emitting particles of smaller sizes will less likely form a ship track than ships producing larger particles. They hypothesize that the type of fuel burnt determines the size of the emitted particles rather than engine type.

Comparing two cases forming and not-forming a ship track under similar conditions in moderately polluted air *Noone et al.* (2000) also found the size of the emitted particles to be the most important difference between the two cases.

Contrary to the impact of ship exhaust on cloud albedo and microphysics the

effect on MBL chemistry received attention only recently. *Streets et al.* (1997) published estimates of SO_2 emissions from international shipping in Asian waters and of the contribution of ship emissions to the deposition on land around the Asian waters. The first global compilation of NO_x and SO_2 emissions from ocean-going ships was presented by *Corbett and Fischbeck* (1997) and *Corbett et al.* (1999). They estimated global annual emissions of NO_x to be 10.12 teragram (Tg) per year (3.08 Tg N/year) and 8.48 Tg of SO_2 per year (4.24 Tg S/year). The sulfur emitted by ships corresponds to roughly 20 % of the biogenic dimethylsulfide (DMS) emissions from the oceans. In some regions of the Northern Hemisphere ship emissions can be of the same order of magnitude as model estimates of the flux of DMS whereas they are much smaller than DMS emissions in the Southern Hemisphere. *Streets et al.* (2000) published updated values for the sulfur emissions in and sulfur deposition around Asian waters. The emission numbers are about 13 % smaller than the values by *Corbett et al.* (1999) which may be due to the fact that *Streets et al.* (2000) neglected non-transported vessels (military, fishing) that were included in *Corbett et al.* (1999).

Based on the emission inventories by *Corbett and Fischbeck* (1997) and *Corbett et al.* (1999), *Capaldo et al.* (1999) used a global chemical transport model to study the global effects of ship emissions on the sulfur cycle and the effect on radiative forcing. They found that ship emissions can be a dominant contributor to SO_2 concentrations over much of the world's ocean and in several coastal regions. Furthermore a substantial fraction of the anthropogenic perturbation of the Earth's radiation budget might be due to ship derived particles (indirect radiative forcing) and a significant contribution to non-sea salt sulfate might be caused by ship emissions.

In another study with a different global chemical transport model *Lawrence and Crutzen* (1999) investigated the effects of NO_x emissions on the budget of O_3 and OH and found that in heavily traversed ocean regions the OH burden was predicted to increase up to fivefold. This would reduce the atmospheric lifetimes of reactive trace gases and could have an effect on aerosol particle production and cloud properties as OH is an important oxidant for DMS. O_3 concentrations were estimated to increase by a factor of more than 2 over the central North Atlantic and Pacific.

Using an updated emission inventory *Kasibhatla et al.* (2000) confirmed the effects predicted by *Lawrence and Crutzen* (1999) but, due to a different geographic distribution of the emissions, the effects were more widespread and peak enhancements not as large. Comparing the model predictions with results from measurement campaigns they found a difference in NO_x of about a factor of 10, therefore showing no support for the model predicted enhancements of NO_x. They conclude that the parameterized description of plume dynamics and or missing knowledge of the plume chemistry could be the cause for an overestimation of the effects of ship emissions. Nevertheless it would be very helpful to do comparisons with a greater observational dataset than the one they used.

To estimate the effects of detailed gas phase and aerosol chemistry as well as that of plume expansion and mixing with clean background air a box model and

a modified version of the one-dimensional MBL model described in section 3 were used. The models will be described in the next section, followed by a discussion of the results of the box model and one-dimensional model studies.

All modeling studies of the chemical effects of ship emissions that were published so far were made using global chemistry transport models (CTM), so the detailed approach that was undertaken here is the first attempt to do so.

Chapter 7

Model description and modifications

The box model that was used to estimate the effects of ship exhausts is based on the box model of *Sander and Crutzen* (1996) and *Vogt et al.* (1996), which has been updated (http://www.mpch-mainz.mpg.de/~sander/mocca). In their model the evolution of gas and aqueous phase chemistry as well as interactions between the phases are modeled similarly as in MISTRA (see section 3.2). The particulate phase is divided into a sea salt and a sulfate aerosol bin.

For the study of ship exhaust, the chemical evolution of gas and aqueous phase species in the background and plume air is calculated separately and mixing between background and plume air is applied as discussed in the next section.

7.1 Mixing of background and plume air

The approach that is used for the mixing of plume and background air has been adopted from studies of the evolution of aircraft exhaust (e.g. *Kärcher* (1999)). The plume expansion in these parameterizations is described with an expansion coefficient that has to be determined empirically. In the description of point sources on the surface (e.g. power plant plumes) often Gaussian plume expansion is assumed (see e.g. *Seinfeld and Pandis* (1998)). The parameters needed for the latter approach can be determined from atmospheric stability data with further assumptions on boundary conditions. In the frame of the models that were used here the largest restriction is the inability to deal with inhomogeneities of the plume evolution. This restriction can only be overcome with the use of three-dimensional models (e.g. LES). As only limited information on ship plume expansion is available from the literature it was most feasible to use the approach from aircraft exhaust studies that needs only one parameter for the description of the plume evolution.

For the box model two reservoirs of air are considered: the plume and the background reservoir. Both are assumed to be well-mixed. Dilution of the plume takes place by expansion of the plume and associated entrainment of background

air. The expansion of the plume is in the vertical and in the horizontal across the ship's course (see Figure 7.1). It can be formulated as:

$$w_{pl}(t) = w_0 \left(\frac{t}{t_0} \right)^{\alpha} \tag{7.1}$$

$$h_{pl}(t) = h_0 \left(\frac{t}{t_0} \right)^{\beta} \tag{7.2}$$

where w_{pl} and h_{pl} are the width and height, respectively, of the plume at time t, t_0 is a reference time, here chosen to be 1 second after plume release and w_0 and h_0 are reference dimension of the plume at time t_0. They were estimated to be 10 m and 5.5 m, respectively, and correspond approximately to the cross-sectional area of a plume after 1 second. α and β are the plume expansion rates in the horizontal and vertical, respectively.

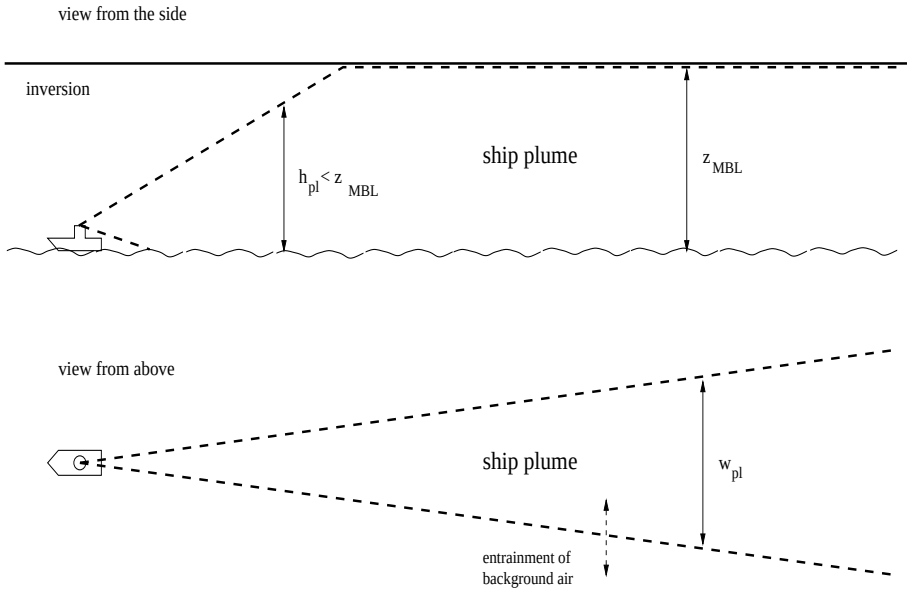

Figure 7.1: Schematic of the assumed plume expansion in the box as well as 1D model. The bold horizontal line indicates the inversion that caps the MBL. The dashed lines show the extent of the ship plume.

Mixing along the ship course does not affect the concentrations significantly as the gradient in this direction is small. The change in concentration in the plume c_{pl} through mixing can be written as:

$$\left. \frac{dc_{pl}}{dt} \right|_{mix} = (c_{bg} - c_{pl}) \frac{1}{A_{pl}} \frac{dA_{pl}}{dt} \tag{7.3}$$

with the background concentration c_{bg} and the cross section of the plume A_{pl}. The expansion of the plume is only considered across the ship course and in the

vertical. The plume cross section is given as $A_{pl} = w_{pl}h_{pl}$. Using this definition for A_{pl} one gets:

$$\begin{aligned} \frac{1}{A_{pl}}\frac{dA_{pl}}{dt} &= \frac{1}{\frac{w_0}{t_0^\alpha}\frac{h_0}{t_0^\beta}t^{\alpha+\beta}}\frac{w_0}{t_0^\alpha}\frac{h_0}{t_0^\beta}(\alpha+\beta)t^{\alpha+\beta-1} \\ &= \frac{\alpha+\beta}{t} \end{aligned} \tag{7.4}$$

The top of the MBL is assumed to be impenetrable by the plume, therefore the expansion of the plume is only horizontally when h_{pl} reaches z_{MBL}, here z_{MBL} is the height of the MBL. Equation 7.3 can now be written as:

$$\left.\frac{dc_{pl}}{dt}\right|_{mix} = \begin{cases} \frac{\alpha+\beta}{t}(c_{bg}-c_{pl}) & h_{pl}(t) < z_{MBL} \\ \frac{\alpha}{t}(c_{bg}-c_{pl}) & h_{pl}(t) = z_{MBL} \end{cases} . \tag{7.5}$$

Values for α and β were estimated from the expansion of ship tracks as reported in the literature. The plume evolution is strongly dependent on atmospheric conditions like wind speed, wind shear, etc. It is therefore impossible to give numbers for α and β that are valid for all atmospheric conditions. Table 7.1 lists the estimates of plume expansion derived from data found in the literature. "Best values" for α and β were estimated and sensitivity studies performed to see the importance of the choice of these values. In Figure 7.2 the evolution of $w_{pl}(t)$ with time for different values of α is shown. Based on *Durkee et al.* (2000a) the average time lag for appearance of the ship track after emission from a ship is 25 min in a MBL with an average height of 500 m. Therefore my "best guess" for β is 0.55 (see Figure 7.2). This estimate assumes coupling between the sub-cloud and cloud layers or, in the cloud-free case, a well mixed MBL.

Using the "best guess" values for α and β, the plume width after 1 hour is 4.6 km and the plume height about 900 m (if the height of the MBL is greater than this number). The plume cross section increased from 55 m^2 at t_0 to 4.1 $\cdot 10^6$ m^2 which corresponds to a dilution factor of nearly 10^5.

A similar approach was used for the one-dimensional model, but here only dilution in the horizontal was parameterized as transport of chemical species and tracers in the vertical is a resolved process. The same values for α were used. At t_0 emissions are spread to the depth of the model layer ($dz = 10$ m) centered around 35 m (assumed to be the height of the funnel).

An implicit assumption of the described implementation of mixing is that the plume is immediately well mixed and that the input of background air has an immediate influence on the chemistry of the complete plume. In reality one would expect higher concentrations of pollutants in the center of the plume cross-section and lower values to the edges where clean air is mixed in.

The mass of the emitted compounds is conserved during the mixing process as the dilution of the plume air is only by entrainment of background air into the expanding plume and not by detrainment of plume air.

Table 7.1: Estimates of values for α

source	ship track width	distance from ship	time since emission	derived α
Durkee et al. (2000a), ship moves into wind, A	3100 m	40000 m	3390 s[1]	0.72
Durkee et al. (2000a), ship moves into wind, B	3800 m	40000 m	1710 s[1]	0.83
Durkee et al. (2000a), ship moves with wind, C	10500 m	40000 m	7690 s[1]	0.8
Durkee et al. (2000a), ship moves with wind, D	6100 m	40000 m	9300 s[1]	0.7
Ferek et al. (1998)[2]	7500 m		20000 s	0.65
"best guess"				0.75

[1] Calculated based on relative windspeeds as given in *Durkee et al.* (2000a). [2] Rough estimate from Figure 2 in *Ferek et al.* (1998); α is calculated with equation 7.1. The letters A - D indicate the cases discussed in *Durkee et al.* (2000a).

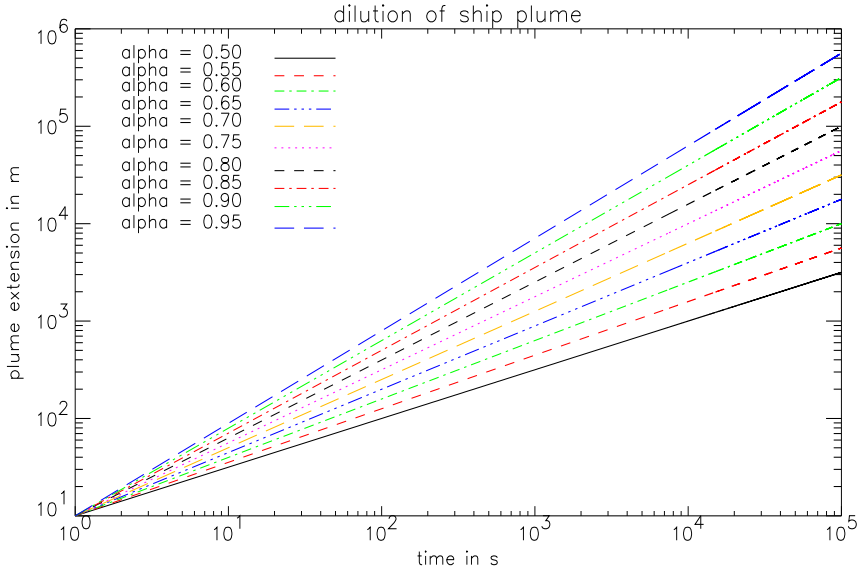

Figure 7.2: Horizontal plume expansion as a function of time for different values of α (see equation 7.1), $w_0 = 10$ m, $t_0 = 1$ s.

7.2 Emission rate estimates

Corbett et al. (1999) provided global estimates for the emissions of SO_2 and NO. Their inventory is based on data and estimates of the global ship fleet and transport routes, fuel consumption, and emission per consumed fuel. They assumed average NO_x emission factors of 57 g/kg_{fuel} for medium-speed diesel engines and 87 g/kg_{fuel} for slow-speed engines. These numbers are similar to the numbers provided by *EPA* (2000). According to *EPA* (2000) allmost all NO_x is emitted as NO, so here only NO was assumed to be emitted by ships. The

Table 7.2: Emissions strength of gases.

	NO	CO	SO_2	HCHO
emission (g/kWh)	10[1]	1[1]		
emission factor (g/kg_{fuel})	50[2]	5[2]	40[3]	
exhaust mixing ratio (μmol/mol)	1000[1]	100[1]	360[4]	5[5]

[1] From *EPA* (2000) for a typical engine load of 80 %. [2] Calculated using a typical fuel consumption of 200 g_{fuel}/kWh (*EPA* (2000)). [3] Calculated using a fuel sulfur content of 2 % and SO_2 (in $g(SO_2)/kg_{fuel}$) = 20 × fuel sulfur content (in %) (*Corbett et al.* (1999)). [4] Calculated from the data given previously, yielding a molar ratio of 0.36 between the mixing ratios of SO_2 and NO in the exhaust. [5] 0.05 × CO (*EPA* (1972)), used as surrogate for aldehydes.

values calculated from measurements during the MAST campaign yield lower values between 2 and 25 g/kg_{fuel} (*Hobbs et al.* (2000)). The reason why the emission estimates of *Hobbs et al.* (2000) are smaller than the other values from the literature (*Corbett et al.* (1999), *EPA* (2000), *Streets et al.* (2000)) is not resolved yet. In the model runs estimates for the mixing ratios of NO and CO in ship exhaust plumes by *EPA* (2000) were used, because they are consistent with two other emission inventory studies that were all conducted indepently and they are consistent to the emission data used by previous model studies. Values for SO_2 and HCHO as a surrogate for aldehyde emissions were estimated based on *EPA* (1972), *Corbett et al.* (1999) and *EPA* (2000) (see Table 7.2).

Particle emissions for the one-dimensional model were estimated based on the data of *Hobbs et al.* (2000). A lognormal size distribution was used with a mode radius $R_N = 0.04\ \mu$m, a standard deviation of $\sigma = 1.5$ and $N_{tot} = 1{\cdot}10^6\ 1/cm^3$ (see explanation of Table 4.2 for the calculaion of the corresponding size distribution) for the ship particle mode of the dry plume aerosol at t_0.

Hobbs et al. (2000) found that the particles in ship tracks are mainly composed of organic material with high boiling points, possibly combined with sulfuric acid particles that were produced in the gas phase in the high SO_2 regime of the plume. They found the typical water-soluble fraction of the particles to be 10 %. In the model all particles of the same size are assumed to have the same physical properties. As the background particles with small sizes are soluble in the model, the emitted particles have to be treated as soluble as well. To account for this, the number of emitted particles has been reduced. They are assumed to be composed of H_2SO_4. Using the average particle emission flux of 10^{16} part/s given by *Hobbs et al.* (2000), this would result in 720 part/cm^3 additional to the background values after one hour for a ship speed of 10 m/s and in a MBL with a height of 300 m. This estimate is confirmed by their figures. the emission estimate that is used here results in the model in about 40 part/cm^3 additional to the background values over a MBL depth of 700 m consistent with the soluble fraction of the plume exhaust.

The measurements of *Hobbs et al.* (2000) did not show significant elevations

of the mass concentrations of ions in bulk aerosol samples compared to the background. This is probably due to the small sizes and masses of the emitted particles. Under the high SO_2 concentrations in plumes and the quite large surface area of the combustion particles, scavenging of SO_2 from the gas phase could produce mixed particles that could be activated easier to cloud droplets than unmodified particles.

Chapter 8

Box model ship plume studies

The box model was used to study the effects of different initial values for the background NO_x and O_3 concentrations, of different plume expansion rates (different values for α), and of aerosol chemistry (sections 8.1 to 8.3). In sections 8.4 and 8.5 the effects of multiple ship passages are examined. All box model runs were made for cloud-free conditions.

8.1 Background NO_x and O_3

In Figure 8.1 the evolution with time of the major gas phase species for box model runs without the inclusion of aerosol chemistry is shown. The ship plume is emitted at 12:00 on the first model day. Shown are the mixing ratios and concentrations in undisturbed background runs (e.g. O_3), in runs with the emission of a ship plume (e.g. p O_3) and the difference (e. g. O_3 diff (pl − bg)). The concentrations of the background run are used in the entrainment routine (equation 7.5).

In the runs with high initial background concentrations of NO_x these high values were artificially sustained by corresponding NO_x sources to see the effect of ship emissions in high NO_x regimes, e.g. coastal regions. The accumulated odd oxygen (O_x, see definition in section 4.6) production rates ("acc O_x bg" in the figure heading) show a net chemical production of O_x for the runs with initial NO_x mixing ratios greater than 50 pmol/mol. For the other runs net chemical O_x destruction takes place.

For all cases the overall evolution of the plume air is similar: O_3 is destroyed immediately after plume release by reaction with NO (note that the accumulated O_x rates in the plots do not show this because the produced NO_2 is part of the O_x family), whereas later O_3 is produced by NO_x catalyzed reactions. Differences between background and plume concentrations of more than 10 % are present for OH only on the first day and for SO_2, NO_x and HNO_3 on the first and second day after plume release. As can be seen from Figure 8.1 increases in O_3 in the plume air compared to the background air are small, on the order of 1 nmol/mol, i.e. 5 %. Increases in OH are on the order of 100 % on the first day after plume emission and around 5 % on the second day.

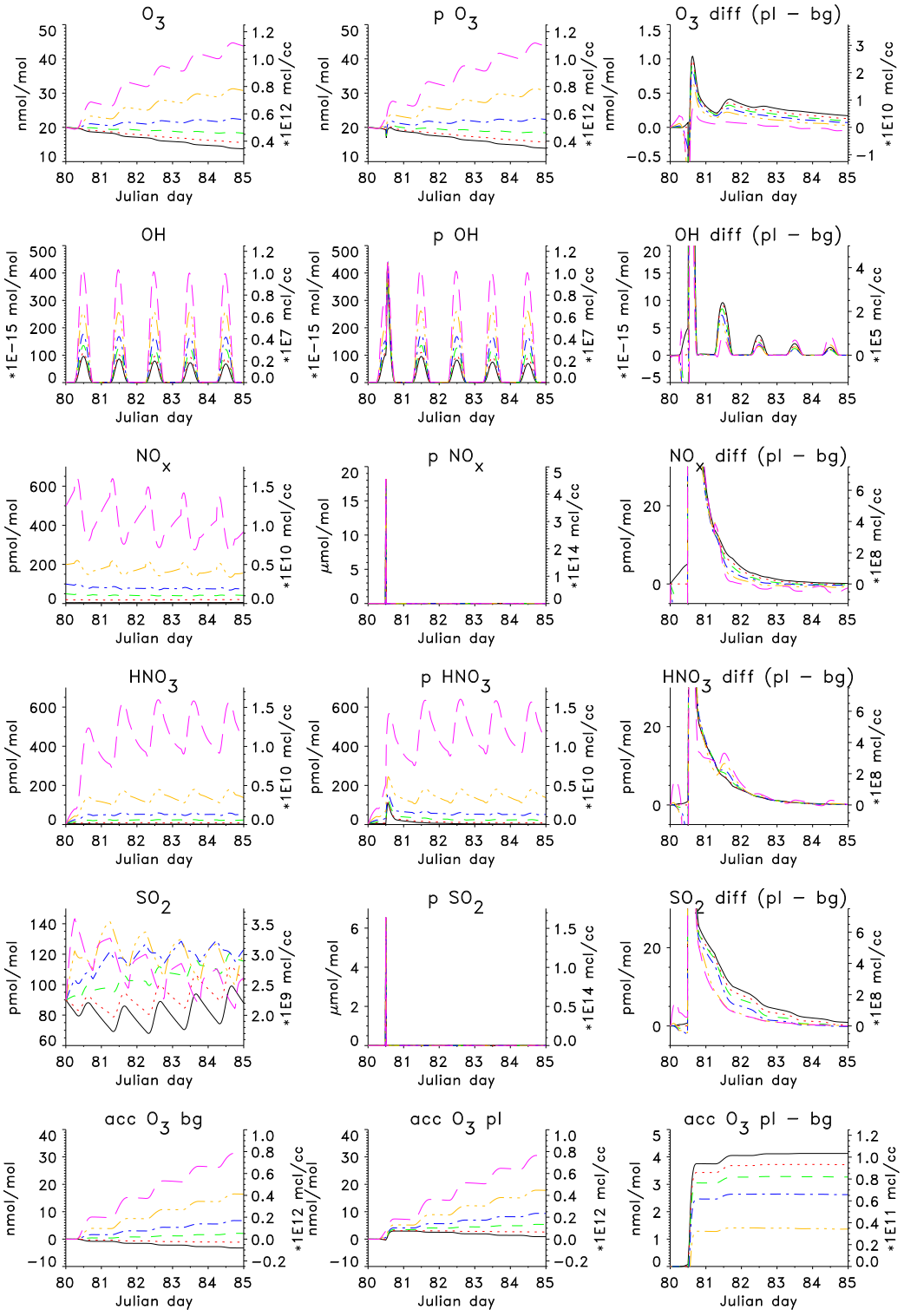

Figure 8.1: Evolution with time for the major gas phase species and accumulated O_3 production rates for emission of a ship plume at 12:00 on the first day (=Julian day 80). The lines show runs with different background NO_x mixing ratios: black, solid line: 5 pmol/mol; red, dotted: 20 pmol/mol; green, dashed: 50 pmol/mol; blue, dash-dotted: 100 pmol/mol; orange, dash-dot-dot-dotted: 200 pmol/mol; pink, long-dashed: 500 pmol/mol. The left column shows the undisturbed background air, the middle column the conditions of the plume air and the right column the difference between both.

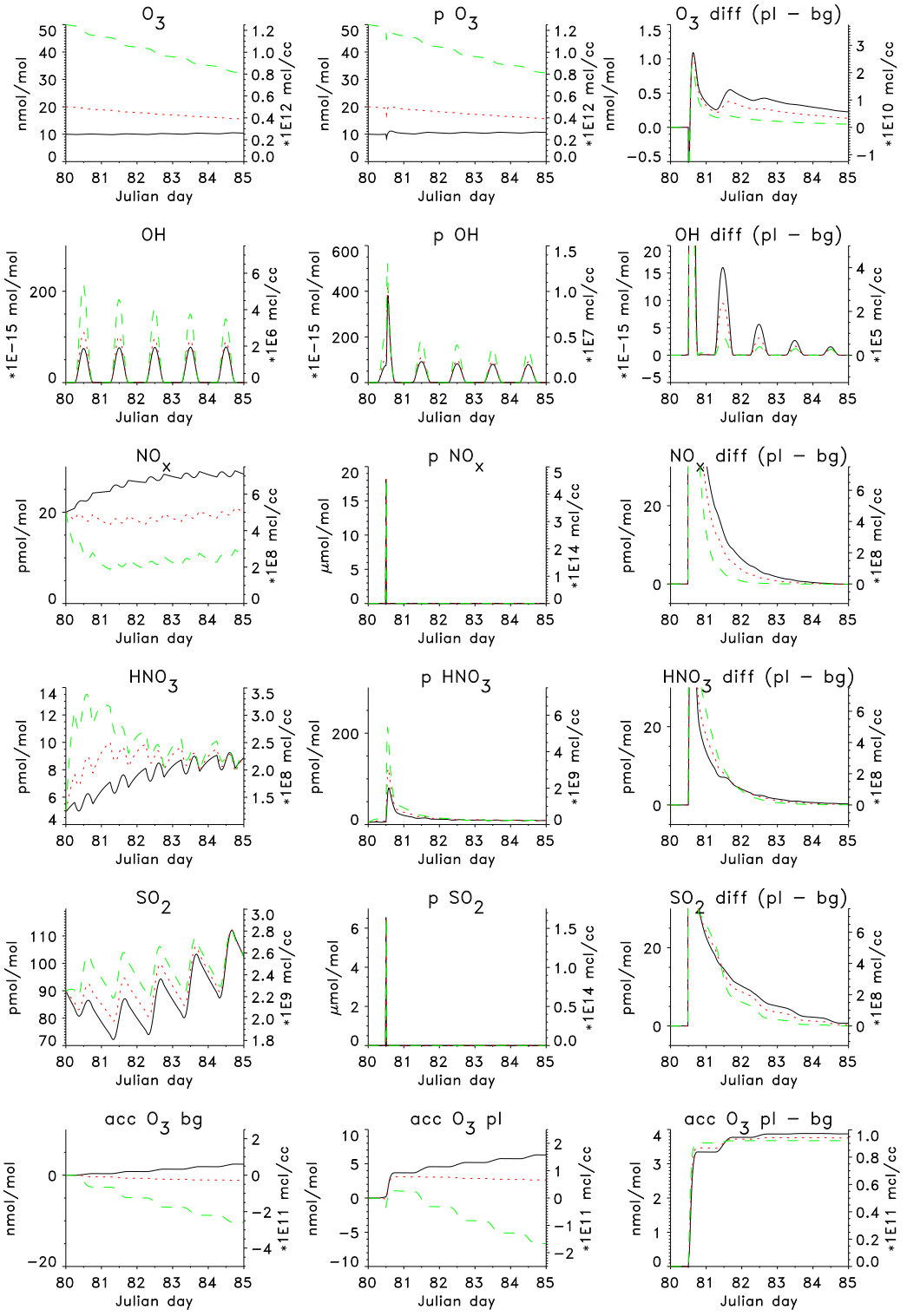

Figure 8.2: Same as Figure 8.1, but for runs with different initital O_3 mixing ratios: black, solid line: 10 nmol/mol; red, dotted: 20 nmol/mol; green, dashed: 50 nmol/mol.

Two days after plume release when the plume width reached an extension of 85 km the difference between background and plume air is below 5 % for all species.

The increase in SO_2 with time in some runs with background air is due to oxidation of DMS that is emitted from the ocean.

The impact and lifetime of ship emissions are largest for the run with the smallest NO_x background mixing ratios. In the runs with more than 100 pmol/mol NO_x in the background air the difference in HNO_3 between plume and background shows a small peak even on the second day after plume release. This is caused by high OH concentrationsin the background. Because OH is the most important sink for NO_x and SO_2, the low background concentrations of OH result in highest concentrations in the runs with smallest initial NO_x mixing ratios .

Further model runs were made to study the effects of different initial O_3 mixing ratios. For these runs initial NO_2 was set to 20 pmol/mol. Figure 8.2 shows the evolution with time for initial O_3 mixing ratios of 10, 20 and 50 nmol/mol. In the 50 nmol/mol case strong O_3 destruction occurs in the background air. Higher OH mixing ratios lead to a decrease in NO_x and an increase in HNO_3 in this run, whereas the opposite is true for the 10 nmol/mol run. When comparing the differences between plume and background air it is obvious from Figure 8.2, that the impact of ship emissions are strongest and most persistent for low O_3 regimes.

8.2 Influence of mixing

To show the influence of dilution on the evolution of the plume runs with different values for α, the horizontal plume expansion rate, were done. Values of $\alpha = 0.62$ (plume width after 4.5 days = 29 km), $\alpha = 0.75$ (156 km, "best guess"), $\alpha = 0.87$ (729 km), and $\alpha = 1.0$ (3888 km) were used. Results from these model runs are shown in Figure 8.3.

In the case of $\alpha = 1.0$ mixing is very quick and 2 days after plume emission background and plume air cannot be distinguished anymore.

For $\alpha = 0.62$ the opposite is the case, mixing is very slow and in all species differences between background and plume air are visible on the fourth day after plume release. The conversion of O_3 to NO_2 on the first day after plume release is very strong, production of O_3 is still occuring on the second day after plume release. OH increases are large with up to 65 % compared to the background on the second day.

In the runs with intermediate values for α the features are as expected from these two extreme values. The accumulated O_x production rates show a strong dependence on α, with highest O_x production in the run with smallest α (= slowest plume expansion rate).

As can be seen from the Figures and from the area influenced by the plume as shown in Figure 7.2 mixing is important mainly in the first 5 to 6 hours after emission of the plume. After this time the volume of the plume is already quite large, so that the entrainment of background air is a rather slow process now.

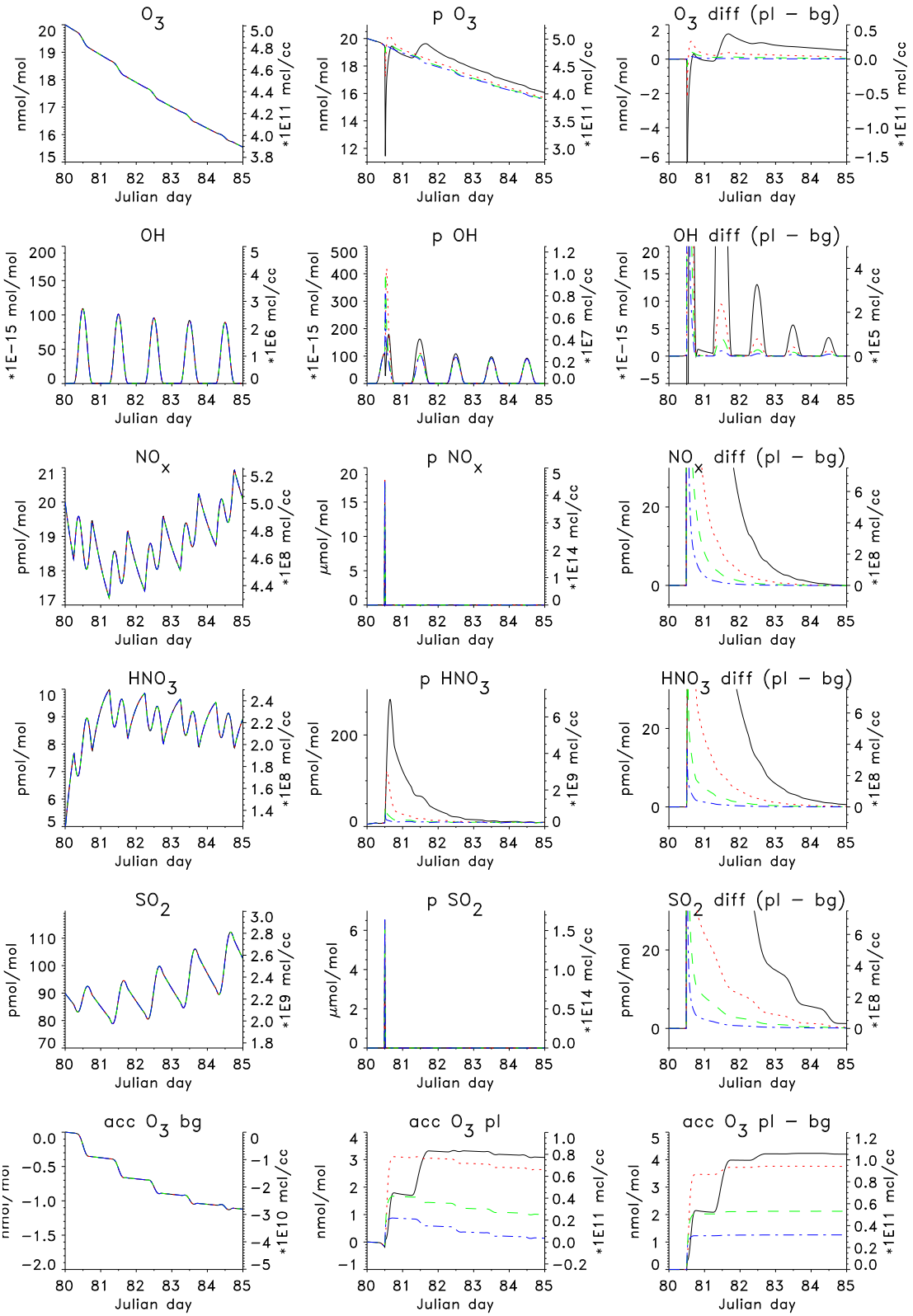

Figure 8.3: Same as Figure 8.1, but for runs with different plume expansion rates: black, solid line: $\alpha = 0.62$, red, dotted: $\alpha = 0.75$, green, dashed: $\alpha = 0.87$; blue, dash-dotted: $\alpha = 1$.

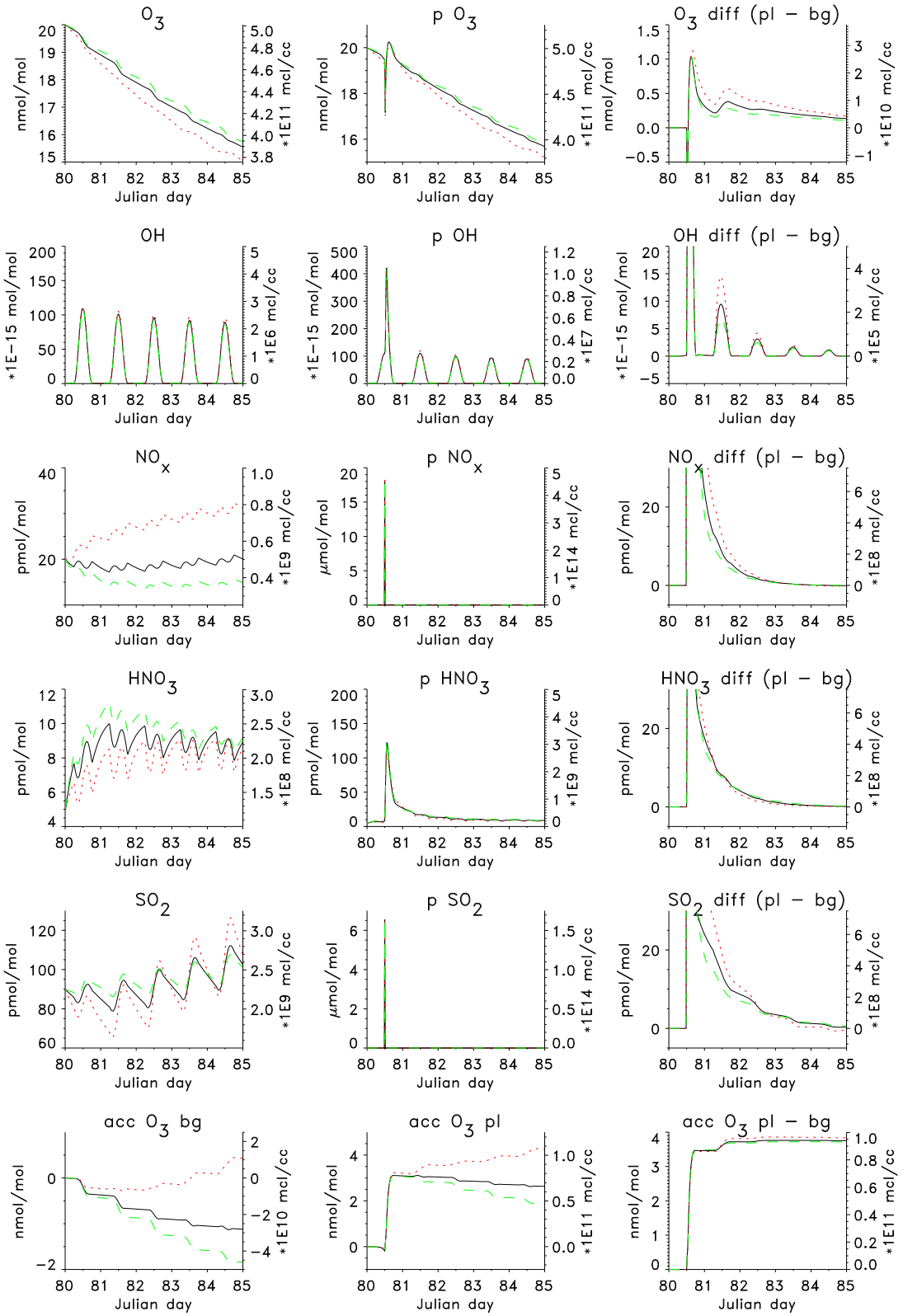

Figure 8.4: Same as Figure 8.1, but for runs with different MBL heights: black, solid line: $z_{MBL} = 1000$ m, red, dotted: $z_{MBL} = 600$ m, green, dashed: $z_{MBL} = 1400$ m.

A consequence of this is that processes that sustain high concentrations of the pollutants in the first hours of plume evolution lead to higher levels of pollutants in the plume later on. The height of the MBL defines the maximum height to which the pollutants can rise without extra buoyancy, because the inversion at the top of the MBL provides a barrier for the vertical transport of pollutants. A shallow MBL means that the pollutants are confined to a smaller volume of air and therefore the concentrations are higher. As relative changes in concentrations due to entrainment of background air are strongest in the first hours after plume release, a shallower MBL has the same net effect as small values of α for the horizontal mixing. This is shown in Figure 8.4, where the differences between background and plume air are apparent for the different MBL heights. When comparing the different runs in Figure 8.4 one has to keep in mind that dry deposition to the sea surface is more important in the cases with a shallow MBL than in cases with a high MBL.

8.3 Effects of heterogeneous chemistry

A correct treatment of the emission and subsequent mixing of aerosol between plume and background air is not possible for technical reasons with the box model used in the previous sections. This section is therefore restricted to a short comparison of the effets of heterogeneous chemistry on background aerosol (sulfate and sea salt) neglecting the emission of particles. Effects from the emission of particles will be studied with the one-dimensional model in chapter 9.

To allow for a spin-up of the aqueous phase chemistry in these runs the ship exhaust is emitted at noon of the third model day.

Figure 8.5 shows plots with different initial mixing ratios of NO_x and O_3, a run with reduced mixing velocity and a run without heterogeneous chemistry. The trends are similar as in the runs without inclusion of aerosol chemistry. The decline in HNO_3 is more rapid than without inclusion of aerosol chemistry because it is taken up by the particles, mainly by the sea salt aerosols. H_2SO_4 that is produced from gas phase oxidation of SO_2 by OH is also taken up by the particles. This results in a drop of sea salt aerosol pH from roughly 5.7 to about 4.7 (similar for all runs). As a consequence HCl degasses.

Through surface reactions (see Table D.3) and reactions in the gas phase, Cl_2 is formed in the plume air, where mixing ratios are up to twice as high as in the background air. The high NO mixing ratios result in a strong decrease in BrO due to the reaction

$$NO + BrO \longrightarrow NO_2 + Br.$$

This reaction has no net effect on O_x but reduces BrO strongly.

As discussed in section 4.2, $BrNO_3$ is formed by the reaction of BrO with NO_2. Subsequent reactions in the aerosol can lead to the liberation of Br_2 and BrCl from the particles.

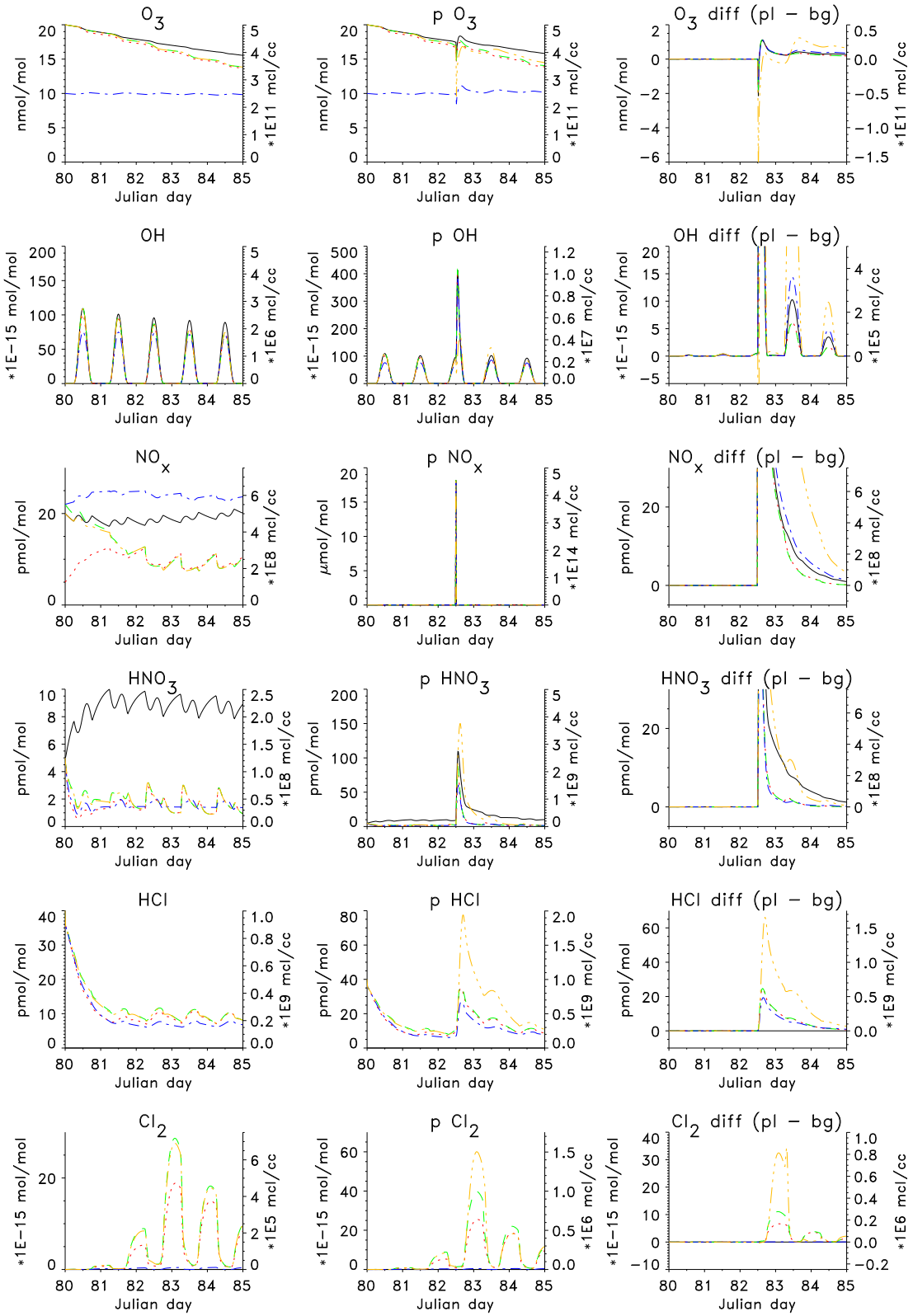

Figure 8.5: Same as Figure 8.1, but for runs including aerosol chemistry: black, solid line: no aerosol chemistry; red, dotted: init NO_x = 5 pmol/mol; green, dashed: init NO_x = 20 pmol/mol; blue, dash-dotted: init O_3 = 10 nmol/mol; orange, dash-dot-dot-dotted: $\alpha = 0.62$.

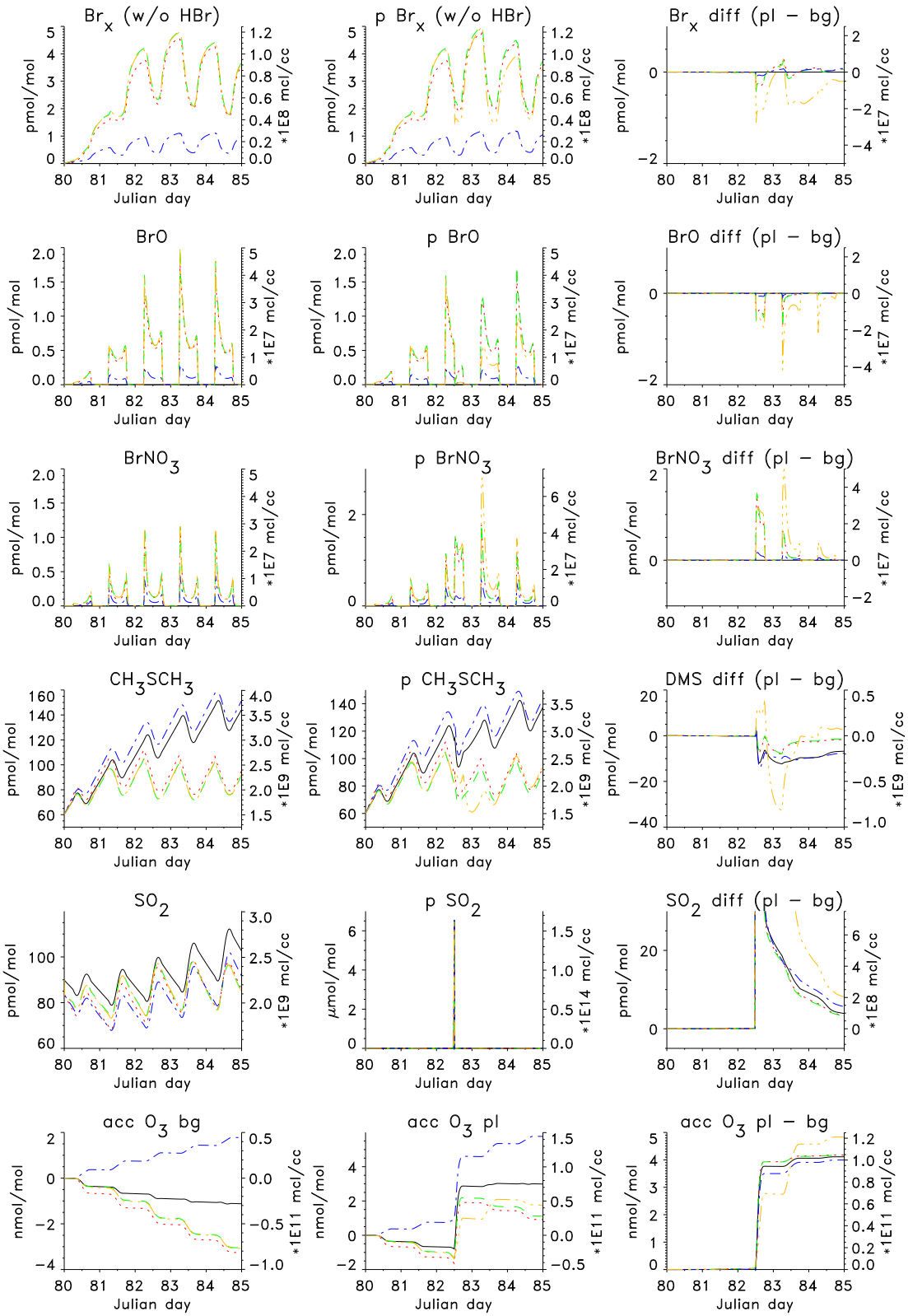

Figure 8.5: Continued. Br_x is the sum of all gas phase bromine species except HBr.

This bromine activation cycle cannot balance the decline in HOBr production by $BrO + HO_2$, as both, BrO and HO_2, are strongly reduced in the highly concentrated plume. The production of HBr in the plume leads to a decrease in Br_x on the first day after plume emission. Only later when NO mixing ratios are already small due to dilution, an increase in Br_x in the plume compared to the background can be seen in all runs except for the one with slow plume evolution, This is caused by reactions involving $BrNO_3$.

Production of DMSO is reduced in the run with aerosol chemistry compared to the undisturbed background because of the reduction in BrO mixing ratios. The increase in OH leads to a small increase in DMSO by the reaction DMS + OH but this increase is too small to compensate for the decline in the BrO related DMSO production (see also section 4.12). Additionally the loss of DMSO by the reaction DMSO + OH increases strongly, thereby enhancing the decline of DMSO mixing ratios.

8.4 Effects of multiple ship emissions

Until now the emission of only one ship has been studied. To get a more realistic picture the effects of the emissions of several ships have to be discussed. For this purpose a method of averaging the plume air of several ships with background air in a certain area is presented.

From the emission inventory of *Corbett et al.* (1999) annual mean emission fluxes in mass (nitrogen, sulfur) per area and time can be extracted. Given the emission of one ship per second, the number of ships per area that are needed to produce the listed emissions can also be calculated. For the most frequently crossed regions (North-Atlantic and North-Pacific) values from *Corbett et al.* (1999) are about 10^{-9} g(N)/(m^2 s) for a fleet that emits on average 74.5 g(NO_x)/kg_{fuel}. *Hobbs et al.* (2000) list the fuel consumption for ships studied during the MAST campaign with a mean of 0.84 kg_{fuel}/s. The fuel consumption was estimated from the nominal engine power as listed in ship registries and the observed ship speed. The numbers they estimated for NO emission on a mass per fuel base are significantly smaller than the numbers in *Corbett et al.* (1999) so use of the numbers of emission per ship from *Hobbs et al.* (2000) together with the numbers for large scale emissions from *Corbett et al.* (1999) would lead to inconsistencies (see also discussion in section 8.5). The use of the fuel consumption of *Hobbs et al.* (2000) is uncritical because the estimate of emissions does not influence the fuel consumption rate.

Based on these data and assuming all that NO_x is emitted as NO, an "average ship" emits 29.6 g(N)/s. This leads to 3.39 $\cdot 10^{-11}$ ships/m^2 that have to be present all year round in the more frequently crossed regions to produce the emissions that were estimated by *Corbett et al.* (1999). Taking the uncertainty of this estimate into account, sensitivity studies are made using values from 1 to 10 $\cdot 10^{-11}$ ships/m^2.

To estimate the impact of several ships in an area of a certain size the following

assumptions are made: i) All ships are homogeneously distributed over this area because the ocean regions considered are quite large and different destinations lead to different ship routes. ii) As most traffic in the more frequently traveled oceans crosses these regions from Asia to North-America and from North-America to Europe (or in the opposite direction) all routes are parallel.

In more frequented areas ships might emit their exhaust in air that has been polluted by a previous ship. To assess the probability of this, the lifetime of a ship plume during which it can clearly be distinguished from background air is estimated to be 2 days, based on the model runs discussed in previous sections. If mixing of plume with background air is assumed to be quicker (e.g. $\alpha = 0.87$) a plume lifetime of 1 day would result (see section 8.2). The mean lifetime of ship tracks during the MAST study was 7.3 h (*Durkee et al.* (2000a)). This lifetime was estimated from the effects of ship emissions on cloud albedo as measured from satellites. The definition for plume lifetime that is used here is different from their concept, as it is chosen to be the time that elapses until differences in the concentrations of the main gas phase species (O_3, SO_2, NO_x) between plume and background air are less than 5 to 10 %.

For convenience the following calculations are based on the emissions of ships in a certain area. The size of this "grid box" is determined by the distance that a ship travels during the chemical lifetime of its plume. From section 8.1 the chemical lifetime of a plume is known to be about 2 days. During 2 days a ship that has a speed of 10 m/s travels 1730 km. In the chosen grid box area of 1730 km by 1730 km between about 30 and 300 ships are cruising at any point in time based on the "ship density" given above. Two days after plume emission the plume width is w_{pl} = 85 km using $\alpha = 0.75$ (see equation 7.1). Therefore the area that is influenced by one ship in 2 days is $7.4 \cdot 10^{10}$ m^2 (0.5×85 km $\times$ 1730 km) or 2.5 % of the grid box area. When 300 ships are present in the grid box the plumes would overlap.

Based on these estimates seven mixing scenarios will be discussed: 30, 101 and 300 ships per grid box of 1730 km by 1730 km, each case with plume emission in background and prepolluted air and one with 101 ships, emission in plume air, but with a reduced plume lifetime.

If all ships are homogeneously distributed over the grid box their total plume over the estimated lifetime of two days has to be accounted for, because, in the same way as the plume of ships that are close to a border of the grid box would influence the neighboring box, the box under consideration is also influenced by neighboring boxes (see Figure 8.6).

For the cases of entrainment of background air the plumes are divided into different phases of plume development and a corresponding fractional plume volume is calculated for each phase (see Figure 8.7). The concentration in the plume in each phase is weighted with the respective fractional volume and number of ships. Using the remainder of the box volume as weight for the background air a mean mixing ratio can be calculated.

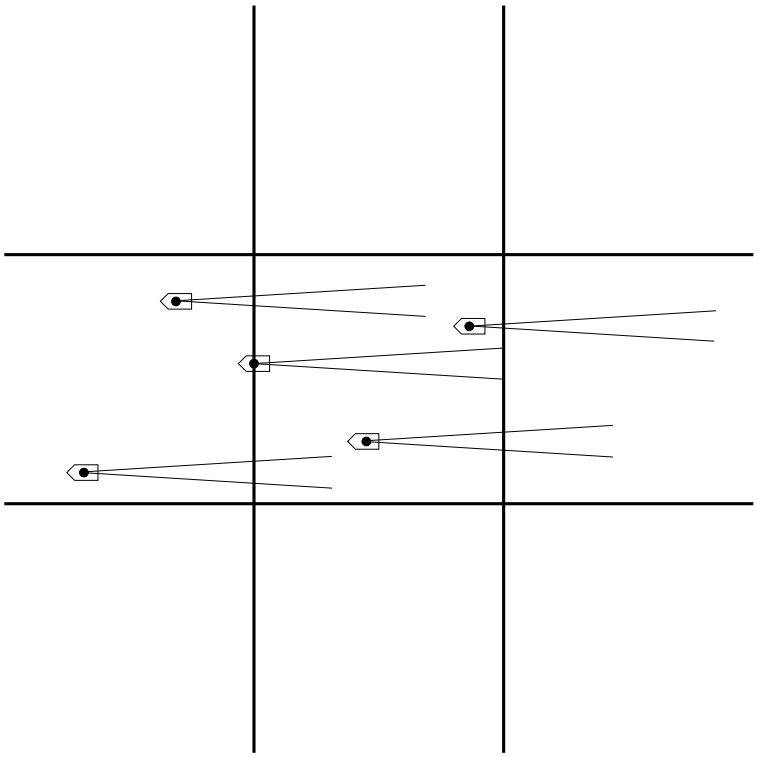

Figure 8.6: Influence of neighboring boxes on the mean mixing ratio.

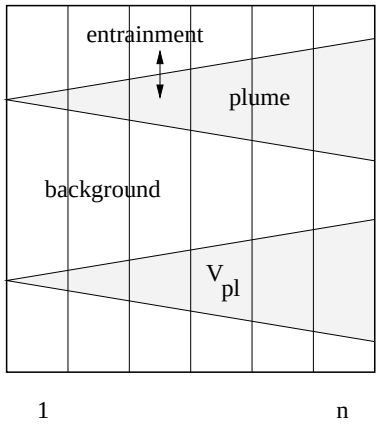

Figure 8.7: 1 to n are the different phases of plume development and V_{pl} is the corresponding fractional plume volume which is weighted by the number of ships in the grid box.

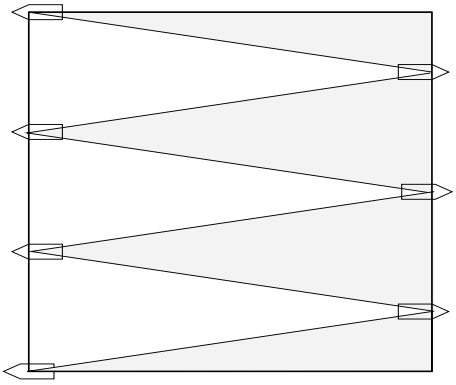

Figure 8.8: Schematic of the calculation of the maximum ship number in a grid box. Shown are the plumes of ships going e.g. from weast-to-east and of others going from east-to-west.

For the case of entrainment of prepolluted air further assumptions have to be made. Depending on the time that elapsed since plume emission of a first ship, the next ship would emit in air which is polluted to various degrees, which has implications for the gradient of pollutants between the airmasses that determines

the dilution rate (see equation 7.3).

Assuming half of the ships to travel from west-to-east and the other half to go in the opposite direction and assuming the distance between two ships that travel parallel to be the plume width at the end of its lifetime, one can calculate the maximum number of non-overlaping ship plumes for a certain area per grid box. If this number is smaller than the number of ships per grid box calculated from the ship density, then overlap of plumes has to occur. For a grid box of 1730 km by 1730 km the maximum number of ships going in parallel is 40 (20 west-to-east and 20 east-to-west, see Figure 8.8). In the case of 300 ships this implies that 7.5 plumes (=300/40) overlap, resulting in a mean time between 2 ships of 6.5 h (=48 h/7.5). In the case of 101 ships 2.5 plumes would overlap, leading to a mean time between 2 successive ships of 19 h. For 30 ships per grid box no overlap would have to occur, but since it is likely to occur statistically an estimate for this case is also given. The number of ships traveling parallel was reduced to 20 and the time for the encounter of an old plume was set to 24 h. It is assumed, that the air that is mixed into the new plume has been influenced by a previous ship traveling 6.5, 19 or 24 h, respectively, earlier. For the mean concentrations for these scenarios runs with plume emissions at different local times have been averaged to account for differences in the plume chemistry when photochemistry is involved (during day) and when it is not (during night).

This averaging approach is only one of several possibilities, but all of them are associated with large uncertainties that are difficult to assess. One problem certainly is the degree of pollution in the air that is entrained into an expanding plume. For heavily traveled ocean regions the approach that is used here is clearly an underestimation because the pollutants of only one preceeding ship are accounted for, whereas in the atmosphere most likely several plumes of various plume ages would overlap. Then no "background" air can be defined any longer, which is used in the approach that is applied here for the dilution of the predecessor plume. It would be very desirable to be able to include effects of more realistically overlaping plumes but this would have to be done with a mesoscale three-dimensional model where different plumes can be resolved.

The resulting mean mixing ratios are listed in Table 8.1. The "30 ships, clean" case can be seen as most relevant for less heavily traveled regions and the "101 ships, poll" case as most relevant for the North-Atlantic and North-Pacific. For coastal regions the "300 ships, poll" case might apply. According to these data the lower limit of 30 ships cruising in an area of 1730 km by 1730 km and emitting into background air would be nearly indistinguishable from the background air. A fleet of 300 ships emitting into background air would increase OH by 3 %, NO_x by 57 % and SO_2 by 2 % compared to a case without ship emissions.

The effects of emission into prepolluted air are more apparent, especially for the fleet of 300 ships. Here O_3 is predicted to increase by 4 % compared to background air, OH would increase by 67 %. NO_x would increase by a factor of 13.6 and SO_2 by 64 %.

In the more realistic case of 101 ships in an area of 1730 km by 1730 km, O_3 would increase by 3 %, OH by 13 %, SO_2 by 33 % and NO_x would increase by a

factor of 5.

While the increase in NO_x and SO_2 are quite large, the consequences for e.g. O_3 would be limited. As already discussed above, the "30 ships, clean" case from Table 8.1 would be representative for most ocean regions except for the North-Atlantic and North-Pacific and coastal regions. This estimate shows, that globally only minor effects of ship emissions on the mixing ratios of O_3, OH, NO_x, and SO_2 would be expected, even if the plumes of several ships would overlap.

The run with enhanced entrainment of air into the plume (marked with [1] in Table 8.1, for conditions in the North-Atlantic and North-Pacific) shows a moderate decrease of the effect of ship emissions on O_3 and OH (compared to the "101 ships, poll" case with a mixing time of 2 days). Increases in NO_x, HNO_3, and SO_2 would still be significant.

For more discussion and comparison with results from runs with continuous emissions, global model results, and measurements see section 8.5.

Table 8.1: Mean mixing ratios for multiple ships.

case	O_3	OH	NO_x	HNO_3	SO_2
	[nmol/mol]	[molec/cm^3]	[pmol/mol]	[pmol/mol]	[pmol/mol]
background	20.4	$6.0 \cdot 10^5$	6.8	1.6	88.1
30 ships, clean	20.5	$6.1 \cdot 10^5$	7.2	1.6	88.2
101 ships, clean	20.5	$6.1 \cdot 10^5$	8.1	1.7	88.7
300 ships, clean	20.5	$6.2 \cdot 10^5$	10.7	1.8	89.8
30 ships, poll	20.9	$6.7 \cdot 10^5$	15.7	3.4	103.4
101 ships, poll	21.2	$7.4 \cdot 10^5$	33.8	6.3	117.4
300 ships, poll	21.2	$10.0 \cdot 10^5$	92.9	15.3	144.4
101 ships, poll [1]	20.6	$6.1 \cdot 10^5$	30.7	5.5	106.8
cont. gas [2]	26.4	$14.1 \cdot 10^5$	109.6	82.0	246.5
cont. aerosol [2]	24.6	$11.9 \cdot 10^5$	81.6	16.4	232.9

Mean mixing ratios in a grid box of 1730 km by 1730 km. 30 ships in this area correspond to an emission of $2.7 \cdot 10^{-10}$ g(N)/(m^2 s), 101 ships correspond to $1 \cdot 10^{-9}$ g(N)/(m^2 s) and 300 ships to $2.7 \cdot 10^{-9}$ g(N)/(m^2 s), respectively. In the "clean" cases background air is mixed into the plume, whereas in the "poll" cases air that has been influenced by a previous ship is mixed into the plume. For a description of the "poll" cases see text. In the "background" case no ship emissions are considered. In all runs background aerosol chemistry (sulfate and sea salt) was included and a constant source of O_3 (from the free troposphere) was applied to yield constant O_3 mixing ratios over the averaging time for the "background" run. Plume lifetime for these runs was 2 days. [1] $\alpha = 0.87$, $\beta = 0.65$, plume lifetime was reduced to 1 day and the area of the grid box used for averaging was adjusted. [2] Average values from the runs discussed in section 8.5. The O_3 values are even higher in steady state, 30 nmol/mol for the run with aerosol chemistry ("cont. aerosol") and 40 nmol/mol for the run without aerosol chemistry ("cont. gas").

8.5 Comparison with results from global models

Kasibhatla et al. (2000) and *Davis et al.* (2000) suggested that the impact of ship

emissions on NO_x concentrations in the MBL might by overestimated by global models compared to measurements. To check this and to be able to compare the results from the box model with the results from global models (*Lawrence and Crutzen* (1999), *Kasibhatla et al.* (2000)) model runs were perfomred where the emissions were treated like in a global chemistry transport model by assuming a continuous source. In the left column of Figure 8.9 a run with background conditions is shown whereas continuous emissions are used in another run shown as "ship" in the middle column of Figure 8.9.

The estimates for the emissions are typical values for the North-Atlantic from *Corbett et al.* (1999). According to these data, emission of NO is about 10^{-9} g(N)/(m^2 s) which translates to $4.3 \cdot 10^9$ molec(NO)/(cm^2 s). Emission of SO_2 is roughly $1.3 \cdot 10^{-9}$ g(S)/(m^2 s) or $2.45 \cdot 10^9$ molec(SO_2)/(cm^2 s). Using a similar scaling approach as for the data in Table 7.2 emissions for CO were estimated to be $4 \cdot 10^8$ molec/(cm^2 s) and $2 \cdot 10^7$ molec/(cm^2 s) for HCHO. Two runs are presented, one neglecting aerosol chemistry as in most CTMs and a second one including aerosol chemistry. Due to the resctrictions discussed above here again no particles are emitted in the run with aerosol chemistry.

These runs (see Figure 8.9) show significant production of O_3. A steady state for O_3 would be reached after 15 days at levels around 30 and 40 nmol/mol including a continuous source for the runs with and without aerosol chemistry, respectively, and at levels of 20 and 24 nmol/mol for background air. The mixing ratios of OH are roughly doubled.

NO_x levels increased to 100 - 120 pmol/mol in the run without aerosol chemistry and to 70 - 100 pmol/mol in the run including aerosol chemistry. The difference in steady state between these 2 runs of about 20 - 25 pmol/mol implies an additional sink of roughly 20 - 25 pmol/(mol day) in the run including aerosol chemistry. The heterogeneous reactions responsible for this difference are uptake of NO_3, N_2O_5, and XNO_3 (X = Cl, Br) on the aerosol. In the model the most important path is uptake of $BrNO_3$ on the sulfate aerosol (for a discussion of this process see section 4.2 and *Sander et al.* (1999)) accounting for roughly two-thirds of the total loss of NO_x. For a discussion of the importance of uptake on cloud droplets see section 9.3.

The effects of heterogeneous chemistry on chlorine and bromine in the plume are very similar to the ones discussed in section 8.3. The diurnal variation in the difference in Br_x between the background and the polluted air is caused by an increase in the production of HBr through reactions of Br with HCHO. HBr is subsequently recycled by the aerosol (see also section 4.4).

The results for NO_x, OH and O_3 from these runs are comparable to but somewhat smaller than that from global models (*Lawrence and Crutzen* (1999), *Kasibhatla et al.* (2000)). Chemistry on aerosol particles appears to explain only part of the great differences between measurements of NO_x and global model results (again it has to be added that only background aerosol was used here).

When the results from the runs with a continuous source of ship emissions are compared with the averaged values from the study of overlaping plumes from section 8.4 that add up to the same emission flux (case "101 ships, poll", see

Table 8.1) differences of about a factor of 3 in NO_x, a factor of 2 on OH, SO_2 and HNO_3 are apparent. As already mentioned on page 83 the dilution of plume air does not affect the mass balance of the emitted species because dilution in the model is only by entrainment of background air and not by detrainment of plume air.

These differences are related to the extremely high NO_x mixing ratios and very rapid dilution in plume air compared to constantly high NO_x values in the air affected by a continuous source. The differences are a result of different lifetimes of NO_x in air with high NO_x and OH concentrations (plume air, see Figure 8.5) and in air with moderate increases in these 2 species (continuous emissions, see Figure 8.9).

The lifetime of NO_x in the plume is strongly reduced compared to background situations. Peak concentrations of OH in the plume are about OH=1.1 $\cdot 10^7$ molec/cm^3 (see Figure 8.5). Using a rate coefficient of $k = 9.1 \cdot 10^{-12}$ cm^3/(molec s) (*Sander et al.* (2000) at p=1013.25 hPa, T=298 K), the NO_x e-folding lifetime due to the reaction $NO_2 + OH \longrightarrow HNO_3$ would be about 2.76 h compared to 14.7 h in the background air (based on a OH concentration of about $2 \cdot 10^6$ molec/cm^3, see Figure 8.5). The mean lifetime of NO_2 in the first 6 hours after plume emission (which occured at 12:00) is about 7.5 h in plume air compared to 26.9 h in undisturbed air, i.e. NO_2 is lost 3.6 times as fast as in the background air. Comparing this with data for the runs with continuous emissions, one finds peak OH concentrations of OH=$5 \cdot 10^6$ molec/cm^3 (see Figure 8.9) leading to a lifetime of about 6.1 h, i.e. the loss of NO_2 is more than twice as fast in the case where the very high plume concentrations are considered than in the run with continuous emissions from ships.

The mean lifetime of NO_2 in the runs with continuous emissions between 12:00 and 18:00 (i.e. the same time span as given above) is 12.7 h, i.e. 1.7 times longer than in the run with description of plume chemistry. NO_2 loss is strongest in the first hours after plume emission, so the large differences in NO_2 lifetime during this period are most relevant for a comparison between the two discussed emission scenarios. From these estimates it is obvious that the correct treatment of plume evolution is critical in assessing the effects of ship emissions. HNO_3, the product of $NO_2 + OH$, is taken up by particles that eventually sediment or is directly deposited to the ocean surface and thereby lost from the atmosphere.

For completeness the 24 h mean values for the lifetime of NO_2 are given, but, as just explained they are not the relevant property to look at to assess the effects of ship emissions. The 24 hours mean lifetimes are 55.5 h for background air, 23.2 h for plume emission at the beginning of the 24 h averaging period and 24.7 h for the continuous case. *Kasibhatla et al.* (2000) used prescribed OH - fields in their CTM resulting in a NO_2 lifetime of 0.75 – 1 days. They already pointed to the possibility that NO_x destruction could be faster on spatial scales not resolved by their model.

The NO_x mixing ratios determined with the averaging of overlaping plumes are still higher than the measured values reported by *Kasibhatla et al.* (2000) and *Davis et al.* (2000).

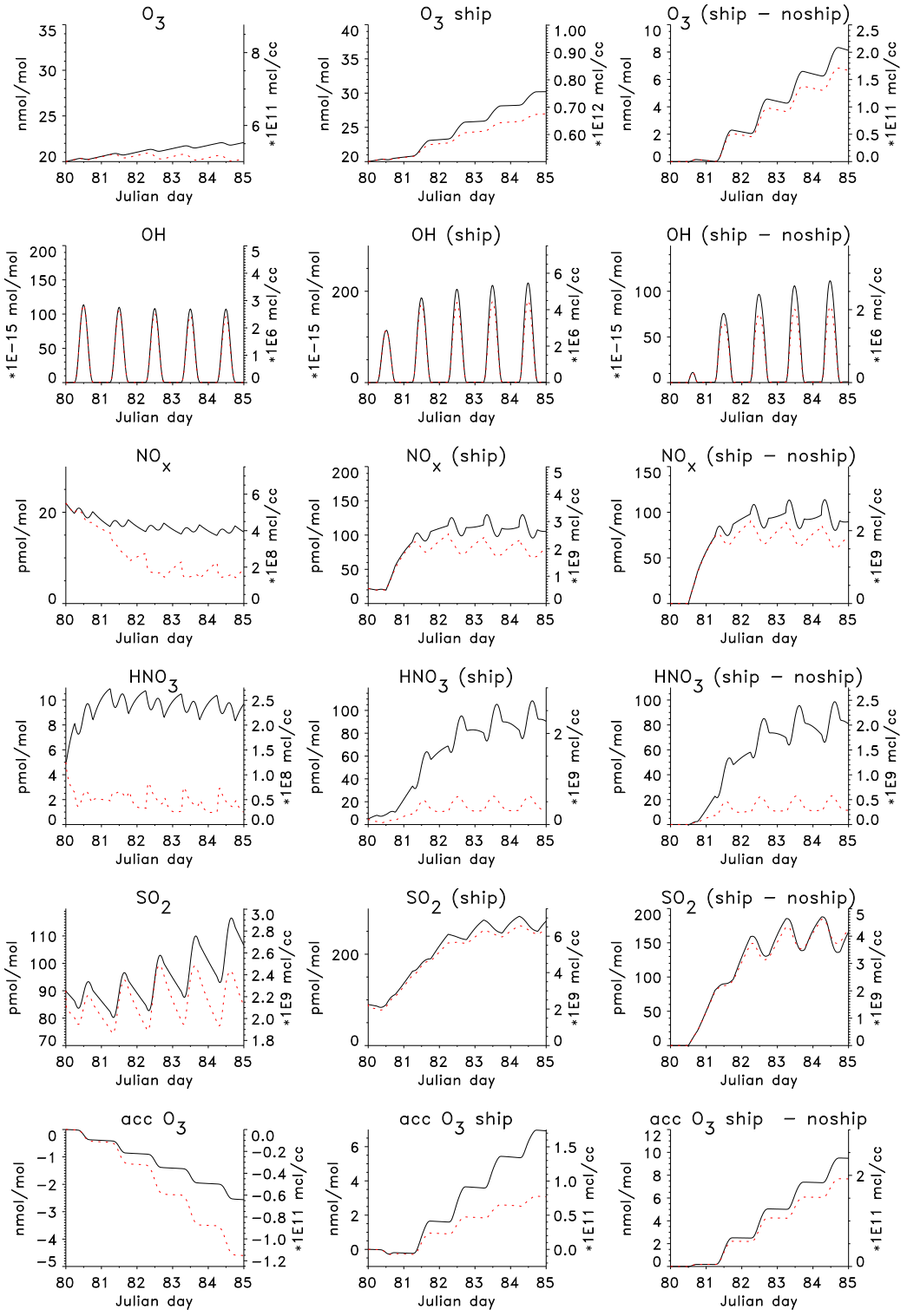

Figure 8.9: Same as Figure 8.1, but for continuous emission of ship exhaust. Run without aerosol chemistry (black, solid line) and run including aerosol chemistry (red, dotted line). The left column shows mixing ratios in undisturbed air, the middle column mixing ratios in air disturbed by a continuous source of ship exhaust and the right column the differences. A constant O_3 source was applied to yield constant O_3 values for the undisturbed run including aerosol chemistry.

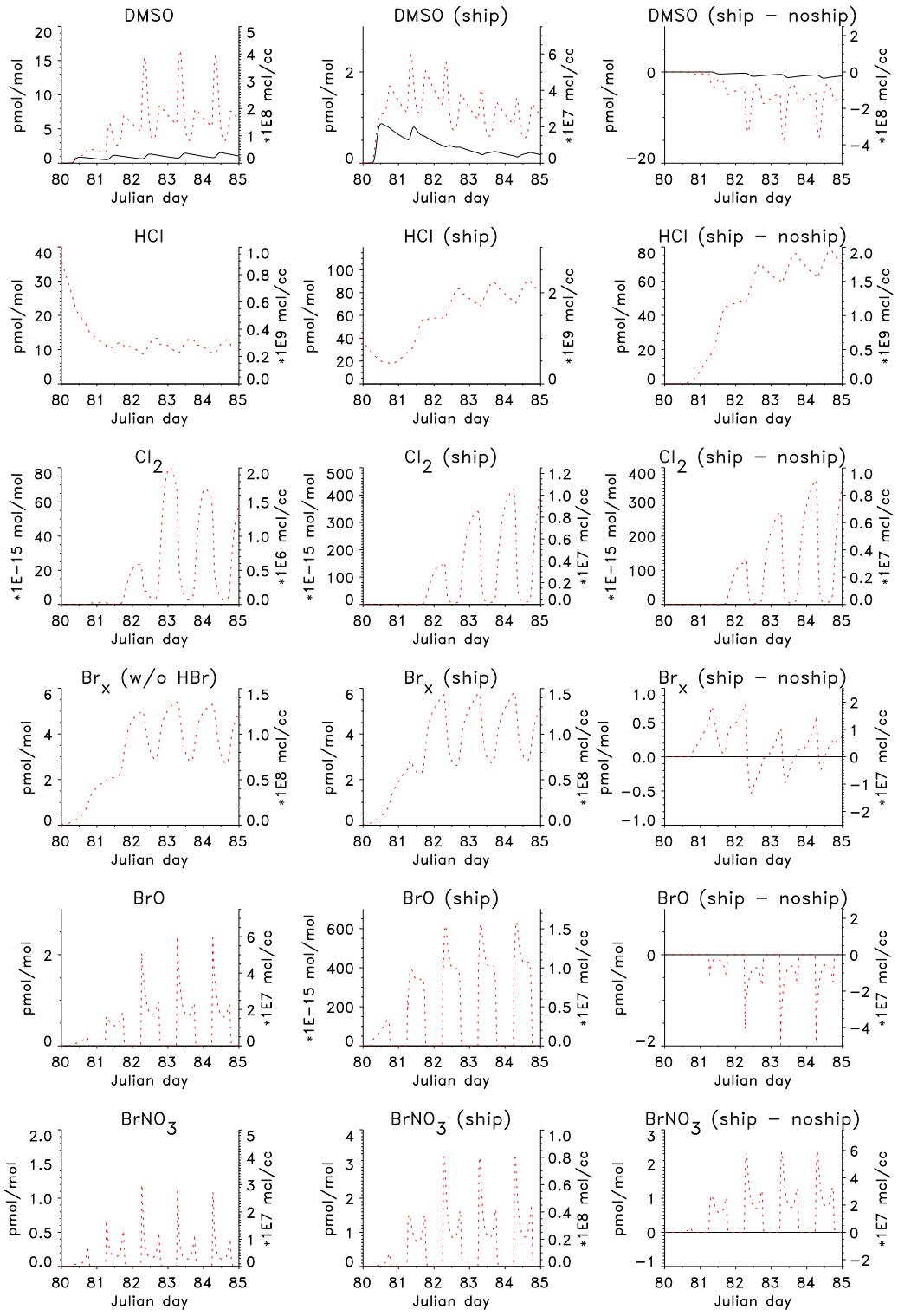

Figure 8.9: Continued.

Explanations for this contradiction in the results could be one or more of the following: The averaging approach for plume air could still overestimate

NO_x mixing ratios. Important chemical processes might not be accounted for. Furthermore problems could exist in the emission inventory that was used.

The emission of NO_x per ship in units of $g(NO)/kg_{fuel}$ as given by *Corbett et al.* (1999) would give an average of 74.5 $g(NO)/kg_{fuel}$, the data from *EPA* (2000) would approximately yield 50 $g(NO)/kg_{fuel}$, whereas the data by *Hobbs et al.* (2000) are less than 20 $g(NO)/kg_{fuel}$, which is a factor of 3 - 4 lower than the data of *Corbett et al.* (1999) that were used in this study.

If ship emissions were overestimated by *Corbett et al.* (1999) by this factor and if the difference in the treatment of ship emissions as continuous emissions versus plume emissions is correctly estimated to be a factor of 3 then it would not be surprising to see that ship emissions would not lead to detectable differences in NO_x over the oceans.

Therefore there is clearly a need for more data on global ship emissions, for measurements over the more heavily traversed ocean regions and for more information on possible chemical reactions on combustion particles.

In coastal regions or e.g. in the oceans off Asia where highest growth rates in ship traffic are expected (*Corbett et al.* (1999)) ship emissions definitely play a role for air quality, now and in the future. Between 1988 and 1995 emission from ships in Asian waters are estimated to have grown by 5.9 % per year (*Streets et al.* (2000)). The effect of sulfur emissions will be discussed in chapter 9.

Chapter 9

1D model ship plume studies

The one-dimensional MBL model that was presented in chapter 3 and modified as discussed in chapter 7 to include entrainment of background air and emissions from ships was also used for ship plume studies. In this chapter the results of simulations of the chemical and physical evolution of a ship plume using this modified model are discussed. Emission of the ship exhaust is at a height of 35 m at 9:00 on the second model day to allow for some spin-up of the aerosol chemistry.

In sections 9.1 and 9.2 the effects of ship plumes in a cloud-free MBL are considered, sections 9.3 and 9.4 deal with the effects in a cloudy MBL.

9.1 Major features of a ship plume in the cloud-free MBL

First a comparison of model results with measurements in early plume stages is made. *Frick and Hoppel* (2000) used an airship to measure gases and particles in ship plumes. They provide data for a plume of an "unidentified ship" with an age of about 8 min at a height of 90 m before the plume encountered any significant cloud cover. SO_2 increased from background values of 0.1 nmol/mol to 10 nmol/mol, whereas O_3 dropped from 40 to 25 nmol/mol. Condensation nuclei (CN) concentrations were about 3 - 4 $\cdot 10^4$ cm^{-3}.

On another occasion they transected a plume of the *Sea Pearl* with an age of approximately 2 to 3 min. In this case O_3 decreased by about 10 nmol/mol and SO_2 increased up to 50 nmol/mol and CN concentrations sometimes exceeded 1 $\cdot 10^5$ cm^{-3}.

Russell et al. (1999) list "track" conditions for the *Star Livorno* in clean background air, where SO_2 rose to 3.7 nmol/mol. O_3 dropped from 26 to 21 nmol/mol. The NO mixing ratio was 0.3 nmol/mol and the NO/NO_2 ratio, that is usually less than 1 when NO and NO_2 are in a photochemical steady state, was 6 indicating fresh plume air where no (confirmed by Lynn Russell, pers. comm., 2000). The total particle number was 1.8 $\cdot 10^4$ cm^{-3}.

Using the emission estimates from section 7.2, the modeled numbers in the

lower MBL after 8 min were 2.5 nmol/mol for SO_2, O_3 decreased from 24 nmol/mol to 20 nmol/mol. The total particle number in the model is 4 $\cdot 10^3$ cm^{-3} which is about 10 % of the measured values and is therefore in agreement with the downscaled emission of particles.

After 3 min the SO_2 mixing ratio in the model is around 10 nmol/mol, O_3 decreased by 12 nmol/mol. Total particle number concentration is greater than 1 $\cdot 10^4$ cm^{-3}.

The modeled concentrations in the early plume stage are in the correct order of magnitude. They are smaller than the values measured by the airship (*Frick and Hoppel* (2000)) but close to the numbers of *Russell et al.* (1999). Differences in MBL height between the model (700 m) and in the field (300 m for the *Sea Pearl* case and 450 m for the *Star Livorno*) might be responsible for part of the differences, because vertical dilution is less strong in a shallower MBL. In another model run with a shallow MBL of about 300 m (not shown), the surface mixing ratio of SO_2 15 min after plume emission was 75 % greater than in the run with a MBL height of 700 m. This indicates that even in the first minutes after plume emission vertical mixing is important. The assumption of homogeneous mixing ratios throughout the modeled plume (see p. 83) might have lead to an overestimation of dilution in the minutes after plume release when the plume might still be quite confined in the atmosphere. Unfortunately no data were sampled by the airship more than 10 km (or 30 min) away from the ships (Glendon Frick, pers. comm., 2000).

In general the plume evolution in the one-dimensional model is similar to the ones discussed for the box model in the previous chapter, so I will concentrate on the additional information from the one-dimensional model, i.e. the vertical evolution and the importance of particle emissions. Furthermore, influence of the emissions on the sulfur cycle, emission during night, and the possible formation of reservoir species will be discussed.

Figure 9.1 shows vertical profiles of major gas phase constituents 15, 30 and 45 minutes after plume release. After 15 min the ship emissions are still mainly in the lower half of the MBL. The extreme high concentrations that occurred in the first minutes after plume release are already strongly relaxed by dilution. The gases that are directly emitted show a strong reduction and upmixing during the timespan of 30 min that is shown in Figure 9.1. The gases that are influenced indirectly mostly show an increase of the perturbation during this time. O_3 has a two-fold behaviour. In the first minutes of the plume emission it is titrated by NO, but roughly one hour after plume release production by catalytic cycles involving NO_2 is strong enough to raise the O_3 concentrations above background values.

The reaction of NO with BrO in the layers below 300 m results in the strong reduction of BrO there (for an undisturbed vertical profile of BrO see Figure 4.7). BrO starts recovering in the lower layers already when the destruction in higher layers is still increasing. Above about 400 m Br (not shown) is not produced significantly from reactions with BrO because NO mixing ratios are a lot smaller there than during the early plume stages in lower layers. Furthermore, the ratio

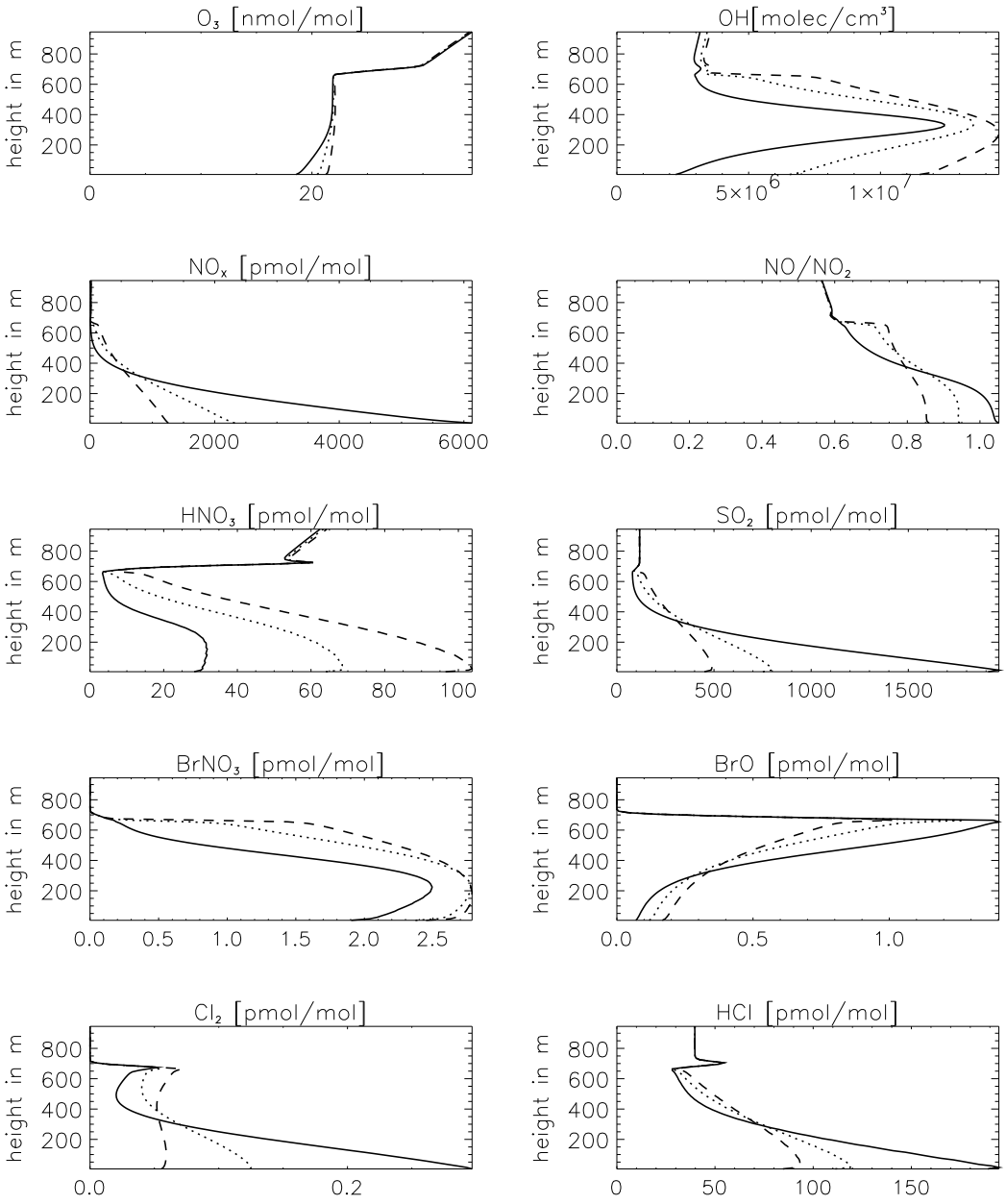

Figure 9.1: Vertical profile of the main gas phase species for the cloud-free case with ship emission at 9:00 on the second model day. Solid line: 15 min, dotted line: 30 min, dashed line: 45 min after plume release.

of NO/NO_2 decreased from about 1 to less than 0.8 during the transport of NO_x to higher layers. Together this makes the reaction $BrO + NO_2 \longrightarrow BrNO_3$ a lot more important than $BrO + NO \longrightarrow Br + NO_2$.

OH increases steadily at all heights during the 30 min shown in Figure 9.1 but it has a very obvious maximum around 300 m. This is caused by two competing processes: production of OH mainly by reaction of NO with HO_2 and destruction

of OH by reaction with CO. Both NO and CO are emitted by ships, but in the first minutes after plume emission the production of OH by reaction of HO_2 with NO (or of $O(^1D)$ with H_2O) is reduced due to low HO_2 ($O_3/O(^1D)$) mixing ratios in the lowest model layers. NO was transported to higher layers by vertical mixing making $NO + HO_2$ more important for the production of OH there than $O(^1D)$ with H_2O. In lower layers not only the production of OH is reduced but the destruction is increased due to the emission of CO. Around 300 m the net OH producing effects have a maximum. The layers above roughly 300 m have yet only moderately been influenced by ship emissions, so OH increases relative to background conditions are smaller there. Two hours after plume release the maximum in the vertical profile of OH disappeared (not shown).

Figure 9.2 depicts the evolution of the plume air in 450 m compared to the base run that was dicussed in chapter 4. The plot starts 3 hours after plume emission. Perturbations in NO_x, HNO_3, $BrNO_3$, and BrO disappeared about one day after plume release. The difference in SO_2 is strongly decreasing, whereas the perturbations in O_3, Cl_2, and HCl have a longer lifetime. The lifetime of the perturbations is longer than in most of the box model runs discussed in the previous chapter where the height of the MBL was 1000 m compared to the 700 m used in the one-dimensional runs. As explained in section 8.2 (see also Figure 8.4), a shallower MBL slows down dilution.

Perturbations in longlived species that are present after the end of the initial mixing phase with strong entrainment of background air are maintained, because for these species dilution by entrainment had temporarily been the most important loss process which is then missing. This phase lasts about 6 hours as can be seen from the behaviour of a longlived tracer that was present only in the background air with steadily rising concentrations. In the plume air the tracer concentration approaches background values soon after plume emission (which is also the start of entrainment) but does not rise as in the background after about 6 hours (see Figure 9.3) indicating that entrainment is only of limited importance later on. After 6 hours the width of a plume that expands with an $\alpha = 0.75$ is about 18 km, corresponding to a dilution ratio of 1:1800.

In this context not only O_3 but also the sum of all gas and aqueous phase chlorine (except for sea salt Cl^-) can be regarded as longlived. Chlorine is rapidly cycled between the different species and the gas and the aqueous phases. Reactions of hydrocarbons with e.g. Cl in the plume would yield HCl as product which can be taken up by the aerosol and recycled in similar steps as described in section 4.4 for bromine. Dry deposition leads only to a moderate loss of Cl_2 and HCl in the model as can be seen from Figure 9.2.

Dry deposition is not very important for these species so the relatively high chlorine values are "self-sustained" by cycling between the different reservoirs. A similar behaviour could be expected for the bromine species that have similar reaction paths. The difference is that bromine was already largely partioned to the gas phase, so no significant amounts of additional bromine could be released from the sea salt. Only a redistribution among the different bromine species occurred. The formation rates and therefore also the mixing ratio of $BrNO_3$

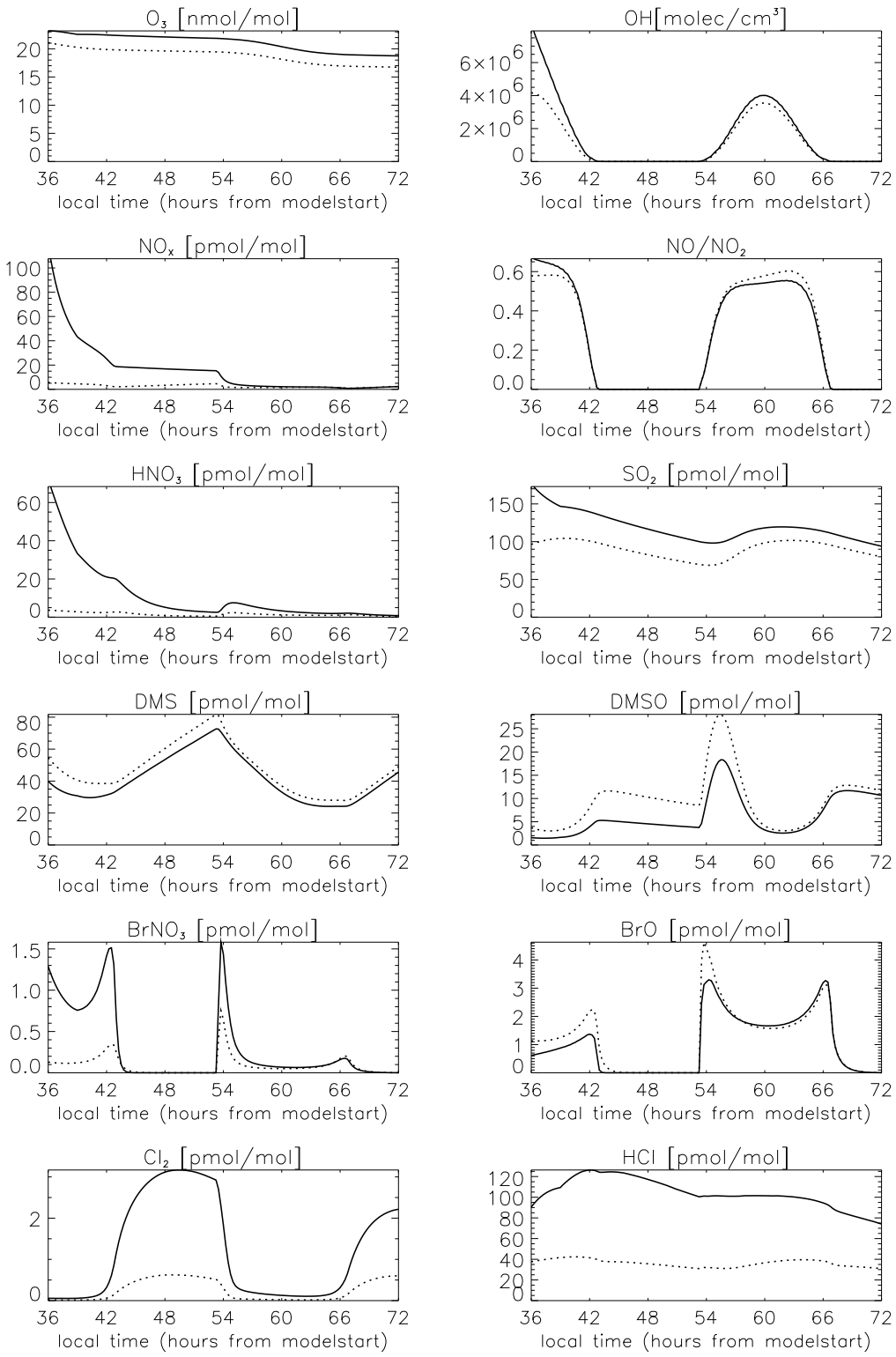

Figure 9.2: Evolution with time of the main gas phase species for a cloud-free run with ship emission at 9:00 on the second model day (solid line) and the base case from chapter 4 without ship emissions (dotted line) in 450 m height.

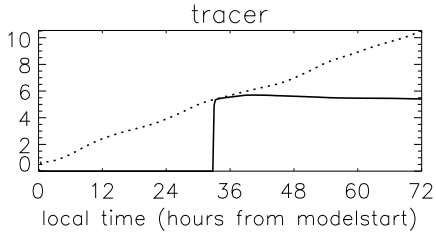

Figure 9.3: Evolution with time of a passive tracer that is present only in the background air (arbitrary units). The concentrations of the tracer in the plume air is shown as solid line, whereas it is shown as dotted line for the background.

decreases on the second day after plume emission due to lower NO_2 levels. If in a different airmass the bromine acivation from the sea salt aerosol would have been less complete before the emission of ship exhaust, additional bromine would have been released. Then the behaviour of chlorine and bromine would be the same.

Emission of SO_2 by ships have several consequences for the MBL as discussed e.g. by *Capaldo et al.* (1999) and *Durkee et al.* (2000b) and as already mentioned briefly above. SO_2 can condense on existing particles making them more hydrophilic and more likely to be activated as CCN, it can be taken up by cloud droplets and, if the droplets do not rain out, be incorporated in the aerosol upon droplet evaporation, or it can form new aerosol particles by gas-to-particle conversion. As most of these processes have an impact on droplet number concentration, droplet radius and cloud lifetime they are of importance for the radiative balance of the earth. Of the processes just mentioned, only new particle formation is not included in the model.

Three hours after plume release the SO_2 concentration in the plume air is about twice as high as in the background and 39 hours after plume emission it is roughly 15 % higher. The increase in S(VI) in the sulfate aerosol is about 4 % and due to the long lifetime of the particles the surplus above the background values is decreasing only slowly. In the shorter lived sea salt aerosols the S(VI) increase is about 100 % 3 hours after plume emission and reduced to roughly 4 % at the end of the model run.

DMS is reduced by the high OH concentrations, mainly producing SO_2. The decrease in DMSO due to ship emissions has already been explained in section 8.3. If DMSO is destroyed by OH SO_2 is produced. Taking all DMS reaction paths together, the conversion of DMS to SO_2 is increased in the ship plume from about 0.25 nmol/(mol day) in the background to roughly 0.5 nmol/(mol day) in the first hours after plume emissions before the rates decrease to background values. This is not much compared with the direct emission of SO_2 by ships but, especially in heavily traveled ocean regions, the lifetime of DMS is considerably reduced by the high OH concentrations.

According to *Pham et al.* (1995) methenosulfonic acid (MSA) is assumed to be a product of the reaction of DMSO with OH. Due to high OH concentrations in the plume its production is higher than in the background air as long as

DMSO + OH is high. After a few hours, however, when DMSO decreased in the plume air MSA concentrations are smaller than in the background air.

In the reaction of NO_2 with $CH_3C(O)O_2$ peroxyacetylenitrate (PAN) is formed, which decomposes thermally. Due to the rather high temperatures in the presented model runs, PAN that is formed in the plume rapidly decomposes. But when it is cooler, e.g. at high latitudes or in winter, the formation of PAN would act as a reservoir for NO_2 and could be transported to regions that were previously unaffected by ship exhaust.

A similar process was discussed by *van Dingenen et al.* (1994), namely the formation of a PAN-like peroxynitrate intermediate species in the reaction of DMS with NO_3 which *van Dingenen et al.* (1994) called MSPN ($CH_3S(O)_2O_2NO_2$). MSPN is stable at low temperatures and would be a reservoir for sulfur as well as for nitrogen. Formation of MSPN might be important when NO_3 mixing ratios during night are still high after emission of a ship plume during daylight or especially from emissions during night. Like in the case for PAN, MSPN could be transported to the free troposphere or more remote areas and be a source of nitrogen and sulfur there. Due to large uncertainties with the overall reaction scheme of DMS the intermediate formation of MSPN has not been included in the model.

Figure 9.4 shows a comparison between a run with ship emissions at midnight and emissions at 9:00. NO_3 mixing ratios exceed 1 pmol/mol in the run with emissions at midnight, 15 times higher than in the undisturbed run. If emissions take place at 9:00 NO_3 is still substantially higher in the following night than in the background air (roughly 5 times) but it does not reach the levels of the case with emission during night. If the ship exhaust is emitted during night the reaction of NO_3 with DMS becomes important, it produces the decrease in DMS that is visible in Figure 9.4. The formation of $ClNO_2$ and $BrNO_2$ in surface reactions of N_2O_5 at the aerosol particles in the "midnight" run which are rapidly photolyzed leads to a strong increase of $BrNO_3$ after sunrise. This does not lead to an increase in BrO because the reaction of BrO with NO is still the most important loss process for BrO. The behaviour for chlorine is similar to that of bromine.

The longer term evolution of ship exhaust with emission during night and day is quite similar.

9.2 Aerosol chemistry in the ship plume

As already explained in section 7.2 only the emission of soluble particles by the ship is included in the model runs with the one-dimensional model.

Reactions on carbonaceous combustion aerosol particles might play a role in the early stages of plume development when the concentrations of combustion particles have not yet been diminished to a significant extent by dilution. *Jacob* (2000) and *Ravishankara* (1997) state that reactions on the surfaces of combustion aerosols will only be of importance in the atmosphere as long as the surface

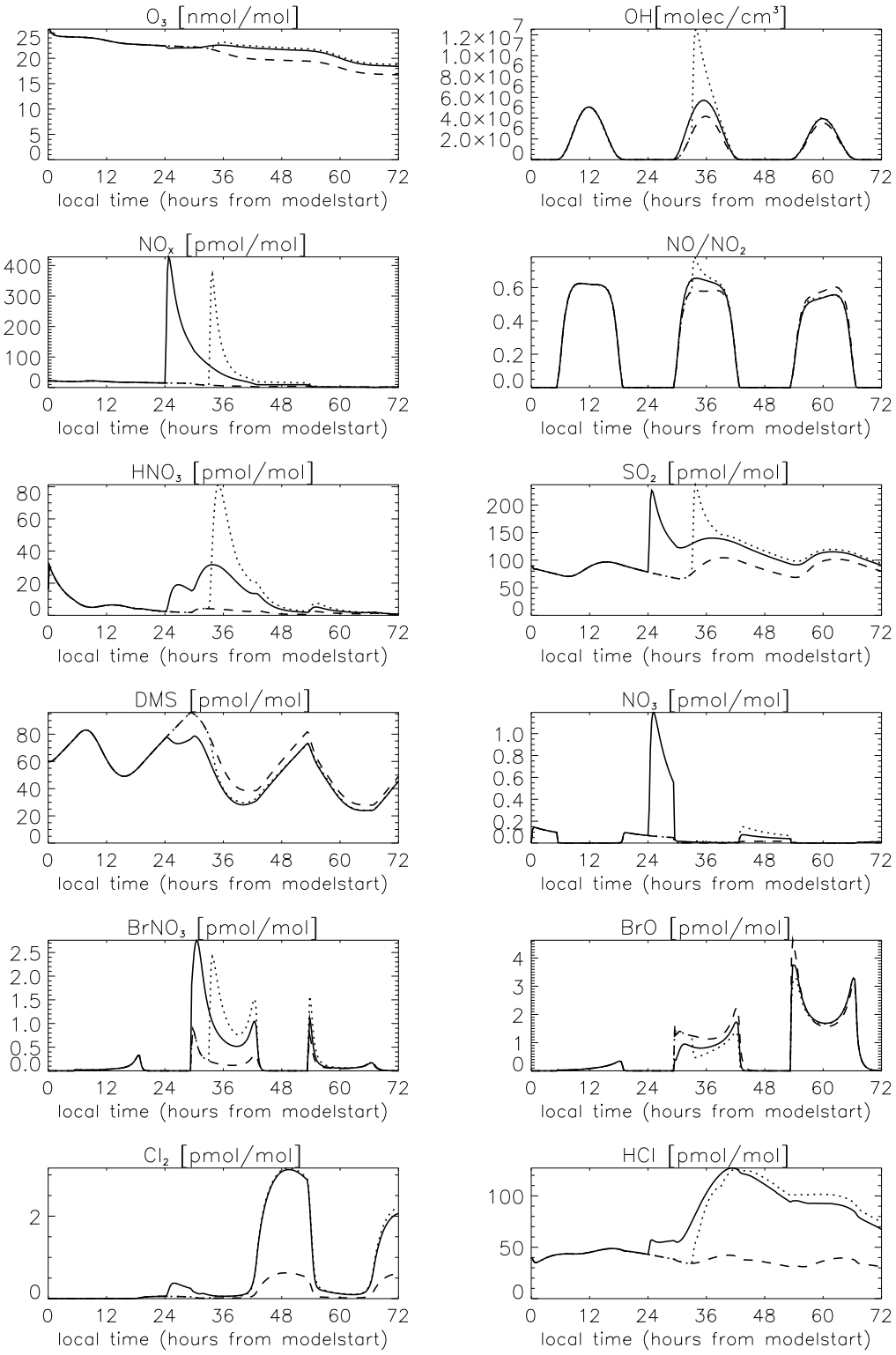

Figure 9.4: Same as Figure 9.2 but for a cloud-free run with ship emission (solid line) at 0:00 on the second day and a run with emissions at 9:00 on the second day (dotted line) and an undisturbed run (dashed line) (in 450 m).

remains in an active state. In a ship plume, however, uptake of SO_2 on the surface and therefore a change in the surface characteristics is likely.

Under the conditions in the early plume stage with very high NO and low O_3 concentrations, reactions of NO_2 on combustion aerosol surfaces could be important as a source of NO (*Kalberer et al.* (1996)) or HONO (*Gerecke et al.* (1998), *Ammann et al.* (1998)). HONO photolyzes rapidly thereby producing OH and NO. The production of OH in this reaction could compensate for a reduced production of OH from O_3 photolysis (O_3 concentrations are low in the early plume stages). *Kirchner et al.* (2000) studied the reaction of NO_2 and HNO_3 on different types of combustion aerosols. They found that reactions on the surfaces of aerosol particles prodced by diesel passenger cars are slower than on soot that was produced from a spark generator and is frequently used in other kinetic studies of uptake on combustion aerosol. *De Santis and Allegrini* (1992) showed that sulfate production can be enhanced in the presence of NO_2 on combustion aerosol surfaces.

Because of the large uncertainties in the reaction products and rates and a possible de-activation of combustion aerosol surfaces, no reactions on combustion aerosols were included at this stage of the work but they should be considered in future studies when more information is available.

The effect of soluble particle emissions (with the restrictions stated above) on the gas phase chemistry in a ship's plume are negligible as can be seen from Figure 9.5, where major gas phase species are plotted for a run with particle emissions, a run with a five-fold increase in the number of particles emitted and a run without the emission of particles. Only Cl_2 shows an increase of 10 % in the run with high particle emissions.

The perturbations in S(VI) and NO_3^- show large differences in the sulfate and sea salt aerosol (see Figure 9.6). Although the lifetime of the sea salt aerosol due to sedimentation is shorter than for the sulfate aerosol and the differences in S(VI) and NO_3^- between the aerosol particles of the plume and the background air should disappear quicker in the sea salt aerosols this is only reflected by S(VI). Increased levels of NO_3^- (compared to the background) are maintained in the shortlived sea salt aerosols whereas they are reduced quickly to background levels in the longlived sulfate aerosols. aerosol bin. The reason for this is twofold. HNO_3 increases strongly after plume emission, so it is taken up by the aerosols to maintain Henry and dissociation equilibria which results in high NO_3^- concentrations in the aerosol. The decrease in NO_3^- in the sulfate aerosol which is caused by degassing of HNO_3 reflects the decrease of HNO_3 in the gas phase. This happens because the aqueous fraction (see Appendix B) for HNO_3 is less than unity for solutions with a pH smaller than 3 (see *Seinfeld and Pandis* (1998), p. 356) which is the case for the sulfate aerosol. The aqueous fraction of HNO_3 with respect to the sea salt aerosol is close to unity, therefore sea salt aerosol always takes up HNO_3. NO_3^- is not reduced in the sea salt aerosol even on the second model day after plume release, because the production of HNO_3 by reaction of NO_2 with OH is still 67 % higher one day after plume emission than in the undisturbed run. Apart from dry deposition, the only sink for HNO_3 is uptake by the aerosol.

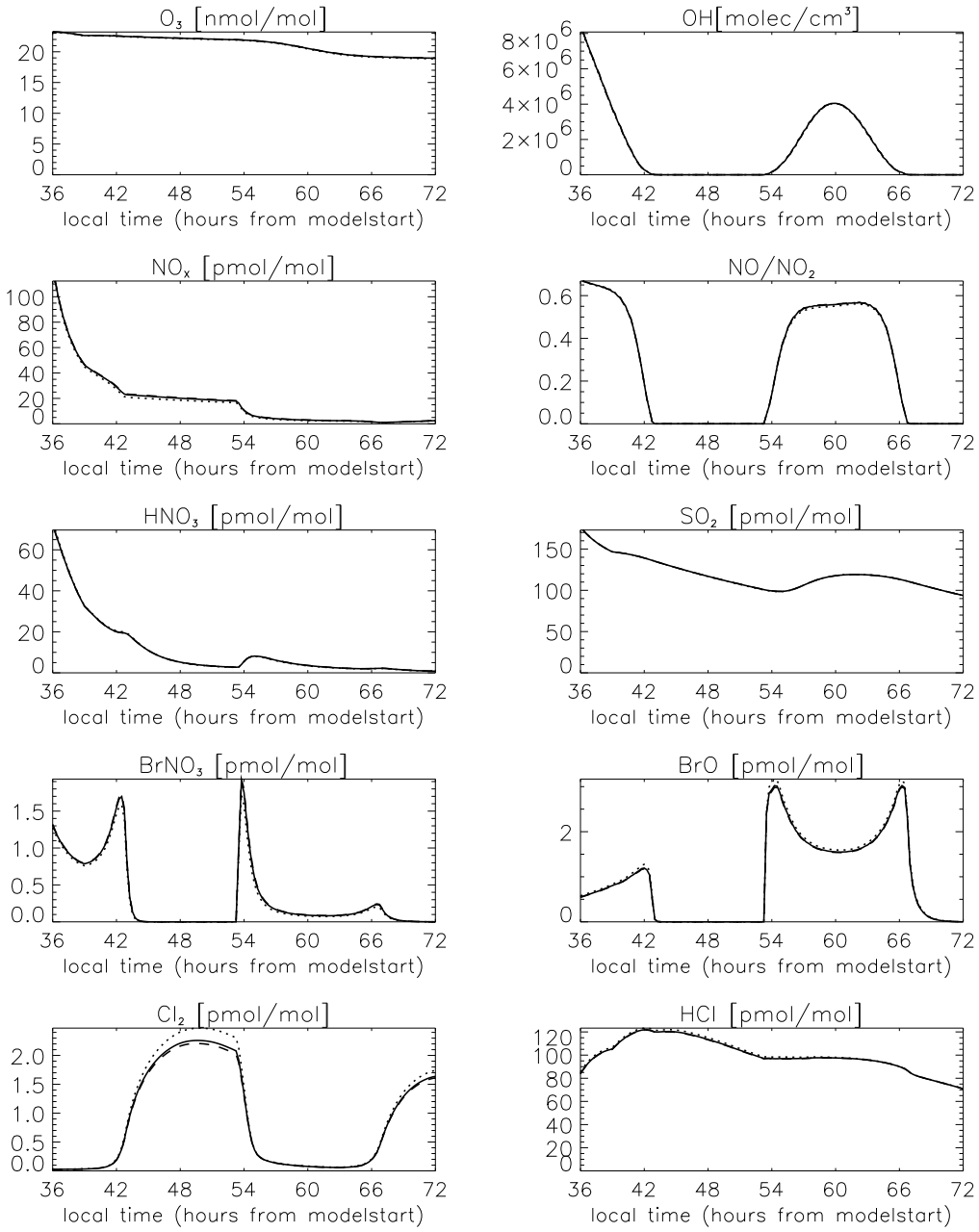

Figure 9.5: Same as Figure 9.2 but for a run with ship emission (solid line), a run with five-fold particle emissions (dotted line) and a run without particle emissions (dashed line) (in 450 m).

S(VI) concentrations in the sulfate aerosol are only slightly (about 5 %) elevated above background values. In the sea salt aerosol S(VI) is about 70 % higher than in the background and this surplus decreases rapidly as expected from the lifetime of the sea salt aerosol.

The consequence of uptake of HNO_3 by the sea salt aerosol is displacement of HCl to the gas phase. The decrease of 2.5 % in Cl^- is enough to produce a

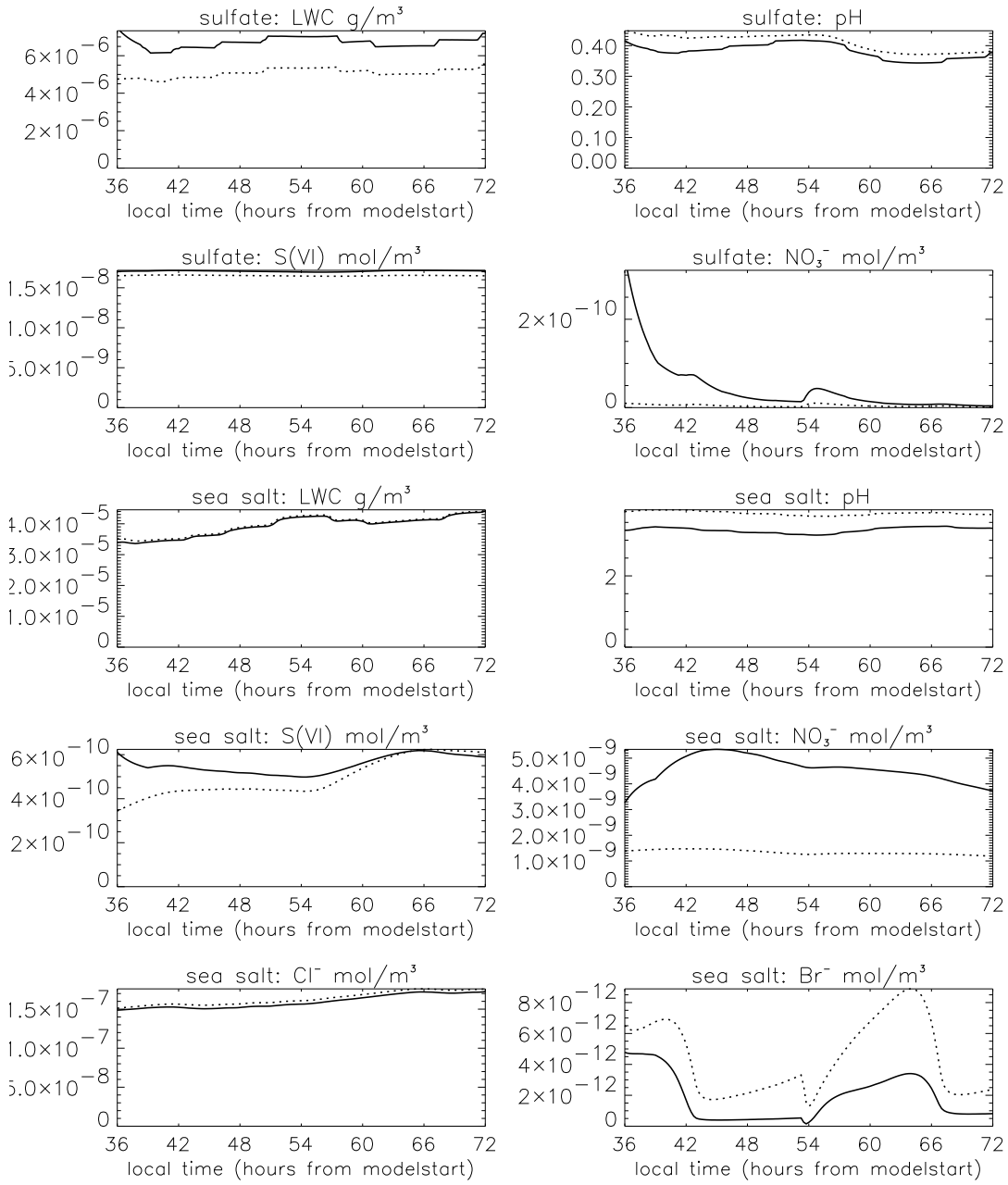

Figure 9.6: Evolution with time of the main aerosol phase species for a cloud-free run with ship emission at 9:00 on the second model day (solid line) and the base case from chapter 4 without ship emissions (dotted line) in 450 m height.

rather strong increase in gas phase HCl of 40 - 60 pmol/mol, as shown in Figures 9.1 and 9.2. Acidification decreases the sea salt aerosol pH by 0.5 pH units. The rather strong relative decrease in Br^- has little consequences for the gas phase because the concentrations in the gas phase are large compared with Br^- in sea salt.

The bulk aerosol samples of *Hobbs et al.* (2000) show similar chemical aerosol

compositions (in $\mu g/m^3$) in- and outside of the ship plume which confirms the model results. Note that for "bulk" samples the sea salt and sulfate aerosols are combined, the perturbations in S(VI) that are apparent in the sea salt aerosol in Figure 9.6 would therefore be "disguised" by the high mass of the background sulfate aerosol. Of the main constituents only NO_3^- is elevated slightly above ambient levels in the measurements. Enhancements in sulfate were found in the plume of only one ship. Organic compounds that are typical for emissions of diesel engines were found but they did not contribute much to aerosol mass. *Hobbs et al.* (2000) assume that this finding is due to the fact, that the emitted particles are very small and therefore do not significantly contribute to the total aerosol mass.

Six hours after plume emission about 53 % of the excess sulfur is in the gas phase as SO_2, 24 % is in the sulfate aerosol in the form of S(VI) and 7 % is in the sea salt aerosol. Roughly 16 % has already been deposited to the sea surface.

9.3 Major features of a ship plume in the cloudy MBL

Spin-up of aqueous chemistry is quicker in a cloud-topped than in a cloud-free MBL (see chapter 5), so the ship plume was emitted already on the first day for the cloud-topped MBL.

Three runs are compared, one without emission of a plume (the base run from chapter 5), one with emission at 7:00 when the cloud- and sub-cloud layers are still coupled (called "7:00 run") and one with emission at 9:00 when the coupling is already weak (called "9:00 run") (for a short discussion on dynamical coupling effects in the MBL see page 64).

In the first 3 to 5 hours after plume emission there are large differences between the 7:00 and the 9:00 run, because more of the pollutants have been transported into the cloud layers in the "7:00 run". Figure 9.7 shows the vertical profile of the base run, the "7:00 run" and the "9:00 run" at 12:00, i.e. 5 h and 3 h, respectively, after plume release. The (gas phase) mixing ratio in the cloud layers of the quite insoluble NO_x is higher in the "7:00 run" than in the "9:00 run" although the emissions were 2 h earlier and dilution acted 2 h longer. The cause for this is the stronger coupling of cloud and sub-cloud layers and therefore stronger vertical transport in the "7:00" run. In the "9:00 run" there is a strong vertical gradient on the first day between pollutants in the cloud- and sub-cloud layers. Soluble gases like HNO_3 and SO_2 are lower in the "7:00 run" than in the "9:00 run" when the runs are compared after the same time elapse after plume emission. This can be seen from Figure 9.8 that depicts the evolution with time for the main gas phase species in 250 m (i.e. below the cloud base) for these runs. The model results of *Liu et al.* (2000) confirm these findings as they showed similar differences in tracer transport depending on the coupling of cloud and sub-cloud layers.

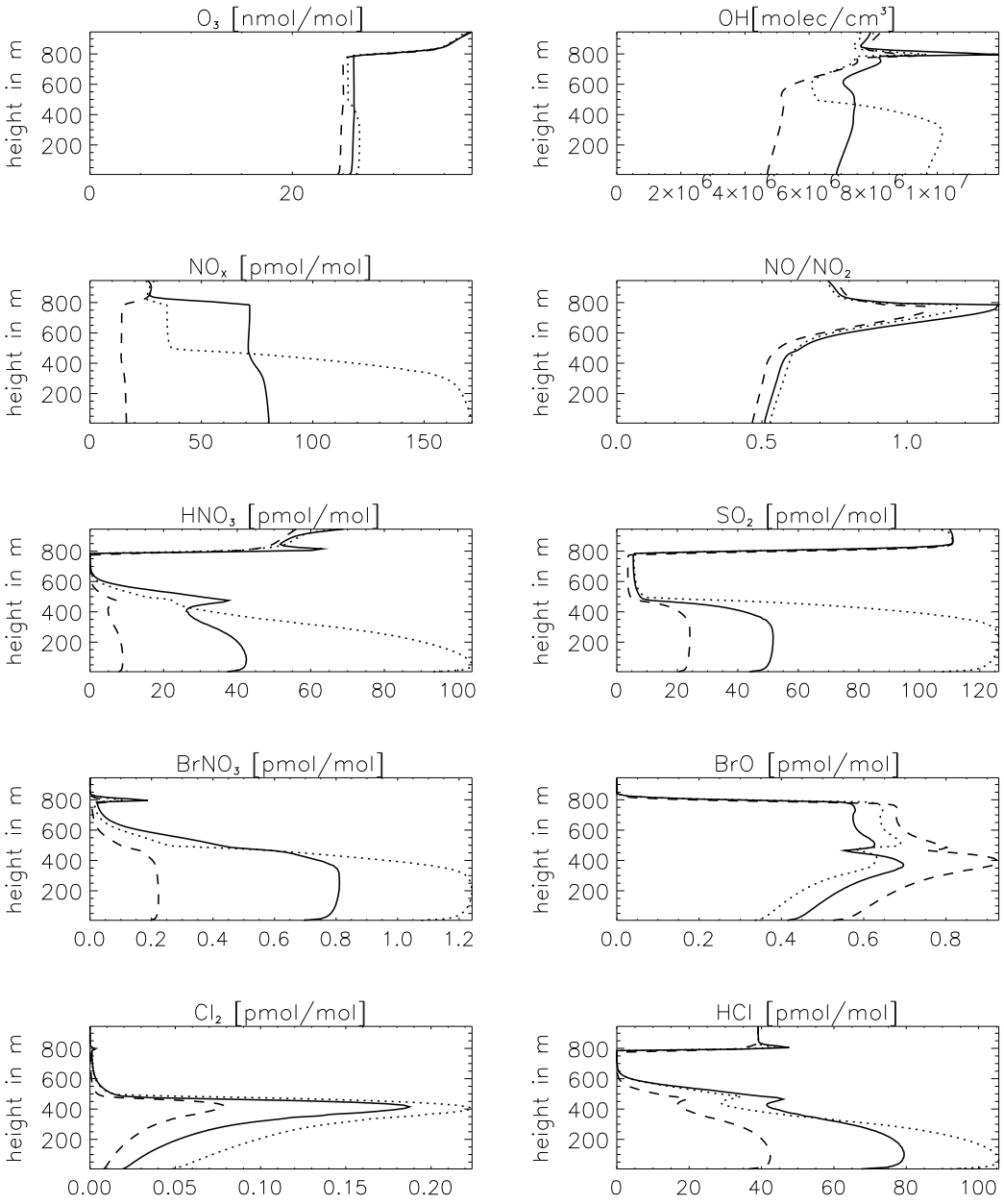

Figure 9.7: Vertical profile of the main gas phase species at 12:00 on the first model day for the cloudy runs with ship emission at 7:00 (solid line) and at 9:00 (dotted line) and for the background run (dashed line). The peak of OH at cloud top stems from the photolysis of HONO that degassed from detrained, evaporating cloud droplets.

The decrease of HNO_3 in the "7:00" and background runs between 12:00 and 13:00 is caused by an increase in the depth of the sub-cloud layer leading to a stronger dilution of freshly produced HNO_3. Later on the cloud base sinks again (see Figure 5.1) and HNO_3 production takes place in a shallower sub-cloud region resulting in higher mixing ratios there. The re-coupling of cloud- and sub-cloud

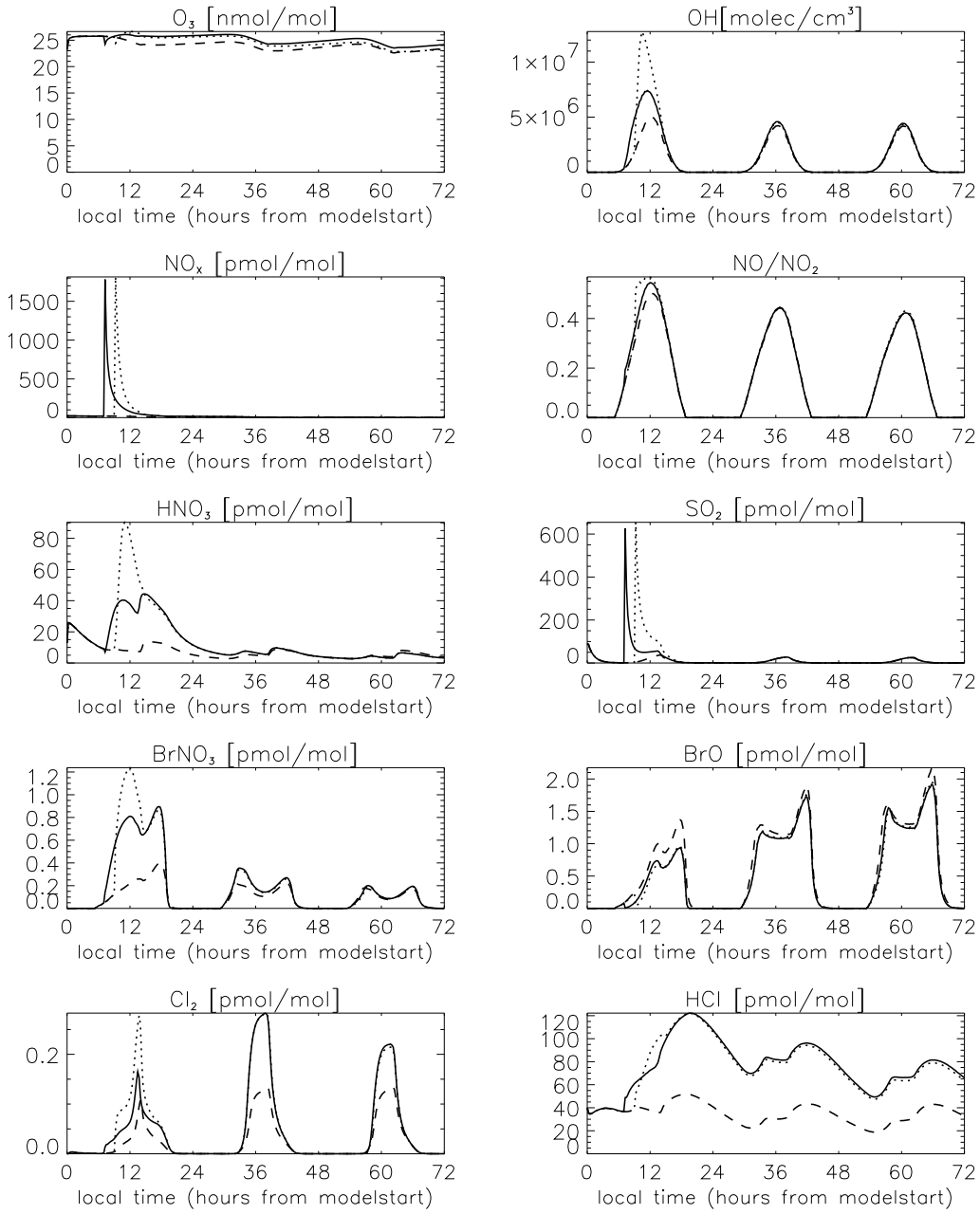

Figure 9.8: Evolution with time for the main gas phase species in 250 m for the cloudy runs with ship emission at 7:00 (solid line) and at 9:00 (dotted line) and for the background run (dashed line).

layers in the evening leads again to a stronger decrease in e.g. HNO_3 and SO_2.

On the afternoon of the second day most differences between the disturbed runs and the base run have disappeared. Differences in O_3 between the three runs are maintained with the highest values in the "7:00 run" (see explanation in section 9.1). Chlorine and bromine show the same behaviour as in the cloud-free runs (see section 9.1). Except for O_3, the differences between the "7:00 run"

and "9:00 run" disappear after re-coupling of cloud- and sub-cloud layer in the evening of the first day.

The ratio NO/NO_2 is greater in clouds than in cloud-free air and it increases with increasing liquid water content (see Figure 9.7). This is mainly caused by an increase with height in the photolysis rates of NO_2 that are greater due to multiple scattering higher up in the cloud (see also discussion on page 71). NO/NO_2 is further enhanced by photolysis of HONO which is produced in the aqueous phase (mainly in droplets grown on sulfate aerosol) and degasses.

The lifetime of excess NO_3^- in the droplets is shorter than that of excess S(VI) (not shown) because upon evaporation of droplets at cloud base HNO_3 is liberated from the droplets grown on sulfate aerosols. Excess sulfate stays in the particles upon droplet evaporation. After plume emission the pH of the cloud droplets decreases from 4.7 to 4.3 in the droplets grown on sulfate aerosol and from 5.0 to 4.6 in the droplets grown on sea salt aerosol.

The lifetime of soluble pollutants in the cloudy MBL is shorter than in the cloud-free MBL and that of insoluble species is roughly of the same order.

A word of caution has to be added. As already discussed on page 114 additional effects or changes in the chemistry discussed in this section might occur, if the chemistry in the particulate phase would be influenced by particle emissions that are not included in the model (i.e. direct combustion residues).

9.4 Cloud development

The development of cloud dynamics and microphysics in ship tracks have been studied intensively. A parameter that is frequently measured is the effective radius r_e, which can be retrieved from in situ and remote sensing platforms; r_e is a measure of the volume to surface ratio of the cloud droplets. It is defined as:

$$r_e = \frac{\int n(r) r^3 dr}{\int n(r) r^2 dr}, \tag{9.1}$$

where r is the droplet radius and $n(r)dr$ the number of droplets with radii between r and $r + dr$. In ship tracks r_e usually decreases compared to undisturbed clouds, whereas increases are found in the number concentration of cloud droplets, N_d, as well as interstitial particles, N_i. Sometimes the cloud top increases and the liquid water content (LWC) and column integrated liquid water content, the so called liquid water path, are often greater than background values (*Taylor and Ackerman* (1999), *Frick and Hoppel* (2000), *Russell et al.* (1999), *Hindman and Bodowski* (1996), *Hobbs et al.* (2000)).

Taylor and Ackerman (1999) utilized a similar one-dimensional model to the one used here to model the evolution of ship tracks in stratiform clouds. To obtain the correct number of cloud droplets they made several assumptions. First they used an aerosol particle source strength of $3 \cdot 10^{16}$ s^{-1} for soluble particles, a factor of 30 compared to the data given in *Hobbs et al.* (2000). Second their particle

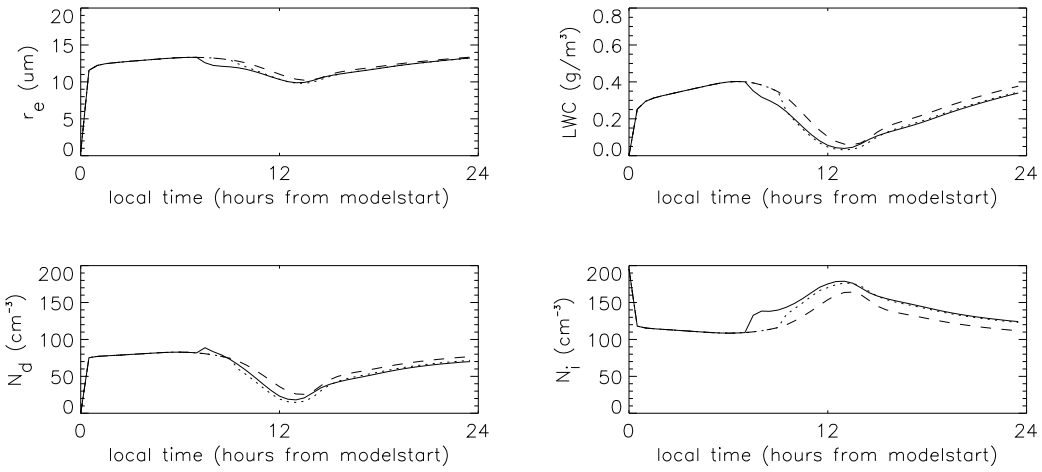

Figure 9.9: Evolution with time of the effective radius r_e, the LWC, the droplets concentration N_d and the concentration of the interstitial aerosol N_i, for the run with plume injection at 7:00 (solid line), the run with plume injection at 9:00 (dotted line), and the undisturbed background run (dashed line) in 600 m height.

spectrum was a lot broader than the measured spectra by *Hobbs et al.* (2000) (*Taylor and Ackerman* (1999), Andy Ackerman, pers. comm., 2000; note that in the paper they incorrectly state to use measured size distributions). They justify this enhancement with a "likely under activation of CCN by the model (due to under-predicted peak-supersaturations)". Their objective was not to predict the number of CN or CCN correctly but to get the measured amount of cloud droplets in the ship track.

Apart from the large enhancement in particle source strength in the model of *Taylor and Ackerman* (1999), the particles were emitted into air with very small background aerosol and cloud droplet number concentrations. They did not consider dilution of the plume by entrainment of background air but assumed the plume emissions to be spread out immediately over a width of 5 km.

In the model runs of *Taylor and Ackerman* (1999) the increase in the number of cloud droplets in the ship track is overestimated compared to the measurements but the decrease of r_e is predicted correctly. The liquid water path increases in their model runs, though the increase is delayed by several hours compared to the observations.

Keeping the differences in the model set-up between *Taylor and Ackerman* (1999) and my model in mind, it is not surprising to see differences in the evolution of the ship track in their and my model runs. The main effect of ship exhaust particles on cloud evolution, however, is correctly simulated here. Figure 9.9 shows differences between the cloud parameters in the undisturbed run, the run with emission of a ship plume at 7:00 and a run with emission at 9:00.

In the first hours after plume emission, the differences between the cloud properties in the ship tracks and in the undisturbed run show the expected behaviour

in the model: The effective radius r_e drops and interstitial aerosol as well as cloud droplet number concentrations rise. The cloud height (not shown) increases by 10 m in the ship track. The LWC drops compared to the undisturbed run. This is caused by a stronger decoupling of cloud and sub-cloud layers in the ship track run, leading to a reduced moisture supply from the sea surface. This effect has already been discussed by *Ackerman et al.* (1995). Here it is mainly caused by a decrease of droplet sedimentation due to smaller particles which leads to an upward shift of the layer in which droplets evaporate most efficiently. Therefore evaporational cooling of cloud base is weaker and decoupling occurs more rapidly.

The increase in cloud droplet number concentration (N_d) is only shortlived in the model runs. This might be explained by the weak particle source, especially when one keeps in mind the changes that were made by *Taylor and Ackerman* (1999) to obtain measured enhancements in N_d.

Chapter 10

Summary and conclusions

There is strong observational evidence for active chemistry of bromine in sea salt aerosol particles both by laboratory (production of Br_2 and BrCl from sea salt solutions) and field studies (bromine deficit).

Using a one-dimensional model of the MBL, results from earlier box model studies for cloud-free conditions could be confirmed. These are the activation of bromine from sea salt aerosol by an acid catalyzed mechanism that follows starter reactions in the sea salt aerosol. These transform the rather unreactive Br^- to reactive substances like $HOBr_{aq}$ and Br_{aq}. The importance of catalytic gas phase reaction cycles that involve bromine for the destruction of O_3 was also confirmed. Roughly 30 % of the total O_3 destruction in the model was due to halogen reactions. The potential role of BrO in the oxidation of DMS and production of DMSO was supported. This points to possibly underestimated total oxidation rates of DMS in studies that do not incorporate halogen chemistry. The role of HOBr and HOCl in the oxidation of S(IV) in aerosol is also in agreement with previous box model results. Furthermore the importance of iodine chemistry in the MBL for the activation of Br and Cl from the sea salt aerosol and in the destruction of O_3 was confirmed and speculations on processes involving the OIO radical which has recently been detected in the MBL were made.

Additionally it could be shown that under low NO_x situations that prevail in the remote MBL the diurnal variation of BrO and ClO show a maximum in the early morning and late afternoon and a local minimum around noon. This diurnal variation was also found in species that are produced from XO (e.g. DMSO, XNO_3). The reason for this behaviour is the different wavelength dependence of the photolytic source of the precursors of BrO and its most important reaction partner HO_2. HO_2 production is initiated by O_3 photolysis at rather short wavelengths, whereas BrO production by photolysis of Br_2 and BrCl followed by reaction with O_3 occurs at longer wavelengths. During dawn and dusk the radiation spectrum in the troposphere is shifted towards longer wavelengths causing production of BrO but not of HO_2. The early morning BrO peaks could be the reason for "sunrise ozone destruction" that has been observed in field measurements.

The model further showed a distinct vertical profile of BrO with maxima

below the inversion that caps the MBL. This is linked to the vertical profile of sea salt aerosol pH which has its minimum below the inversion where relative humidity is highest. The reason for this astonishing behaviour was found to be the high Cl^- loading of the sea salt particles and the exchange of HCl via Henry and dissociation equilibria with the gas phase that acts as a supply for acidity for the aerosol.

In the simulations the presence of sulfate aerosol particles was important for the recycling of less reactive bromine species like HBr and HOBr to more reactive species like Br_2 and BrCl. As this cycling is quick the sulfate aerosol was not found to be an important reservoir for bromine.

If the availability of acids is restricted, bromine activation is reduced in the model. Bromine activation is also slowed down in low O_3 regions, because the reaction of Br with O_3 is an important step in the bromine activation mechanism. On the other hand bromine activation can be accelerated in more polluted regions.

As a consequence of the shift in the tropospheric radiation spectrum at high solar zenith angles the mixing ratios of BrO and ClO were predicted to be higher in winter than in summer and the relative importance of halogen reactions in O_3 destruction and DMS oxidation increased significantly. This is true only for comparable availability of gas phase acidity and similar sea salt aerosol fluxes.

The influence of the presence of stratiform clouds on halogen and aerosol chemistry was also subject of this thesis. Significant differences in the diurnal variation of many species as well as in the phase partitioning of bromine compared to cloud-free runs were found. Even in sub-cloud layers the effects were strong e.g. Cl_x and Br_x are mainly partitioned to the aqueous phase during night which is not the case in the cloud-free runs. The turbulent state of the MBL is important for the vertical transport of substances. In the cloud-free MBL usually the whole MBL is well mixed whereas in the cloudy MBL this is mainly true only during the night. During day the cloud and sub-cloud layers are decoupled resulting in reduced vertical exchange.

Apart from H_2O_2, HOCl and HOBr are important oxidants of S(IV) in cloud particles. The relative importance of the latter two species changed compared to oxidation in aerosol particles due to dilution effects.

At higher wind speeds and resulting higher fluxes of sea salt aerosol to the atmosphere, total S(IV) production increases significantly in cloud-free situations, whereas in cloudy situations there is mainly a shift from oxidation in cloud droplets towards sea salt aerosol particles.

Comparisons of results from field campaigns with models that do not include cloud processes may be very misleading in the light of the fundamental differences that were found between cloudy and cloud-free model runs. Many measurements in the MBL are made near the sea surface but this part of the MBL is also influenced by clouds in higher layers. Information about cloud cover, vertical extent of the cloud, etc. from field campaigns would be very helpful to adequately describe the circumstances under which the measurements were made and to be able to interpret the results correctly. Furthermore, in the light of the distinct vertical profiles that were found for many compounds, one should be careful with

the extrapolation of surface measurements to the entire MBL.

The discussion of the effects of ship emissions on the MBL lead to very interesting new insights.

From the studies of the exhaust plume of single ships the chemical lifetime (defined as time when differences between plume and background air are reduced to 5 % or less) was estimated to be 2 days.

Dilution of the ship plume via entrainment of background air was treated as in studies of aircraft emission. It is a very important process that significantly alters model results. Dilution has the strongest effects during roughly the first 6 hours after plume release. The height of the MBL is important for the lifetime of pollutants. The concentrations are higher in a shallower MBL, because the temperature inversion at the top of the MBL is an effective barrier for upward transport of pollutants. For longlived species the differences that are present after the "strong mixing period" (first 6 hours) are conserved.

Strongest effects of ship emissions and largest plume lifetimes were found for the cleanest conditions that were studied.

Increased concentrations of NO_x in the plume air lead to higher catalytical photochemical production rates of O_3 and therefore also of OH. Due to increased OH concentrations in the plume, the lifetime of DMS is reduced in plume air. Reservoir species for nitrogen and sulfur can be formed in plume air during night or in cold regions. These have the potential to be transported to regions that have previously been unaffected by ship emissions.

The effects of overlapping plumes in heavily traversed ocean regions was also investigated. Caused by a strongly reduced lifetime of e.g. NO_x in the early stages of a ship plume, it was found that the parameterization of ship emissions in global chemistry models as a constant source at the sea surface leads to an overestimation of the effects of ship emissions.

The chemistry of background aerosols has only little effect on gas phase chemistry in a ship plume. Only the mixing ratios of chlorine are significantly enlarged in plume air. In the discussed model runs most bromine was partitioned to the gas phase so in the plume no additional bromine (compared to the background) was released from the sea salt aerosol which would be the case for less depleted sea salt aerosol. In the early plume stages BrO reacts rapidly with NO thereby strongly reducing BrO mixing ratios but without a net effect on the O_x family as NO_2 is produced in this reaction. Later on bromine is redistributed mainly towards $BrNO_3$ in plume air.

The modeled evolution of the pollutants in the plume was compared to measurements and found to be realistically described. No significant increase in aerosol mass was found in the ship plume which is also in agreement with measurements.

When the ship plume was emitted in a model run with a cloud-topped MBL the effective radius of the cloud droplets dropped and the number of interstitial aerosols and cloud droplets increased which is known from measurements to happen in the MBL.

The importance of the coupling of the cloud and sub-cloud layers was shown.

If pollutants are emitted into a coupled MBL, rapid transport to the cloud takes place. This is the case only to a smaller extent for the decoupled MBL. On the other hand, emissions of ship particles and the corresponding decrease in effective droplet radius speeds up the decoupling of the MBL in the morning.

Results from field campaigns with simultaneous measurements of both gas and particulate phase chemical composition are becoming more and more available. More comparisons with these results should be made in the future. The availability of faster computers will make the introduction of more size bins for the description of aqueous phase chemistry possible.

Appendix A

Treatment of turbulent transport

The exact description of turbulence remains one of the unsolved problems of classical physics. This is due to the non-linear characteristic of turbulence. *Stull* (1988) desribes in detail the different concepts and equations that are briefly discussed here.

Turbulent fluxes appear in the prognostic equations of fluids. They can be derived by the so-called Reynold's averaging of the conservation equations, e.g. Newton's second law for the conservation of momentum. A fundamental problem in the description of turbulent flows is known as "the closure problem". As the number of unknowns in the set of equations for turbulent flow is larger than the number of equations, the set of equations is not closed. Therefore parameterizations have to be made that maintain the fundamental properties of turbulent flow, e.g. that gradients of the conserved variables disappear when the fluid is well-mixed. A property that is invariant for individual fluid elements is said to be conserved. Applied to the atmosphere this means that no gradients exist in a well mixed part of it (e.g. the MBL) for the absolute humidity or the mass mixing ratios or molar fraction of chemical species or particles.

The frequently used gradient transport theory parameterizes the turbulent fluxes with the help of a turbulent exchange coefficient that is abbreviated as K (this is the reason for the often used term "K - theory"). The turbulent flux is parameterized as (here only written for the vertical turbulent flux):

$$\overline{w'\Phi'} = -K\frac{\partial\overline{\Phi}}{\partial z}, \tag{A.1}$$

w' is the turbulent fluctuation of the vertical velocity w and Φ' is the turbulent fluctuation for a variable Φ. The prognostic variables for particle concentrations ($f(a,r)$) and chemical species (c_g and $c_{a,i}$) as they are used in the model are no conserved variables because they are not independent on the density of air. This is due to the choice to define them in particles per volume of air and in mol of a substance per volume of air, respectively. As only mass mixing ratios or molar fractions would be conserved variables that have no gradient in a well mixed fluid the mean density of the air, ρ, has to be used as a factor. Therefore the turbulent fluxes are parameterized in the model as:

$$\overline{w' f(a,r)'} = -K \frac{\rho}{m(a,r)} \frac{\partial f(a,r) m(a,r)/\rho}{\partial z} \tag{A.2}$$

$$\overline{w' c'} = -K \rho \frac{\partial c/\rho}{\partial z}. \tag{A.3}$$

where c stands for gas phase as well as aqueous phase species and $m(a,r)$ is the mass of one particle with dry radius a and total radius r. Now the turbulent fluxes are proportional to the gradients of the conserved variables $f(a,r)m(a,r)/\rho$ and c/ρ and they are therefore in agreement with the gradient transport theory. To transform the conserved variables back to the prognostic variables that are used in the model, they have to multiplied again with ρ. This ensures also that the unit of the turbulent flux $\overline{w'\Phi'}$ is correct.

In the prognostic equations (equation 3.1 to 3.6, 3.10 and 3.13) changes due to turbulent movements are by the divergence of the turbulent fluxes, so there the derivation of the turbulent fluxes with respect to height appears. In equation 3.6 the mass of a single particle $m(a,r)$ is omitted because it is a constant and cancels out.

Appendix B

Calculation of the aqueous fraction

The distribution ratio of a species between gas and aqueous phase is defined as the ratio of gas phase concentration and aqueous concentration (see e.g. *Seinfeld and Pandis* (1998), chapter 6.2.1):

$$f_A = \frac{c_a}{c_g}, \tag{B.1}$$

where both c_g and c_a are given in mol/m^3_{air}. If Henry's equilibrium is assumed, equation B.1 can be written as

$$f_A = k_H^{cc*} w_l \tag{B.2}$$

with the effective Henry's constant k_H^{cc*} that takes dissociation effects in the aqueous phase into account. The aqueous fraction is defined as the ratio of the concentration in the aqueous phase and the total concentration:

$$X_{aq} = \frac{c_a}{c_a + c_g} = \frac{f_A}{1 + f_A} = \frac{k_H^{cc*} w_l}{1 + k_H^{cc*} w_l}. \tag{B.3}$$

Figure B.1 shows the aqueous fraction for different liqud water contents as a function of the effective Henry's constant. As unit for the Henry's constant the most commonly used one was taken: mol/(l atm) = M/atm.

The Figure shows that for typical cloud liquid water contents (0.1 to 1 g/m^3) an effective Henry's constant of 10^7 M/atm is sufficient to have an aqueous fraction of nearly unity. This is the case for e.g. HNO_3. The Henry's constant for NO_2 is only $4 \cdot 10^{-3}$ M/atm, so it is nearly completed partitioned towards the gas phase.

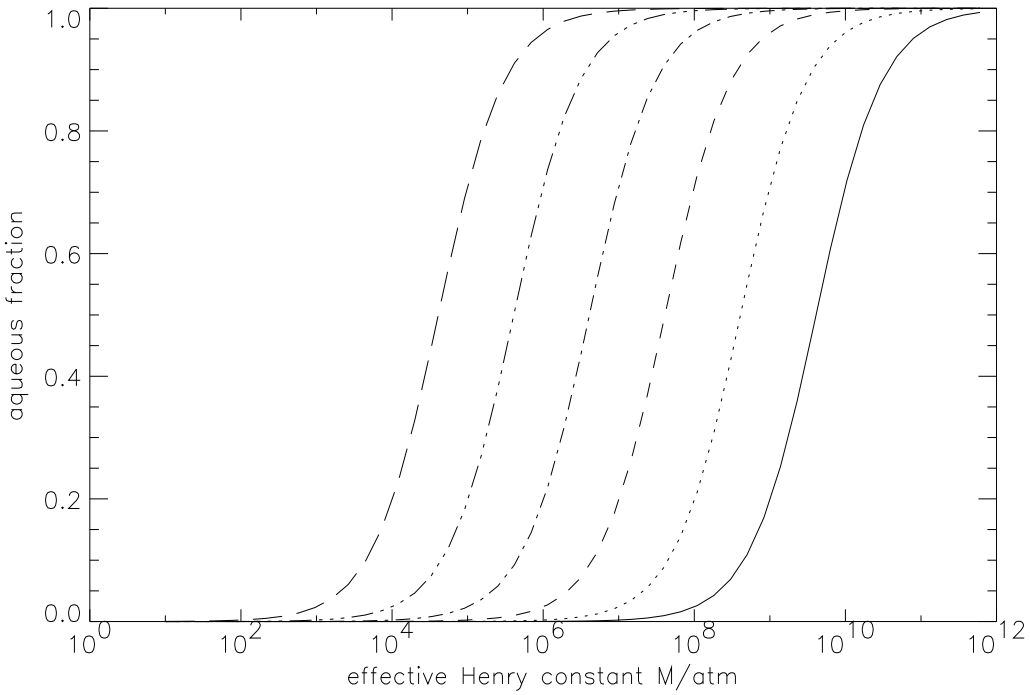

Figure B.1: Aqueous fraction as function of the Henry's constant for different liquid water contents. Long-dashed line: $w_l = 1$ g/m^3, dash-dot-dot-dotted line: $w_l = 0.1$ g/m^3, dash-dotted line: $w_l = 0.01$ g/m^3, dashed line: $w_l = 10^{-3}$ g/m^3, dotted line: $w_l = 10^{-4}$ g/m^3, solid line: $w_l = 10^{-5}$ g/m^3

Appendix C

Variation of pH with relative humidity: An analytical solution

This section is part of von Glasow and Sander *(2001) and gives an analytical solution for the variation of sea salt aerosol pH with relative humidty. As it was written in collaboration with Rolf Sander it was not included in the main text but is shown here for completeness.*

In order to better understand this surprising phenomenon of falling pH with rising relative humidity, we have analyzed the system in a very simplified form analytically. We only consider the main components of acidified sea-salt aerosol: Cl^- and H^+. We implicitly assume the system to be in thermodynamic equilibrium according to Henry's law which is justified as the timescale for gas phase diffusion as well as for transfer between gas and aqueous phase is on the order of a few seconds (*Jacob* (2000)).

For a strong acid, Henry's law can be written as:

$$[H^+] \times [Cl^-] = k'_{\mathrm{H}} \times c_{\mathrm{g}}(\mathrm{HCl}) \tag{C.1}$$

where $[H^+]$ and $[Cl^-]$ are the aqueous phase concentrations of H^+ and Cl^-, respectively. To simplify the following calculations, we strictly use SI units here, which means that the unit of $[H^+]$ and $[Cl^-]$ is $\mathrm{mol/m^3_{aq}}$. $c_{\mathrm{g}}(\mathrm{HCl})$ is the gas phase concentration of HCl in $\mathrm{mol/m^3_{air}}$. k'_{H} is the Henry's law constant (k_H) of HCl multiplied with the equilibrium constant for the dissociation of HCl (k_A):

$$k'_{\mathrm{H}} = k_H k_A = 5 \times 10^{10} \, \frac{(\mathrm{mol/m^3_{aq}})^2}{\mathrm{mol/m^3_{air}}} \quad \left(2 \times 10^6 \, \mathrm{M^2/atm}\right) \tag{C.2}$$

The mass balance equations for H^+ and Cl^- are:

$$[H^+] \times L + c_{\mathrm{g}}(\mathrm{HCl}) = A \tag{C.3}$$

$$[Cl^-] \times L + c_{\mathrm{g}}(\mathrm{HCl}) = S \tag{C.4}$$

where L is the dimensionless liquid water content (in $\mathrm{m^3_{aq}/m^3_{air}}$). A and S are the total concentrations of acid and salt, respectively. To ensure they are independent

of the liquid water content, they are expressed in mol/m^3_{air}. Charge balance is implicitly guaranteed since Na^+ is given by :

$$[Na^+] + [H^+] = [Cl^-] \quad \Longleftrightarrow \quad [Na^+] = \frac{S-A}{L}. \tag{C.5}$$

As Na^+ is chemically unreactive it need not be considered explicitly in the following calculations.

The unknown variables $c_g(HCl)$ and $[Cl^-]$ are eliminated by combining equations (C.1), (C.3), and (C.4) which yields:

$$[H^+]^2 + \left(\frac{S-A}{L} + L\,k'_H\right)[H^+] - A\,k'_H = 0 \tag{C.6}$$

This quadratic equation can be solved unequivocally (there is also another solution but is has no physical significance):

$$\begin{aligned}[H^+] = & - \frac{1}{2}\left(\frac{S-A}{L} + L\,k'_H\right) \\ & + \sqrt{\frac{1}{4}\left(\frac{S-A}{L} + L\,k'_H\right)^2 + A\,k'_H}\end{aligned} \tag{C.7}$$

In Figures C.1 and C.2 we show for several selected values of S and A how $[H^+]$ changes with L. The bold line in both plots represents the base case for typical, slightly acidified sea-salt aerosol. Here, $S = 0.1$ μmol/m^3_{air} (i.e. 3.6 μg/m^3_{air} of Cl^-). The total acid is $A = 1$ nmol/m^3_{air} which corresponds to a mixing ratio of 24 pmol/mol if it were all in the gas phase. Under these conditions the aerosol pH decreases with increasing liquid water content up to about $L = 10^{-9}$ m^3_{aq}/m^3_{air} (10^{-5} g/m^3). When L increases further, the dilution effect takes over and the pH rises again.

In addition to the base case, it is instructive to look at other regimes. First, we define an abbreviation:

$$Y \equiv \frac{1}{2}\left(\frac{S-A}{L} + Lk'_H\right) \tag{C.8}$$

Equation (C.7) becomes:

$$\begin{aligned}[H^+] &= -Y + \sqrt{Y^2 + A\,k'_H} \\ &= -Y + Y\sqrt{1 + \frac{A\,k'_H}{Y^2}}\end{aligned} \tag{C.9}$$

For large L and for an excess of salt in the particles ($S \gg A$, which is the case for sea salt aerosol) this can be simplified because $Y^2 \gg A\,k'_H$ and the approximation $\sqrt{1+\varepsilon} \approx 1 + \varepsilon/2$ is used:

$$\begin{aligned}[H^+] &= -Y + Y\left(1 + \frac{A\,k'_H}{2Y^2}\right) \\ &= \frac{A\,k'_H}{2Y} = \frac{A\,L\,k'_H}{S - A + L^2 k'_H}\end{aligned} \tag{C.10}$$

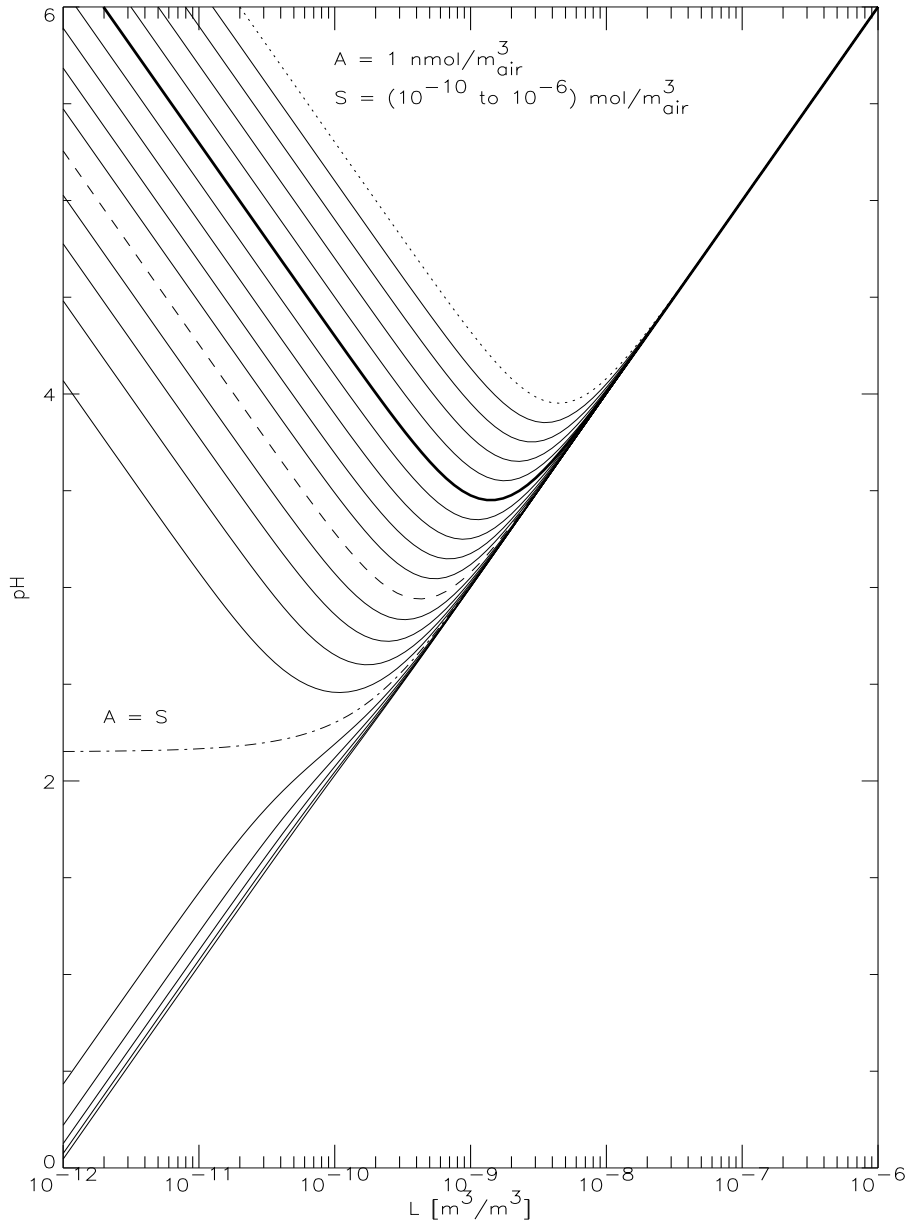

Figure C.1: Variation of sea salt aerosol pH as a function of the dimensionless liquid water content (LWC, in m^3_{aq}/m^3_{air}). The total amount of acid (A) is kept constant and the amount of salt (S) is varied between 10^{-10} to 10^{-6} mol/m^3_{air}. Dotted line: $S = 10^{-6} mol/m^3_{air}$, bold line: $S = 10^{-7} mol/m^3_{air}$ (typical case for the MBL), dashed line: $S = 10^{-8} mol/m^3_{air}$, dash-dotted line: $S = 10^{-9} mol/m^3_{air}$. $S = 10^{-10} mol/m^3_{air}$ is hidden in the diagonal line where the salt is well diluted and the pH increases monotonically with increasing LWC. This is the case for most other types of atmospheric aerosol particles. Sea salt aerosol LWC is in the range of 10^{-11} to 10^{-9} m^3_{aq}/m^3_{air} and in clouds the LWC content is usually greater than 10^{-7} m^3_{aq}/m^3_{air}.

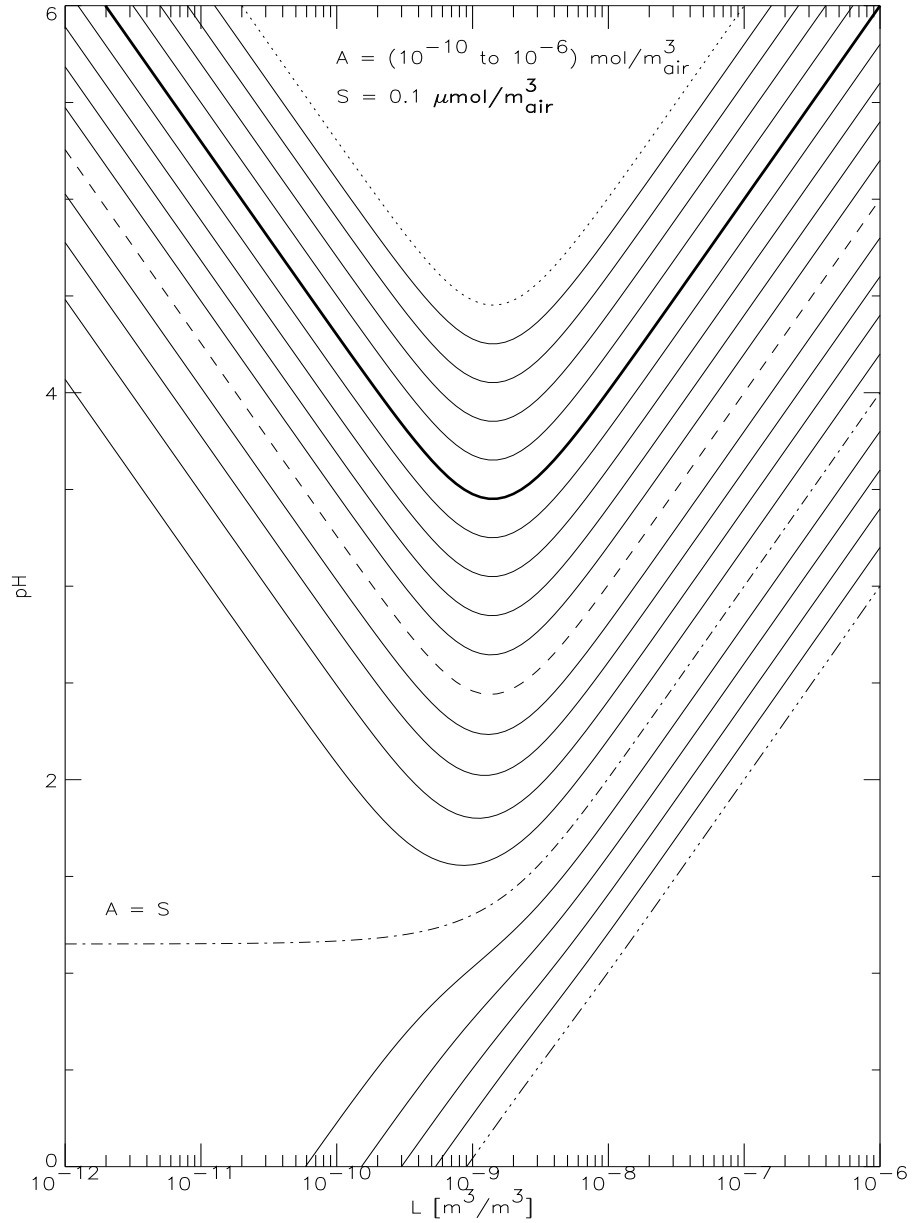

Figure C.2: Variation of sea salt aerosol pH as a function of the dimensionless liquid water content (LWC, in m^3_{aq}/m^3_{air}). The total amount of salt (S) is kept constant and the amount of acid (A) is varied between 10^{-10} to 10^{-6} mol/m^3_{air}. Dotted line: $A = 10^{-10}$ mol/m^3_{air}, bold line: $A = 10^{-9}$ mol/m^3_{air} (typical case for the MBL), dashed line: $A = 10^{-8}$ mol/m^3_{air}, dash-dotted line: $A = 10^{-7}$ mol/m^3_{air}, dash-dot-dot-dot-line: $A = 10^{-6}$ mol/m^3_{air}. Sea salt aerosol LWC is in the range of 10^{-11} to 10^{-9} m^3_{aq}/m^3_{air} and in clouds the LWC content is usually greater than 10^{-7} m^3_{aq}/m^3_{air}.

This equation can be used to calculate the ratio between HCl in the gas phase and $[H^+]$:

$$\frac{c_g(HCl)}{[H^+]\,L} = \frac{A - [H^+]\,L}{[H^+]\,L} = \frac{S - A}{L^2 k'_H} \tag{C.11}$$

This ratio equals 1 at $L = \sqrt{(S-A)/k'_H}$. It is interesting to note that at this value of L the concentration $[H^+]$ (in equation (C.10)) has a maximum:

$$\frac{d[H^+]}{dL} = 0 \Leftrightarrow L = \sqrt{\frac{S-A}{k'_H}} \tag{C.12}$$

Thus the lowest pH occurs at a liquid water content when HCl is distributed evenly between the phases.

Another interesting regime is at $S = A$, i.e. when the aerosol concentrations of H^+ and Cl^- are equal. It can be seen in Figures C.1 and C.2 that this marks a turning point in the correlation between aerosol pH and L. At low L the dissolution of some HCl does not affect the gas phase concentration significantly. In this case equation (C.7) reduces to $[H^+] = \sqrt{A\,k'_H}$, which means that the aerosol acidity is independent of L.

The solubility of a gas decreases with increasing salt concentration (e.g. *Sander* (1999)). We did sensitivity studies where we decreased the Henry's constant by a factor of 10 and 100, respectively. The shape of the lines in Figures C.1 and C.2 remains the same, they are only shifted to higher pH values for reduced solubility. As equation (C.12) implies, the minimum in pH is at a higher liquid water content for reduced solubility.

Appendix D

Tables of reaction rates

This chapter comprises a complete listing of all gas phase (Table D.1, page 138) and aqueous phase (Table D.2, page 144) reaction rates used, as well as rates for the heterogeneous (particle surface) reactions (Table D.3, page 150), aqueous phase equilibrium constants (Table D.4, page 151), Henry constants and accomodations coefficients (Table D.5, page 152).

Table D.1: Gas phase reactions.

no	reaction	n	A [$(\mathrm{cm}^{-3})^{1-n}\mathrm{s}^{-1}$]	$-E_a$ / R [K]	reference
G1	$NO_2 + h\nu \longrightarrow NO + O_3$	1	[1]		*DeMore et al.* (1997)
G2	$NO + O_3 \longrightarrow NO_2 + O_2$	2	3.0×10^{-12}	-1500	*Sander et al.* (2000)
G3	$NO_2 + O_3 \longrightarrow NO_3 + O_2$	2	1.2×10^{-13}	-2450	*DeMore et al.* (1997)
G4	$NO + NO_3 \longrightarrow 2NO_2$	2	1.5×10^{-11}	170	*DeMore et al.* (1997)
G5	$NO_2 + NO_3 \xrightarrow{M} N_2O_5$	3	[2]		*Sander et al.* (2000)
G6	$N_2O_5 \xrightarrow{M} NO_2 + NO_3$	1	[2]		*Sander et al.* (2000)
G7	$NO_3 + h\nu \longrightarrow NO + O_2$	1	[1]		*Wayne et al.* (1991)
G8	$NO_3 + h\nu \longrightarrow NO_2 + O_3$	1	[1]		*Wayne et al.* (1991)
G9	$NO_3 + HO_2 \longrightarrow HNO_3 + O_2$	2	3.50×10^{-12}		*DeMore et al.* (1997)
G10	$O_3 + h\nu \longrightarrow O_2 + O^1D$	1	[1]		*DeMore et al.* (1997)
G11	$O^1D + O_2 \longrightarrow O_3$	2	3.2×10^{-11}	70	*DeMore et al.* (1997)
G12	$O^1D + N_2 \longrightarrow O_3$	2	1.8×10^{-11}	110	*DeMore et al.* (1997)
G13	$O^1D + H_2O \longrightarrow 2\ OH$	2	2.2×10^{-10}		*DeMore et al.* (1997)
G14	$NO + OH \xrightarrow{M} HONO$	2	[2]		*DeMore et al.* (1997)
G15	$HONO + h\nu \longrightarrow NO + OH$	1	[1]		*DeMore et al.* (1997)
G16	$NO_2 + OH \xrightarrow{M} HNO_3$	2	[2]		*Sander et al.* (2000)
G17	$HNO_3 + h\nu \longrightarrow NO_2 + OH$	1	[1]		*DeMore et al.* (1997)
G18	$HNO_3 + OH \longrightarrow NO_3 + H_2O$	2	[2]		*Atkinson et al.* (1997)
G19	$N_2O_5 + H_2O \longrightarrow 2HNO_3$	2	2.6×10^{-22}		*Mentel et al.* (1996)
G20	$N_2O_5 + h\nu \longrightarrow NO_2 + NO_3$	1	[1]		*DeMore et al.* (1997)
G21	$HONO + OH \longrightarrow NO_2$	2	1.8×10^{-11}	-390	*DeMore et al.* (1997)
G22	$CO + OH \xrightarrow{O_2} HO_2 + CO_2$	2	[2]		*DeMore et al.* (1997)
G23	$O_3 + OH \longrightarrow HO_2 + O_2$	2	1.5×10^{-12}	-880	*Sander et al.* (2000)
G24	$NO + HO_2 \longrightarrow NO_2 + OH$	2	3.5×10^{-12}	250	*DeMore et al.* (1997)
G25	$NO_2 + HO_2 \xrightarrow{M} HNO_4$	2	[2]		*Atkinson et al.* (1997)
G26	$HNO_4 \xrightarrow{M} NO_2 + HO_2$	1	[2]		*Atkinson et al.* (1997)
G27	$O_3 + HO_2 \longrightarrow OH + 2O_2$	2	2.0×10^{-14}	-680	*Sander et al.* (2000)
G28	$HO_2 + HO_2 \longrightarrow H_2O_2 + O_2$	2	[2]		*DeMore et al.* (1997)
G29	$HO_2 + OH \longrightarrow H_2O + O_2$	2	4.8×10^{-11}	250	*DeMore et al.* (1997)

Table D.1: Continued.

no	reaction	n	A $[(\mathrm{cm}^{-3})^{1-n}\mathrm{s}^{-1}]$	$-E_a$ / R [K]	reference
G30	$H_2O_2 + h\nu \longrightarrow 2OH$	1	[1]		*DeMore et al.* (1997)
G31	$H_2O_2 + OH \longrightarrow HO_2 + H_2O$	2	2.9×10^{-12}	-160	*DeMore et al.* (1997)
G32	$HNO_4 + h\nu \longrightarrow NO_2 + HO_2$	1	[1]		*DeMore et al.* (1997)
G33	$HNO_4 + h\nu \longrightarrow OH + NO_3$	1	[1]		*DeMore et al.* (1997)
G34	$HNO_4 + OH \longrightarrow NO_2 + H_2O + O_2$	2	1.3×10^{-12}	380	*DeMore et al.* (1997)
G35	$SO_2 + OH \longrightarrow SO_4 + HO_2$	2	[2]		*Lurmann et al.* (1986)
G36	$HCHO + h\nu \longrightarrow 2HO_2 + CO$	1	[1]		*DeMore et al.* (1997)
G37	$HCHO + h\nu \longrightarrow CO + H_2$	1	[1]		*DeMore et al.* (1997)
G38	$HCHO + OH \xrightarrow{O_2} HO_2 + CO + H_2O$	2	1.00×10^{-11}		*DeMore et al.* (1997)
G39	$HCHO + HO_2 \longrightarrow HOCH_2O_2$	2	6.7×10^{-15}	600	*DeMore et al.* (1997)
G40	$HOCH_2O_2 + NO \longrightarrow HCOOH + HO_2 + NO_2$	2	4.2×10^{-12}	180	*Lurmann et al.* (1986)
G41	$HOCH_2O_2 + HO_2 \longrightarrow HCOOH + H_2O + O_2$	2	2.00×10^{-12}		*Lurmann et al.* (1986)
G42	$2\ HOCH_2O_2 \longrightarrow 2HCOOH + 2HO_2 + 2O_2$	2	1.00×10^{-13}		*Lurmann et al.* (1986)
G43	$HCOOH + OH \xrightarrow{O_2} HO_2 + H_2O + CO_2$	2	4.0×10^{-13}		*DeMore et al.* (1997)
G44	$HCHO + NO_3 \xrightarrow{O_2} HNO_3 + HO_2 + CO$	2	5.8×10^{-16}		*DeMore et al.* (1997)
G45	$ALD + OH \longrightarrow CH_3CO_3 + H_2O$	2	6.9×10^{-12}	250	*Lurmann et al.* (1986)
G46	$ALD + NO_3 \longrightarrow HNO_3 + CH_3CO_3$	2	1.40×10^{-15}		*DeMore et al.* (1997)
G47	$ALD + h\nu \longrightarrow CH_3OO + HO_2 + CO$	1	[1]		*Lurmann et al.* (1986)
G48	$ALD + h\nu \longrightarrow CH_4 + CO$	1	[1]		*Lurmann et al.* (1986)
G49	$CH_3CO_3 + NO_2 \longrightarrow PAN$	2	4.70×10^{-12}		*Lurmann et al.* (1986)
G50	$PAN \longrightarrow CH_3CO_3 + NO_2$	1	1.9×10^{16}	-13543	*DeMore et al.* (1997)
G51	$CH_3CO_3 + NO \longrightarrow CH_3OO + NO_2 + CO_2$	2	4.2×10^{-12}	180	*Lurmann et al.* (1986)
G52	$CH_3OO + NO \xrightarrow{O_2} HCHO + NO_2 + HO_2$	2	3.0×10^{-12}	280	*DeMore et al.* (1997)
G53	$CH_4 + OH \xrightarrow{O_2} CH_3OO + H_2O$	2	2.4×10^{-12}	-1710	*Lurmann et al.* (1986)
G54	$C_2H_6 + OH \longrightarrow C_2H_5O_2 + H_2O$	2	1.7×10^{-11}	-1232	*Lurmann et al.* (1986)
G55	$C_2H_5O_2 + NO \longrightarrow ALD + HO_2 + NO_2$	2	4.2×10^{-12}	180	*Lurmann et al.* (1986)
G56	$CH_3OO + CH_3OO \longrightarrow 1.4HCHO + 0.8HO_2 + O_2$	2	1.5×10^{-13}	220	*Lurmann et al.* (1986)
G57	$2C_2H_5O_2 \longrightarrow 1.6ALD + 1.2HO_2$	2	5.00×10^{-14}		*Lurmann et al.* (1986)
G58	$HO_2 + CH_3OO \longrightarrow ROOH + O_2$	2	3.8×10^{-13}	800	*DeMore et al.* (1997)

Table D.1: Continued.

no	reaction	n	A $[(\mathrm{cm}^{-3})^{1-n}\mathrm{s}^{-1}]$	$-E_a$ / R [K]	reference
G59	$HO_2 + C_2H_5O_2 \longrightarrow ROOH + O_2$	2	7.5×10^{-13}	700	*DeMore et al.* (1997)
G60	$HO_2 + CH_3CO_3 \longrightarrow ROOH + O_2$	2	4.5×10^{-13}	1000	*DeMore et al.* (1997)
G61	$C_2H_4 + OH \longrightarrow EO_2$	2	1.66×10^{-12}	474	*Lurmann et al.* (1986)
G62	$EO_2 + NO \longrightarrow NO_2 + 2.0HCHO + HO_2$	2	4.2×10^{-12}	180	*Lurmann et al.* (1986)
G63	$C_2H_4 + O_3 \longrightarrow HCHO + 0.4CHO_2 + 0.12HO_2 + 0.42CO + 0.06CH_4$	2	1.2×10^{-14}	-2633	*Lurmann et al.* (1986)
G64	$EO_2 + EO_2 \longrightarrow 2.4HCHO + 1.2HO_2 + 0.4ALD$	2	5.00×10^{-14}		*Lurmann et al.* (1986)
G65	$HO_2 + EO_2 \longrightarrow ROOH + O_2$	2	3.00×10^{-12}		*Lurmann et al.* (1986)
G66	$ROOH + OH \longrightarrow 0.7\ CH_3OO + 0.3\ HCHO + 0.3\ OH$	2	3.8×10^{-12}	200	*DeMore et al.* (1997), see note
G67	$ROOH + h\nu \longrightarrow HCHO + OH + HO_2$	1	[1]		*DeMore et al.* (1997), see note
G68	$HCl + OH \longrightarrow H_2O + Cl$	2	2.6×10^{-12}	-350	*DeMore et al.* (1997)
G69	$Cl + O_3 \longrightarrow ClO + O_2$	2	2.3×10^{-11}	-200	*Sander et al.* (2000)
G70	$Cl + CH_4 \xrightarrow{O_2} HCl + CH_3OO$	2	9.6×10^{-12}	-1360	*Sander et al.* (2000)
G71	$Cl + C_2H_6 \xrightarrow{O_2} HCl + C_2H_5O_2$	2	7.7×10^{-11}	-90	*DeMore et al.* (1997)
G72	$Cl + C_2H_4 \xrightarrow{O_2} HCl + C_2H_5O_2$	2	$1. \times 10^{-10}$		see note
G73	$Cl + HCHO \xrightarrow{O_2} HCl + HO_2 + CO$	2	8.1×10^{-11}	-30	*DeMore et al.* (1997)
G74	$ClO + HO_2 \longrightarrow HOCl + O_2$	2	4.8×10^{-13}	700	*DeMore et al.* (1997)
G75	$ClO + NO \longrightarrow Cl + NO_2$	2	6.4×10^{-12}	290	*DeMore et al.* (1997)
G76	$ClO + NO_2 \xrightarrow{M} ClNO_3$	2	[2]		*Sander et al.* (2000)
G77	$ClO + CH_3OO \longrightarrow Cl + HCHO + HO_2$	2	3.3×10^{-12}	-115	*DeMore et al.* (1997)
G78	$ClO + ClO \longrightarrow Cl_2O_2$	2	[2]		*Sander et al.* (2000)
G79	$Cl_2O_2 \longrightarrow ClO + ClO$	1	[2]		*Sander et al.* (2000)
G80	$Cl + H_2O_2 \longrightarrow HCl + HO_2$	2	1.1×10^{-11}	-980	*DeMore et al.* (1997)
G81	$ROOH + Cl \longrightarrow CH_3OO + HCl$	2	5.7×10^{-11}		*Wallington et al.* (1990), see note
G82	$ClNO_3 \longrightarrow ClO + NO_2$	1	[2]		*Anderson and Fahey* (1990)
G83	$Cl + ClNO_3 \longrightarrow Cl_2 + NO_3$	2	9.6×10^{-12}	140	*Yokelson et al.* (1995)
G84	$HOCl + h\nu \longrightarrow Cl + OH$	1	[1]		*DeMore et al.* (1997)
G85	$ClNO_2 + h\nu \longrightarrow Cl + NO_2$	1	[1]		*DeMore et al.* (1997)
G86	$ClNO_3 + h\nu \longrightarrow Cl + NO_3$	1	[1]		*DeMore et al.* (1997)
G87	$Cl_2 + h\nu \longrightarrow 2\ Cl$	1	[1]		*DeMore et al.* (1997)

Table D.1: Continued.

no	reaction	n	A $[(\mathrm{cm}^{-3})^{1-n}\mathrm{s}^{-1}]$	$-E_a$ / R [K]	reference
G88	$Cl_2O_2 + h\nu \longrightarrow Cl + Cl + O_2$	1	[1]		*DeMore et al.* (1997)
G89	$OClO + h\nu \xrightarrow{O_2,O_3} O_3 + ClO$	1	[1]		*DeMore et al.* (1997)
G90	$HBr + OH \longrightarrow Br + H_2O$	2	1.1×10^{-11}		*DeMore et al.* (1997)
G91	$Br + O_3 \longrightarrow BrO + O_2$	2	1.7×10^{-11}	-800	*DeMore et al.* (1997)
G92	$Br + HO_2 \longrightarrow HBr + O_2$	2	1.5×10^{-11}	-600	*DeMore et al.* (1997)
G93	$Br + C_2H_4 \xrightarrow{O_2} HBr + C_2H_5O_2$	2	$5. \times 10^{-14}$		see note
G94	$Br + HCHO \xrightarrow{O_2} HBr + CO + HO_2$	2	1.7×10^{-11}	-800	*DeMore et al.* (1997)
G95	$Br_2 + Cl \longrightarrow BrCl + Br$	2	1.2×10^{-10}		*Mallard et al.* (1993)
G96	$BrCl + Br \longrightarrow Br_2 + Cl$	2	3.3×10^{-15}		*Mallard et al.* (1993)
G97	$Br + Cl_2 \longrightarrow BrCl + Cl$	2	1.1×10^{-15}		*Mallard et al.* (1993)
G98	$BrCl + Cl \longrightarrow Br + Cl_2$	2	1.5×10^{-11}		*Mallard et al.* (1993)
G99	$BrO + HO_2 \longrightarrow HOBr + O_2$	2	3.4×10^{-12}	540	*DeMore et al.* (1997)
G100	$BrO + NO \longrightarrow Br + NO_2$	2	8.8×10^{-12}	260	*DeMore et al.* (1997)
G101	$BrO + NO_2 \xrightarrow{M} BrNO_3$	2	[2]		*Sander et al.* (2000)
G102	$BrO + ClO \longrightarrow Br + OClO$	2	9.5×10^{-13}	550	*Sander et al.* (2000)
G103	$BrO + ClO \longrightarrow Br + Cl + O_2$	2	2.3×10^{-12}	260	*Sander et al.* (2000)
G104	$BrO + ClO \longrightarrow BrCl + O_2$	2	4.1×10^{-13}	290	*Sander et al.* (2000)
G105	$BrO + BrO \longrightarrow 2\ Br + O_2$	2	2.36×10^{-12}	40	*DeMore et al.* (1997)
G106	$BrO + BrO \longrightarrow Br_2 + O_2$	2	2.79×10^{-14}	860	*DeMore et al.* (1997)
G107	$BrO + CH_3OO \longrightarrow HOBr + HCHO$	2	4.1×10^{-12}		*Aranda et al.* (1997)
G108	$BrO + CH_3OO \longrightarrow Br + HCHO + HO_2$	2	1.6×10^{-12}		*Aranda et al.* (1997)
G109	$ROOH + Br \longrightarrow CH_3OO + HBr$	2	2.66×10^{-12}	-1610	*Mallard et al.* (1993), see note
G110	$BrNO_3 \longrightarrow BrO + NO_2$	1	[2]		*Orlando and Tyndall* (1996)
G111	$Br + BrNO_3 \longrightarrow Br_2 + NO_3$	2	4.9×10^{-11}		*Orlando and Tyndall* (1996)
G112	$HOBr + h\nu \longrightarrow Br + OH$	1	[1]		*Ingham et al.* (1999)
G113	$BrNO_2 + h\nu \longrightarrow Br + NO_2$	1	[1]		*Scheffler et al.* (1997)
G114	$BrNO_3 + h\nu \longrightarrow Br + NO_3$	1	[1]		*DeMore et al.* (1997)
G115	$Br_2 + h\nu \longrightarrow 2\ Br$	1	[1]		*Hubinger and Nee* (1995)
G116	$BrCl + h\nu \longrightarrow Br + Cl$	1	[1]		*DeMore et al.* (1997)
G117	$BrO + h\nu \xrightarrow{O_2} Br + O_3$	1	[1]		*DeMore et al.* (1997)

Table D.1: Continued.

no	reaction	n	A [$(\mathrm{cm}^{-3})^{1-n}\mathrm{s}^{-1}$]	$-E_a$ / R [K]	reference
G118	$CH_3SCH_3 + OH \xrightarrow{O_2} CH_3SOCH_3 + HO_2$	2	[2]		*Atkinson et al.* (1997)
G119	$CH_3SCH_3 + OH \longrightarrow SO_2 + 2\ CH_3OO$	2	[2]		*Atkinson et al.* (1997)
G120	$CH_3SCH_3 + NO_3 \xrightarrow{O_2,O_3} CH_3SO_2 + HNO_3 + HCHO$	2	1.9×10^{-13}	520	*Atkinson et al.* (1999)
G121	$CH_3SCH_3 + Cl \xrightarrow{NO,2O_3} CH_3SO_2 + HCl + HCHO + NO_2$	2	3.3×10^{-10}		*Atkinson et al.* (1999)
G122	$CH_3SCH_3 + Br \xrightarrow{NO,2O_3} CH_3SO_2 + HBr + HCHO + NO_2$	2	9.0×10^{-11}	-2386	*Jefferson et al.* (1994)
G123	$CH_3SCH_3 + BrO \longrightarrow CH_3SOCH_3 + Br$	2	2.54×10^{-14}	850	*Ingham et al.* (1999)
G124	$CH_3SOCH_3 + OH \longrightarrow 0.6\ SO_2 + HCHO + 0.6\ CH_3OO + 0.4\ HO_2 + 0.4\ CH_3SO_3H$	2	1.0×10^{-10}		*Hynes and Wine* (1996) [3]
G125	$CH_3SCH_3 + OH \xrightarrow{NO,2O_3} CH_3SO_2 + HCHO + NO_2$	2	1.12×10^{-11}	-253	*Atkinson et al.* (1999)
G126	$CH_3SO_2 \longrightarrow SO_2 + CH_3OO$	1	1.9×10^{13}	-8661	*Barone et al.* (1995)
G127	$CH_3SO_2 + O_3 \longrightarrow CH_3SO_3$	2	$3. \times 10^{-13}$		*Barone et al.* (1995)
G128	$CH_3SO_3 + HO_2 \longrightarrow CH_3SO_3H$	2	$5. \times 10^{-11}$		*Barone et al.* (1995)
Gi1	$I + O_3 \longrightarrow IO + O_2$	2	2.3×10^{-11}	-870	*DeMore et al.* (1997)
Gi2	$I + HO_2 \longrightarrow HI + O_2$	2	1.5×10^{-11}	-1090	*DeMore et al.* (1997)
Gi3	$I + BrO \longrightarrow IO + Br$	2	1.2×10^{-11}		*DeMore et al.* (1997)
Gi4	$I + NO_2 \xrightarrow{M} INO_2$	2	[2]		*DeMore et al.* (1997)
Gi5	$I + NO_3 \longrightarrow IO + NO_2$	2	4.5×10^{-10}		*Chambers et al.* (1992)
Gi6	$HI + OH \longrightarrow I + H_2O$	2	3.0×10^{-11}		*Campuzano-Jost and Crowley* (1999)
Gi7	$IO + HO_2 \longrightarrow HOI + O_2$	2	8.4×10^{-11}		*DeMore et al.* (1997)
Gi8	$IO + NO \longrightarrow I + NO_2$	2	9.1×10^{-12}	240	*DeMore et al.* (1997)
Gi9	$IO + NO_2 \xrightarrow{M} INO_3$	2	[2]		*DeMore et al.* (1997)
Gi10	$IO + IO \longrightarrow I_2O_2$	2	$0.5 \times 1.5 \times 10^{-11}$	500	*DeMore et al.* (1997)
Gi11	$IO + IO \longrightarrow 2\ I + O_2$	2	$0.12 \times 1.5 \times 10^{-11}$	500	*DeMore et al.* (1997)
Gi12	$IO + IO \longrightarrow OIO + I$	2	$0.38 \times 1.5 \times 10^{-11}$	500	*DeMore et al.* (1997)
Gi13	$IO + ClO \longrightarrow I + Cl + O_2$	2	5.1×10^{-12}	280	*DeMore et al.* (1997)
Gi14	$IO + BrO \longrightarrow OIO + Br$	2	8.5×10^{-11}		*Bedjanian et al.* (1998)
Gi15	$INO_2 \longrightarrow I + NO_2$	1	2.4		estimated from data in *Jenkin et al.* (1985)
Gi16	$INO_3 \longrightarrow IO + NO_2$	1	$5. \times 10^{-3}$		*Barnes et al.* (1991)

Table D.1: Continued.

no	reaction	n	A $[(\mathrm{cm}^{-3})^{1-n}\mathrm{s}^{-1}]$	$-E_a$ / R [K]	reference
Gi17	$IO + h\nu \xrightarrow{O_2} I + O_3$	1	[1]		*Laszlo et al.* (1995)
Gi18	$HOI + h\nu \longrightarrow I + OH$	1	[1]		*Bauer et al.* (1998)
Gi19	$I_2 + h\nu \longrightarrow 2\ I$	1	[1]		*Wesely* (1989)
Gi20	$I_2O_2 + h\nu \longrightarrow 2\ I + O_2$	1	[1]		estimated by *Davis et al.* (1996), 9 × G79
Gi21	$ICl + h\nu \longrightarrow I + Cl$	1	[1]		*Seery and Britton* (1964)
Gi22	$IBr + h\nu \longrightarrow I + Br$	1	[1]		*Seery and Britton* (1964)
Gi23	$INO_2 + h\nu \longrightarrow I + NO_2$	1	[1]		*Bröske and Zabel* (1998), R. Bröske, pers. comm.
Gi24	$INO_3 + h\nu \longrightarrow I + NO_3$	1	[1]		same as G114, but redshifted by 50 nm
Gi25	$CH_3I + h\nu \longrightarrow I + CH_3OO$	1	[1]		*Roehl et al.* (1997)
Gi26	$C_3H_7I + h\nu \longrightarrow I + ROOH$	1	[1]		*Roehl et al.* (1997)
Gi27	$CH_2ClI + h\nu \longrightarrow I + Cl + 2\ HO_2 + CO$	1	[1]		*Roehl et al.* (1997)
Gi28	$CH_2I_2 + h\nu \longrightarrow 2\ I + 2\ HO_2 + CO$	1	[1]		*Roehl et al.* (1997)
Gi29	$C_3H_7I + OH \longrightarrow CH_3OO + I$	2	1.2×10^{-12}		J. Crowley, pers. comm.
Gi30	$I_2O_2 \longrightarrow 2\ IO$	1	31.0		assumed (thermolysis of Cl_2O_2 at 20 °C)
Gi31	$OIO + OH \longrightarrow HOI$	2	7.0×10^{-12}		assumed, see section (4.13)
Gi32	$OIO + NO \longrightarrow NO_2 + IO$	2	8.5×10^{-12}		assumed, see section (4.13)
Gi33	$CH_3SCH_3 + IO \longrightarrow CH_3SOCH_3 + I$	2	1.2×10^{-14}		*DeMore et al.* (1997)

n is the order of the reaction. [1] photolysis rates calculated online, [2] special rate functions (pressure dependent and/or humidity dependent), [3] products after *Pham et al.* (1995). Notes: ALD is a generic aldehyde (see *Lurmann et al.* (1986)), the rates for ROOH were assumed as that of CH_3OOH. The reactions Gi1 - Gi33 are included only in the sensitivity runs including iodine reactions. The rate coefficients are calculated with $k = A \times \exp(\frac{-E_a}{RT})$.

Table D.2: Aqueous phase reactions.

no	reaction	n	k_0 $[(\mathrm{M}^{1-n})\mathrm{s}^{-1}]$	$-E_a$ / R [K]	reference
A1	$O_3 + OH \longrightarrow HO_2$	2	1.1×10^8		*Sehested et al.* (1984)
A2	$OH + OH \longrightarrow H_2O_2$	2	5.5×10^9		*Buxton et al.* (1988)
A3	$OH + HO_2 \longrightarrow H_2O$	2	7.1×10^9		*Sehested et al.* (1968)
A4	$OH + O_2^- \longrightarrow OH^-$	2	1.0×10^{10}		*Sehested et al.* (1968)
A5	$H_2O_2 + OH \longrightarrow HO_2$	2	2.7×10^7	-1684	*Christensen et al.* (1982)
A6	$HO_2 + HO_2 \longrightarrow H_2O_2$	2	9.7×10^5	-2500	*Christensen and Sehested* (1988)
A7	$HO_2 + O_2^- \xrightarrow{H^+} H_2O_2 + O_2$	2	1.0×10^8	-900	*Christensen and Sehested* (1988)
A8	$O_3 + O_2^- \xrightarrow{H_2O} OH + OH^- + 2\ O_2$	2	1.5×10^9		*Sehested et al.* (1983)
A9	$NO_3 + OH^- \xrightarrow{H^+} NO_3^- + OH + H^+$	2	8.2×10^7	-2700	*Exner et al.* (1992)
A10	$HONO + H_2O_2 \longrightarrow HNO_3$	2	4.6×10^3	-6800	*Damschen and Martin* (1983)
A11	$NO_2^- + O_3 \longrightarrow NO_3^- + O_2$	2	5.0×10^5	-6950	*Damschen and Martin* (1983)
A12	$NO_2 + NO_2 \longrightarrow HNO_3 + HONO$	2	1.0×10^8		*Lee and Schwartz* (1981)
A13	$NO_4^- \longrightarrow NO_2^- + O_2$	1	8.0×10^{-1}		*Warneck* (1999)
A14	$NO_2^- + OH \longrightarrow NO_2 + OH^-$	2	1.0×10^{10}		*Barker et al.* (1970)
A15	$HONO + OH \longrightarrow NO_2$	2	1.0×10^{10}		assumed (=A14)
A16	$HO_2 + NO_2 \longrightarrow HNO_4$	2	1.8×10^9		*Warneck* (1999)
A17	$CH_3OH + OH \xrightarrow{O_2} HCHO + HO_2 + H_2O$	2	9.7×10^8		*Buxton et al.* (1988)
A18	$CH_3OO + HO_2 \longrightarrow CH_3OOH$	2	4.3×10^5		estimated by *Jacob* (1986)
A19	$CH_3OO + O_2^- \xrightarrow{H_2O} CH_3OOH + OH^- + O_2$	2	5.0×10^7		estimated by *Jacob* (1986)
A20	$CH_3OOH + OH \longrightarrow CH_3OO$	2	2.7×10^7	-1715	estimated by *Jacob* (1986)
A21	$CH_3OOH + OH \longrightarrow HCHO + OH$	2	1.1×10^7	-1715	estimated by *Jacob* (1986)
A22	$HCHO + OH \xrightarrow{O_2} HCOOH + HO_2$	2	7.7×10^8	-1020	*Chin and Wine* (1994)
A23	$HCOOH + OH \xrightarrow{O_2} HO_2 + CO_2 + H_2O$	2	1.1×10^8	-991	*Chin and Wine* (1994)
A24	$HCOO^- + OH \xrightarrow{O_2} OH^- + HO_2 + CO_2$	2	3.1×10^9	-1240	*Chin and Wine* (1994)
A25	$HCO_3^- + OH \longrightarrow CO_3^- + H_2O$	2	8.5×10^6		*Ross et al.* (1992)
A26	$CO_3^- + O_2^- \xrightarrow{H_2O} HCO_3^- + OH^- + O_2$	2	6.5×10^8		*Ross et al.* (1992)
A27	$CO_3^- + H_2O_2 \longrightarrow HCO_3^- + HO_2$	2	4.3×10^5		*Ross et al.* (1992)

Table D.2: Continued.

no	reaction	n	k_0 $[(M^{1-n})s^{-1}]$	$-E_a$ / R [K]	reference
A28	$CO_3^- + HCOO^- \xrightarrow{H_2O,O_2} HCO_3^- + HCO_3^- + HO_2$	2	1.5×10^5		*Ross et al.* (1992)
A29	$Cl^- + OH \longrightarrow ClOH^-$	2	4.3×10^9		*Jayson et al.* (1973)
A30	$NO_3 + Cl^- \longrightarrow NO_3^- + Cl$	2	3.4×10^8		*Buxton et al.* (1999b)
A31	$Cl^- + HOCl + H^+ \longrightarrow Cl_2 + H_2O$	3	2.2×10^4	-3508	*Wang and Margerum* (1994)
A32	$Cl_2 \xrightarrow{H_2O} Cl^- + HOCl + H^+$	1	2.2×10^1	-8012	*Wang and Margerum* (1994)
A33	$Cl + H_2O \longrightarrow H^+ + ClOH^-$	2	1.3×10^3		*Jayson et al.* (1973)
A34	$Cl_2^- + HO_2 \longrightarrow 2\ Cl^- + H^+ + O_2$	2	4.5×10^9		*Ross et al.* (1992)
A35	$Cl_2^- + O_2^- \longrightarrow 2\ Cl^- + O_2$	2	1.0×10^9		*Lelieveld and Crutzen* (1991)
A36	$ClOH^- \longrightarrow Cl^- + OH$	1	6.1×10^9		*Jayson et al.* (1973)
A37	$H^+ + ClOH^- \longrightarrow Cl + H_2O$	2	2.1×10^{10}		*Jayson et al.* (1973)
A38	$Cl + Cl \longrightarrow Cl_2$	2	8.8×10^7		*Wu et al.* (1980)
A39	$Cl_2^- + Cl_2^- \longrightarrow Cl_2 + 2Cl^-$	2	1.8×10^9		*Jacobi et al.* (1999)
A40	$HO_2 + HOCl \longrightarrow Cl + O_2 + H_2O$	2	7.5×10^6		assumed (=A41)
A41	$O_2^- + HOCl \longrightarrow Cl + OH^- + O_2$	2	7.5×10^6		*Long and Bielski* (1980)
A42	$HO_2 + Cl_2 \longrightarrow Cl_2^- + H^+ + O_2$	2	1.0×10^9		*Bjergbakke et al.* (1981)
A43	$O_2^- + Cl_2 \longrightarrow Cl_2^- + O_2$	2	1.0×10^9		assumed (=A42)
A44	$O_3 + Cl^- \longrightarrow ClO^- + O_2$	2	3.0×10^{-3}		*Hoigné et al.* (1985)
A45	$NO_3^- + Cl \longrightarrow NO_3 + Cl^-$	2	1.0×10^8		*Buxton et al.* (1999b)
A46	$Cl_2^- + CH_3OOH \longrightarrow 2\ Cl^- + H^+ + CH_3OO$	2	5.0×10^4		estimate by J. E. Williams (pers. comm.)
A47	$NO_2^- + Cl_2^- \longrightarrow 2\ Cl^- + NO_2$	2	6.0×10^7		*Jacobi* (1996)
A48	$H_2O_2 + Cl \longrightarrow HO_2 + Cl^- + H^+$	2	2.7×10^7	-1684	assumed (=A5)
A49	$Br^- + OH \longrightarrow BrOH^-$	2	1.1×10^{10}		*Kläning and Wolff* (1985)
A50	$Br^- + NO_3 \longrightarrow Br + NO_3^-$	2	4.0×10^9		*Neta and Huie* (1986)
A51	$Br^- + HOCl + H^+ \longrightarrow BrCl + H_2O$	3	1.3×10^6		*Kumar and Margerum* (1987)
A52	$Cl^- + HOBr + H^+ \longrightarrow BrCl + H_2O$	3	5.6×10^9		*Wang et al.* (1994)
A53	$BrCl \xrightarrow{H_2O} Cl^- + HOBr + H^+$	1	1.0×10^5		*Wang et al.* (1994)
A54	$Br^- + HOBr + H^+ \longrightarrow Br_2 + H_2O$	3	1.6×10^{10}		*Beckwith et al.* (1996)
A55	$Br_2 \xrightarrow{H_2O} Br^- + HOBr + H^+$	1	9.7×10^1		*Beckwith et al.* (1996)
A56	$Br^- + SO_4^- \longrightarrow Br + SO_4^{2-}$	2	3.5×10^9		*Ross et al.* (1992)

Table D.2: Continued.

no	reaction	n	k_0 $[(\mathrm{M}^{1-n})\mathrm{s}^{-1}]$	$-E_a$ / R [K]	reference
A57	$Br_2^- + HO_2 \longrightarrow 2\ Br^- + H^+ + O_2$	2	1.0×10^8		*Wagner and Strehlow* (1987)
A58	$Br_2^- + O_2^- \longrightarrow 2\ Br^- + O_2$	2	1.7×10^8		*Wagner and Strehlow* (1987)
A59	$Br_2^- + H_2O_2 \longrightarrow 2\ Br^- + H^+ + HO_2$	2	5.0×10^2		*Chameides and Stelson* (1992)
A60	$Br_2^- + Br_2^- \longrightarrow 2\ Br^- + Br_2$	2	1.9×10^9		*Ross et al.* (1992)
A61	$Br_2^- + HSO_3^- \longrightarrow Br^- + Br^- + H^+ + SO_3^-$	2	5.0×10^7		*Jacobi* (1996)
A62	$Br_2^- + SO_3^{2-} \longrightarrow Br^- + Br^- + SO_3^-$	2	3.3×10^7		*Jacobi* (1996)
A63	$BrOH^- \longrightarrow Br^- + OH$	1	3.3×10^7		*Kläning and Wolff* (1985)
A64	$BrOH^- \longrightarrow Br + OH^-$	1	4.2×10^6		*Kläning and Wolff* (1985)
A65	$BrOH^- + H^+ \longrightarrow Br$	2	4.4×10^{10}		*Kläning and Wolff* (1985)
A66	$Br^- + ClO^- + H^+ \longrightarrow BrCl + OH^-$	3	3.7×10^{10}		*Kumar and Margerum* (1987)
A67	$Br^- + O_3 \longrightarrow BrO^-$	2	2.1×10^2	-4450	*Haag and Hoigné* (1983)
A68	$HO_2 + HOBr \longrightarrow Br + O_2$	2	1.0×10^9		*Herrmann et al.* (1999)
A69	$O_2^- + HOBr \longrightarrow Br + OH^- + O_2$	2	3.5×10^9		*Schwarz and Bielski* (1986)
A70	$HO_2 + Br_2 \longrightarrow Br_2^- + H^+ + O_2$	2	1.1×10^8		*Sutton and Downes* (1972)
A71	$O_2^- + Br_2 \longrightarrow Br_2^- + O_2$	2	5.6×10^9		*Sutton and Downes* (1972)
A72	$Cl_2 + Br^- \longrightarrow BrCl_2^-$	2	7.7×10^9		*Losno et al.* (1998)
A73	$Br_2^- + CH_3OOH \longrightarrow 2\ Br^- + H^+ + CH_3OO$	2	1.0×10^5		estimate by J. E. Williams (pers. comm.)
A74	$NO_2^- + Br_2^- \longrightarrow 2\ Br^- + NO_2$	2	1.7×10^7	-1720	*Shoute et al.* (1991)
A75	$Br_2^- + HO_2 \xrightarrow{H^+} Br_2 + H_2O_2$	2	9.1×10^7		*Wagner and Strehlow* (1987)
A76	$HOBr + H_2O_2 \longrightarrow Br^- + H^+ + O_2$	2	1.2×10^6		*von Gunten and Oliveras* (1998)
A77	$HSO_3^- + O_3 \longrightarrow SO_4^{2-} + H^+ + O_2$	2	3.7×10^5	-5500	*Hoffmann* (1986)
A78	$SO_3^{2-} + O_3 \longrightarrow SO_4^{2-} + O_2$	2	1.5×10^9	-5300	*Hoffmann* (1986)
A79	$HSO_3^- + OH \longrightarrow SO_3^- + H_2O$	2	4.5×10^9		*Buxton et al.* (1988)
A80	$SO_3^{2-} + OH \longrightarrow SO_3^- + OH^-$	2	5.5×10^9		*Buxton et al.* (1988)
A81	$HSO_3^- + HO_2 \longrightarrow SO_4^{2-} + OH + H^+$	2	3.0×10^3		upper limit (D. Sedlak, pers. comm.)
A82	$HSO_3^- + O_2^- \longrightarrow SO_4^{2-} + OH$	2	3.0×10^3		upper limit (D. Sedlak, pers. comm.)
A83	$HSO_3^- + H_2O_2 \longrightarrow SO_4^{2-} + H^+ + H_2O$	2	$5.2 \times 10^6 \times \frac{[H^+]}{[H^+]+0.1\mathrm{M}}$	-3650	*Martin and Damschen* (1981)
A84	$HSO_3^- + NO_3 \longrightarrow SO_3^- + NO_3^- + H^+$	2	1.4×10^9	-2000	*Exner et al.* (1992)

Table D.2: Continued.

no	reaction	n	k_0 $[(\mathrm{M}^{1-n})\mathrm{s}^{-1}]$	$-E_a$ / R [K]	reference
A85	$HSO_3^- + CH_3OOH + H^+ \longrightarrow SO_4^{2-} + 2\ H^+ + CH_3OH$	3	1.6×10^7	-3800	*Lind et al.* (1987)
A86	$SO_3^{2-} + CH_3OOH + H^+ \longrightarrow SO_4^{2-} + CH_3OH + H^+$	3	1.6×10^7	-3800	*Lind et al.* (1987)
A87	$HSO_3^- + Cl_2^- \longrightarrow SO_3^- + 2\ Cl^- + H^+$	2	1.7×10^8		*Jacobi et al.* (1996)
A88	$SO_3^{2-} + Cl_2^- \longrightarrow SO_3^- + 2\ Cl^-$	2	6.2×10^7		*Jacobi et al.* (1996)
A89	$HSO_3^- + HSO_5^- + H^+ \longrightarrow 2\ SO_4^{2-} + 3\ H^+$	3	$7.1 \times 10^{6\ 2}$		*Betterton and Hoffmann* (1988)
A90	$HSO_3^- + SO_4^- \longrightarrow SO_3^- + SO_4^{2-} + H^+$	2	8.0×10^8		*Huie and Neta* (1987)
A91	$SO_3^{2-} + SO_4^- \longrightarrow SO_3^- + SO_4^{2-}$	2	4.6×10^8		*Huie and Neta* (1987)
A92	$HSO_3^- + SO_5^- \longrightarrow SO_4^- + SO_4^{2-} + H^+$	2	7.5×10^4		*Huie and Neta* (1987)
A93	$SO_3^{2-} + SO_5^- \longrightarrow SO_4^- + SO_4^{2-}$	2	9.4×10^6		*Huie and Neta* (1987)
A94	$HSO_3^- + SO_5^- \longrightarrow SO_3^- + HSO_5^-$	2	2.5×10^4		*Huie and Neta* (1987), *Deister and Warneck* (1990)
A95	$SO_3^{2-} + SO_5^- \xrightarrow{H^+} SO_3^- + HSO_5^-$	2	3.6×10^6		*Huie and Neta* (1987), *Deister and Warneck* (1990)
A96	$HSO_3^- + HNO_4 \longrightarrow HSO_4^- + NO_3^- + H^+$	2	3.1×10^5		*Warneck* (1999)
A97	$SO_3^- + O_2 \longrightarrow SO_5^-$	2	1.5×10^9		*Huie and Neta* (1984)
A98	$SO_4^- + NO_3^- \longrightarrow SO_4^{2-} + NO_3$	2	5.0×10^4		*Exner et al.* (1992)
A99	$SO_4^- + Cl^- \longrightarrow SO_4^{2-} + Cl$	2	2.5×10^8		*Buxton et al.* (1999a)
A100	$SO_5^- + O_2^- \xrightarrow{H^+} HSO_5^- + O_2$	2	2.3×10^8		*Buxton et al.* (1996)
A101	$SO_5^- + SO_5^- \longrightarrow$ products	2	1.0×10^8		*Ross et al.* (1992)
A102	$BrO^- + SO_3^{2-} \longrightarrow Br^- + SO_4^{2-}$	2	1.0×10^8		*Troy and Margerum* (1991)
A103	$HOBr + SO_3^{2-} \longrightarrow Br^- + HSO_4^-$	2	5.0×10^9		*Troy and Margerum* (1991)
A104	$HOBr + HSO_3^- \longrightarrow Br^- + HSO_4^- + H^+$	2	5.0×10^9		assumed (=A103)
A105	$HOCl + SO_3^{2-} \longrightarrow Cl^- + HSO_4^-$	2	7.6×10^8		*Fogelman et al.* (1989)
A106	$HOCl + HSO_3^- \longrightarrow Cl^- + HSO_4^- + H^+$	2	7.6×10^8		assumed (=A105)
A107	$HSO_5^- + Br^- \longrightarrow HOBr + SO_4^{2-}$	2	1.0	-5338	*Fortnum et al.* (1960)
A108	$HSO_5^- + Cl^- \longrightarrow HOCl + SO_4^{2-}$	2	1.8×10^{-3}	-7352	*Fortnum et al.* (1960)
A109	$HSO_3^- + HCHO \longrightarrow CH_2OHSO_3^-$	2	4.3×10^{-1}		*Boyce and Hoffmann* (1984)
A110	$SO_3^{2-} + HCHO \xrightarrow{H^+} CH_2OHSO_3^-$	2	1.4×10^4		*Boyce and Hoffmann* (1984)
A111	$CH_2OHSO_3^- + OH^- \longrightarrow SO_3^{2-} + HCHO$	2	3.6×10^3		*Seinfeld and Pandis* (1998)

Table D.2: Continued.

no	reaction	n	k_0 $[(M^{1-n})s^{-1}]$	$-E_a$ / R [K]	reference
A112	$SO_4^{2-} + Cl \longrightarrow SO_4^- + Cl^-$	2	2.1×10^8		*Buxton et al.* (1999a)
A113	$NO_3 + SO_4^{2-} \longrightarrow NO_3^- + SO_4^-$	2	1.0×10^5		*Logager et al.* (1993)
A114	$SO_4^- + H_2O \longrightarrow SO_4^{2-} + H^+ + OH$	2	1.1×10^1	-1110	*Herrmann et al.* (1995)
A115	$SO_4^- + H_2O_2 \longrightarrow SO_4^{2-} + H^+ + HO_2$	2	1.2×10^7		*Wine et al.* (1989)
A116	$OH + SO_4^- \longrightarrow HSO_5^-$	2	1.0×10^9		*Jiang et al.* (1992)
A117	$SO_4^- + HO_2 \longrightarrow SO_4^{2-} + H^+$	2	3.5×10^9		*Jiang et al.* (1992)
A118	$SO_4^- + O_2^- \longrightarrow SO_4^{2-}$	2	3.5×10^9		assumed (=A117)
A119	$O_3 + h\nu \longrightarrow OH + OH + O_2$	1			assumed: 2 × G10
A120	$H_2O_2 + h\nu \longrightarrow OH + OH$	1			assumed: 2 × G30
A121	$HOCl + h\nu \longrightarrow OH + Cl$	1			assumed: 2 × G84
A122	$Cl_2 + h\nu \longrightarrow Cl + Cl$	1			assumed: 2 × G87
A123	$HOBr + h\nu \longrightarrow OH + Br$	1			assumed: 2 × G112
A124	$Br_2 + h\nu \longrightarrow Br + Br$	1			assumed: 2 × G115
A125	$BrCl + h\nu \longrightarrow Cl + Br$	1			assumed: 2 × G116
A126	$NO_2^- + h\nu \xrightarrow{H^+} NO + OH$	1			*Zellner et al.* (1990)
A127	$NO_3^- + h\nu \xrightarrow{H^+} NO_2 + OH$	1			only in sensitivity run *Zellner et al.* (1990), *Burley and Johnston* (1992)
Ai1	$HOI + I^- + H^+ \longrightarrow I_2$	3	4.4×10^{12}		*Eigen and Kustin* (1962)
Ai2	$HOI + Cl^- + H^+ \longrightarrow ICl$	3	2.9×10^{10}		*Wang et al.* (1989)
Ai3	$ICl \longrightarrow HOI + Cl^- + H^+$	1	2.4×10^6		*Wang et al.* (1989)
Ai4	$HOI + Br^- + H^+ \longrightarrow IBr$	3	3.3×10^{12}		*Troy et al.* (1991)
Ai5	$IBr \longrightarrow HOI + H^+ + Br^-$	1	8.0×10^5		*Troy et al.* (1991)
Ai6	$HOCl + I^- + H^+ \longrightarrow ICl$	3	3.5×10^{11}		*Nagy et al.* (1988)
Ai7	$HOBr + I^- \longrightarrow IBr + OH^-$	2	5.0×10^9		*Troy and Margerum* (1991)
Ai8	$IO + O_2^- \xrightarrow{H^+} HOI + O_2$	2	0.		see note
Ai9	$IO_2^- + H_2O_2 \longrightarrow IO_3^-$	2	6.0×10^1		*Furrow* (1987)

Table D.2: Continued.

no	reaction	n	k_0 [$(M^{1-n})s^{-1}$]	$-E_a$ / R [K]	reference
Ai10	$IO + IO \longrightarrow HOI + IO_2^- + H^+$	2	1.5×10^9		*Buxton et al.* (1986)
Ai11	$I^- + O_3 \xrightarrow{H^+} HOI$	2	4.2×10^9	-9311	*Magi et al.* (1997)
Ai12	$Cl_2 + HOI \longrightarrow IO_2^- + 2Cl^- + 3H^+$	2	1.0×10^6		*Lengyel et al.* (1996)
Ai13	$HOI + HOCl \longrightarrow IO_2^- + Cl^- + 2\ H^+$	2	5.0×10^5		*Citri and Epstein* (1988)
Ai14	$HOI + HOBr \longrightarrow IO_2^- + Br^- + 2\ H^+$	2	1.0×10^6		*Chinake and Simoyi* (1996)
Ai15	$IO_2^- + HOCl \longrightarrow IO_3^- + Cl^- + H^+$	2	1.5×10^3		*Lengyel et al.* (1996)
Ai16	$IO_2^- + HOBr \longrightarrow IO_3^- + Br^- + H^+$	2	1.0×10^6		*Chinake and Simoyi* (1996)
Ai17	$IO_2^- + HOI \longrightarrow IO_3^- + I^- + H^+$	2	6.0×10^2		*Chinake and Simoyi* (1996)
Ai18	$I_2 + HSO_3^- \longrightarrow 2\ I^- + HSO_4^- + 2\ H^+$	2	1.0×10^6		*Olsen and Epstein* (1991)

n is the order of the reaction. [1] photolysis rates calculated online. The reactions Ai1 - Ai18 are included only in the sensitivity runs including iodine reactions. The temperature dependence is $k = k_0 \times \exp(\frac{-E_a}{R}(\frac{1}{T} - \frac{1}{T_0}))$, $T_0 = 298$ K.

Table D.3: Heterogeneous reactions.

no	reaction	k	reference
H1	$N_2O_5 \xrightarrow{H_2O} HNO_{3aq} + HNO_{3aq}$	$\overline{k_t}(N_2O_5)w_{l,i}[H_2O]/Het_T$	*Behnke et al.* (1994), *Behnke et al.* (1997)
H2	$N_2O_5 \xrightarrow{Cl^-} ClNO_2 + NO_3^-$	$\overline{k_t}(N_2O_5)w_{l,i}f(Cl^-)[Cl^-]/Het_T$	*Behnke et al.* (1994), *Behnke et al.* (1997)
H3	$N_2O_5 \xrightarrow{Br^-} BrNO_2 + NO_3^-$	$\overline{k_t}(N_2O_5)w_{l,i}f(Br^-)[Br^-]/Het_T$	*Behnke et al.* (1994), *Behnke et al.* (1997)
H4	$ClNO_3 \xrightarrow{H_2O} HOCl_{aq} + HNO_{3aq}$	$\overline{k_t}(ClNO_3)w_{l,i}[H_2O]/Het_T$	see note
H5	$ClNO_3 \xrightarrow{Cl^-} Cl_{2aq} + NO_3^-$	$\overline{k_t}(ClNO_3)w_{l,i}f(Cl^-)[Cl^-]/Het_T$	see note
H6	$ClNO_3 \xrightarrow{Br^-} BrCl_{aq} + NO_3^-$	$\overline{k_t}(ClNO_3)w_{l,i}f(Br^-)[Br^-]/Het_T$	see note
H7	$BrNO_3 \xrightarrow{H_2O} HOBr_{aq} + HNO_{3aq}$	$\overline{k_t}(BrNO_3)w_{l,i}[H_2O]/Het_T$	see note
H8	$BrNO_3 \xrightarrow{Cl^-} BrCl_{aq} + NO_3^-$	$\overline{k_t}(BrNO_3)w_{l,i}f(Cl^-)[Cl^-]/Het_T$	see note
H9	$BrNO_3 \xrightarrow{Br^-} Br_{2aq} + NO_3^-$	$\overline{k_t}(BrNO_3)w_{l,i}f(Br^-)[Br^-]/Het_T$	see note
H10	$CH_3SO_3H \xrightarrow{H_2O} CH_3SO_3^- + H^+$	$\overline{k_t}(CH_3SO_3H)w_{l,i}$	
Hi1	$INO_3 \xrightarrow{H_2O} HOI_{aq} + HNO_{3aq}$	$\overline{k_t}(INO_3)w_{l,i}$	
Hi2	$HI \xrightarrow{H_2O} H^+ + I^-$	$\overline{k_t}(HI)w_{l,i}$	
Hi3	$I_2O_2 \xrightarrow{H_2O} HOI_{aq} + H^+ + IO_2^-$	$\overline{k_t}(I_2O_2)w_{l,i}$	
Hi4	$INO_2 \xrightarrow{H_2O} HOI_{aq} + HONO_{aq}$	$\overline{k_t}(INO_2)w_{l,i}$	
Hi5	$OIO \xrightarrow{H_2O} IO_2^- + H^+ + OH_{aq}$	$0.1 \times \overline{k_t}(OIO)w_{l,i}$	assumed, see section (4.13)
Hi6	$OIO \xrightarrow{H_2O} HOI_{aq} + HO_{2aq}$	$0.9 \times \overline{k_t}(OIO)w_{l,i}$	assumed, see section (4.13)

The reactions Hi1 - Hi6 are included only in the sensitivity runs including iodine reactions. For a definition of $\overline{k_t}$ and $w_{l,i}$ see section 3. $Het_T = [H_2O + f(Cl^-)[Cl^-] + f(Br^-)[Br^-]$, with $f(Cl^-) = 5.0 \times 10^2$ and $f(Br^-) = 3.0 \times 10^5$. H4 - H9: the total rate is determined by $\overline{k_t}$, the distribution among the different reaction paths was assumed to be the same as for reactions H1 - H3.

Table D.4: Aqueous phase equilibrium constants.

no	reaction	m	n	K_0 [M^{n-m}]	-$\Delta H/R$ [K]	reference
EQ1	$CO_{2aq} \longleftrightarrow H^+ + HCO_3^-$	1	2	4.3×10^{-7}	-913	*Chameides* (1984)
EQ2	$NH_{3aq} \longleftrightarrow OH^- + NH_4^+$	1	2	1.7×10^{-5}	-4325	*Chameides* (1984)
EQ3	$H_2O_{aq} \longleftrightarrow H^+ + OH^-$	1	2	1.0×10^{-14}	-6716	*Chameides* (1984)
EQ4	$HCOOH_{aq} \longleftrightarrow H^+ + HCOO^-$	1	2	1.8×10^{-4}		*Weast* (1980)
EQ5	$HSO_3^- \longleftrightarrow H^+ + SO_3^{2-}$	1	2	6.0×10^{-8}	1120	*Chameides* (1984)
EQ6	$H_2SO_{4aq} \longleftrightarrow H^+ + HSO_4^-$	1	2	1.0×10^{3}		*Seinfeld and Pandis* (1998)
EQ7	$HSO_4^- \longleftrightarrow H^+ + SO_4^{2-}$	1	2	1.2×10^{-2}	1120	*Weast* (1980)
EQ8	$HO_{2aq} \longleftrightarrow O_2^- + H^+$	1	2	1.6×10^{-5}		*Weinstein-Lloyd and Schwartz* (1991)
EQ9	$SO_{2aq} \longleftrightarrow H^+ + HSO_3^-$	1	2	1.7×10^{-2}	2090	*Chameides* (1984)
EQ10	$Cl_2^- \longleftrightarrow Cl_{aq} + Cl^-$	1	2	5.2×10^{-6}		*Jayson et al.* (1973)
EQ11	$HOCl_{aq} \longleftrightarrow H^+ + ClO^-$	1	2	3.2×10^{-8}		*Lax* (1969)
EQ12	$HBr_{aq} \longleftrightarrow H^+ + Br^-$	1	2	1.0×10^{9}		*Lax* (1969)
EQ13	$Br_2^- \longleftrightarrow Br_{aq} + Br^-$	1	2	9.1×10^{-6}		*Mamou et al.* (1977)
EQ14	$HOBr_{aq} \longleftrightarrow H^+ + BrO^-$	1	2	2.3×10^{-9}	-3091	*Kelley and Tartar* (1956)
EQ15	$BrCl_{aq} + Cl^- \longleftrightarrow BrCl_2^-$	2	1	3.8	1143	*Wang et al.* (1994)
EQ16	$BrCl_{aq} + Br^- \longleftrightarrow Br_2Cl^-$	2	1	1.8×10^{4}		*Wang et al.* (1994)
EQ17	$Br_{2aq} + Cl^- \longleftrightarrow Br_2Cl^-$	2	1	1.3		*Wang et al.* (1994)
EQ18	$HNO_{3aq} \longleftrightarrow H^+ + NO_3^-$	1	2	1.5×10^{1}		*Davis and de Bruin* (1964)
EQ19	$HCl_{aq} \longleftrightarrow H^+ + Cl^-$	1	2	1.7×10^{6}		*Marsh and McElroy* (1985)
EQ20	$HONO_{aq} \longleftrightarrow H^+ + NO_2^-$	1	2	5.1×10^{-4}	-1260	*Schwartz and White* (1981)
EQ21	$HNO_{4aq} \longleftrightarrow NO_4^- + H^+$	1	2	1.0×10^{-5}	8700	*Warneck* (1999)
EQi1	$ICl_{aq} + Cl^- \longleftrightarrow ICl_2^-$	2	1	7.7×10^{1}		*Wang et al.* (1989)
EQi2	$IBr_{aq} + Br^- \longleftrightarrow IBr_2^-$	2	1	2.9×10^{2}		*Troy et al.* (1991)

The equilibria EQi1 - EQi2 are included only in the sensitivity runs including iodine reactions. The temperature dependence is $K = K_0 \times \exp(\frac{-\Delta H}{R}(\frac{1}{T} - \frac{1}{T_0}))$, $T_0 = 298$ K.

Table D.5: Henry constants and accomodation coefficients.

specie	K_H^0 [M/atm]	$-\Delta_{soln}H/R$ [K]	reference	α^0	$-\Delta_{obs}H/R$ [K]	reference
O_3	1.2×10^{-2}	2560	*Chameides* (1984)	0.002	(at 292 K)	*DeMore et al.* (1997)
O_2	1.3×10^{-3}	1500	*Wilhelm et al.* (1977)	0.01	2000	estimated
OH	3.0×10^{1}	4300	*Hanson et al.* (1992)	0.01	(at 293 K)	*Takami et al.* (1998)
HO_2	3.9×10^{3}	5900	*Hanson et al.* (1992)	0.2	(at 293 K)	*DeMore et al.* (1997)
H_2O_2	1.0×10^{5}	6338	*Lind and Kok* (1994)	0.077	2769	*Worsnop et al.* (1989)
NO_2	6.4×10^{-3}	2500	*Lelieveld and Crutzen* (1991)	0.0015	(at 298 K)	*Ponche et al.* (1993)
NO_3	2.0	2000	*Thomas et al.* (1993)	0.04	(at 273? K)	*Rudich et al.* (1996)
N_2O_5	∞	—		0.1	(at 195-300 K)	*DeMore et al.* (1997)
HONO	4.9×10^{1}	4780	*Schwartz and White* (1981)	0.04	(at 247-297 K)	*DeMore et al.* (1997)
HNO_3	1.7×10^{5}	8694	*Lelieveld and Crutzen* (1991)	0.5	(at RT)	*Abbatt and Waschewsky* (1998)
HNO_4	1.2×10^{4}	6900	*Régimbal and Mozurkewich* (1997)	0.1	(at 200 K)	*DeMore et al.* (1997)
NH_3	5.8×10^{1}	4085	*Chameides* (1984)	0.06	(at 295 K)	*DeMore et al.* (1997)
CH3OO	6.0	$=HO_2$	*Pandis and Seinfeld* (1989)	0.01	2000	estimated
ROOH	3.0×10^{2}	5322	*Lind and Kok* (1994)	0.0046	3273	*Magi et al.* (1997)
HCHO	7.0×10^{3}	6425	*Chameides* (1984)	0.04	(at 260-270 K)	*DeMore et al.* (1997)
HCOOH	3.7×10^{3}	5700	*Chameides* (1984)	0.014	3978	*DeMore et al.* (1997)
CO_2	3.1×10^{-2}	2423	*Chameides* (1984)	0.01	2000	estimated
HCl	1.2	9001	*Brimblecombe and Clegg* (1989)	0.074	3072	*Schweitzer et al.* (2000)
HOCl	6.7×10^{2}	5862	*Huthwelker et al.* (1995)	=HOBr	=HOBr	estimated
$ClNO_3$	∞	—		0.1	(at RT)	*Koch and Rossi* (1998)
Cl_2	9.1×10^{-2}	2500	*Wilhelm et al.* (1977)	0.038	6546	*Hu et al.* (1995)
HBr	1.3	10239	*Brimblecombe and Clegg* (1989)	0.031	3940	*Schweitzer et al.* (2000)
HOBr	9.3×10^{1}	=HOCl	*Vogt et al.* (1996)	0.5	(at RT)	*Abbatt and Waschewsky* (1998)
$BrNO_3$	∞	—		0.8	0	*Hanson et al.* (1996)
Br_2	7.6×10^{-1}	4094	*Dean* (1992)	0.038	6546	*Hu et al.* (1995)
BrCl	9.4×10^{-1}	5600	*Bartlett and Margerum* (1999)	$=Cl_2$	$=Cl_2$	estimated
DMSO	5.0×10^{4}	=HCHO	*De Bruyn et al.* (1994)	0.048	2578	*De Bruyn et al.* (1994)
SO_2	1.2	3120	*Chameides* (1984)	0.11	0	*DeMore et al.* (1997)
H_2SO_4	∞	—		0.65	(at 303 K)	*Pöschl et al.* (1998)
CH_3SO_3H	∞	—		0.076	1762	*De Bruyn et al.* (1994)

Table D.5: Continued.

specie	k_H^0 [M/atm]	$-\Delta_{soln}H/R$ [K]	reference	α^0	$-\Delta_{soln}H/R$ [K]	reference
HI	∞	—		0.036	4130	*Schweitzer et al.* (2000)
IO	4.5×10^2	=HOI	see note	0.5	2000	estimated
HOI	4.5×10^2	=HOCl	*Chatfield and Crutzen* (1990)	=HOBr	=HOBr	estimated
INO_2	∞	—		0.1	2000	estimated
INO_3	∞	—		0.1	2000	estimated
I_2	3.0	4431	*Palmer et al.* (1985)	0.01	2000	estimated
ICl	1.1×10^2	=BrCl	see note	0.01	2000	estimated
IBr	2.4×10^1	=BrCl	see note	0.01	2000	estimated
I_2O_2	∞	—		0.1	2000	estimated

For ROOH the values of CH_3OOH have been assumed. The temperature dependence is for the Henry constants is $K_H = K_H^0 \times \exp(\frac{-\Delta_{soln}H}{R}(\frac{1}{T} - \frac{1}{T_0}))$, $T_0 = 298$ K and for the accomodation coefficients $dln(\frac{\alpha}{1-\alpha})/d(\frac{1}{T}) = \frac{-\Delta_{obs}H}{R}$.

Appendix E

List of symbols

variable	description	unit
A_{pl}	cross section of the ship plume	m^2
a	dry aerosol radius	m
$\bar{v}$	mean molecular speed	m/s
C	condensation rate	$kg/(m^3 s)$
$c_{a,i}$	concentration of aqueous phase species in bin i	mol/m^3_{air}
c_{bg}	background concentration	mol/m^3_{air}
c_g	concentration of gas phase species	mol/m^3_{air}
c_p	specific heat of dry air at constant pressure	J/(kg K)
c_w	specific heat of water	J/(kg K)
D	aerosol diffusivity	m^2/s
D	chemical destruction	1/s
D_g	gas phase diffusion coefficient	m^2/s
D'_v	diffusivity of water vapor	m^2/s
E	surface gas phase emission flux	$mol/(m^2\ s)$
E_n	net radiative flux density	W/m^2
e	turbulent kinetic energy	$1/(m^2\ s)$
F	flux of sea salt particles from the ocean	$1/(m^2\ s)$
$F_d(a,r)$	net radiative flux at the particle's surface	W
$F(\lambda)$	spectral actinic flux	$W/(m^2\ m)$
$f(a,r)$	two-dimensional particle size distribution function	$1/m^3$
f	Coriolis parameter	1/s
h_0	reference height of the ship plume	m
H^*	effective Henry constant	$mol/(m^3\ Pa)$
h_{pl}	height of the ship plume	m
J_{X}	photolysis rate (or photo dissociation coefficient)	1/s
$J^a_{i,\mathrm{X}}$	photolysis rate for a purely absorbing atmosphere	1/s
K_e	exchange coefficient for e	m^2/s
K_h	turbulent exchange coefficients for heat	m^2/s
K_m	turbulent exchange coefficients for momentum	m^2/s
k^{cc}_H	dimensionless Henry constant	1

variable	description	unit
k_H	Henry constant	mol/(m^3 Pa)
k'	thermal conductivity of moist air	W/(m K)
k_t	mass transfer coefficient	m^3_{air}/(m^3_{aq} s)
$k_{t,i}$	mass transfer coefficient for aqueous bin i	m^3_{air}/(m^3_{aq} s)
$\overline{k_t}$	mean transfer coefficient for a particle population	m^3_{air}/(m^3_{aq} s)
l	mixing length	m
L	latent heat of condensation	J/kg
L	Monin-Obukhov length	m
M	molar mass	g/mol
$m_w(a,r)$	liquid water mass of the particle	kg
n_{kc}	number of the aqueous classes	1
p_0	air pressure at the surface	Pa
p	air pressure	Pa
P	chemical production	mol/(m^3 s)
P_{pc}	transport of chemical species from the aerosol to the cloud droplet regimes	mol/(m^3 s)
q	specific humidity	kg/kg
r_a	aerodynamic resistance	s/m
r_b	quasi-laminar layer resistance	s/m
r_c	surface resistance	s/m
R	gas constant for dry air	J/(mol K)
R_v	specific gas constant for water vapor	J/(kg K)
r	total particle radius	m
Sc	Schmidt number	1
S_∞	ambient supersaturation	1
S_r	supersaturation at the droplet's surface	1
St	Stokes number	1
T	temperature	K
t	time	s
u	wind speed in x-direction	m/s
u_{10}	wind speed in 10 m height	m/s
u_*	friction velocity	m/s
u_g	geostrophic wind	m/s
v	wind speed in y-direction	m/s
$v_{a,i}^{dry}$	dry deposition velocity of particles	m/s
v_g^{dry}	dry deposition velocity of gases	m/s
v_g	geostrophic wind	m/s
$\overline{v}$	mean molecular speed	m/s
w	vertical/subsidence velocity	m/s
w_0	reference width of the ship plume	m
$w_{l,i}$	liquid water content of aqueous bin i	kg/m^3
w_{pl}	width of the ship plume	m
w_t	particle sedimentation velocity	m/s
z_0	roughness length	m

variable	description	unit
α	accommodation coefficient	1
α	horizontal plume expansion rate	1
β	vertical plume expansion rate	1
δ_i	describes the effect of scattering by air molecules, aerosol and cloud particles	1
κ	von Kármán constant	1
λ	mean free path length	m
λ	wavelength	m
ν	dynamic viscosity of air	kg/(m s)
Φ	generic meteorological variable	-
Φ_s	stability function	1
ϕ_{X}	quantum yield	1
ρ	air density	$\mathrm{kg/m^3}$
ρ_s	saturation vapor density	$\mathrm{kg/m^3}$
ρ_w	density of water	$\mathrm{kg/m^3}$
σ_{X}	absorption cross section	$\mathrm{m^2}$
Θ	potential temperature	K

Appendix F

Photolysis rates

Figure F.1 shows photolysis rates for a cloudy and non-cloudy model run near the surface (in 50 m height) and at 750 m, which is below the top of the cloud for the cloudy run. The asymmetry of the photolysis rates with respect to local noon in the cloudy MBL is a consequence of the column integrated liquid water content, the so-called liquid water path. It has a minimum after noon, see Figure 5.1. The increase of photolysis rates below cloud top is due to multiple scattering of photons, see page 71.

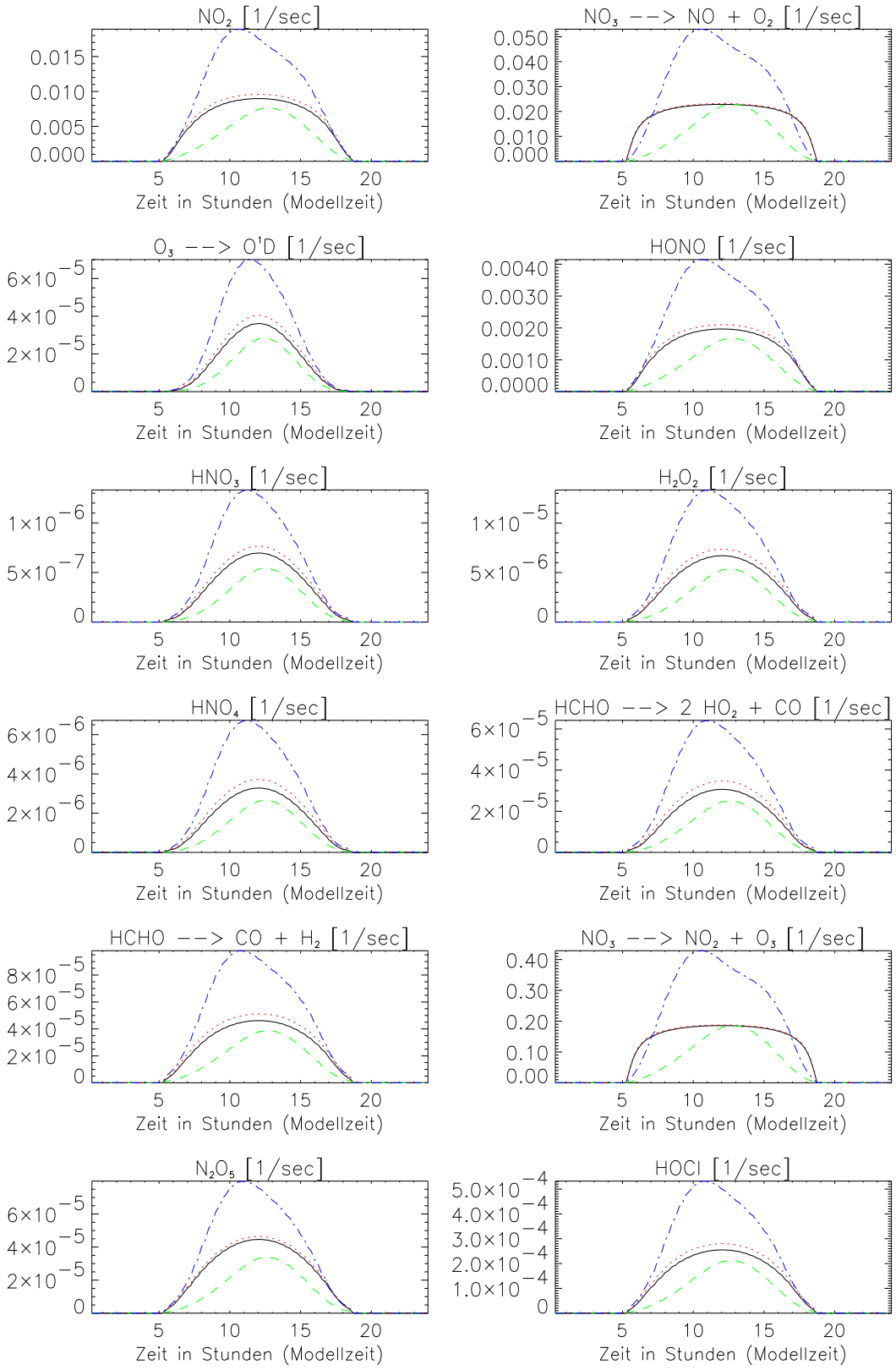

Figure F.1: Photolysis rates for a cloudy and a cloud-free MBL. 50 m cloud-free: black, solid line, 50 m cloudy: green, dashed line; 750 m cloud-free: red, dotted line, 750 m cloudy: blue, dash-dotted line.

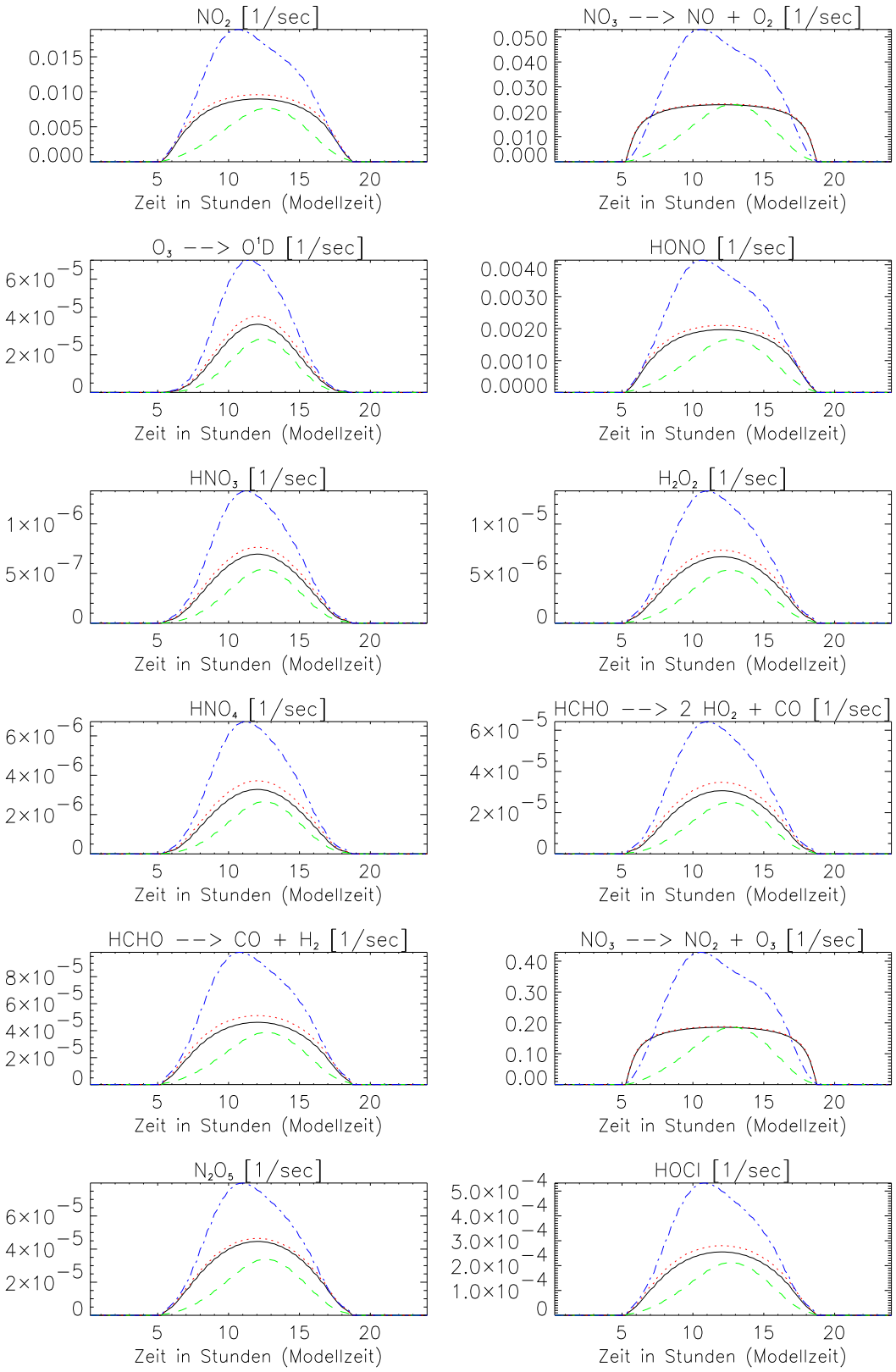

Figure F.1: Continued.

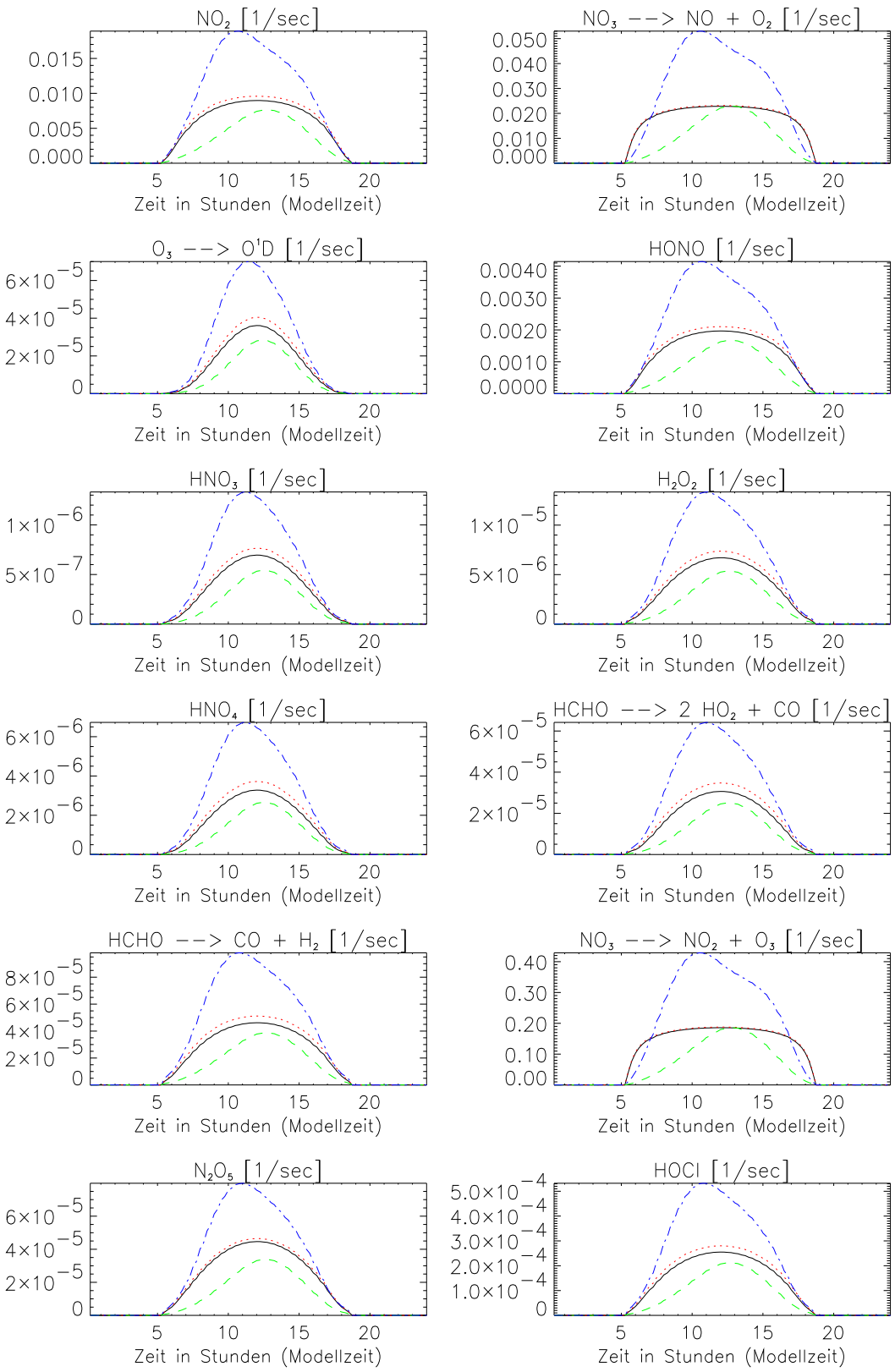

Figure F.1: Continued.

Appendix G

Major reaction cycles

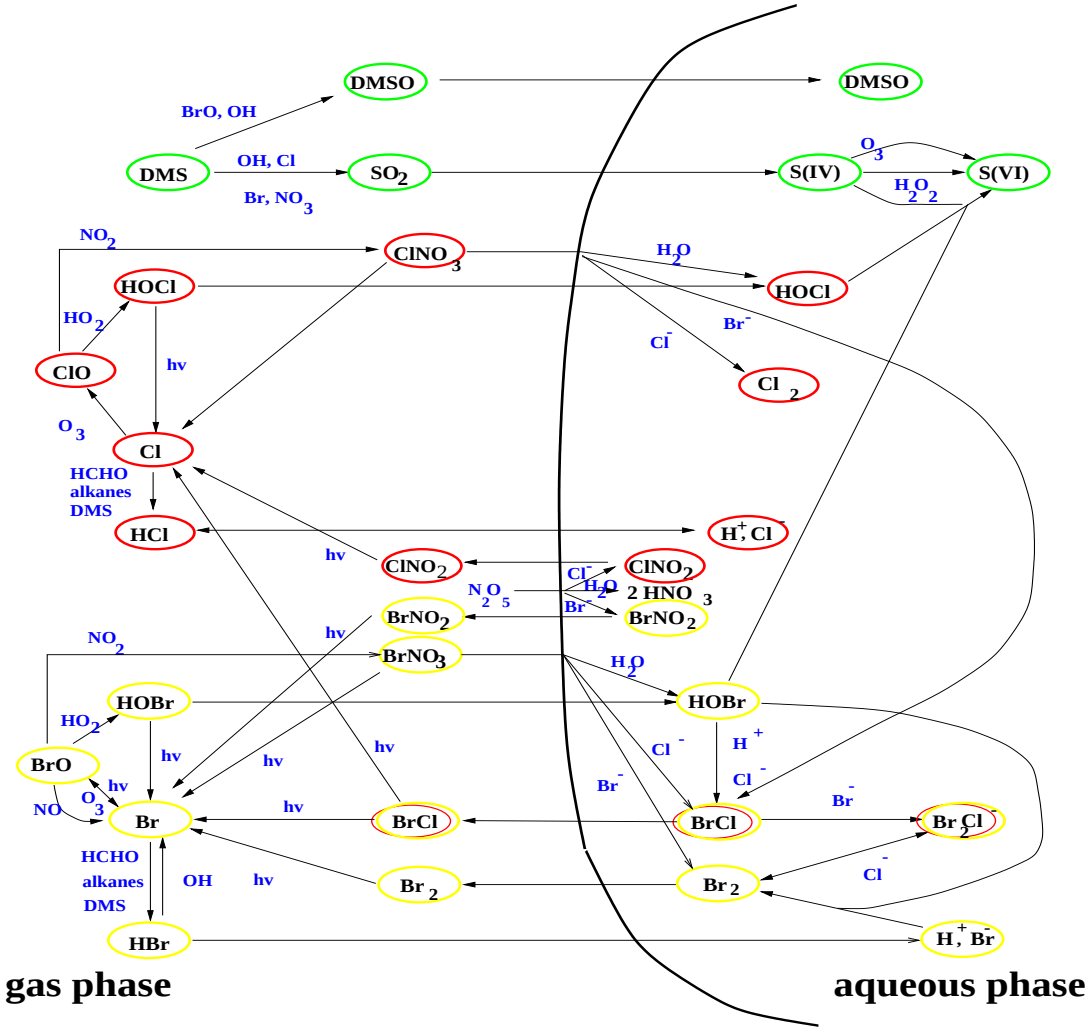

Figure G.1: Schematic diagram of the major bromine, chlorine, and sulfur related reactions in the gas and aqueous phase.

Bibliography

Abbatt, J. P. D. and G. C. G. Waschewsky. Heterogeneous interactions of HOBr, HNO_3, O_3 and NO_2 with deliquescent NaCl aerosols at room temperature. *J. Phys. Chem. A*, *102*, 3719 – 3725, 1998.

Ackerman, A. S., O. B. Toon, and P. V. Hobbs. Numerical modeling of ship tracks produced by injections of cloud condensation nuclei into marine stratiform clouds. *J. Geophys. Res.*, *100*, 7121 – 7133, 1995.

Albrecht, B. A. Aerosols, Cloud Microphysics, and Fractional Cloudiness. *Science*, *245*, 1227 – 1230, 1989.

Alicke, B., K. Hebestreit, J. Stutz, and U. Platt. Iodine oxide in the marine boundary layer. *Nature*, *397*, 572 – 573, 1999.

Allan, B. J., G. McFiggans, J. M. C. Plane, and H. Coe. Observation of Iodine Oxide in the Remote Marine Boundary Layer. *J. Geophys. Res.*, *105*, 14 363 – 14 370, 2000.

Ammann, M., M. Kalberer, D. T. Jost, L. Tobler, E. Rössler, D. Piguet, H. W. Gäggeler, and U. Baltensperger. Heterogeneous production of nitrous acid on soot in polluted air masses. *Nature*, *395*, 157 – 160, 1998.

Anderson, L. C. and D. W. Fahey. Studies with $ClONO_2$: Thermal dissociation rate and catalytic conversion to NO using an NO/O_3 chemiluminescence detector. *J. Phys. Chem.*, *94*, 644 – 652, 1990.

Andreas, E. L. A New Sea Spray Generation Function for Wind Speeds up to 32 m s^{-1}. *J. Phys. Oceanogr.*, *28*, 2175 – 2184, 1998.

Andreas, E. L., J. B. Edson, E. C. Monahan, M. P. Rouault, and S. D. Smith. The spray contribution to net evaporation from the sea: A review of recent progress. *Bound. Lay. Met.*, *72*, 3 – 52, 1995.

Andrews, J. E., P. Brimblecombe, T. D. Jickells, and P. S. Liss. *An Introduction to Environmental Chemistry*. Blackwell Science, 1996.

Aranda, A., G. Le Bras, G. La Verdet, and G. Poulet. The BrO + CH_3O_2 reaction: Kinetics and role in the atmospheric ozone budget. *Geophys. Res. Letters*, *24*, 2745 – 2748, 1997.

Atkinson, A., D. L. Baulch, R. A. Cox, R. F. Hampson, Jr., J. A. Kerr, M. J. Rossi, and J. Troe. Evaluated kinetic and photochemical data for atmospheric chemistry: Supplement VI. *J. Phys. Chem. Ref. Data*, *26*, 1329 – 1499, 1997.

Atkinson, R., D. L. Baulch, R. A. Cox, J. R. F. Hampson, J. A. Kerr, M. J. Rossi, and J. Troe. Summary of Evaluated Kinetic and Photochemical Data for Atmspheric Chemistry. *Web Version*, *http://www.iupac-kinetic.ch.cam.ac.uk*, 1999.

Ayers, G. P., J. M. Cainey, R. W. Gillett, E. S. Saltzman, and M. Hooper. Sulfur dioxide and dimethyl sulfide in marine air at Cape Grim, Tansania. *Tellus*, *49B*, 292 – 299, 1997a.

Ayers, G. P. and R. W. Gillett. DMS and its oxidation products in the remote marine atmosphere; implications for climate and atmospheric chemistry. *J. Sea Res.*, *43*, 275 – 286, 2000.

Ayers, G. P., R. W. Gillett, J. M. Cainey, and A. L. Dick. Chloride and Bromide Loss from Sea-Salt Particles in Southern Ocean Air. *J. Atmos. Chem.*, *33*, 299 – 319, 1999.

Ayers, G. P., H. Granek, and R. Boers. Ozone in the Marine Boundary Layer at Cape Grim: Model Simulation. *J. Atmos. Chem.*, *27*, 179 – 195, 1997b.

Baker, A. R., D. Thompson, M. L. A. M. Campos, S. J. Perry, and T. D. Jickells. Iodine concentration and availability in atmospheric aerosol. *Atmos. Environ.*, *34*, 4331 – 4336, 2000.

Bandy, A. R., D. C. Thornton, B. W. Blomquist, S. Chen, T. P. Wade, J. C. Ianni, G. M. Mitchell, and W. Nadler. Chemistry of dimethyl sulfide in the equatorial Pacific atmosphere. *Geophys. Res. Letters*, *23*, 741 – 744, 1996.

Barker, G. C., P. Fowles, and B. Stringer. Pulse radiolytic induced transient electrical conductance in liquid solutions. *Trans. Faraday Soc.*, *66*, 1509–1519, 1970.

Barnes, I., K. H. Becker, and J. Starcke. Fourier-transform IR spectroscopic observation of gaseous nitrosyl iodine, nitryl iodine, and iodine nitrate. *J. Phys. Chem.*, *95*, 9736–9740, 1991.

Barone, S. B., A. A. Turnipseed, and A. R. Ravishankara. Role of adducts in the atmospheric oxidation of dimethyl sulfide. *Faraday Discuss.*, *100*, 39 – 54, 1995.

Barrie, L. and U. Platt. Arctic tropospheric chemistry: an overview. *Tellus*, *49B*, 450 – 454, 1997.

Barrie, L. A., J. W. Bottenheim, and W. R. Hart. Polar Sunrise Experiment 1992 (PSE 1992): Preface. *J. Geophys. Res.*, *99*, 25 313 – 25 314, 1994.

Barrie, L. A., J. W. Bottenheim, R. C. Schnell, P. J. Crutzen, and R. A. Rasmussen. Ozone destruction and photochemical reactions at polar sunrise in the lower Arctic atmosphere. *Nature*, *334*, 138 – 141, 1988.

Bartlett, W. P. and D. W. Margerum. Temperature dependencies of the Henry's law constant and the aqueous phase dissociation constant of bromine chloride. *Environ. Sci. Technol.*, *33*, 3410–3414, 1999.

Bauer, D., T. Ingham, S. A. Carl, G. K. Moortgat, and J. N. Crowley. Ultraviolet-visible absorption cross sections of gaseous HOI and its photolysis at 355 nm. *J. Phys. Chem. A*, *102*, 2857–2864, 1998.

Beckwith, R. C., T. X. Wang, and D. W. Margerum. Equilibrium and kinetics of bromine hydrolysis. *Inorg. Chem.*, *35*, 995–1000, 1996.

Bedjanian, Y., G. L. Bras, and G. Poulet. Kinetics and Mechanisms of the IO + BrO Reaction. *J. Phys. Chem. A*, *102*, 10 501 – 10 511, 1998.

Behnke, W., M. Elend, U. Krüger, and C. Zetzsch. The Influence of NaBr/NaCl Ratio on the Br^--Catalyzed Production of Halogenated Radicals. *J. Atmos. Chem.*, *34*, 87 – 99, 1999.

Behnke, W., C. George, V. Scheer, and C. Zetzsch. Production and decay of $ClNO_2$ from the reaction of gaseous N_2O_5 with NaCl solution: Bulk and aerosol experiments. *J. Geophys. Res.*, *102*, 3795–3804, 1997.

Behnke, W., V. Scheer, and C. Zetzsch. Formation of $ClNO_2$ and HNO_3 in the Presence of N_2O_5 and Wet Pure NaCl- and Wet Mixed $NaCl/Na_2SO_4$ - Aerosol. *J. Aerosol Sci.*, *24, Suppl.1*, S115 – S116, 1993.

Behnke, W., V. Scheer, and C. Zetzsch. Production of $BrNO_2$, Br_2 and $ClNO_2$ from the Reaction between Sea Spray Aerosol and N_2O_5. *J. Aerosol Sci.*, *25, Suppl.1*, S227 – S228, 1994.

Betterton, E. A. and M. R. Hoffmann. Oxidation of aqueous SO_2 by peroxymonosulfate. *J. Phys. Chem.*, *92*, 5962–5965, 1988.

Bjergbakke, E., S. Navartnam, B. J. Parsons, and A. J. Swallow. Reaction between $HO_2\cdot$ and chlorine in aqueous solution. *J. Am. Chem. Soc.*, *103*, 5926–5928, 1981.

Blake, N. J., D. R. Blake, O. W. Wingenter, B. C. Sive, C. H. Kang, D. C. Thornton, A. R. Bandy, E. Atlas, F. Flocke, J. M. Harris, and F. S. Rowland. Aircraft measurements of the latitudinal, vertical, and seasonal variations of NMHCs, methyl nitrate, methyl halides, and DMS during the First Aerosol Characterization Experiment (ACE 1). *J. Geophys. Res.*, *104*, 21 803 – 21 817, 1999.

Bott, A. A numerical model of the cloud-topped planetary boundary-layer: Impact of aerosol particles on the radiative forcing of stratiform clouds. *Q. J. R. Meteorol. Soc.*, *123*, 631 – 656, 1997.

Bott, A. A numerical model of the cloud-topped planetary boundary-layer: Chemistry in marine stratus and the effects on aerosol particles. *Atmos. Environ.*, *33*, 1921 – 1936, 1999.

Bott, A. A Flux Method for the Numerical Solution of the Stochastic Collection Equation: Extension to Two-Dimensional Particle Distributions. *J. Atmos. Sci.*, *57*, 284 – 294, 2000.

Bott, A., T. Trautmann, and W. Zdunkowski. A numerical model of the cloud-topped planetary boundary-layer: Radiation, turbulence and spectral microphysics in marine stratus. *Q. J. R. Meteorol. Soc.*, *122*, 635–667, 1996.

Bottenheim, J. W., L. A. Barrie, E. Atlas, L. E. Heidt, H. Niki, R. A. Rasmussen, and P. B. Shepson. Depletion of lower tropospheric ozone during Arctic spring: The polar sunrise experiment 1988. *J. Geophys. Res.*, *95*, 18 555 – 18 568, 1990.

Boyce, S. D. and M. R. Hoffmann. Kinetics and mechanism of the formation of hydroxymethanesulfonic acid at low pH. *J. Phys. Chem.*, *88*, 4740–4746, 1984.

Boyd, A. A., G. Marston, and R. P. Wayne. Kinetic Studies of the Reaction between NO_3 and OClO at T=300K and p=2-8 Torr. *J. Phys. Chem.*, *100*, 130 – 137, 1996.

Brasseur, G. P., J. J. Orlando, and G. S. Tyndall, editors. *Atmospheric Chemistry and Global Change*. Oxford University Press, New York, Oxford, 1999.

Brimblecombe, P. and S. L. Clegg. Erratum. *J. Atmos. Chem.*, *8*, 95, 1989.

Bröske, R. and F. Zabel. Spectroscopic and kinetic properties of XNO_2 (X = Br, I). *Ann. Geophys. Suppl. II*, *16*, C717, 1998.

Burley, J. D. and H. S. Johnston. Ionic mechanisms for heterogeneous stratospheric reactions and ultraviolet photoabsorption cross-sections for $NO2^+$, HNO_3, and NO_3^- in sulfuric-acid. *Geophys. Res. Letters*, *19*, 1359 – 1362, 1992.

Buxton, G. V., M. Bydder, and G. A. Salmon. The reactivity of chlorine atoms in aqueous solution Part II: The equilibrium $SO_4^- + Cl^- \longleftrightarrow Cl + SO_4^{2-}$. *Phys. Chem. Chem. Phys.*, *1*, 269 – 273, 1999a.

Buxton, G. V., C. L. Greenstock, W. P. Helman, and A. B. Ross. Critical review of rate constants for reactions of hydrated electrons, hydrogen atoms and hydroxyl radicals ($\cdot OH/\cdot O^-$) in aqueous solution. *J. Phys. Chem. Ref. Data*, *17*, 513–886, 1988.

Buxton, G. V., C. Kilner, and R. M. Sellers. Pulse radiolysis of HOI and IO^- in aqeuous solution, formation and characterization of I^{II}. In *6th. Symp. on Radiation Chemistry*, pages 155 – 159. 1986.

Buxton, G. V., S. McGowan, G. S. Salmon, J. E. Williams, and N. D. Wood. A study of the spectra and reactivity of oxysulphur-radical anions involved in the chain oxidation of S(IV): A pulse and γ-radiolysis study. *Atmos. Environ.*, *30*, 2483–2493, 1996.

Buxton, G. V., G. A. Salmon, and J. Wang. The equilibrium $NO_3 + Cl^- \longleftrightarrow NO_3^- + Cl$: A laser flash photolysis and pulse radiolysis study of the reactivity of NO_3 with chloride ion in aqueous solution. *Phys. Chem. Chem. Phys.*, *1*, 3589 – 3593, 1999b.

Campuzano-Jost, P. and J. N. Crowley. Kinetics of the Reaction of OH with HI between 246 and 353 K. *J. Phys. Chem. A*, *103*, 2712 – 2719, 1999.

Capaldo, K., J. J. Corbett, P. Kasibhatla, P. Fischbeck, and S. N. Pandis. Effects of ship emissions on sulphur cycling and radiative climate forcing over the ocean. *Nature*, *400*, 743 – 764, 1999.

Capaldo, K. P. and S. N. Pandis. Dimethylsulfide chemistry in the remote marine atmosphere: Evaluation and sensitivity analysis of available mechanisms. *J. Geophys. Res.*, *102*, 23 251 – 23 267, 1997.

Chambers, R. M., A. C. Heard, and R. P. Wayne. Inorganic gas-phase reactions of the nitrate radical: $I_2 + NO_3$ and $I + NO_3$. *J. Phys. Chem.*, *96*, 3321–3331, 1992.

Chameides, W. L. The Photochemistry of a Remote Marine Stratiform Cloud. *J. Geophys. Res.*, *89*, 4739 – 4755, 1984.

Chameides, W. L. and D. D. Davis. The Free Radical Chemistry of Cloud Droplets And Its Impact Upon the Composition of Rain. *J. Geophys. Res.*, *87*, 4863 – 4877, 1982.

Chameides, W. L. and A. W. Stelson. Aqueous-Phase Chemical Processes in Deliquescent Sea-Salt Aerosols: A Mechanism That Couples the Atmospheric Cycles of S and Sea Salt. *J. Geophys. Res.*, *97*, 20 565 – 20 580, 1992.

Chance, K. Analysis of BrO Measurements from the Global Ozone Monitoring Experiment. *Geophys. Res. Letters*, *25*, 3335 – 3338, 1998.

Charlson, R. J., J. E. Lovelock, M. O. Andreae, and S. G. Warren. Oceanic phytoplankton, atmospheric sulphur, cloud albedo and climate. *Nature*, *326*, 655 – 661, 1987.

Chatfield, R. B. and P. J. Crutzen. Are There Interactions of Iodine and Sulfur Species in Marine Air Photochemistry? *J. Geophys. Res.*, *95*, 22 319 – 22 341, 1990.

Chen, G., D. D. Davis, P. Kasibhatla, A. R. Bandy, D. C. Thornton, B. J. Huebert, A. D. Clarke, and B. W. Blomquist. A Study of DMS Oxidation in the Tropics: Comparison of Christmas Island Field Observations of DMS, SO_2, and DMSO with Model Simulations. *J. Atmos. Chem.*, *37*, 137 – 160, 2000.

Chin, M. and P. H. Wine. A temperature-dependent competitive kinetics study of the aqueous-phase reactions of OH radicals with formate, formic acid, acetate, acetic acid, and hydrated formaldehyde. In G. R. Helz, R. G. Zepp, and D. G. Crosby, editors, *Aquatic and Surface Photochemistry*, pages 85–96. A. F. Lewis, NY, 1994.

Chinake, C. R. and R. H. Simoyi. Kinetics and mechanism of the complex bromate-iodine reaction. *J. Phys. Chem.*, *100*, 1643–1656, 1996.

Christensen, H. and K. Sehested. HO_2 and O_2^- radicals at elevated temperatures. *J. Phys. Chem.*, *92*, 3007–3011, 1988.

Christensen, H., K. Sehested, and H. Corfitzen. Reactions of hydroxyl radicals with hydrogen peroxide at ambient and elevated temperatures. *J. Phys. Chem.*, *86*, 1588–1590, 1982.

Citri, O. and I. R. Epstein. Mechanistic study of a coupled chemical oscillator: the bromate-chlorite-iodide reaction. *J. Phys. Chem.*, *92*, 1865–1871, 1988.

Coakley, J. A. J., P. A. Durkee, K. Nielsen, J. P. Taylor, S. Platnick, B. A. Albrecht, D. Babb, F.-L. Chang, W. R. Tahnk, C. S. Bretherton, and P. V. Hobbs. The Appearance and Disappearance of Ship Tracks on Large Spatial Scales. *J. Atmos. Sci.*, *57*, 2765 – 2778, 2000.

Conover, J. H. Anomalous Cloud Lines. *J. Atmos. Sci.*, *23*, 778 – 785, 1966.

Corbett, J. J. and P. Fischbeck. Emissions from Ships. *Science*, *278*, 823 – 824, 1997.

Corbett, J. J., P. S. Fischbeck, and S. N. Pandis. Global nitrogen and sulfur inventories for oceangoing ships. *J. Geophys. Res.*, *104*, 3457 – 3470, 1999.

Cox, R. A., W. J. Bloss, R. L. Jones, and D. M. Rowley. OIO and the atmospheric cycle of iodine. *Geophys. Res. Letters*, *26*, 1857 – 1860, 1999.

Crowley, J. N., C. Zetsch, P. Mirabel, J.-P. Sawerysyn, M. Rossi, and Y. Gershenzon. Halogens in the marine environment: laboratory investigations of heterogeneous chemistry. Technical Report EC Grant: ENV4-CT97-0394, HAMLET, 1998.

Crutzen, P. J. and U. Schmailzl. Chemical budgets of the stratosphere. *Planet. Space. Sci.*, *31*, 1009 – 1032, 1983.

Damian-Iordache, V. *KPP - Chemistry Simulation Development Environment*. Ph.D. thesis, University of Iowa, 1996.

Damschen, D. E. and L. R. Martin. Aqueous aerosol oxidation of nitrous acid by O_2, O_3 and H_2O_2. *Atmos. Environ.*, *17*, 2005–2011, 1983.

Davies, R. Response of Cloud Supersaturation to Radiative Forcing. *J. Atmos. Sci.*, *42*, 2820–2825, 1985.

Davis, D., J. Crawford, S. Liu, S. McKeen, A. Bandy, D. Thornton, F. Rowland, and D. Blake. Potential impact of iodine on tropospheric levels pf ozone and other critical oxidants. *J. Geophys. Res.*, *101*, 2135 – 2147, 1996.

Davis, D. D., G. Grodzinsky, P. Kasibhatla, J. Crawford, G. Chen, S. Liu, A. Bandy, D. Thornton, H. Guan, and S. Sandholm. Impact of Ship Emissions on Marine Boundary Layer NO_x and SO_2 Distributions over the Pacific Basin. *in prep. for JGR?*, 2000.

Davis, W., Jr. and H. J. de Bruin. New activity coefficients of 0-100 per cent aqueous nitric acid. *J. Inorg. Nucl. Chem.*, *26*, 1069 – 1083, 1964.

De Bruyn, W. J., J. A. Shorter, P. D. andD. R. Worsnop, M. S. Zahniser, and C. E. Kolb. Uptake of gas phase sulfur species methanesulfonic acid, dimethylsulfoxide, and dimethyl sulfone by aqueous surface. *J. Geophys. Res.*, *99*, 16 927 – 16 932, 1994.

De Santis, F. and I. Allegrini. Heterogeneous reactions of SO_2 and NO_2 on carbonaceous surfaces. *Atmos. Environ.*, *16*, 3061 – 3064, 1992.

Dean, J. A. *Lange's Handbook of Chemistry*. McGraw-Hill, Inc., 1992.

Deister, U. and P. Warneck. Photooxidation of SO_3^{2-} in aqueous solution. *J. Phys. Chem.*, *94*, 2191–2198, 1990.

DeMore, W. B., S. P. Sander, D. M. Golden, R. F. Hampson, M. J. Kurylo, C. J. Howard, A. R. Ravishankara, C. E. Kolb, and M. J. Molina. Chemical Kinetics and Photochemical Data for Use in Stratospheric Modeling. Technical Report JPL Publication 97-4, Jet Propulsion Laboratory, Pasadena, CA, 1997.

Dickerson, R. R., K. P. Rhoads, T. P. Carsey, S. J. Oltmans, J. P. Burrows, and P. J. Crutzen. Ozone in the Remote Marine Boundary Layer: A Possible Role for Halogens. *J. Geophys. Res.*, *104*, 21 385 – 21 395, 1999.

Disselkamp, R. S., C. D. Howd, E. G. Chapman, W. R. Barchet, and S. D. Colson. BrCl production in $NaBr/NaCl/HNO_3/O_3$ solutions representative of sea-salt aerosols in the marine boundary layer. *Geophys. Res. Letters*, *26*, 2183 – 2186, 1999.

Driedonks, A. G. M. and P. G. Duynkerke. Current Problems in the Stratocumulus-Topped Atmospheric Boundary Layer. *Bound. Lay. Met.*, *46*, 275 – 303, 1989.

Duce, R. A., R. Arimoto, B. J. Ray, C. K. Unni, and P. J. Harder. Atmospheric trace elements at Enewetak Atoll: 1, Concentrations, sources, and temporal variability. *J. Geophys. Res.*, *88C*, 5321–5342, 1983.

Duce, R. A., J. W. Winchester, and T. W. van Nahl. Iodine, bromine, and chlorine in the Hawaiian marine atmosphere. *J. Geophys. Res.*, *70*, 1775 – 1799, 1965.

Durkee, P. A., R. E. Chartier, A. Brown, E. J. Trehubenko, S. D. Rogerson, C. Skupniewicz, K. E. Nielsen, S. Platnick, and M. D. King. Composite Ship Track Characteristics. *J. Atmos. Sci.*, *57*, 2542 – 2553, 2000a.

Durkee, P. A., K. J. Noone, and R. T. Bluth. The Monterey Area Ship Track Experiment. *J. Atmos. Sci.*, *57*, 2523 – 2541, 2000b.

Duynkerke, P. G. The Diurnal Variation of a Marine Stratocumuls Layer: A Model Sensitivity Study. *J. Atmos. Sci.*, *117*, 1710 – 1725, 1989.

Eigen, M. and K. Kustin. The kinetics of halogen hydrolysis. *J. Am. Chem. Soc.*, *84*, 1355–1361, 1962.

EPA. Compilation of Air Pollutant Emission Factors. Technical report, United States Environmental Protection Agency, 1972.

EPA. Analysis of Commercial Marine Vessels Emissions and Fuel Consumption Data. Technical Report EPA420-R-00-002, United States Environmental Protection Agency, 2000.

Erickson, I., D. J., C. Seuzaret, W. C. Keene, and S. L. Gong. A general circulation model based calculation of HCl and $ClNO_2$ production from sea salt dechlorination: Reactive Chlorine Emissions Inventory. *J. Geophys. Res.*, *104*, 8347 – 8372, 1999.

Exner, M., H. Herrmann, and R. Zellner. Laser-based studies of reactions of the nitrate radical in aqueous solution. *Ber. Bunsenges. Phys. Chem.*, *96*, 470–477, 1992.

Falbe-Hansen, H. S. S., N. R. Jensen, T. Pedersen, and J. Hjorth. Atmospheric gas-phase reactions of dimethylsulphoxide and dimethylsulphone with OH and NO_3 radicals, Cl atoms and ozone. *Atmos. Environ.*, *34*, 1543 – 1551, 2000.

Fan, S.-M. and D. J. Jacob. Surface ozone depletion in Arctic spring sustained by bromine reactions on aerosols. *Nature*, *359*, 522 – 524, 1992.

Ferek, R. J., D. A. Hegg, P. V. Hobbs, P. Durkee, and K. Nielson. Measurement of ship-induced tracks in clouds off the Washington coast. *J. Geophys. Res.*, *103*, 23 199 – 23 206, 1998.

Fickert, S., J. W. Adams, and J. N. Crowley. Activation of Br_2 and BrCl via uptake of HOBr onto aqueous salt solutions. *J. Geophys. Res.*, *104*, 23 719 – 23 727, 1999.

Fickert, S., F. Helleis, J. W. Adams, G. K. Moortgat, and J. N. Crowley. Reactive Uptake of $ClNO_2$ on Aqueous Bromide Solutions. *J. Phys. Chem. A*, *102*, 10 689 – 10 696, 1998.

Finlayson-Pitts, B. J., M. J. Ezell, and J. N. Pitts, Jr. Formation of chemically active chlorine compounds by reactions of atmospheric NaCl particles with gaseous N_2O_5 and $ClONO_2$. *Nature*, *337*, 241 – 244, 1989.

Finlayson-Pitts, B. J. and J. N. P. Jr. *Chemistry of the Upper and Lower Atmosphere*. Academic Press Inc, 1999.

Fogelman, K. D., D. M. Walker, and D. W. Margerum. Non-metal redox kinetics: Hypochlorite and hypochlorous acid reactions with sulfite. *Inorg. Chem.*, *28*, 986–993, 1989.

Fortnum, D. H., C. J. Battaglia, S. R. Cohen, and J. O. Edwards. The kinetics of the oxidation of halide ions by monosubstituted peroxides. *J. Am. Chem. Soc.*, *82*, 778–782, 1960.

Frick, G. M. and W. A. Hoppel. Airship Measurements of Ship's Exhaust Plumes and Their Effect on Marine Boundary Layer Clouds. *J. Atmos. Sci.*, *57*, 2625 – 2648, 2000.

Fridlind, A. M. and M. Z. Jacobson. A study of gas-aerosol equilibrium and aerosol pH in the remote marine boundary layer during the First Aerosol Characterization Experiment (ACE 1). *J. Geophys. Res.*, *105*, 17 325 – 17 340, 2000.

Furrow, S. Reactions of iodine intermediates in iodate-hydrogen peroxide oscillators. *J. Phys. Chem.*, *91*, 2129–2135, 1987.

Galbally, I. E., S. T. Bentley, and C. P. M. Meyer. Mid-latitude marine boundary-layer ozone destruction at visible surise observed at Cape Grim, Tasmania, 41°S. *Geophys. Res. Letters*, *27*, 3841 – 3844, 2000.

Gerecke, A., A. Thielmann, L. Gutzwiller, and M. J. Rossi. The chemical kinetics of HONO formation resulting from heterogeneous interaction of NO2 with flame soot. *Geophys. Res. Letters*, *25*, 2453 – 2456, 1998.

Ghosal, S., A. Shbeeb, and J. C. Hemminger. Surface Segregation of Bromine doped NaCl: Implications for the Seasonal Variations in Arctic Ozone. *Geophys. Res. Letters*, *27*, 1879 – 1882, 2000.

Gombosi, T. I. *Gaskinetic Theory*. Cambridge University Press, 1994.

Gong, S. L., L. A. Barrie, and J.-P. Blanchet. Modeling sea-salt aerosols in the atmosphere: 1. Model development. *J. Geophys. Res.*, *102*, 3805 – 3818, 1997.

Graedel, T. E. and W. C. Keene. Tropospheric budget of reactive chlorine. *Global Biogeochem. Cycles*, *9*, 47 – 77, 1995.

Haag, W. R. and J. Hoigné. Ozonation of bromide-containing waters: Kinetics of formation of hypobromous acid and bromate. *Environ. Sci. Technol.*, *17*, 261 – 267, 1983.

Hanson, D. R., J. B. Burkholder, C. J. Howard, and A. R. Ravishankara. Measurement of OH and HO_2 radical uptake coefficients on water and sulfuric acid surfaces. *J. Phys. Chem.*, *96*, 4979–4985, 1992.

Hanson, D. R., A. R. Ravishankara, and E. R. Lovejoy. Reaction of $BrONO_2$ with H_2O on submicron sulfuric acid aerosol and the implications for the lower stratosphere. *J. Geophys. Res.*, *101D*, 9063–9069, 1996.

Hausmann, M. and U. Platt. Spectroscopic measurement of bromine oxide and ozone in the high Arctic during Polar Sunrise Experiment 1992. *J. Geophys. Res.*, *99*, 25 399 – 25 413, 1994.

Hebestreit, K., G. Hönninger, J. Stutz, B. Alicke, and U. Platt. Measurements of halogen oxides in the troposphere. *Geophys. Res. Abs.*, *2*, 1061, 2000.

Hebestreit, K., J. Stutz, D. Rosen, V. Matveiv, M. Peleg, M. Luria, and U. Platt. DOAS Measurements of Tropospheric Bromine Oxide in Mid-Latitudes. *Science*, *283*, 55 – 57, 1999.

Herrmann, H., B. Ervens, P. Nowacki, R. Wolke, and R. Zellner. A chemical aqueous phase radical mechanism for tropospheric chemistry. *Chemosphere*, *38*, 1223 – 1232, 1999.

Herrmann, H., A. Reese, and R. Zellner. Time resolved UV/VIS diode array absorption spectroscopy of SO_x^- (x=3, 4, 5) radical anions in aqueous solution. *J. Mol. Struct.*, *348*, 183–186, 1995.

Hindman, E. E. and R. J. Bodowski. A Marine Stratus Layer Modified by Nuclei from a Ship Plume. *J. Appl. Met.*, *35*, 1596 – 1600, 1996.

Hirokawa, J., K. Onaka, Y. Kajii, and H. Akimoto. Heterogeneous processes involving sodium halide particles and ozone: Molecular bromine release in the marine boundary layer in the absence of nitrogen oxides. *Geophys. Res. Letters*, *25*, 2449 – 2452, 1998.

Hobbs, P. V., T. J. Garrett, R. J. Ferek, S. R. Strader, D. A. Hegg, G. M. Frick, W. A. Hoppel, R. F. Gasparovic, L. M. Russell, D. W. Johnson, C. O'Dowd, P. A. Durkee, K. E. Nielsen, and G. Innis. Emissions from Ships with respect to Their Effects on Cloud. *J. Atmos. Sci.*, *57*, 2570 – 2590, 2000.

Hoffmann, M. R. On the kinetics and mechanism of oxidation of aquated sulfur dioxide by ozone. *Atmos. Environ.*, *20*, 1145 – 1154, 1986.

Hoigné, J., H. Bader, W. R. Haag, and J. Staehelin. Rate constants of reactions of ozone with organic and inorganic compounds in water — III Inorganic compounds and radicals. *Wat. Res.*, *19*, 993–1004, 1985.

Hoppel, W. A. and G. M. Frick. Submicron aerosol size distributions measured over the tropical and south Pacific. *Atmos. Environ.*, *24A*, 645 – 659, 1990.

Hu, J. H., Q. Shi, P. Davidovits, D. R. Worsnop, M. S. Zahniser, and C. E. Kolb. Reactive uptake of Cl_2(g) and Br_2(g) by aqueous surfaces as a function of Br^- and I^- ion concentration: The effect of chemical reaction at the interface. *J. Phys. Chem.*, *99*, 8768–8776, 1995.

Hubinger, S. and J. B. Nee. Absorption spectra of Cl_2, Br_2 and BrCl between 190 and 600 nm. *J. Photochem. Photobiol. A: Chem.*, *86*, 1–7, 1995.

Huie, R. E. and P. Neta. Chemical behavior of SO_3^- and SO_5^- radicals in aqueous solutions. *J. Phys. Chem.*, *88*, 5665–5669, 1984.

Huie, R. E. and P. Neta. Rate constants for some oxidations of S(IV) by radicals in aqueous solutions. *Atmos. Environ.*, *21*, 1743–1747, 1987.

Huthwelker, T., S. L. Clegg, T. Peter, K. Carslaw, B. P. Luo, and P. Brimblecombe. Solubility of HOCl in water and aqueous H_2SO_4 to stratospheric temperatures. *J. Atmos. Chem.*, *21*, 81–95, 1995.

Hynes, A. J. and P. H. Wine. The atmospheric chemistry of dimethylsulfoxide (DMSO) kinetics and mechanism of the OH + DMSO reaction. *J. Atmos. Chem.*, *24*, 23 – 27, 1996.

Ingham, T., D. Bauer, R. Sander, P. J. Crutzen, and J. N. Crowley. Kinetics and Products of the Reactions BrO + DMS and Br + DMS at 298 K. *J. Phys. Chem. A*, *103*, 7199 – 7209, 1999.

Ingham, T., M. Cameron, and J. N. Crowley. Photodissociation of IO (355 nm) and OIO (532 nm): Quantum Yields for O(^{3}P)/I Production. *J. Phys. Chem. A*, *104*, 8001 – 8010, 2000.

Jacob, D. J. Chemistry of OH in Remote Clouds and Its Role in the Production of Formic Acid and Peroxymonosulfate. *J. Geophys. Res.*, *91*, 9807 – 9826, 1986.

Jacob, D. J. Heterogeneous chemistry and tropospheric ozone. *Atmos. Environ.*, *34*, 2131 – 2159, 2000.

Jacobi, H.-W. *Kinetische Untersuchungen und Modellrechnungen zur troposphärischen Chemie von Radikalanionen und Ozon in wässriger Phase*. Ph.D. thesis, Universität Essen, 1996.

Jacobi, H.-W., H. Herrmann, and R. Zellner. Kinetic investigation of the Cl_2^- radical in the aqueous phase. In P. Mirabel, editor, *Air Pollution Research Report 57: Homogenous and hetrogenous chemical Processes in the Troposphere*, pages 172–176. Office for official Publications of the European Communities, Luxembourg, 1996.

Jacobi, H.-W., F. Wicktor, H. Herrmann, and R. Zellner. A laser flash photolysis kinetic study of reactions of the Cl_2^- radical anion with oxygenated hydrocarbons in aqueous solution. *Int. J. Chem. Kinet.*, *31*, 169–181, 1999.

Jaenicke, R. Aerosol Physics and Chemistry. In *Landolt-Börnstein "'Zahlenwerte und Funktionen aus Naturwissenschaften und Technik"'*, V 4b, pages 391–457. Springer, 1988.

Jayson, G. G., B. J. Parsons, and A. J. Swallow. Some simple, highly reactive, inorganic chlorine derivatives in aqueous solution. *J. Chem. Soc. Faraday Trans.*, *69*, 1597–1607, 1973.

Jefferson, A., J. M. Nicovich, and P. H. Wine. Temperature-dependent kinetics studies of the reactions $Br(^2P_{3/2}) + CH_3SCH_3 \leftrightarrow CH_3SCH_2 + HBr$. Heat of formation of the CH_3SCH_2 radical. *J. Phys. Chem.*, *98*, 7128 – 7135, 1994.

Jenkin, M. E., R. A. Cox, and D. E. Candeland. Photochemical aspects of tropospheric iodine behaviour. *J. Atmos. Chem.*, *2*, 359–375, 1985.

Jiang, P.-Y., Y. Katsumura, R. Nagaishi, M. Domae, K. Ishikawa, K. Ishigure, and Y. Yoshida. Pulse radiolysis study of concentrated sulfuric acid solutions. Formation mechanism, yield and reactivity of sulfate radicals. *J. Chem. Soc. Faraday Trans.*, *88*, 1653–1658, 1992.

Jobson, B. T., D. D. Parrish, P. Goldan, W. Kuster, F. C. Fehsenfeld, D. R. Blake, N. J. Blake, and H. Niki. Spatial and temporal variability of nonmethane hydrocarbon mixing ratios and their relation to photochemical lifetime. *J. Geophys. Res.*, *103*, 13 557 – 13 567, 1998.

Kalberer, M., K. Tabor, M. Ammann, Y. Parrat, E. Weingartner, D. Piguet, E. Rössler, D. T. Jost, A. Türler, H. W. Gäggeler, and U. Baltensperger. Heterogeneous Chemical Processing of $^{13}NO_2$ by Monodisperse Carbon Aerosols at Very Low Concentrations. *J. Phys. Chem.*, *100*, 15 487 – 15 493, 1996.

Kärcher, B. Aviation-produced aerosol and contrails. *Surveys in Geophysics*, *20*, 113 – 167, 1999.

Kasibhatla, P., H. L. II, W. J. Moxim, S. N. Pandis, J. J. Corbett, M. C. Peterson, R. E. Honrath, G. J. Frost, D. D. Parrish, and T. B. Ryerson. Do emissions from ships have a significant impact on concentrations of nitrogen oxides in the marine boundary layer ? *Geophys. Res. Letters*, *27*, 2229 – 2232, 2000.

Keene, W. C., A. A. P. Pszenny, D. J. Jacob, R. A. Duce, J. N. Galloway, J. J. Schultz-Tokos, H. Sievering, and J. F. Boatman. The geochemical cycling of reactive chlorine through the marine troposphere. *Global Biogeochem. Cycles*, *4*, 407 – 430, 1990.

Keene, W. C., R. Sander, A. A. P. Pszenny, R. Vogt, P. J. Crutzen, and J. N. Galloway. Aerosol pH in the marine boundary layer: A review and model evaluation. *J. Aerosol Sci.*, *29*, 339 – 356, 1998.

Keene, W. C. and D. L. Savoie. The pH of deliquesced sea-salt aerosol in polluted marine air. *Geophys. Res. Letters*, *25*, 2181 – 2184, 1998.

Keene, W. C. and D. L. Savoie. Correction to "The pH of deliquesced sea-salt aerosol in polluted marine air". *Geophys. Res. Letters*, *26*, 1315 – 1316, 1999.

Kelley, C. M. and H. V. Tartar. On the system: bromine-water. *J. Am. Chem. Soc.*, *78*, 5752–5756, 1956.

Kerminen, V.-M., K. Teinilä, R. Hillamo, and T. Pakkanen. Substitution of chloride in sea-salt particles by inorganic and organic anions. *J. Aerosol Sci.*, *29*, 929 – 942, 1998.

Kim, Y., H. Sievering, J. Boatman, D. Wellman, and A. Pszenny. Aerosol size distribution and aerosol water content measurements during Atlantic Stratocumulus Transition Experiment/Marine Aerosol and Gas Exchange. *J. Geophys. Res.*, *100*, 23 027 – 23 038, 1995.

Kirchner, U., V. Scheer, and R. Vogt. FTIR Spectroscopic Investigation of the Mechanism and Kinetics of the Heterogeneous Reactions of NO_2 and HNO_3 with Soot. *J. Phys. Chem. A*, *104*, 8908 – 8915, 2000.

Kläning, U. K. and T. Wolff. Laser flash photolysis of HClO, ClO^-, HBrO, and BrO^- in aqueous solution. Reactions of Cl- and Br-atoms. *Ber. Bunsenges. Phys. Chem.*, *89*, 243–245, 1985.

Knipping, E. M., M. J. Lakin, K. L. Foster, P. Jungwirth, D. J. Tobias, R. B. Gerber, D. Dabdub, and B. J. Finlayson-Pitts. Experiments and Molecular/Kinetics Simulations of Ion-Enhanced Interfacial Chemistry on Aqueous NaCl Aerosols. *Science*, *288*, 301 – 306, 2000.

Koch, T. G. and M. J. Rossi. Direct measurement of surface residence times: Nitryl chloride and chlorine nitrate on alkali halides at room temperature. *J. Phys. Chem. A*, *102*, 9193–9201, 1998.

Kritz, M. and J. Rancher. Circulation of Na, Cl, and Br in the Tropical Marine Atmosphere. *J. Geophys. Res.*, *85*, 1633 – 1639, 1980.

Kumar, K. and D. W. Margerum. Kinetics and mechanism of general-acid-assisted oxidation of bromide by hypochlorite and hypochlorous acid. *Inorg. Chem.*, *26*, 2706–2711, 1987.

Landgraf, J. *Modellierung photochemisch relevanter Strahlungsvorgänge in der Atmosphäre unter Berücksichtigung des Einflusses von Wolken*. Ph.D. thesis, Universität Mainz, 1998.

Landgraf, J. and P. Crutzen. An Efficient Method for 'On-Line' Calculations of Photolysis and Heating Rates. *J. Atmos. Sci.*, *55*, 863 – 878, 1998.

Laszlo, B., M. J. Kurylo, and R. E. Huie. Absorption cross sections, kinetics of formation, and self-reaction of the IO radical produced via the laser photolysis of $N_2O/I_2/N_2$ mixtures. *J. Phys. Chem.*, *99*, 11 701–11 707, 1995.

Lawrence, M. G. and P. J. Crutzen. Influence of NO_x emissions from ships on tropospheric photochemistry and climate. *Nature*, *402*, 167 – 170, 1999.

Lax, E. *Taschenbuch für Chemiker und Physiker*. Springer Verlag, Berlin, 1969.

Lee, C.-T. and W.-C. Hsu. The measurement of liquid water mass associated with collected hygroscopic particles. *J. Aerosol Sci.*, *31*, 189 – 197, 2000.

Lee, Y.-N. and S. E. Schwartz. Reaction kinetics of nitrogen dioxide with liquid water at low partial pressure. *J. Phys. Chem.*, *85*, 840–848, 1981.

Lelieveld, J. and P. J. Crutzen. The Role of Clouds in Tropospheric Photochemistry. *J. Atmos. Chem.*, *12*, 229 – 267, 1991.

Lelieveld, J., P. J. Crutzen, and H. Rodhe. Zonal average cloud characteristics for global atmospheric chemistry modelling. Technical Report CM-76, Dep. of Meteorology, University of Stockholm (MISU), 1989.

Lengyel, I., J. Li, K. Kustin, and I. R. Epstein. Rate constants for reactions between iodine- and chlorine-containing species: A detailed mechanism of the chlorine dioxine/chlorite reaction. *J. Am. Chem. Soc.*, *118*, 3708–3719, 1996.

Li, Z. and Z. Tao. A kinetic study on reactions of OBrO with NO, OClO, and ClO at 298 K. *Chem. Phys. Lett.*, *306*, 117 – 123, 1999.

Lind, J. A. and G. L. Kok. Correction to "Henry's law determinations for aqueous solutions of hydrogen peroxide, methylhydroperoxide, and peroxyacetic acid" by John A. Lind and Gregory L. Kok. *J. Geophys. Res.*, *99D*, 21 119, 1994.

Lind, J. A., A. L. Lazrus, and G. L. Kok. Aqueous phase oxidation of sulfur(IV) by hydrogen peroxide, methylhydroperoxide, and peroxyacetic acid. *J. Geophys. Res.*, *92D*, 4171–4177, 1987.

Liu, Q., Y. L. Kogan, D. K. Lilly, D. W. Johnson, G. E. Innis, P. A. Durkee, and K. E. Nielsen. Modeling of Ship Effluent Transport and Its Sensitivity to Boundary Layer Structure. *J. Atmos. Sci.*, *57*, 2779 – 2791, 2000.

Logager, T., K. Sehested, and J. Holcman. Rate constants of the equilibrium reactions $SO_4 + HNO_3 \longleftrightarrow HSO_4^- + NO_3$ and $SO_4 + NO_3 \longleftrightarrow SO_4^{2-} + NO_3$. *Radiat. Phys. Chem.*, *41*, 539 – 543, 1993.

Long, C. A. and B. H. J. Bielski. Rate of reaction of superoxide radical with chloride-containing species. *J. Phys. Chem.*, *84*, 555–557, 1980.

Losno, R., J. L. Colin, L. Spokes, T. Jickells, M. Schulz, A. Rebers, M. Leermakers, C. Meuleman, and W. Baeyens. Non-Rain Deposition Significantly Modifies Rain Samples at a Coastal Site. *Atmos. Environ.*, *32*, 3445 – 3455, 1998.

Loughlin, P. E., T. Trautmann, A. Bott, W. G. Panhans, and W. Zdunkowski. The effects of different radiation parameterisations on cloud evolution. *Q. J. R. Meteorol. Soc.*, *123*, 1985–2007, 1997.

Lurmann, F. W., A. C. Lloyd, and R. Atkinson. A Chemical Mechanism for Use in Long-Range Transport/Acid Deposition Computer Modeling. *J. Geophys. Res.*, *91*, 10 905 – 10 936, 1986.

Magi, L., F. Schweitzer, C. Pallares, S. Cherif, , P. Mirabel, and C. George. Investigation of the uptake rate of ozone and methyl hydroperoxide by water surfaces. *J. Phys. Chem. A*, *101*, 4943–4949, 1997.

Mallard, W. G., F. Westley, J. T. Herron, R. F. Hampson, and D. H. Frizzel. *NIST Chemical Kinetics Database: Version 5.0*. National Institute of Standards and Technology, Gaithersburg, MD, 1993.

Mamou, A., J. Rabani, and D. Behar. On the oxidation of aqueous Br^- by OH radicals, studied by pulse radiolysis. *J. Phys. Chem.*, *81*, 1447–1448, 1977.

Marsh, A. R. W. and W. J. McElroy. The dissociation constant and Henry's law constant of HCl in aqueous solution. *Atmos. Environ.*, *19*, 1075 – 1080, 1985.

Martin, L. R. and D. E. Damschen. Aqueous oxidation of sulfur dioxide by hydrogen peroxide at low pH. *Atmos. Environ.*, *15*, 1615–1621, 1981.

McElroy, C. T., C. A. McLinden, and J. C. McConnell. Evidence for bromine monoxide in the free troposphere during the Arctic polar sunrise. *Nature*, *397*, 338 – 341, 1999.

McFiggans, G., J. M. C. Plane, B. J. Allan, L. J. Carpenter, H. Coe, and C. O'Dowd. A Modellig Study of Iodine Chemistry in the Marine Boundary Layer. *J. Geophys. Res.*, *105*, 14 371 – 14 377, 2000.

Mellor, G. L. and T. Yamada. Development of a Turbulence Closure Model for Geophysical Fluid Problems. *Rev. Geoph. Space Ph.*, *20*, 851–875, 1982.

Mentel, T. F., D. Bleilebens, and A. Wahner. A study of nighttime nitrogen oxide oxidation in a large reaction chamber — The fate of NO_2, N_2O_5, HNO_3, and O_3 at different humidities. *Atmos. Environ.*, *30*, 4007–4020, 1996.

Misra, A. and P. Marshall. Computational Investigations of Iodine Oxides. *J. Phys. Chem. A*, *102*, 9056 – 9060, 1998.

Mochida, M., H. Akimoto, H. van den Bergh, and M. J. Rossi. Heterogeneous Kinetics of the Uptake of HOBr on Solid Alkali Metal Halides at Ambient Temperature. *J. Phys. Chem. A*, *102*, 4819 – 4828, 1998a.

Mochida, M., J. Hirokawa, and H. Akimoto. Unexpected large uptake of O_3 on sea salts and the observed Br_2 formation. *Geophys. Res. Letters*, *27*, 2629 – 2632, 2000.

Mochida, M., J. Hirokawa, Y. Kajii, and H. Akimoto. Heterogeneous reactions of Cl_2 with sea salts at ambient temperature: Implications for halogen exchange in the atmosphere. *Geophys. Res. Letters*, *25*, 3927 – 3930, 1998b.

Monahan, E. C., D. E. Spiel, and K. L. Davidson. A model of marine aerosol generation via whitecaps and wave disruption. In E. C. Monahan and G. M. Niocaill, editors, *Oceanic Whitecaps*, pages 167 – 174. D. Reidel, Norwell, Mass, 1986.

Monks, P. S., L. J. Carpenter, S. A. Penkett, G. P. Ayers, R. W. Gillet, I. E. Galbally, and C. P. Meyer. Fundamental Ozone Photochemistry in the Remote Marine Boundary Layer: The SOAPEX Experiment, Measurements and Theory. *Atmos. Environ.*, *32*, 3647 – 3664, 1998.

Monks, P. S., G. Salisbury, G. Holland, S. A. Penkett, and G. P. Ayer. A seasonal comparison of ozone photochemistry in the remote marine boundary layer. *Atmos. Environ.*, *34*, 2547 – 2561, 2000.

Moyers, J. L. and R. A. Duce. Gaseous and particulate bromine in the marine atmosphere. *J. Geophys. Res.*, *77*, 5330–5338, 1972.

Mozurkewich, M. Mechanisms for the release of halogens from sea-salt particles by free radical reactions. *J. Geophys. Res.*, *100*, 14 199 – 14 207, 1995.

Nagao, I., K. Matsumoto, and H. Tanaka. Sunrise ozone destruction found in the sub-tropical marine boundary layer. *Geophys. Res. Letters*, *26*, 3377 – 3380, 1999.

Nagy, J. C., K. Kumar, and D. W. Margerum. Non-metal redox kinetics: Oxidation of iodide by hypochlorous acid and by nitrogen trichloride measured by the pulsed-accelerated-flow method. *Inorg. Chem.*, *27*, 2773–2780, 1988.

Neta, P. and R. E. Huie. Rate constants for reactions of NO_3 radicals in aqueous solutions. *J. Phys. Chem.*, *90*, 4644–4648, 1986.

Noone, K. J., E. Öström, R. J. Ferek, T. Garrett, P. V. Hobbs, D. W. Johnson, J. P. Taylor, L. M. Russell, R. C. Flagan, J. H. Seinfeld, C. D. O'Dowd, M. H. Smith, P. A. Durkee, K. Nielsen, J. G. Hudson, R. A. Pockalny, L. de Bock, R. E. van Grieken, R. F. Gasparovic, and I. Brooks. A Case Study of Ships Forming and Not Forming Tracks in Moderately Polluted Clouds. *J. Atmos. Sci.*, *54*, 2729 – 2747, 2000.

Olsen, R. J. and I. R. Epstein. Bifurcation analysis of chemical reaction mechanisms. I. Steady state bifurcation structure. *J. Chem. Phys.*, *94*, 3083–3095, 1991.

Orlando, J. J. and G. S. Tyndall. Rate coefficients for the thermal decomposition of $BrONO_2$ and the heat of formation of $BrONO_2$. *J. Phys. Chem.*, *100*, 19 398 – 19 405, 1996.

Oum, K., M. J. Lakin, D. O. D. Haan, T. Brauers, and B. J. Finlayson-Pitts. Formation of Molecular Chlorine from the Photolysis of Ozone and Aqueous Sea-Salt Particles. *Science*, *279*, 74 – 77, 1998.

Palmer, D. A., R. W. Ramette, and R. E. Mesmer. The hydrolysis of iodine: Equilibria at high temperatures. *J. Nucl. Mater.*, *130*, 280–286, 1985.

Pandis, S. N. and J. H. Seinfeld. Sensitivity Analysis of a Chemical Mechanism for Aqueous-Phase Atmospheric Chemistry. *J. Geophys. Res.*, *94*, 1105 – 1126, 1989.

Pham, M., J.-F. Müller, G. P. Brasseur, C. Granier, and G. Mégie. A three-dimensional study of the tropospheric sulfur cycle. *J. Geophys. Res.*, *100*, 26 061 – 26 092, 1995.

Pitzer, K. S. Ion interaction approach: Theory and data correlation. In *Activity Coefficients in Electrolyte Solutions, edited by K. S. Pitzer*, pages 75 – 153. CRC Press, Boca Raton, 1991.

Plane, J. M. C., B. J. Allan, G. McFiggans, and R. A. Cox. Radical chemistry in the remote marine boundary layer. *Geophys. Res. Abs.*, *2*, 1070, 2000.

Platt, U. and G. K. Moortgat. Heterogeneous and Homogeneous Chemistry of Reactive Halogen Compounds in the Lower Troposphere. *J. Atmos. Chem.*, *34*, 1 – 8, 1999.

Ponche, J. L., C. George, and P. Mirabel. Mass transfer at the air/water interface: Mass accommodation coefficients of SO_2, HNO_3, NO_2 and NH_3. *J. Atmos. Chem.*, *16*, 1–21, 1993.

Pöschl, U., M. Canagaratna, J. T. Jayne, L. T. Molina, D. R. Worsnop, C. E. Kolb, and M. J. Molina. Mass accommodation coefficient of H_2SO_4 vapor on aqueous sulfuric acid surfaces and gaseous diffusion coefficient of H_2SO_4 in N_2/H_2O. *J. Phys. Chem. A*, *102*, 10 082–10 089, 1998.

Pruppacher, H. R. and J. D. Klett. *Microphysics of Clouds and Precipitation*. Kluwer Academic Pub., Dordrecht/Boston/London, 1997.

Pszenny, A., W. Keene, C. O'Dowd, M. Smith, and P. Quinn. Sea salt aerosols, tropospheric sulphur cycling, and climate forcing. *IGBP Newsletter*, *33*, 13 – 19, 1998.

Pszenny, A. A. P., W. C. Keene, D. J. Jacob, S. Fan, J. R. Maben, M. P. Zetwo, M. Springer-Young, and J. N. Galloway. Evidence of inorganic chlorine gases other hydrogen chloride in marine surface air. *Geophys. Res. Letters*, *20*, 699 – 702, 1993.

Quinn, P. K., T. S. Bates, J. E. johnson, D. S. Covert, and R. J. Charlson. Interactions Between the Sulfur and Reduced Nitrogen Cycles Over the Central Pacific Ocean. *J. Geophys. Res.*, *95*, 16 405 – 16 416, 1990.

Rancher, J. and M. A. Kritz. Diurnal Fluctuations of Br and I in the Tropical Marine Atmosphere. *J. Geophys. Res.*, *85*, 5581 – 5587, 1980.

Ravishankara, A. R. Heterogeneous and Multiphase Chemistry in the Troposphere. *Science*, *276*, 1058 – 1065, 1997.

Régimbal, J.-M. and M. Mozurkewich. Peroxynitric acid decay mechanisms and kinetics at low pH. *J. Phys. Chem. A*, *101*, 8822–8829, 1997.

Richter, A., F. Wittrock, M. Eisinger, and J. P. Burrows. GOME Observations of Tropospheric BrO in Northern Hemispheric Spring and Summer 1997. *Geophys. Res. Letters*, *25*, 2683 – 2686, 1998.

Roehl, C. M., J. B. Burkholder, G. K. Moortgat, A. R. Ravishankara, and P. J. Crutzen. The temperature dependence of the UV absorption cross sections and the atmospheric implications of several alkyl iodides. *J. Geophys. Res.*, *102D*, 12 819–12 829, 1997.

Ross, A. B., W. G. Mallard, W. P. Helman, B. H. J. Bielski, G. V. Buxton, D. E. Cabelli, C. L. Greenstock, R. E. Huie, and P. Neta. *NDRL-NIST Solution Kinetics Database: - Ver. 1*. National Institute of Standards and Technology, Gaithersburg, MD, 1992.

Rudich, Y., R. K. Talukdar, T. Imamura, R. W. Fox, and A. R. Ravishankara. Uptake of NO_3 on KI solutions: Rate coefficient for the $NO_3 + I^-$ reaction and gas-phase diffusion coefficients for NO_3. *Chem. Phys. Lett.*, *261*, 467–473, 1996.

Rudolph, J., R. Koppmann, and C. Plass-Dülmer. The budgets of ethane and tetrachloroethene: Is there evidence for an impact of reactions with chlorine atoms in the troposphere? *Atmos. Environ.*, *30*, 1887 – 1894, 1996.

Rudolph, J., B. Ramacher, C. Plass-Dülmer, K.-P. Müller, and R. Koppmann. The indirect determination of chlorine atom concentration in the troposphere from changes in the patterns of non-methane hydrocarbons. *Tellus*, *49B*, 592 – 601, 1997.

Ruggaber, A., R. Dlugi, A. Bott, R. Forkel, H. Herrmann, and H.-W. Jacobi. Modelling of radiation quantities and photolysis frequencies in the aqueous phase in the troposphere. *Atmos. Environ.*, *31*, 3137 – 3150, 1997.

Russell, L. M., J. H. Seinfeld, R. C. Flagan, R. J.Ferek, D. A. Hegg, P. V. Hobbs, W. Wobrock, A. I. Flossmann, C. D. O'Dowd, K. E. Nielsen, and P. A. Durkee. Aerosol dynamics in ship track. *J. Geophys. Res.*, *104*, 31 077 – 31 095, 1999.

Sander, R. Modeling Atmospheric Chemistry: Interactions between Gas-Phase Species and Liquid Cloud/Aerosol Particles. *Surveys in Geophysics*, *20*, 1 – 31, 1999.

Sander, R. and P. J. Crutzen. Model study indicating halogen activation and ozone destruction in polluted air masses transported to the sea. *J. Geophys. Res.*, *101*, 9121 – 9138, 1996.

Sander, R., Y. Rudich, R. von Glasow, and P. J. Crutzen. The role of $BrNO_3$ in marine tropospheric chemistry: A model study. *Geophys. Res. Letters*, *26*, 2857 – 2860, 1999.

Sander, S. P., R. R. Friedl, W. B. DeMore, D. M. Golden, M. J. Kurylo, R. F. Hampson, R. E. Huie, G. K. Moortgat, A. R. Ravishankara, C. E. Kolb, and M. J. Molina. Chemical Kinetics and Photochemical Data for Use in Stratospheric Modeling. Technical Report JPL Publication 00-3, Jet Propulsion Laboratory, Pasadena, CA, 2000.

Scheffler, D., H. Grothe, H. Willner, A. Frenzel, and C. Zetzsch. Properties of Pure Nitryl Bromide. Thermal Behaviour, UV/Vis and FTIR Spectra, and Photoisomerization to *trans*-BrONO in an Argon Matrix. *Inorg. Chem.*, *36*, 335 – 338, 1997.

Schultz, M. G., D. J. Jacob, Y. Wang, J. A. Logan, E. L. Atlas, D. R. Blake, N. J. Blake, J. D. Bradshaw, E. V. Browell, M. A. Fenn, F. Flocke, G. L. Gregory, B. G. Heikes, G. W. Sachse, S. T. Sandholm, R. E. Shetter, H. B. Singh, and R. W. Talbot. On the origin of tropospheric ozone and NO_x over the tropical South Pacific. *J. Geophys. Res.*, *104*, 5829 – 5843, 1999.

Schwartz, S. E. Mass-Transport Considerations Pertinent to Aqueous Phase Reactions of Gases in Liquid-Water Clouds. In W. Jaeschke, editor, *Chemistry of Multiphase Atmospheric Systems*, pages 415 – 471. NATO ASI Series, Vol. G6, 1986.

Schwartz, S. E. and W. H. White. Solubility equilibria of the nitrogen oxides and oxyacids in dilute aqueous solution. In J. R. Pfafflin and E. N. Ziegler, editors, *Advances in Environmental Science and Engineering*, volume 4, pages 1–45. Gordon and Breach Science Publishers, NY, 1981.

Schwarz, H. A. and B. H. J. Bielski. Reactions of HO_2 and O_2^- with iodine and bromine and the I_2^- and I atom reduction potentials. *J. Phys. Chem.*, *90*, 1445–1448, 1986.

Schweitzer, F., P. Mirabel, and C. George. Uptake of hydrogen halides by water droplets. *J. Phys. Chem. A*, *104*, 72–76, 2000.

Sciare, J., E. Baboukas, M. Kanakidou, U. Krischke, S. Belviso, H. Bardouki, and N. Mihalopoulos. Spatial and temporal variability of atmospheric sulfur-containing gases and particles during the Albatross campaign. *J. Geophys. Res.*, *105*, 14 433 – 14 448, 2000.

Seery, D. J. and D. Britton. The continous absorption spectra of chlorine, bromine, bromine chloride, iodine chloride, and iodine bromide. *J. Phys. Chem.*, *68*, 2263–2266, 1964.

Sehested, K., J. Holcman, E. Bjergbakke, and E. J. Hart. A pulse radiolytic study of the reaction OH + O_3 in aqueous medium. *J. Phys. Chem.*, *88*, 4144–4147, 1984.

Sehested, K., J. Holcman, and E. J. Hart. Rate constants and products of the reactions of e_{aq}^-, O_2^- and H with ozone in aqueous solutions. *J. Phys. Chem.*, *87*, 1951–1954, 1983.

Sehested, K., O. L. Rasmussen, and H. Fricke. Rate constants of OH with HO_2, O_2^-, and $H_2O_2^+$ from hydrogen peroxide formation in pulse-irradiated oxygenated water. *J. Phys. Chem.*, *72*, 626–631, 1968.

Seinfeld, J. H. and S. N. Pandis. *Atmospheric Chemistry and Physics*. John Wiley & Sons, New York, Chichester, Weinheim, 1998.

Seisel, S., F. Caloz, F. F. Fenter, H. van den Bergh, and M. J. Rossi. The heterogeneous reaction of NO_3 with NaCl and KBr: A nonphotolytic source of halogen atoms. *Geophys. Res. Letters*, *24*, 2757 – 2760, 1997.

Shaw, M. A. and M. J. Rood. Measurement of the crystallization humidities of ambient aerosol particles. *Atmos. Environ.*, *24A*, 1837 – 1841, 1990.

Shoute, L. C. T., Z. B. Alfassi, P. Neta, and R. E. Huie. Temperature dependence of the rate constants for reaction of dihalide and azide radicals with inorganic reductants. *J. Phys. Chem.*, *95*, 3238–3242, 1991.

Sievering, H., B. Lerner, J. Slavich, J. Anderson, M. M. Posfai, and J. Cainey. O_3 oxidation of SO_2 in sea-salt aerosol water: Size distribution of non-sea-salt sulfate during the First Aerosol Characterization Experiment (ACE 1). *J. Geophys. Res.*, *104*, 21 707 – 21 717, 1999.

Singh, H. B., G. L. Gregory, B. Anderson, E. Browell, G. W. Sachse, D. D. Davis, J. Crawford, J. D. Bradshaw, R. Talbot, D. R. Blake, D. Thornton, R. Newell, and J. Merrill. Low ozone in the marine boundary layer of the tropical Pacific Ocean: Photochemical loss, chlorine atoms, and entrainment. *J. Geophys. Res.*, *101*, 1907 – 1917, 1996a.

Singh, H. B., A. N. Thakur, Y. E. Chen, and M. Kanakidou. Tetrachloroethylene as an indicator of low Cl atom concentrations in the troposphere. *Geophys. Res. Letters*, *23*, 1529 – 1532, 1996b.

Smith, M. H., P. M. Park, and I. E. Consterdine. Marine aerosol concentrations and estimated fluxes over the sea. *Q. J. R. Meteorol. Soc.*, *119*, 809 – 824, 1993.

Spicer, C. W., E. G. Chapman, B. J. Finlayson-Pitts, R. A. Plastridge, J. M. Hubbe, J. D. Fast, and C. M. Berkowitz. Unexpectedly high concentrations of molecular chlorine in coastal air. *Nature*, *394*, 353 – 356, 1998.

Streets, D. G., G. R. Carmichael, and R. L. Arndt. Sulfur dioxide emissions and sulfur deposition frominternatinal shipping in Asian waters. *Atmos. Environ.*, *31*, 1573 – 1582, 1997.

Streets, D. G., S. K. Guttikunda, and G. R. Carmichael. The growing contribution of sulfur emissions from ships in Asian waters, 1988-1995. *Atmos. Environ.*, *34*, 4425 – 4439, 2000.

Stull, R. B. *An Introduction to Boundary Layer Meteorology*. Kluwer Academic Pub., Dordrecht/Boston/London, 1988.

Sutton, H. C. and M. T. Downes. Reactions of the HO_2 radical in aqueous solution with bromine and related compounds. *J. Chem. Soc. Faraday Trans. 1*, *68*, 1498–1507, 1972.

Takami, A., S. Kato, A. Shimono, and S. Koda. Uptake coefficient of OH radical on aqueous surface. *Chem. Phys.*, *231*, 215–227, 1998.

Tang, I. N. Thermodynamic and optical properties of mixed-salt aerosols of atmospheric interest. *J. Geophys. Res.*, *102*, 1883 – 1893, 1997.

Taylor, J. P. and A. S. Ackerman. A case-study of pronounced perturbations to cloud properties and boundary-layer dynamics due to aerosol emissions. *Q. J. R. Meteorol. Soc.*, *125*, 2643 – 2661, 1999.

Thomas, K., A. Volz-Thomas, and D. Kley. *Zur Wechselwirkung von* NO_3*-Radikalen mit wässrigen Lösungen: Bestimmung des Henry- und des Massenakkomodationskoeffizienten*. Ph.D. thesis, Institut für Chemie und Dynamik der Geosphäre 2, Forschungszentrum Jülich GmbH, FRG, 1993.

Toumi, R. BrO as a sink for dimethylsulphide in the marine atmosphere. *Geophys. Res. Letters*, *21*, 117 – 120, 1994.

Trautmann, T., I. Podgorny, J. Landgraf, and P. J. Crutzen. Actinic fluxes and photodissociation coefficients in cloud fields embedded in realistic atmospheres. *J. Geophys. Res.*, *104*, 30 173 – 30 192, 1999.

Troy, R. C., M. D. Kelley, J. C. Nagy, and D. W. Margerum. Non-metal redox kinetics: Iodine monobromide reaction with iodide ion and the hydrolysis of IBr. *Inorg. Chem.*, *30*, 4838–4845, 1991.

Troy, R. C. and D. W. Margerum. Non-metal redox kinetics: Hypobromite and hypobromous acid reactions with iodide and with sulfite and the hydrolysis of bromosulfate. *Inorg. Chem.*, *30*, 3538–3543, 1991.

Tuckermann, M., R. Ackermann, C. Golz, H. Lorenzen-Schmidt, T. Senne, J. Stutz, B. Trost, W. Unold, and U. Platt. DOAS-observation of halogen radical-catalysed arctic boundary layer ozone destruction during the ARCTOC-campaigns 1995 and 1996 in Ny-Alesund, Spitsbergen. *Tellus*, *49B*, 533 – 555, 1997.

van Dingenen, R., N. R. Jensen, J. Hjorth, and F. Raes. Peroxynitrate Formation During the Night-Time Oxidation of Dimethylsulfide: Its Role as a Reservoir Species for Aerosol Formation. *J. Atmos. Chem.*, *18*, 211 – 237, 1994.

Verwer, J. G., E. J. Spee, J. G. Blom, and W. H. Hundsdorfer. A second order Rosenbrock method applied to photochemical dispersion problems. Technical Report MAS-R9717, Centrum voor Wiskunde en Informatica, 1997.

Vogt, R. Iodine Compounds in the Atmosphere. In P. Fabian and O. N. Singh, editors, *The Handbook of Environmental Chemistry. Volume 4, Part E Air Pollution*, pages 113 – 129. 1999.

Vogt, R., P. J. Crutzen, and R. Sander. A mechanism for halogen release from sea-salt aerosol in the remote marine boundary layer. *Nature*, *383*, 327 – 330, 1996.

Vogt, R., R. Sander, R. von Glasow, and P. Crutzen. Iodine Chemistry and its Role in Halogen Activation and Ozone Loss in the Marine Boundary Layer: A Model Study. *J. Atmos. Chem.*, *32*, 375 – 395, 1999.

Volpe, C., M. Wahlen, A. A. P. Pszenny, and A. J. Spivack. Chlorine isotopic composition of marine aerosols: Implications for the release of reactive chlorine and HCl cycling rates. *Geophys. Res. Letters*, *25*, 3831 – 3834, 1998.

von Glasow, R. and R. Sander. Variation of sea salt aerosol pH with relative humidity. *Geophys. Res. Letters*, *28*, 247 – 250, 2001.

von Gunten, U. and Y. Oliveras. Advanced oxidation of bromide-containing waters: Bromate formation mechanisms. *Environ. Sci. Technol.*, *32*, 63 – 70, 1998.

Wagner, I. and H. Strehlow. On the flash photolysis of bromide ions in aqueous solution. *Ber. Bunsenges. Phys. Chem.*, *91*, 1317–1321, 1987.

Wagner, T. and U. Platt. Satellite mapping of enhanced BrO concentrations in the troposphere. *Nature*, *395*, 486 – 490, 1998.

Wallington, T. J., J. M. Andino, J. C. Ball, and S. M. Japar. Fourier transform infrared studies of the reaction of Cl atoms with PAN, PPN, CH_3OOH, HCOOH, CH_3COCH_3 and $CH_3COC_2H_5$ at 295±2 K. *J. Atmos. Chem.*, *10*, 301 – 313, 1990.

Wang, T. X., M. D. Kelley, J. N. Cooper, R. C. Beckwith, and D. W. Margerum. Equilibrium, kinetic, and UV-spectral characteristics of aqueous bromine chloride, bromine, and chlorine species. *Inorg. Chem.*, *33*, 5872–5878, 1994.

Wang, T. X. and D. W. Margerum. Kinetics of reversible chlorine hydrolysis: Temperature dependence and general-acid/base-assisted mechanisms. *Inorg. Chem.*, *33*, 1050 – 1055, 1994.

Wang, Y. L., J. C. Nagy, and D. W. Margerum. Kinetics of hydrolysis of iodine monochloride measured by the pulsed-accelerated-flow method. *J. Am. Chem. Soc.*, *111*, 7838–7844, 1989.

Warneck, P. The relative importance of various pathways for the oxidation of sulfur dioxide and nitrogen dioxide in sunlit continental fair weather clouds. *Phys. Chem. Chem. Phys.*, *1*, 5471 – 5483, 1999.

Warneck, P. and C. Wurzinger. Product Quantum Yield for the 305-nm Photodecomposition of NO_3^- in Aqueous Solution. *J. Phys. Chem. A*, *92*, 6278 – 6283, 1988.

Wayne, R. P., I. Barnes, P. Biggs, J. P. Burrows, C. E. Canosa-Mas, J. Hjorth, G. Le Bras, G. K. Moortgat, D. Perner, G. Poulet, G. Restelli, and H. Sidebottom. The nitrate radical: Physics, chemistry, and the atmosphere. *Atmos. Environ.*, *25A*, 1–203, 1991.

Weast, R. C., editor. *CRC Handbook of Chemistry and Physics, 61st Edition*. CRC Press, Inc., Boca Raton, FL, 1980.

Weinstein-Lloyd, J. and S. E. Schwartz. Low-intensity radiolysis study of free-radical reactions in cloudwater: H_2O_2 production and destruction. *Environ. Sci. Technol.*, *25*, 791–800, 1991.

Wesely, M. L. Parametrization of surface resistances to gaseous deposition in regional-scale numerical models. *Atmos. Environ.*, *23*, 1293 – 1304, 1989.

Wilhelm, E., R. Battino, and R. J. Wilcock. Low-pressure solubility of gases in liquid water. *Chem. Rev.*, *77*, 219–262, 1977.

Wine, P. H., Y. Tang, R. P. Thorn, J. R. Wells, and D. D. Davis. Kinetics of aqueous phase reactions of the SO_4^- radical with potential importance in cloud chemistry. *J. Geophys. Res.*, *94D*, 1085–1094, 1989.

Wingenter, O. W., D. R. Blake, N. J. Blake, B. C. Sive, F. S. Rowland, E. Atlas, and F. Flocke. Tropospheric hydroxyl and atomic chlorine concentrations, and mixing timescales determined from hydrocarbon and halocarbon measurements made over the Southern Ocean. *J. Geophys. Res.*, *104*, 21 819 – 21 828, 1999.

Wingenter, O. W., M. K. Kubo, N. J. Blake, T. W. Smith, Jr., D. R. Blake, and F. S. Rowland. Hydrocarbon and halocarbon measurements as photochemical and dynamical indicators of atmospheric hydroxyl, atomic chlorine, and vertical mixing obtained during Lagrangian flights. *J. Geophys. Res.*, *101*, 4331 – 4340, 1996.

Winkler, P. Relations between Aerosol Acidity and Ion Balance. In W. Jaeschke, editor, *Chemistry of Multiphase Atmospheric Systems*, pages 269 – 298. NATO ASI Series, Vol. G6, 1986.

Woodcock, A. H., C. F. Kientzler, A. B. Arons, and D. C. Blanchard. Giant Condensation Nuclei from Bursting Bubbles. *Nature*, *172*, 1144 – 1145, 1953.

Worsnop, D. R., M. S. Zahniser, C. E. Kolb, J. A. Gardner, L. R. Watson, J. M. van Doren, J. T. Jayne, and P. Davidovits. The temperature dependence of mass accommodation of SO_2 and H_2O_2 on aqueous surfaces. *J. Phys. Chem.*, *93*, 1159–1172, 1989.

Wu, D., D. Wong, and B. Di Bartolo. Evolution of Cl_2^- in aqueous NaCl solutions. *J. Photochem.*, *14*, 303–310, 1980.

Wu, J. Production of Spume Drops by the Wind Tearing of Wave Crests: The Search for Quantification. *J. Geophys. Res.*, *98*, 18 221 – 18 227, 1993.

Yokelson, R. J., J. B. Burkholder, L. Goldfarb, R. W. Fox, M. K. Gilles, and A. R. Ravishankara. Temperature dependent rate coefficient for the Cl + $ClONO_2$ reaction. *J. Phys. Chem.*, *99*, 13 976–13 983, 1995.

Zafiriou, O. C., M. McFarland, and R. H. Bromund. Nitric oxide in seawater. *Science*, *207*, 637 – 639, 1980.

Zdunkowski, W. G., W.-G. Panhans, R. M. Welch, and G. J. Korb. A Radiation Scheme for Circulation and Climate Models. *Contr. Physics Atm.*, *55*, 215–238, 1982.

Zellner, R., M. Exner, and H. Herrmann. Absolute OH Quantum Yield in the Laser Photolysis of Nitrate, Nitrite and Dissolved H_2O_2 at 308 and 351 nm in the Temperature Range 278-353 K. *J. Atmos. Chem.*, *10*, 411 – 425, 1990.

Zetzsch, C. and W. Behnke. Heterogeneous photochemical sources of atomic Cl in the troposphere. *Ber. Bunsenges. Phys. Chem.*, *96*, 488 – 493, 1992.

Zetzsch, C., P. Mirabel, J. Crowley, M. J. Rossi, J.-P. Sawerysyn, and Y. Gershenzon. Sea-salt aerosols: laboratory investigations of heterogeneous halogen activation in the troposphere SALT. Technical Report ENV4-CT95-0037 (SALT), Environment Research Programme: Oxidising capacity of the atmosphere and transport of photooxidants, 1998.

Zetzsch, C., G. Pfahler, and W. Behnke. Heterogeneous formation of chlorine atoms from NaCl in a photosmog system. *J. Aerosol Sci.*, *19*, 1203 – 1206, 1988.